Heterologous expression and artificial maturation of the [FeFe]-hydrogenase from *Desulfovibrio desulfuricans*

-Characterization and comparison with the native enzyme-

INAUGURAL-DISSERTATION

zur

Erlangung des Doktorgrades der Mathematisch-Naturwissenschaftlichen Fakultät der Heinrich-Heine-Universität Düsseldorf

angefertigt am

Max-Planck-Institut für Chemische Energiekonversion

Mülheim an der Ruhr

vorgelegt von

Kathrin Wrede

aus Essen

Die vorliegende Arbeit wurde in der Zeit von Februar 2011 bis Mai 2015 am Max-Planck-Institut für Chemische Energiekonversion (vormals Max-Planck-Institut für Bioanorganische Chemie) in Mülheim an der Ruhr unter der Anleitung von Herrn Prof. Dr. Dr. h. c. Wolfgang Lubitz verfasst.

Gedruckt mit der Genehmigung
der Mathematisch-Naturwissenschaftlichen Fakultät
der Heinrich-Heine-Universität Düsseldorf

Referent: Prof. Dr. Wolfgang Lubitz

Korreferent: Prof. Dr. Karl-Erich Jaeger

Tag der mündlichen Prüfung: 13 Juli 2015

Deklaration

Ich versichere, dass ich die hier vorgelegte Dissertation eigenständig und ohne unerlaubte Hilfe angefertigt habe. Die Dissertation wurde in der vorgelegten oder in ähnlicher Form noch bei keiner anderen Institution eingereicht. Ich habe bislang keine erfolglosen Promotionsversuche unternommen.

Mülheim an der Ruhr, den

Kathrin Wrede

Für André

und

meine Eltern

It doesn't matter how beautiful your theory is.

It doesn't matter how smart you are.

If it doesn't agree with the experiment, it's wrong.

-That's science-

(Richard Feynman)

Danksagung

An erster Stelle möchte ich Herrn Prof. Dr. W. Lubitz für die Überlassung dieses interessanten Themas, die ständige Diskussionsbereitschaft und seine immerwährende Unterstützung bei der Umsetzung meiner Vorstellungen danken.

Herrn Prof. Dr. K.-E. Jaeger danke ich für die Übernahme des Korreferats und sein Interesse am Fortgang dieser Arbeit.

Ein ganz großes Dankeschön geht an Dr. J. Birrell, der mich mit unendlicher Geduld und vor allem seiner Liebe zur Forschung stets motivierte weiter zu machen und mir Chemiker half meine Freude in den Tiefen der Biologie zu finden. Des Weiteren war er maßgeblich am Gelingen dieser Arbeit beteiligt, nicht nur durch die Hilfe bei den EPR-Messungen, unzähligen Diskussionen und das Korrekturlesen dieser Arbeit. Auch der kulturelle Austausch England-Deutschland hat hervorragend geklappt. :)

Herrn Dr. O. Rüdiger und Frau P. Rodriguez danke ich für die Hilfe bei den PFE-Experimenten und ihre stete Diskussionsbereitschaft und das nette Klima im Labor inklusive Spanisch-Crashkurs.

Viele Experimente wären ohne die Hilfe der vielen helfenden Hände, in diesem Umfang gar nicht möglich gewesen. Ich danke Frau G. Klihm und Herrn C. Laurich für die Unterstützung bei den EPR Messungen und den EPR Redox-Titrationen. Des Weiteren danke ich Herrn N. Dickmann für die Aufnahme zahlreicher MALDI-TOF Spektren und Frau M. Frenzer für ihre Hilfe bei den GC-Wasserstoffmessungen.

Der „Kristallfee“ Y. Brandenburger danke ich für die Vielzahl an angesetzten Kristallisationsversuchen und Herrn Dr. H. Ogata für die Messung unseres Hase-Kristalls an der BESSY in Berlin.

Ein ebenfalls großer Dank gebührt dem ganzen Team des Biolabors 1. Etage, euch danke ich nicht nur dafür, dass ihr mich die ganze Zeit mit meinen Launen ertragen habt sondern auch für eure Hilfe im Labor und als gute Büronachbarn, die immer genug Tee und Notfall-Süßigkeiten bereit hielten. Auch alle nicht-wissenschaftlichen Tätigkeiten wie der „Kuchen zu jeder Zeit“ und unsere selbst eingeführten Feiertage (CFF) werden mir immer in Erinnerung bleiben und haben einen wichtigen Beitrag zu dieser Arbeit geleistet.

Auch allen anderen Mitarbeitern des MPIs möchte ich herzlich danken, ich denke es gibt kein Problem was man mit euch nicht lösen kann. Ebenso danke ich allen Junglaboranten und Azubis, die mich in meiner Arbeit unterstützt haben.

Tanja Berndsen möchte ich einfach für alles danken, nicht nur für die wichtige Hilfe die sie mir bei der [FeFe]-Präp war, sondern einfach für alles. Danke, dass du immer für mich da warst und auch weiterhin bist.

Dann gibt es noch das Origin-Krisenmanagement Potsdam, liebe Annika, lieber Dirk, danke, dass ihr mir bei allen größeren und kleineren Problemen zu Seite gestanden habt und mich immer motiviert habt weiter zu machen.

Auch meiner „Telefonfreundin“ Anika Thiel möchte ich herzlich danken, dass sie immer ein offenes Ohr für mich hatte und wir es letztendlich doch geschafft haben zusammen auch noch das Projekt Promotion abzuschließen. Jetzt bleibt endlich Zeit für einfach „nur“ Freundschaft.

Meinen Eltern gebührt ebenfalls ein großer Dank, ohne eure stete Unterstützung auf meinem Weg und euren unermüdlichen Glauben an mich, wäre diese Arbeit nie möglich gewesen.

Der größte Dank gebührt allerdings meinem Ehemann André, nicht nur dafür, dass er immer für mich da war und mich in allen Entscheidungen bedingungslos unterstützt hat, sondern, dass er nach dieser Arbeit immer noch da ist. :) Ich war bestimmt nicht immer einfach in dieser Zeit, aber jetzt ist es geschafft. Danke für deine fortwährende Liebe und dass du bist wie du bist.

Es gibt kein zufälliges Treffen.
Jeder Mensch in unserem Leben ist entweder
ein Test, eine Strafe oder ein Geschenk...

Heterologous expression and artificial maturation of the [FeFe]-hydrogenase from *Desulfovibrio desulfuricans*
-Characterization and comparison with the native enzyme-

A better understanding of the hydrogen reaction cycle in hydrogenases would help to design new bio-based catalysts for hydrogen production. Therefore, the [FeFe]-hydrogenase from *Desulfovibrio desulfuricans* was studied in this thesis.

An important issue in studying proteins is the availability of high amounts of pure protein. Chapter 3 shows the improvement of the cell growth and purification methods for the native enzyme from *Desulfovibrio desulfuricans*. Additionally, and for the first time, the development and establishment for an overexpression system for the [FeFe]-hydrogenase from *D. desulfuricans* is reported. For that the sequences encoding for the protein were codon-optimized. Afterwards a plasmid was constructed that contained these codon optimized sequences for both subunits of the hydrogenase, one of which additionally contained the sequence for an affinity tag for easy purification. From this, high amounts of pure, unmaturated enzyme could be prepared.

Spectroscopic studies of the heterologously expressed, unmaturated enzyme by EPR spectroscopy are reported in Chapter 4, as well as its crystallization. It is shown that artificial maturation of this enzyme with a synthetic $[2Fe]_H$-mimic is possible and leads to fully active protein. The optimization for hydrogen production and consumption assays is also reported. Afterwards the maturated enzyme was studied by EPR and FTIR spectroscopy and compared with the native enzyme.

To get better insight into the involvement of the accessory iron-sulfur clusters in the function of the [FeFe]-hydrogenase, site-directed mutagenesis experiments to change redox potentials of these clusters are reported in Chapter 5. Maturation and activity measurements are shown here to see the effect of the mutations on the protein behaviour. The unmaturated enzymes were studied by EPR spectroscopy and compared to the heterologously expressed wild type protein.

The native [FeFe]-hydrogenase from *D. desulfuricans* shows an inactivation at high potentials (HPI) in protein film electrochemistry (PFE) experiments, which is not fully understood. Therefore, Chapter 6 reports experiments designed to provide further understanding of this phenomenon. It is reported that chloride seems to be essential for HPI and that HPI is also observed in the absence of hydrogen. Furthermore, the unmaturated and maturated [FeFe]-hydrogenase were measured for the first time with this technique to compare it with the native enzyme and to determine the redox potentials of the different clusters.

Heterologe Expression und artifizielle Maturation der [FeFe]-Hydrogenase aus *Desulfovibrio desulfuricans*
-Charakterisierung und Vergleich mit dem nativen Enzym-

Um die Entwicklung neuer, bio-technologisch basierter Katalysatoren zur Wasserstoffgewinnung voran zu treiben, ist ein detailliertes Verständnis von Modellenzymen, beispielsweise der Hydrogenasen, notwendig. Daher fokussiert sich die vorliegende Arbeit auf die Untersuchung der [FeFe]-Hydrogenase aus *Desulfovibrio desulfuricans*.

Der limitierende Faktor bei der Untersuchung von Proteinen ist meist ihr geringes Vorkommen im Wirtsorganismus, sowie ihre langwierige Gewinnung. Kapitel 3 dieser Arbeit beschreibt daher die Optimierung der Zellgewinnung und der Aufreinigungsmethode der [FeFe]-hydrogenase aus dem Ursprungsorganismus. Zusätzlich wurde zum ersten Mal ein Überexpressionssystem für dieses Enzym in *E.coli* entwickelt und etabliert. Dafür wurde ein Plasmid konstruiert, der neben den Codon-optimierten Gensequenzen des Enzyms auch einen Affinitätstag aufweist. Dies ermöglicht eine schnelle und effektive Aufreinigung des gewünschten Proteins. Durch diese Methode, können schnell, große Mengen an reinem, un-maturiertem Protein gewonnen werden.

Kapitel 4 beschreibt sowohl die Untersuchung des heterolog exprimierten, un-maturierten Enzyms mittels EPR Spektroskopie als auch seine Kristallisation. Es konnte gezeigt werden, dass eine künstliche Maturation dieses Proteins mit Hilfe eines synthetischen $[2Fe]_H$-Komplexes möglich ist und dieses, zu vollständig aktivem Enzym führt. Des Weiteren wird die Optimierung der Messtechniken sowohl für den Wasserstoffverbrauch als auch für die Wasserstoffproduktion beschrieben. Im Anschluss werden spektroskopische Untersuchungen (EPR und FTIR Spektroskopie) des vollständig maturierten Enzyms vorgestellt und mit dem nativen Enzym aus *D. desulfuricans* verglichen.

Um den Einfluss der zusätzlichen [Fe-S]-cluster im Elektronentransport des Proteins besser verstehen zu können, wurde die Methode der gezielten Mutagenese (site-directed mutagenesis) gewählt um so, die Redox-Potentiale der einzelnen Cluster gezielt zu verändern. Dies und die Maturation der so gewonnenen Mutanten mittels des synthetischen $[2Fe]_H$-Komplexes, sowie ihre Aktivitätsmessungen werden in Kapitel 5 beschrieben. Die un-maturierten Mutanten wurden ebenfalls EPR spektroskopisch untersucht und mit dem ursprünglich heterolog exprimierten Enzym vergleichen. Die native [FeFe]-Hydrogenase zeigt in elektrochemischen Experimenten (PFE) eine, noch nicht vollständig untersuchte, Inaktivierung bei hohen Potentialen (HPI). In Kapitel 6 werden daher Experimente vorgestellt, die dieses Phänomen weiter untersuchen. Es wird gezeigt, dass Chlorid präsent sein muss, um diesen Zustand zu erzeugen, während Wasserstoff hingegen nicht essentiell zu sein scheint. Des Weiteren wurden auch erste Untersuchungen an un-maturiertem und maturiertem, heterolog exprimierten Protein durchgeführt. Durch diese Methode ließen sich die Redox-Potentiale der einzelnen Cluster des un-maturierten Enzyms erstmals messen.

Abbreviations

[2Fe-2S]-cluster	2-iron-2-sulfur cluster
[3Fe-3S]-cluster	3-iron-3-sulfur cluster
[4Fe-4S]-cluster	4-iron-4-sulfur cluster
A. vinosum	*Allochromatium vinosum*
ADP	adenosine diphosphate
adt	azadithiolate cofactor
APS	adenosine 5’ phosphosulfate
ATP	adenosine triposphate
bp	base pair
BSA	bovine serum albumin
BV	benzylviologen
C. reinhardtii	*Chlamydomonas reinhardtii*
Cam	chloramphenicol
CHES	2-(Cyclohexylamino)ethanesulfonic acid
CpI	*Clostridium pasteurianum*
CT	carboxy terminal
CV	column volume
CvFd	clostridial type of ferredoxin
CW	continuous wave
Cyt	cytochrome
D. desulfuricans (DdH)	*Desulfovibrio desulfuricans*
D. vulgaris	*Desulfovibrio vulgaris*
DNA	deoxyribonucleic acid
DDAO	N,N-dimethyldodecylamine N-oxide
DMSO	dimethyl sulfoxide
DTT	dithiothreitol
E. coli	*Escherichia coli*
EDC	1-ethyl-3(3-dimethylaminopropyl)-carbodiimide
EDTA	ethylene diamine tetraacetic acid
EPR	electron paramagnetic resonance
eq	equivalent
et al.	et alii (and others)
FeAmCit	iron ammonium citrate

FNR	ferredoxin-NADP-reductase
FPLC	fast performance liquide chromatography
FTIR	Fourier Transformation Infrared spectroscoy
h	Planck constant
Hb	haemoglobin
HEPES	4-(2-hydroxyethyl)-1-piperazineethanesulfonic acid
HiPIP	high potential iron-sulfur protein
Hmc	cytochrome complex
Hmd-hydrogenase	H_2-forming methylenyltetrahydromethanopterin dehydrogenase
HOPGE	highly ordered pyrolytic graphite edge electrode
HPI	high potential inactivation
IEC	ion exchange chromatography
IPTG	isopropyl β-D-1-thiogalactopyranoside
isc	iron sulfur cluster
Kan	kanamycin
LDH	lactatedehydrogenase
LSU	large subunit
MALDI-TOF MS	matrix-assisted laser desorption/ionization- time of flight mass spectrometry
MES	2-(N-morpholino)ethanesulfonic acid
MOPS	3-(N-morpholino)propanesulfonic acid
mRNA	messenger ribonucleic acid
MV	methylviologen
MWCO	molecular-weight cutoff
NADP/H	nicotinamide adenine dinucleotide phosphate
NaDT	sodium dithionite
NBD	4-nitro-benzene-diazoniumsalt
Ndh	NAD(P)H-dehydrogenase
neg.	negative
NHS	N-hydroxysuccinimide
NMR	nuclear magnetic resonance
NT	amino terminal
o/n	over night
PAGE	polyacrylamide gel electrophoresis
PC	plastocyanine
PCR	polymerase chain reaction

PEG	polyethylene glycol
PES	polyethersulfone
PFE	protein film electrochemistry
PMSF	phenylmethylsulphonyl fluoride
PNK	polynucleotide 5'-hydroxyl-kinase
pos.	positive
PQ	plastoquinone
ps	post sonication
PS I / II	photosystem I /II
pss	post sonication supernatant
rpm	rounds per minute
RT	room temperature
SAM	S-adenosylmethionine
SCE	standard calomel electrode
SDS	sodium dodecyl sulphate
SEC	size exclusion chromatography
SEIRA	surface enhanced infrared absorption spectroscopy
SHE	standard hydrogen electrode
SRB	sulfate reducing bacteria
SSU	small subunit
TAPS	N-Tris(hydroxymethyl)methyl-3-aminopropanesulfonic acid
TEV	Tobacco etch virus
TOF [s^{-1}]	turn over frequency (µmol H_2 s^{-1} $µmol^{-1}$ hydrogenase)
Tris	tris(hydroxymethyl)aminomethane
TvH	*Trichomonas vaginalis*
UV/vis	ultraviolet/visible

A list of amino acids in their one and three letter code is given in the appendix.

Contents

Chapter 1 Introduction

"A fundamental and principal difficulty of the energy industry is that the rate of formation of fossil fuels is much slower than the rate of their exploitation."[1] In principle this sentence is the summary of the energy problem which needs to be solved. This thesis will show how a group of small enzymes, the hydrogenases, could help to solve some aspects of this energy problem.

1.1 Hydrogenases

1.1.1 *Classification and general introduction*

The hydrogenase enzymes belong to the metalloenzyme family and they catalyse the simplest chemical reaction of all; the reversible reduction of two protons and two electrons to molecular hydrogen.

$$H_2 \rightleftharpoons H^- + H^+ \rightleftharpoons 2\,H^+ + 2\,e^-$$

In vivo, hydrogenases are biased to catalyse this reaction in one direction and, according to this, they can be grouped into H_2-uptake (H_2 oxidation) or H_2-production hydrogenases. Hydrogenases are found mainly in prokaryotes, where they were first discovered,[2] but there are also some eukaryotes known, where a hydrogenase is located in special cell compartments like chloroplasts or hydrogenosomes.[3] Due to their functions they are located either in the periplasm or cytoplasm of gram negative bacterial cells and they can exist as membrane bound or soluble proteins (based on the electron donors or acceptors they interact with).[3,4] Hydrogenases are part of the metabolism of the cells where the oxidation of hydrogen is used as an energy source. This is typical for anaerobic bacteria, due to the relative low reduction potential of hydrogen (-413 mV E°' at pH 7.0) it can reduce energy converting electron donors like sulfate, fumarate or iron.[5] In the green alga *Chlamydomonas reinhardtii*, hydrogenase is coupled to the photosynthetic electron transport chain.[6] During photosynthesis a very negative redox

potential accumulates and, under certain conditions, the formation of hydrogen can be used to get rid of the electron excess (i.e. protons can act as a terminal electron acceptor).

Hydrogenases belong to the enzymatic group of oxidoreductases[7] and can be further characterized by their redox partner protein, for most [FeFe]-hydrogenases this is an iron-sulfur protein; a ferredoxin. In general ferredoxin linked hydrogenases probably function as hydrogen producers. This is because ferredoxins normally have a quite negative potential and are in turn coupled to reactions that yield electrons. The [NiFe]-hydrogenases are normally coupled to cytochromes or quinones, both of which have quite positive potentials and normally exchange electrons with more oxidizing acceptors. The purpose of this is to conserve as much energy as possible. Because *D. desulfuricans* operates as a hydrogen user it probably donates electrons to an acceptor with a high potential hence cytochromes, but obviously the acceptor could also be a ferredoxin with a high potential. But for the [FeFe]-hydrogenase from *Desulfovibrio desulfuricans* it is not absolute clear if the electron acceptor is also a ferredoxin or a cytochrome. The more commonly used classification of hydrogenases is based on the metal-ions in their active site. They can be divided into three classes[8-10]: [FeFe]-hydrogenases, [NiFe]-hydrogenases and [Fe] or Hmd-hydrogenases. The hydrogenase on which this thesis is based is an [FeFe]-hydrogenase. This hydrogenase type is introduced in detail in Section 1.1.2. The biological hydrogen metabolism seems to go back to the early earth age, when the atmosphere was hydrogen-rich.[11] It is reasonable to think that hydrogenases probably came into existence during these early periods on our planet.[3] However, even today's organisms are able to use molecular hydrogen as energy source in certain environments as mentioned above.

[Fe] or Hmd-hydrogenases form the class of hydrogenases with the smallest number of members. These enzymes are found in some methanogenic archaea like *Methanocaldococcus* jannaschii[12] or *Methanothermobacter marburgensis*[13]. They house no [Fe-S]-clusters and no nickel, so they were called metal free hydrogenases for a long time, but a single iron atom was found in their active centre, which is necessary for their activity.[14,15]

The renamed Hmd-hydrogenases ($\underline{H_2}$-forming methylenyltetrahydromethanopterin-dehydrogenase[16]) function very differently from [NiFe]- or [FeFe]-hydrogenases: they catalyse a step in carbon reduction by hydrogen to produce methane.

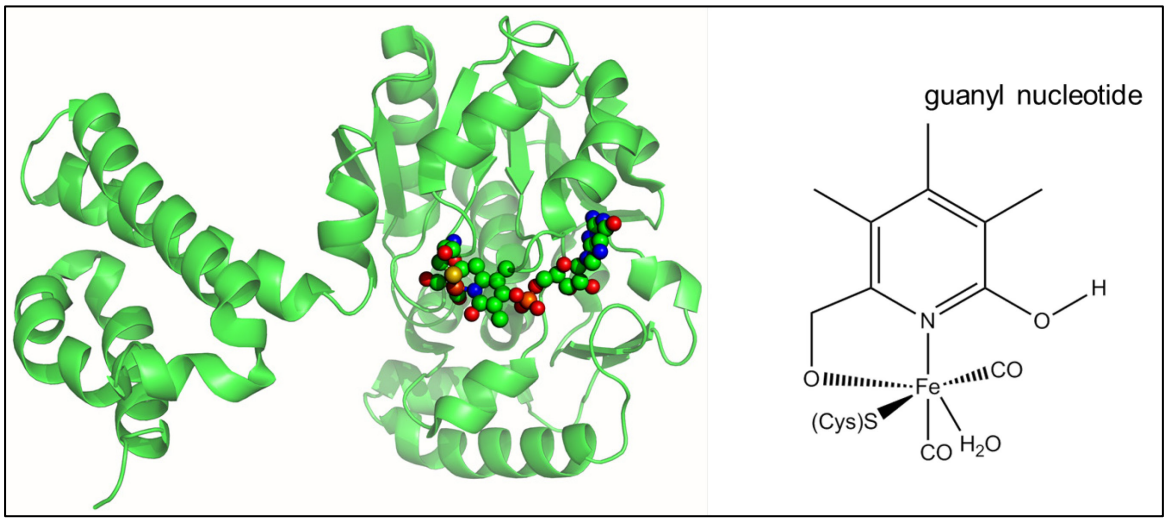

Figure 1-1 Protein structure of Hmd-hydrogenase from *Methanocaldococcus jannaschii* (3F47) with the highlighted active site on the left side and a closer view of the active site on the right. The program pymol[17] was used to create this figure. The protein backbone is shown in cartoon representation and in green. The active site is shown in balls and sticks and coloured by element.

The largest group of hydrogenases is formed by the [NiFe]-hydrogenases which are enzymes with a binuclear [NiFe]-cluster in their active site. The simplest [NiFe]-hydrogenases are heterodimeric enzymes with a binuclear [NiFe]-cluster in their active site, which is located in the large subunit. So far [NiFe]-hydrogenases are only found in prokaryotes.[18] The binuclear centre is bound via four cysteines to the protein. The iron binds two cyanide- and one carbonmonoxide-ligands.[19,20] A subgroup of [NiFe]-hydrogenases are the [NiFeSe]-hydrogenases, in these enzymes one of the cysteine residues coordinated to the nickel is replaced by a selenocysteine (SeCys).[21] In addition to the active site [NiFe]-hydrogenase houses three [Fe-S]-clusters for electron transfer in their small subunit. Standard [NiFe]-hydrogenases contain two [4Fe-4S]-clusters and one [3Fe-4S]-cluster. In contrast to this, in [NiFeSe]-hydrogenases all three clusters are [4Fe-4S]-clusters. Normally the [NiFeSe]-hydrogenases show higher rates in hydrogen production. For example the [NiFe]-hydrogenase from *Desulfovibrio vulgaris Hildenborough* gives rates of 169 s^{-1} while the [NiFeSe]-hydrogenase from the same organism shows 6867 s^{-1}.[22,23]

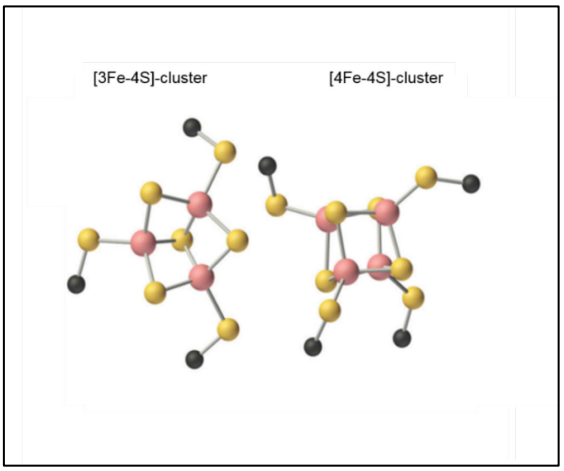

Figure 1-2 Scheme of two types of [Fe-S]-clusters, a [3Fe-4S]-cluster on the left and a [4Fe-4S]-cluster on the right. Both are typically found in standard [NiFe]-hydrogenases.

In comparison to [FeFe]-hydrogenases the [NiFe]-hydrogenases show a higher tolerance to oxygen damage and inhibition by CO.[24,25] A special group of the [NiFe]-hydrogenases is known, which is completely oxygen tolerant. These enzymes contain two additional cysteine residues that coordinate the proximal iron-sulfur cluster. The presence of an unusual [4Fe-3S]-cluster with a six cysteine coordination seems to be responsible for the oxygen tolerance of this class of enzymes.

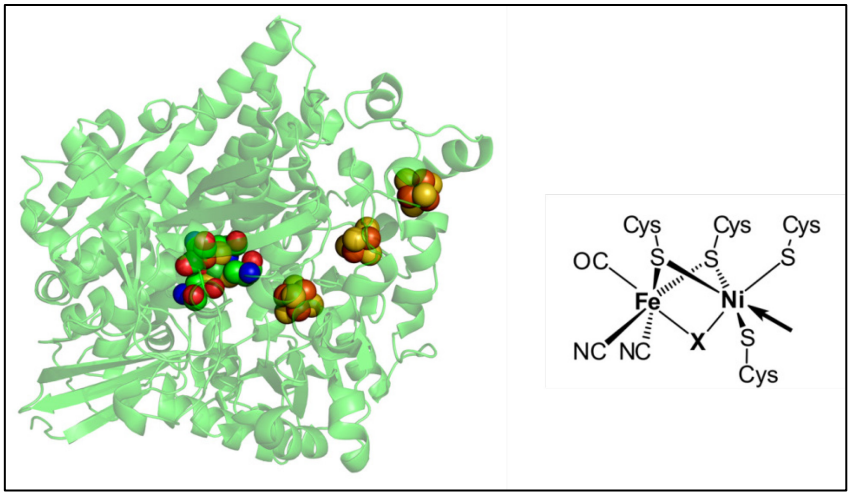

Figure 1-3 Protein structure of [NiFe]-hydrogenase from *Desulfovibrio vulgaris Miyazaki F* (1WUJ) with the highlighted active site and [Fe-S]-cluster on the left side and a closer view of the active site on the right. The free binding site is indicated with an arrow. The program pymol[17] was used to create this figure. The protein backbone is shown in cartoon representation and in green. The active site is shown in balls and sticks and coloured by element.

The third class of hydrogenases, and the topic of this thesis, are the [FeFe]-hydrogenases. They are mostly hydrogen production enzymes and contain a special type of iron-sulfur cluster, the so called H-cluster, which consists of an unusual $[2Fe]_H$ sub-cluster linked to a [4Fe-4S]-cluster (Figures 1-5, 1-6).[26] The sub-cluster contains two cyanide- and three carbonmonoxide-ligands, one of which is in a bridging position, and a bridging dithiolate ligand, an azapropanedithiolate (adt). A cysteine residue links the so-called proximal iron (Fe_p) of the sub-cluster to the [4Fe-4S]-cluster, while the binding site for hydrogen is located at the so-called distal iron (Fe_d). In addition to the H-cluster [FeFe]-hydrogenases from many species harbour additional [Fe-S]-clusters (F-clusters) of different types and numbers. [FeFe]-hydrogenases are highly sensitive to oxygen damage and to inhibition by CO. This type of hydrogenase shows in general higher activity for hydrogen production and consumption in comparison to [NiFe]-hydrogenases, this make them an interesting target for new approaches like electrocatalysts in electrochemical cells or as models for artificial hydrogen production. However, a major disadvantage of these enzymes is their extreme oxygen sensitivity.

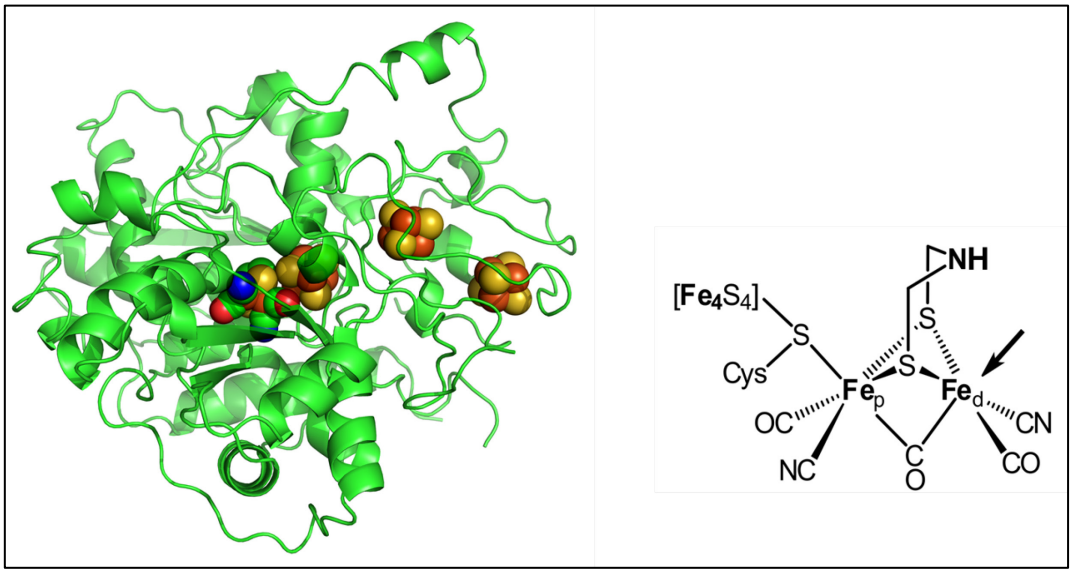

Figure 1-4 Protein structure of [FeFe]-hydrogenase from Desulfovibrio desulfuricans (1HFE) with the highlighted active site and [Fe-S]-cluster on the left side and a closer view of the active site on the right. The free binding site is indicated with an arrow. The program pymol[17] was used to create this figure. The protein backbone is shown in cartoon representation and in green. The active site is shown in balls and sticks and coloured by element.

Figure 1-5 shows both types of bimetallic hydrogenases in direct comparison. Despite the fact that these two classes of enzyme have independent evolutionary origins, the active sites of [NiFe]- and [FeFe]- hydrogenases actually have several common features: coordination of diatomic ligands to an Fe ion, a vacant coordination site that represents a substrate binding site, a thiolate-bridged binuclear centre and plausible proton- and electron-transfer pathways and substrate channels.[27] Normally one iron is strongly affected by the surrounded ligands (CO and CN), which causes the low spin state of the iron (through the Jahn Teller effect). The cyanides are strong σ-donor ligands and can form hydrogen bonds to the surrounding amino acids of the active site, while CO ligands form only very weak hydrogen bonds or no hydrogen bond at all. In [NiFe]-hydrogenases, the four sulfurs from the cysteine residues are coordinated to the nickel ion, two of them are bridging to the iron and the other two are bound to the nickel in a terminal fashion. The low spin iron shows an octahedral coordination with the three ligands and the two bridging thiolates.

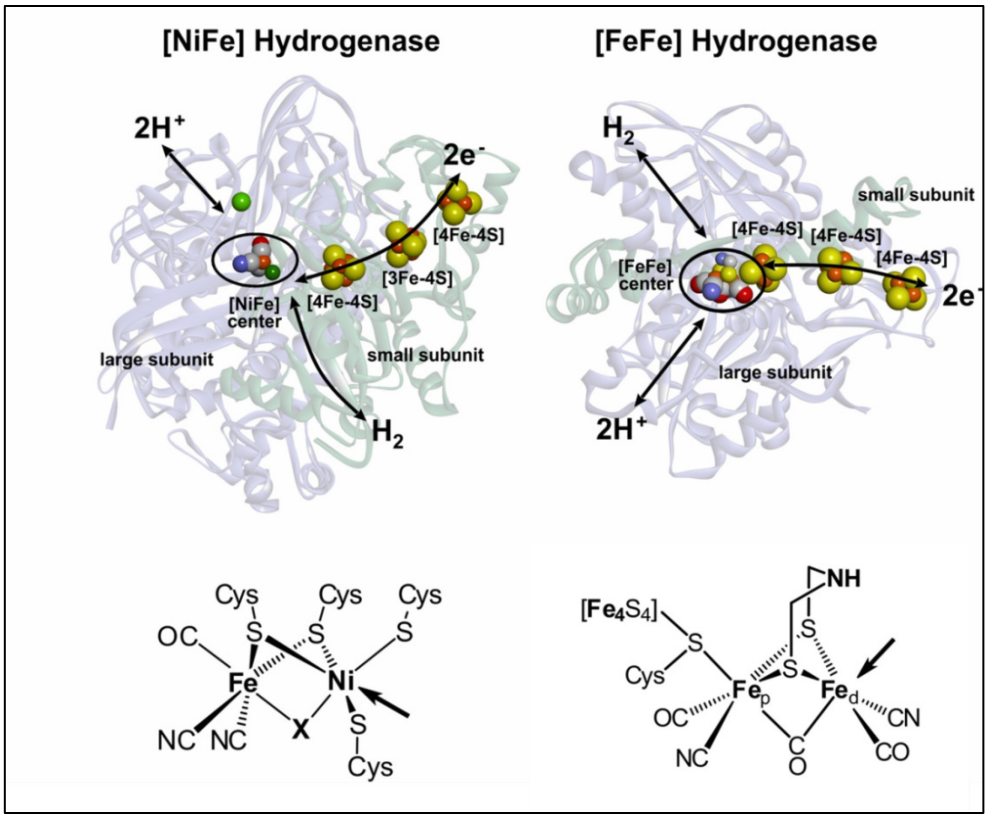

Figure 1-5 Direct comparison between [NiFe]-hydrogenase (left) and [FeFe]-hydrogenase (right) with their active sites and [Fe-S]-clusters. The possible electron transport chain is illustrated, as well as the hydrogen and proton channels.

1.1.2 *[FeFe]-hydrogenase of Desulfovibrio desulfuricans*

As mentioned above, most of the [FeFe]-hydrogenases are mostly biased towards hydrogen production. An exception is the periplasmic [FeFe]-hydrogenase from *Desulfovibrio desulfuricans*, which is a hydrogen uptake hydrogenase and oxidizes hydrogen under physiological conditions.[3,28]

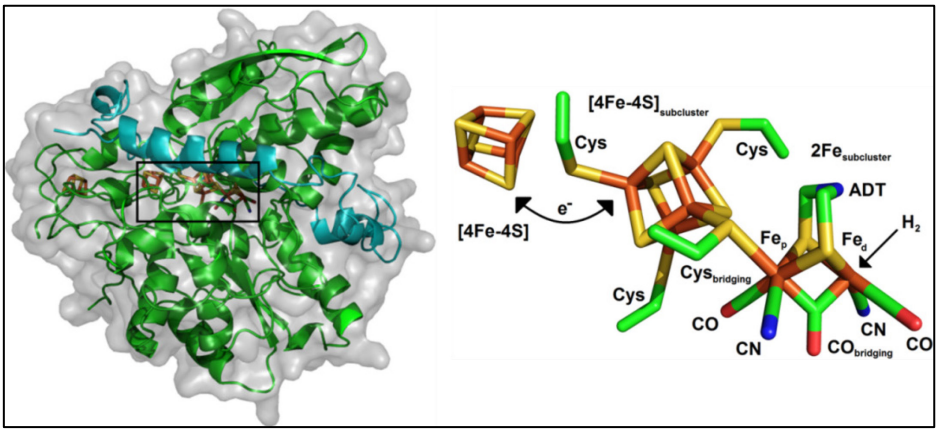

Figure 1-6 Structure of the [FeFe]-hydrogenase from *Desulfovibrio desulfuricans* on the left (PDB: 1HFE). The large and the small subunit are highlighted in green and cyan. The [Fe-S]-cluster and the $[2Fe]_H$-cluster are represented as sticks. On the right site a closer look of the H-cluster and the proximal [4Fe-4S]-cluster is given. ADT = azapropanedithiolate.

The heterodimer consists of a large subunit (*hyd*A) with a mass of 46 kDa and a small subunit (*hyd*B) with a mass of 13.5 kDa. The large subunit harbours the active site (H-cluster) and two additional [4Fe-4S]-clusters while the small subunit, which consists of four α-helices, surrounds the large subunit like a belt, and has most likely a stabilizing function (see Figure 1-6). A simultaneous transcription of both subunits is postulated followed by translation from a polycistronic mRNA, because both the *hyd*A and *hyd*B genes exist in a single operon with two open reading frames. The gene sequence of the enzyme has been known since 1999.[29] Both subunits contain signal peptides that allow the targeting into the periplasm. The small subunit contains a 34 amino acid long sequence at the amino terminus and the large subunit has a 24 amino acid sequence at the carboxy terminus, both of which are removed by peptidases during translocation.[30] This leads to a protein mass of 42 kDa for the large subunit and 11 kDa for the small subunit. The region around the H-cluster is highly conserved in the whole enzyme class and includes about 350 amino acids.[29,31]

Electron transfer chain

Soluble periplasmic hydrogenases are hydrogen oxidizing enzymes. The heterolytic cleavage of hydrogen at the H-cluster produces electrons which can then be transferred via the [Fe-S]-clusters to the surface and to the electron acceptor.[32,33] The nature of the electron acceptor is still not established but, is suggested to be either a ferredoxin or a cytochrome. The distance between the [Fe-S]-clusters is approximately 11Å which is sufficient for electron transfer. A theoretical study has suggested, that the electron transport can activate one of the water channels which supplies protons to the active site.[34] The accessory [Fe-S]-clusters are two [4Fe-4S] bacterial ferredoxin-like domains, which were identified in the sequence by an arrangement of eight cysteine residues.

Proton transfer

In hydrogenases, protons are transferred to the active site through a network of hydrogen bonds. It is not determined if a proton tunnelling mechanism, which is found in other enzymes[35], also plays a role in hydrogenases. For *Desulfovibrio desulfuricans* two possible pathways were proposed from the crystal structure. The first pathway starts at the cyanide ligand of the distal iron and involves two conserved residues (Lys237 and Glu240). Glu240 is connected via three water molecules to the non-conserved Glu245 at the protein surface.[30] The problem of this pathway is that the proton from heterolytic cleavage needs to bind to the cyanide ligand of the distal iron. It is more likely, that an alternative pathway, where this proton binds to a neighbouring water molecule at the distal iron and is then transferred to Cys178 and an additional water molecule, is used.[36] In this pathway the bridgehead atom, which is proposed to be a nitrogen, could be involved in the heterolytic cleavage of molecular hydrogen. The secondary amine of this bridgehead can be protonated on the distal iron side, and then transferred to Cys178 via a Walden inversion.

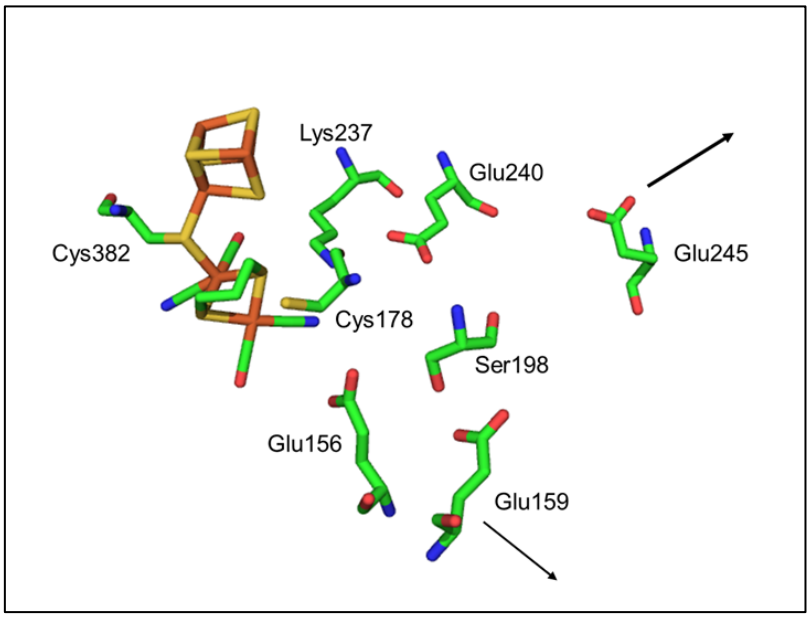

Figure 1-7 Putative proton transfer pathway in [FeFe]-hydrogenase from *Desulfovibrio desulfuricans*. Both possible proton pathways are indicated with an arrow. Figure adapted from[8] and generated with pymol[17].

Gas Access channels

The H-cluster is positioned in the centre of the protein; therefore the substrate (H_2) or inhibitors (O_2 and CO) need to have access from the protein surface to reach the active site via hydrophobic gas channels. According to the crystal structure, the gas channel of [FeFe]-hydrogenases is much shorter than that found in [NiFe]-hydrogenases. This could be one of the reasons why [FeFe]-hydrogenases show higher turnover numbers.[21] Two possible hydrophobic gas access channels have been postulated based on the crystal structure, the so called channels A and B. Both channels meet at a large central cavity next to the active site.[8] Both possible pathways are shown in the following Figure 1-8.

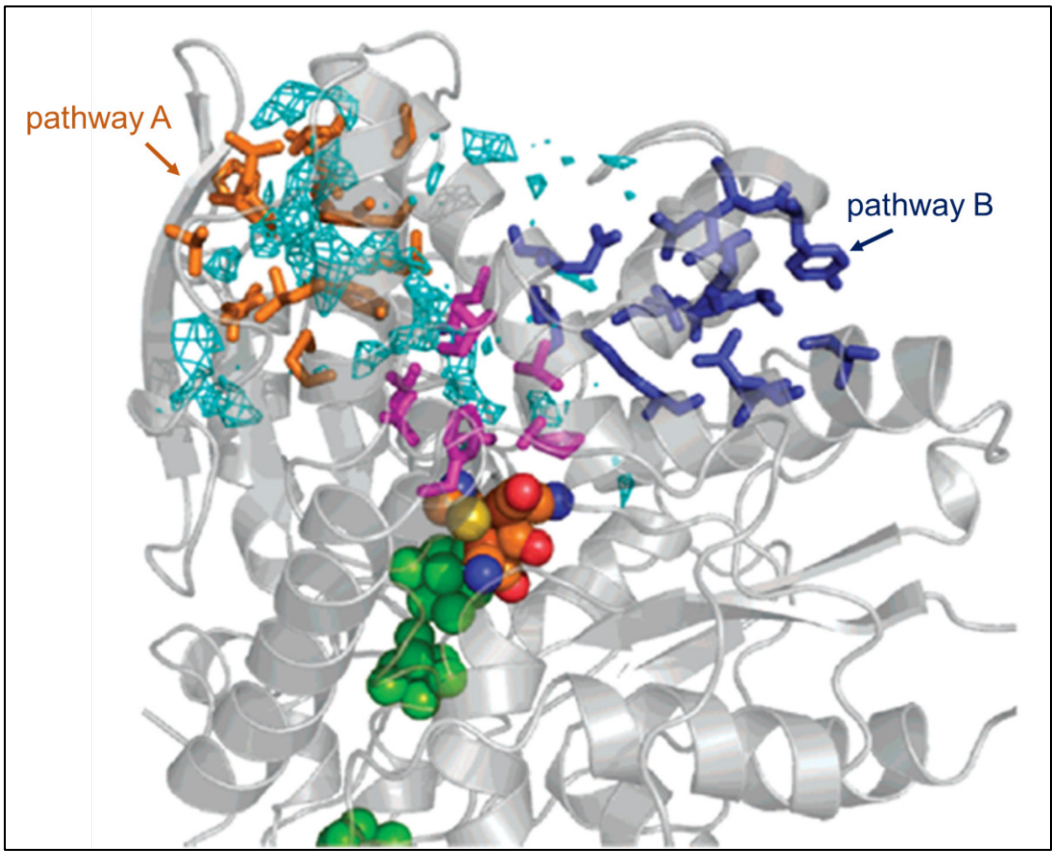

Figure 1-8 Overview of the hydrophobic gas access channels in *Desulfovibrio desulfuricans*. The gas access channel is highlighted in cyan. Pathway A is given in orange and pathway B in blue. The conserved cavity, where both channels meet, next to the active site (coloured spheres), is marked in magenta. The additional [Fe-S]-clusters are given in green spheres.[8]

1.1.3 *Reaction pathway of [FeFe]-hydrogenase from Desulfovibrio desulfuricans*

During the catalytic cycle the hydrogenase passes through different redox states[18] which are presented in the following Figure 1-9.

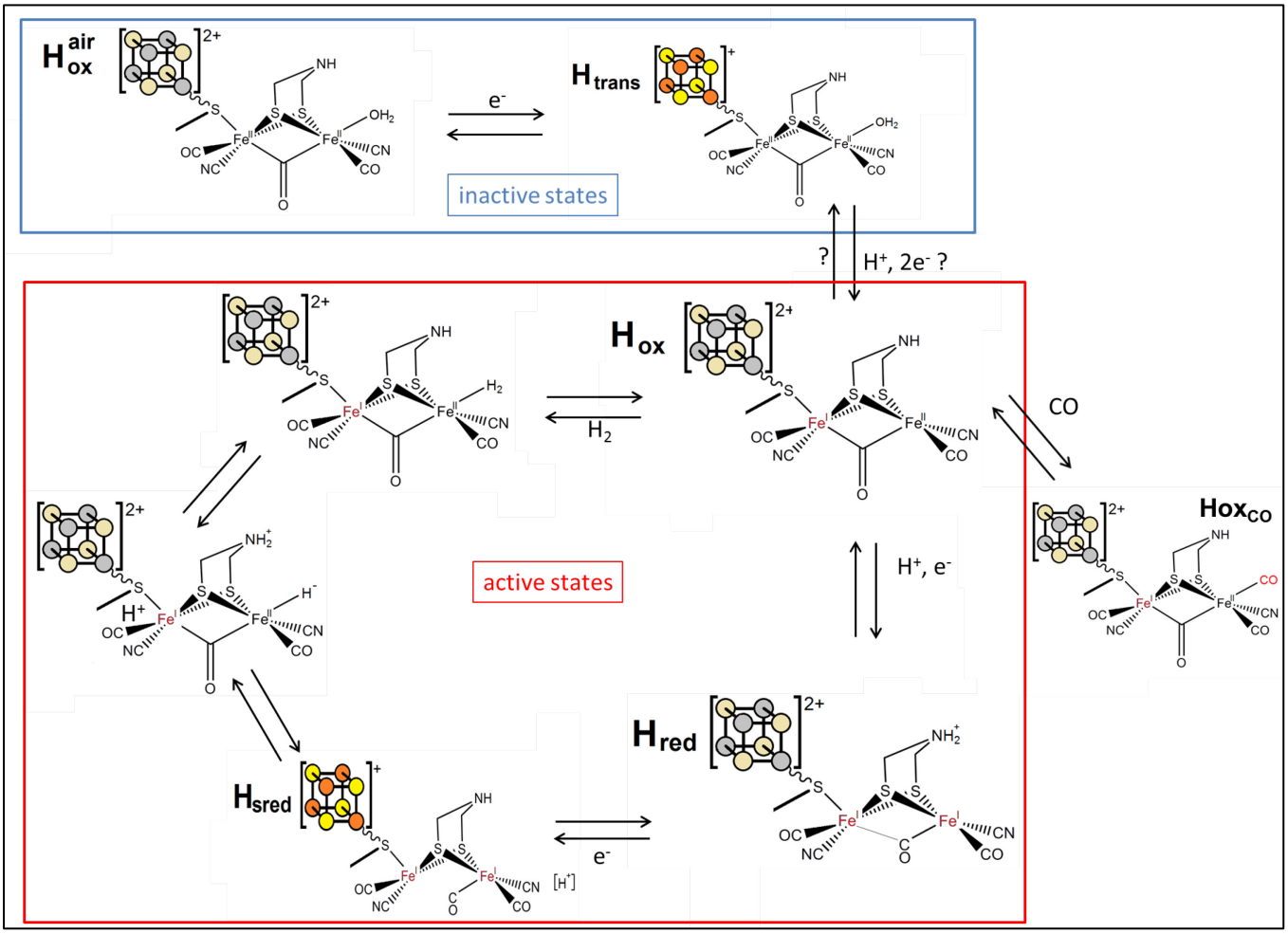

Figure 1-9 Scheme of the reaction cycle of [FeFe]-hydrogenases. The states in the blue box are the inactive states and the one in the red box the active states. The state which is not included in one of the boxes is the CO-inhibited state. The figure is modified from[26,26,37,37].

Most of the [FeFe]-hydrogenases need to be purified under anaerobic conditions in order to preserve the H-cluster. Under these conditions the purified enzyme is a mixture of the H_{ox}, H_{red} and in some species the H_{sred} state, in all these states the enzyme is fully active. A special property of the [FeFe]-hydrogenase from *Desulfovibrio desulfuricans* is the possibility to purify the enzyme under aerobic conditions which leads to an inactive,

EPR- (electron paramagnetic resonance) silent state, the **H_{ox}^{air} state**. In this state the two irons of the sub-cluster are in the 2+ state and also the [4Fe-4S]-cluster is in its 2+ state. It is, remarkable that this hydrogenase can be purified under aerobic conditions. However, when the enzyme is activated (by reduction) it becomes extremely sensitive to oxygen damage. The mechanism by which the H_{ox}^{air} state is formed and whether it can be reformed from the purified enzyme is not known.

Recent evidence has suggested that in general oxygen damage is initiated at the $[2Fe]_H$ sub-cluster of the active site but the mechanism by which this occurs is still unclear.[38] This could be shown for the [FeFe]-hydrogenase from *Chlamydomonas* reinhardtii by X-ray absorption spectroscopy, for *Desulfovibrio desulfuricans* it is not clear where exactly the damage takes place. For [NiFe]-hydrogenases it is known, that purified under aerobic conditions, the enzyme forms a stable intermediate with an oxygen bond (NiA and NiB state). Electrochemical studies showed that the hydrogenase from *Desulfovibrio desulfuricans* undergoes reversible inactivation at high potentials anaerobically[39], this is possibly an unrelated phenomenon. This will be discussed in more detail in Chapter 6 of this thesis.

Reduction of the H_{ox}^{air} state with hydrogen or other reductants yields the **transition state (H_{trans})**. The reduction potential of this process is -75 mV. This state displays a rhombic EPR signal that is proposed to be due to reduction of the [4Fe-4S]-sub-cluster of the H-cluster.[40,41] That means that the $[2Fe]_H$ sub-cluster is still oxidized while the [4Fe-4S]-cluster is reduced by one electron to a 1+ net charge.

An additional two electron reduction yields the **H_{ox}-state**. In this state the reduction-equivalent is transferred from the [4Fe-4S]-sub-cluster of the H-cluster to the $[2Fe]_H$-cluster which has a charge of 1+ for Fe_d and 2+ for Fe_p. This transition occurs at a potential of E_m = -261 mV. Due to its paramagnetic properties this state can be observed in EPR spectroscopy. The reversal of this reductive activation process, that of oxidative inactivation, has only been achieved under very specific conditions.[42]

The **H_{red}-state** can be formed from the H_{ox}-state in two ways. One way is the reduction with electrons from electron donors via the F-clusters or the second way is by oxidation of hydrogen. Heterolytic cleavage of hydrogen first yields a state in which the distal iron has a bound hydride and the bridgehead nitrogen is protonated. Next, the hydride is oxidized to a proton via reduction of the distal iron to Fe(I) and electron transfer to the [4Fe-4S]-cluster, generating the **H_{sred}** state. Probably in *Desulfovibrio desulfuricans* the [4Fe-4S]-cluster is immediately oxidized by the F-clusters, leaving the diamagnetic, EPR

silent, H_{red} state. The second electron from the $[2Fe]_H$ sub-cluster is then transferred to the F-clusters, via the $[4Fe]_H$ of the H-cluster. The potential of the transition from H_{ox} to H_{red} in *Desulfovibrio desulfuricans* [FeFe]-hydrogenase is E_m = -350 mV.

1.1.4 *Maturation of [FeFe]-hydrogenases*

The maturation of [FeFe]-hydrogenases is not very well understood but highly interesting due to the biologically unusual ligands of the $[2Fe]_H$ sub-cluster CO and CN and the unique dithiolate cofactor. Following protein synthesis, the [4Fe-4S] clusters are inserted into the apo-protein by the isc (iron-sulfur-cluster) machinery, and afterwards the H-cluster is incorporated.[43] The H-cluster binding domain is highly conserved and can be identified in the primary sequence by three binding motifs; L1 (TSCCPXW), L2 (MPCXXKXXE) and L3 (EXMACXXGCXXGGGXP).[44] These binding domains are typically located at the N-terminus of the H-cluster binding domain.[41,44]

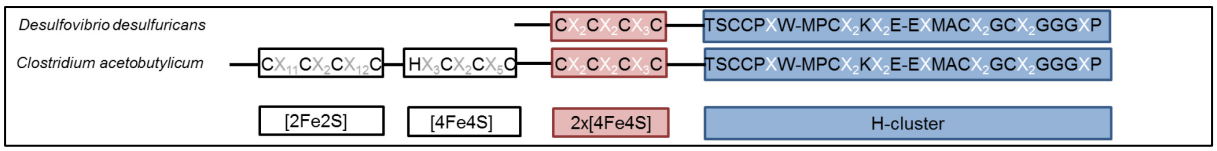

Figure 1-10 Alignment of the [Fe-S]-cluster binding motifs in [FeFe]-hydrogenases.

Iron-sulfur cluster synthesis and insertion is carried out in the isc pathway. In the living cell the proteins HydE, HydF and HydG are necessary for this.[45] HydE and HydG show CX_3CX_2C binding motifs which are characteristic for radical S-adenosylmethionine (SAM) enzymes. HydF in contrast has an N-terminal GTPase domain and a C-terminal domain with conserved cysteine and histidine residues.[43] One possible pathway is described by Peters et al.[46] who proposed that HydE and/or HydG are responsible for the synthesis of the bridging dithiolate in the first step of the chemical modification of a [2Fe]-cluster. Subsequent generation of a glycyl radical by HydE and/or HydG and the reaction of this radical with an Fe(I)-thiolate site resulted in exothermic decomposition, which generates a CO, CN and a H_2O-coordinated Fe(I)-centre.[46] HydF is suggested to function as a scaffold-protein which transports the cluster from HydG to the unmaturated [FeFe]-hydrogenase.

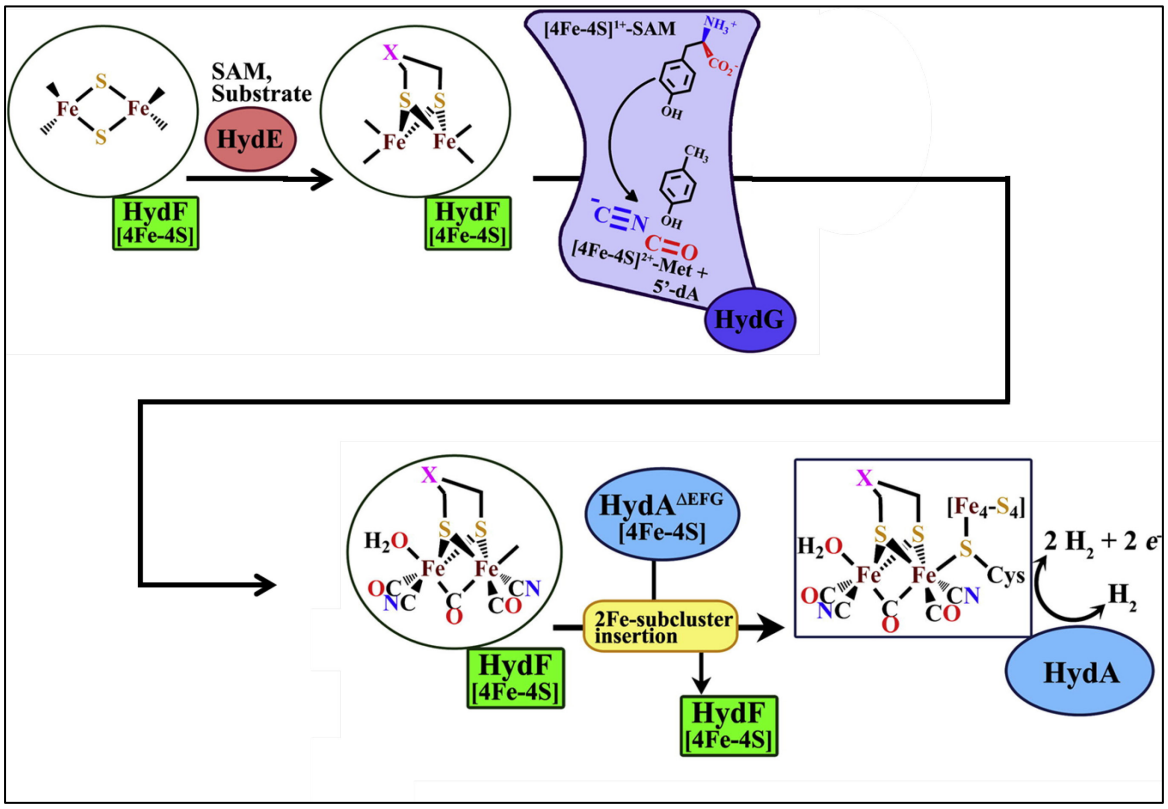

Figure 1-11 Scheme for maturation of [FeFe]-hydrogenases by the enzymes HydE, HydF and HydG. Figure from[43].

More details about the *in vivo* maturation are given in Chapter 4 of this thesis.

1.2 The genus *Desulfovibrio desulfuricans*

1.2.1 *Systematic and biological properties*

Desulfovibrio desulfuricans is a gram-negative, sulfate-reducing eubacterium. It belongs to the group-I-sulfate reducing bacteria (SRB), which are characterized by their sulfate metabolism. Type I bacteria oxidize substrates like pyruvate or lactate only to CO_2.

Table 1-1 Phylogenetic table of *Desulfovibrio desulfuricans*.

superkingdom	bacteria
phylum	proteobacteria
class	deltaproteobacteria
order	desulfovibrionales
family	desulfovibrionaceae
genus	desulfovibrio
species	desulfovibrio desulfuricans

In 1895 W.M. Beyernick was the first to report the isolation of *Desulfovibrio desulfuricans* from a city canal in the Netherlands,[47] initially being named *Spirillum desulfuricans*. The bacterial cells have a vibroid form with polar, single flagellum. *Desulfovibrio desulfuricans* houses at least two types of hydrogenases, one cytoplasmic [NiFe]-hydrogenase and one periplasmic [FeFe]-hydrogenase. Genome sequence analysis shows the potential existence of an additional [NiFeSe]-hydrogenase. It is worth mentioning, that, when growing chemolithotrophically, *Desulfovibrio desulfuricans* catalyses hydrogen uptake though the periplasmic hydrogenase.[47]

Desulfovibrio desulfuricans is found in the upper anaerobic sediment layer of stagnant water but it can tolerate oxygen concentrations near the atmospheric level.[48] The organism is part of a natural redox-cycle, shown in Figure 1-12.

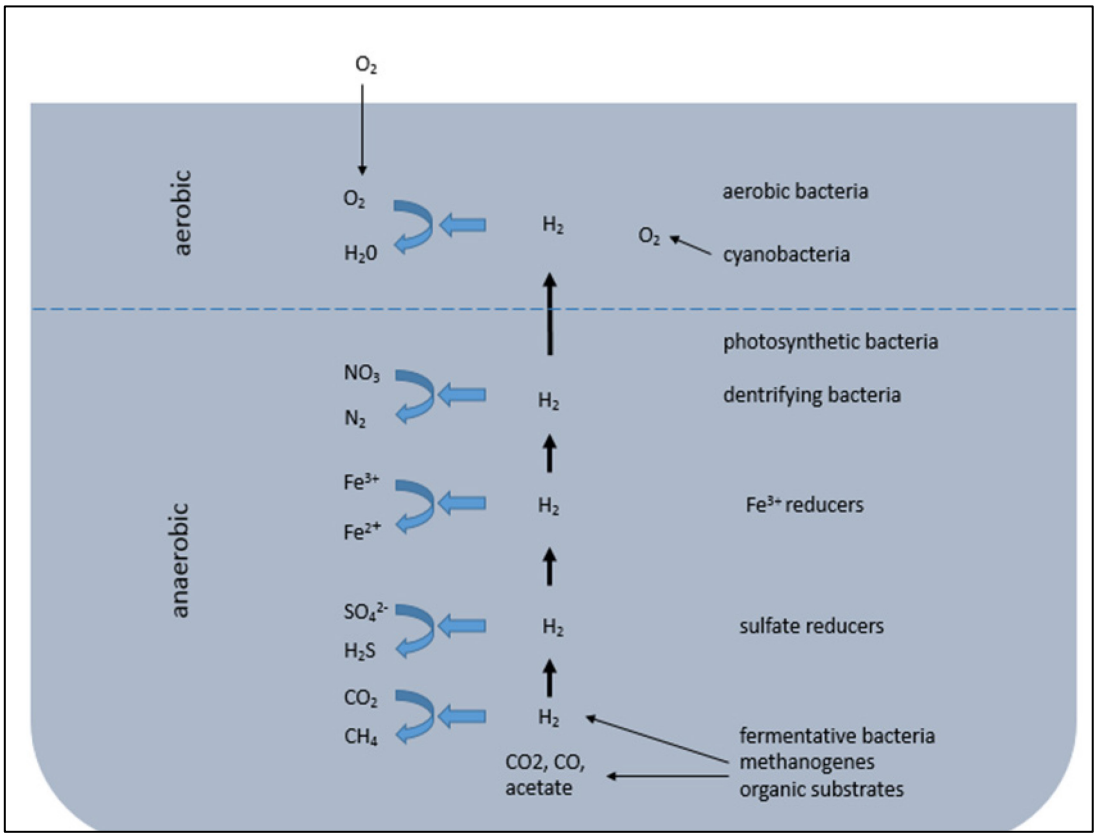

Figure 1-12 Schematic outline of the vertical distribution of different redox reactions catalysed by microorganisms capable of production or consuming hydrogen. At the bottom of stagnant water the redox potential is more negative and increases in upper direction. At the surface, in contact with air, it becomes positive. Modified from[1,49]

Currently, *Desulfovibrio desulfuricans* is just of secondary importance for humans. The metabolic product H_2S causes corrosion at hulls of ships and other submarine metal parts. This biological iron oxidation can lead to large problems. The exact mechanism of this process is not fully understood. It is postulated, that the bacteria consume a hydrogen film, which adheres to iron surfaces due to autoprotolysis of water. In this reaction the iron is oxidized to Fe^{2+} while the sulfate is reduced to sulfide. Both species form FeS which can react as a cathode of a galvanic cell.

The overall reaction can be formulated as follows:

$$4\ Fe + 2\ H_2O + Na_2SO_4 + 2\ H_2CO_3 \rightarrow 3\ Fe(OH)_2 + FeS + 2\ NaHCO_3$$

This process can be seen on a much larger scale in the Black Sea. Here *Desulfovibrio desulfuricans* produces large amounts of H_2S which reacts with iron to form black iron sulphide precipitates, from which the sea derives its name.

1.2.2 *Metabolism: electron donors and acceptors*

An overview of the *Desulfovibrio desulfuricans* metabolism is presented in Figure 1-13, with further details in the text below. Hydrogenases are responsible for forming a proton gradient between the cytoplasm and the periplasm to store energy. The cytoplasmic [NiFe]-hydrogenase normally generates hydrogen using electrons from substrate oxidation. After diffusion to the periplasm, the hydrogen is consumed by the [FeFe]-hydrogenase forming a proton gradient. The electrons, at more oxidizing potential, are used for sulfate reduction.

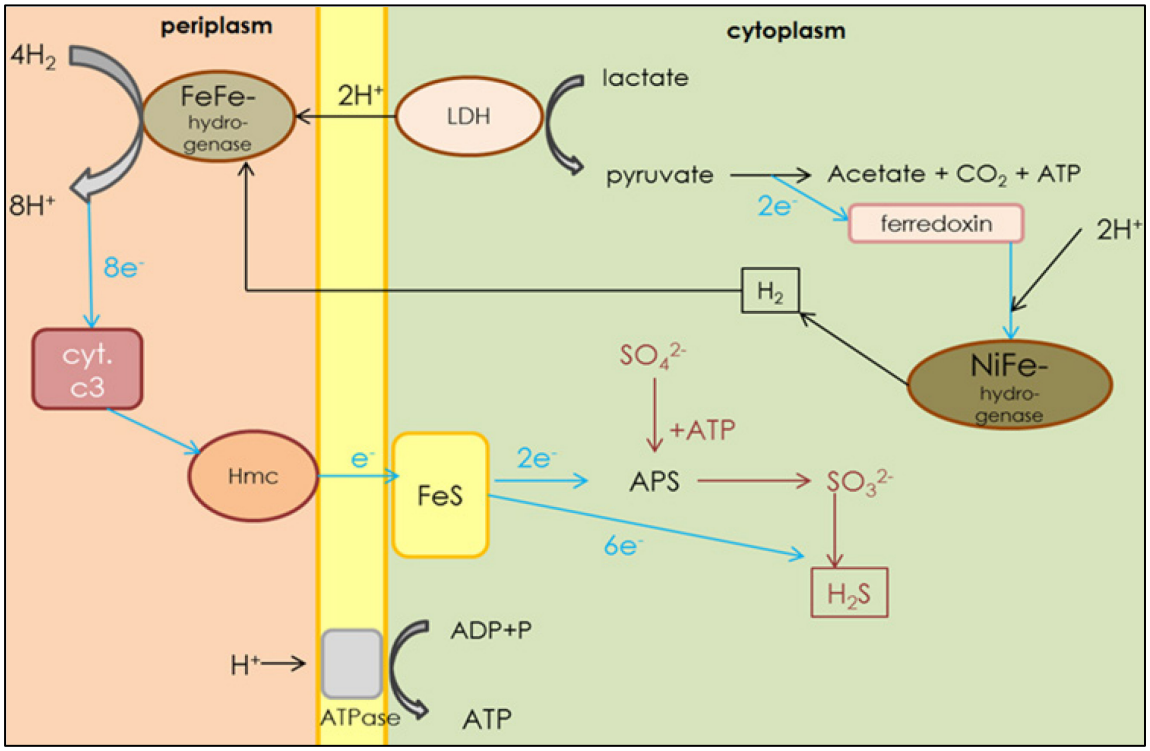

Figure 1-13 Basic overview of *Desulfovibrio desulfuricans metabolism.* NiFe: [NiFe]-hydrogenase, FeFe: [FeFe]-hydrogenase, Hmc: cytochrome complex, cyt. c3: cytochrome c3, FeS: iron sulfur protein, LDH: lactatedehydrogenase.

For the *Desulfovibrio* organism around 100 different substrates including hydrogen, fumarate, pyruvate, lactate and metallic iron are known.[50] *Desulfovibrio desulfuricans* consumes mainly malate or lactate. An important metabolism of these species is the dissimilative reduction of sulfate which is an electron acceptor of these species. The sulfate is reduced to sulfide by several reactions with adenosine-5'-phosphosulfate (APS) and sulfite as intermediates. The following reaction is catalysed by four cytoplasmic enzymes: ATP sulfurylase, APS reductase, sulfite reductase and pyrophosphatase.[47,51]

$$SO_4^{2-} + ATP + 8\ H^+_{in} + 8e^- \rightleftharpoons HS^- + AMP + 2\ P_i$$

From this reaction it is clear that the reduction of sulfate requires an investment of two high energy phosphate bonds. This investment can be balanced by a proton-driven and/or substrate-level phosphorylation of ADP to ATP. The electrons for sulfate reduction come from hydrogen oxidation in the periplasm. This hydrogen oxidation reaction is catalysed by the [FeFe]-hydrogenase by the following reaction:

$$4\ H_2 \longrightarrow 8H^+_{out} + 8\ e^-$$

Both reactions can be combined to the following reaction:

$$4\ H_2 + SO_4^{2-} + ATP + 8\ H^+_{in} \longrightarrow HS^- + AMP + 2\ P_i + 8\ H^+_{out}$$

The proton gradient results from the compartmentalisation hydrogen production and consumption. Protons are consumed in the cytoplasm and released in the periplasm. The mechanism of sulfate reduction is not fully understood, but it is postulated, that a two electron reduction reduces the sulfite to $S_3O_6^{2-}$ which is then reduced to $S_2O_3^{2-}$.

Finally, a thiosulfatereductase catalyses a disproportion to SO_3^{2-} and H_2S. To summarize these steps the following reaction can be formulated:

$$4\ H_2 + SO_4^{2-} + H^+ \longrightarrow HS^- + 4\ H_2O$$

It is obvious that the hydrogen and sulfate metabolism are strongly coupled in *Desulfovibrio desulfuricans*. The hydrogen metabolism functioned as a kind of valve for redox equivalents. On one hand protons and electrons can be used for ATP generation and on the other hand an electron or proton excess can be removed during the reaction to molecular hydrogen, which can easily leave the cells.

There are a couple of different pathways in cells; for example, if hydrogen is available then the cells do not require cytoplasmic hydrogen reduction, because there are other sources of electrons in the periplasm. But there is good evidence that under certain conditions a hydrogen cycling pathway operates allowing lactate oxidation coupled to sulfate reduction.

1.3 How hydrogenases can help to solve the energy problem

1.3.1 *Energy problematic*

The availability of large amounts of energy was a basic requirement for modern industry and human society to grow as fast as in the past few centuries. The wealth of the national economy was based on the possibility to develop fossil fuels like mineral oil, domestic natural gas and coal. These natural, primary energy sources are part of the biological carbon cycle, they are composed of plant and animal materials that have been under high pressure for the past few million years. This imbalance between the long formation process and the fast consumption of fossil fuels results in a shortage of these resources. Due to these facts it is clear that alternative and especially renewable energy sources must be found that support the current energy demand without the need for fossil fuels.

Their limited supply is not the only problem with fossil fuels for humanity. Fossil fuels are carbon compounds which produce the greenhouse gas CO_2 through their combustion. This increasing CO_2 concentration cannot be compensated by the natural CO_2 cycle and leads through the greenhouse effect to global warming and climate changes. A good alternative to fossil fuels is to use the abundance of energy from the wind or sun. These days energy from the sun, solar energy, can be used to heat water or generate electrical energy by photovoltaic cells. One of the biggest challenges nowadays is the development of technologies for capturing and storing this renewable energy as a fuel that can be used on demand. Hydrogen, with its high energy density, is one possibility.[1,52] All photoautotrophic organisms like green plants, photosynthetic bacteria (cyanobacteria, purple bacteria) and green algae can store sun energy, by absorption of light, in carbohydrates or sugar. Some of these organisms also produce hydrogen as a byproduct of photosynthesis under certain conditions.

The electricity from renewable sources can be stored as hydrogen. When this stored energy is required, hydrogen can be oxidized in fuel cells to produce electricity in an efficient and carbon-neutral way.

$$2H_2 + O_2 \longrightarrow 2\ H_2O$$

Today most of the hydrogen is produced with a huge energy input from steam reformation of fossil fuels, and is mostly used by the chemical industry.[53] An alternative method of hydrogen production is electrolysis of water. The electrocatalyst that is mostly used to perform this reaction is the metal platinum, which, because it is extremely rare and expensive, could never be used on a global scale. Other electrolysis methods require large over-potentials in alkaline solutions and high temperatures. An additional problem of platinum is its sensitivity to H_2S or CO_2, both are typical contaminants of hydrogen from steam reforming or fermentative hydrogen production.[21] But, as described earlier, there are already highly efficient natural catalysts known which produce hydrogen and use the cheap and abundant metals iron and nickel: the hydrogenases.

These metalloenzymes catalyse the production or the consumption of hydrogen under “ambient-conditions” i.e. room temperature, physiological pH and atmospheric pressure. The major roles of hydrogenases are oxidation of hydrogen as a source of reducing power or hydrogen production to get rid of an electron excess.[8,54]

1.3.2 *Biological hydrogen production and biofuel cells*

Hydrogen produced by biological or photobiological methods is called “biohydrogen”.[3] Some ideas of this biological hydrogen production should be now introduced:

Photobiological hydrogen production

The green alga *Chlamydomonas reinhardtii* is able to connect photosynthesis with hydrogen metabolism.[55] Water splitting by Photosystem II generates protons and electrons which could be used by hydrogenases to generate hydrogen. The problem of this method is the oxygen sensitivity of hydrogenases, which must be overcome in order to make solar fuel cells based on this principle a viable energy solution. Another problem is the fact that these organisms must also direct electrons to the Calvin cycle to generate sugars. Here, a significant amount of the available energy is lost.

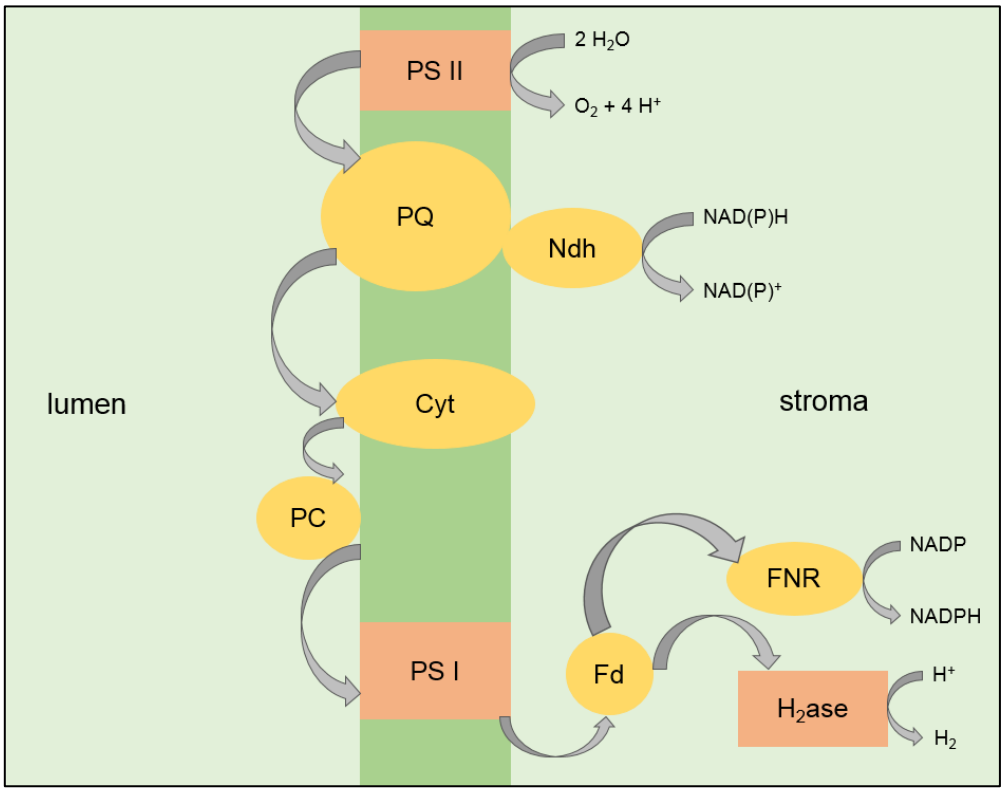

Figure 1-14 Electron transport chain coupled with hydrogenase from *C. reinhardtii*, modified from[56,57]. Water is oxidized at the reaction centre of photosystem II (PS II). The electrons are transferred via plastoquinone (PQ), cytochrome (Cyt) and plastocyanine (PC) to photosystem I (PS I). Ferredoxin transfers the electrons to the hydrogenase, where hydrogen is produced. Normally, i.e. in plants, the electrons are transferred from the ferredoxin to a ferredoxin-NADP-reductase (FNR) where NADPH is produced from NADP. An additional way of generating electrons is the metabolism of starch, which generates NADH that is in turn oxidized by NAD(P)H-dehydrogenase (Ndh).

Fermentative hydrogen production

Some mesophilic bacteria like *Clostridia* or thermophiles like *Pyrococcus* have been shown to achieve complete degradation of substrates like glucose, pyruvate or lactate and production of hydrogen in a combined dark and photofermentation process.[58] The hydrogen produced is contaminated with H_2S or CH_4 which need to be eliminated before use in biofuel cells. An additional problem is the low hydrogen yield. One mole of glucose can theoretically be converted to 6 moles of hydrogen, however, a ratio of two moles hydrogen per mole glucose is typical due to losses by alternative metabolic pathways.[59] During this process another resource becomes available, biomass, which can be used for biogas production. Biogas production has already been industrially established for a few years.

Biofuel cells

A fuel cell is a device that provides electrical energy from a chemical reaction but, unlike a battery, this energy is sustained as long as oxidants and reductants (the fuel) reach the fuel cell.[21] In comparison to a normal combustion engine with an efficiency of 20-25 % biofuel cells can reach efficiencies of 50-60 % and produce only water in the reaction of H_2 and O_2, which means a greenhouse gas free technology. A basic scheme of such a biofuel cell is given in the following Figure 1-15.

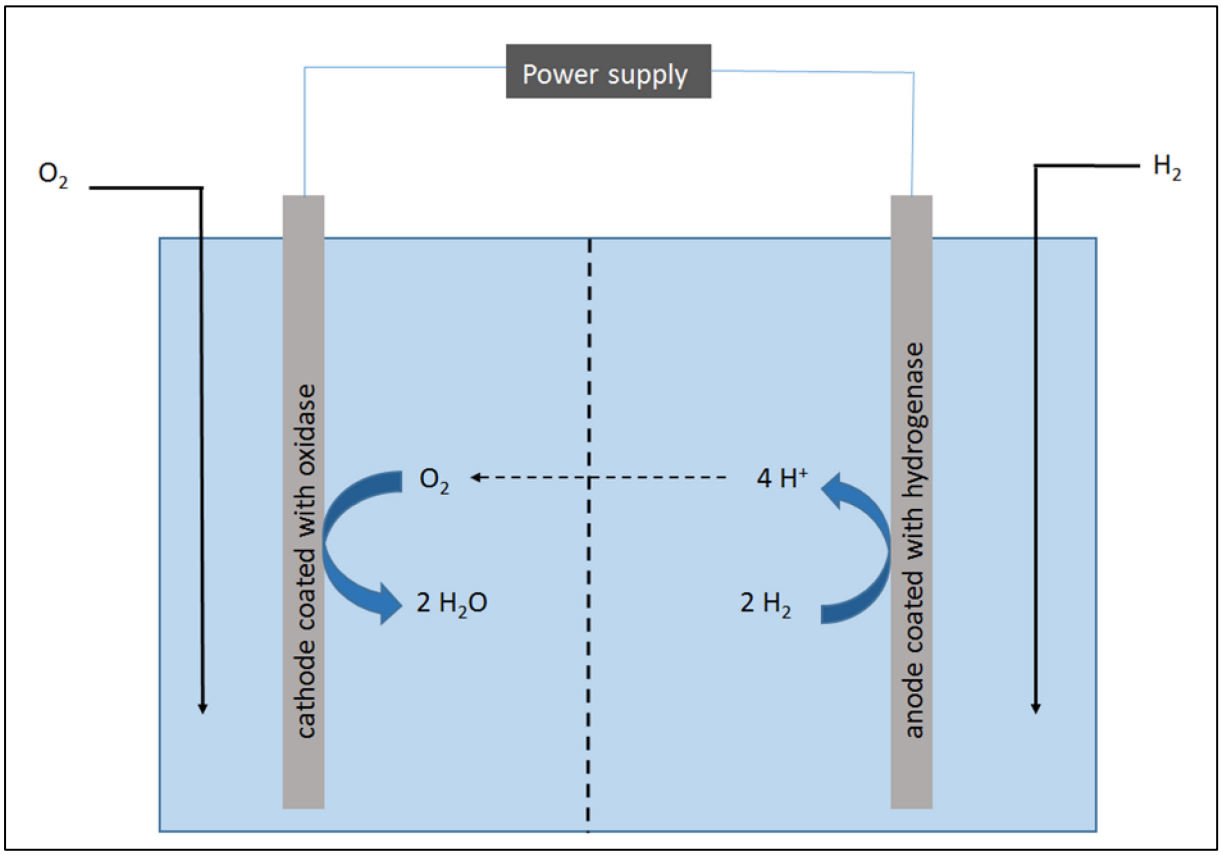

Figure 1-15 General scheme of a biofuel cell which uses enzymes as electrocatalysts. In this example the cathode is covered with an oxidase and the anode with a hydrogenase. Both compartments could be separated via a proton permeable membrane. Scheme was modified from[21].

All these new techniques in greenhouse gas free hydrogen production require a deeper understanding of the key-enzyme hydrogenase. The present thesis tries to give insight into the behaviour of these interesting molecules.

Chapter 2 Material and methods

All chemicals were ordered in the highest available purity grade and purchased from Carl Roth (Karlsruhe), Sigma-Aldrich (München), Serva Electrophoresis (Heidelberg), Thermo Fisher Scientific (Schwerte), New England Biolabs (Frankfurt am Main), and Merck (Darmstadt).
For all solutions water from a Millipore Milli-Q purification system (Merck, Darmstadt) was used.

2.1 Organisms, plasmids, primers

The organism strains and plasmids used are given in Table 2-1.

Table 2-1 Overview of the used organism strains and plasmids.

name	characteristics	reference
D. desulfuricans ATCC7757	chromosome-accession-number: NC_007519.1	Leibnitz Institut DSMZ, Braunschweig
NEB 5-alpha Competent *E.coli*	fhuA2 Δ(argF-lacZ)U169 phoA gln V44 Φ80 Δ(lacZ)M15 gyrA96 recA1 relA1 endA1 thi-1 hsdR17	New England Biolabs, Frankfurt am Main
BL21 (DE3) ΔiscR Competent *E.coli*	F^-ompT $hsdS_B$ ($r_B^-m_B^-$) gal dcm iscR::kan λDE3	Ref[60]
pUC57 with *Dd*Hyd, codon optimised	cloning vector, includes *DdHyd*, amino-terminal (NT) Strep-II tag, Tev-protease cleavage sites on large subunit, restriction sites for sub-cloning into pACYCDuet-1	GenScript, Piscataway NJ USA
pACYCDuet1	Dual expression vector, P15A replicon, lacI ::cm	Novagen, Merck, Darmstadt

All used primers were ordered from Metabion (Steinkirchen) and given in the following Table 2.2.

Table 2-2 Overview of the used primers.

primer	description	sequence (5'-3')
1A reverse	remove nt tag and Tev cleavage site	ctt taa taa gga gat ata cca tg
1A forward	remove nt tag and Tev cleavage site	ctc ccg cac cgt gat gg
2A reverse	add ct tag LSU	cct cgg caa ata aag cct ggt cgc acc c
2A forward	add ct tag LSU	gca gtt tga aaa ata aaa gct tgc ggc cgc
4 reverse	remove pre-sequence SSU	gta taa gaa gga gat ata cat atg
4 forward	remove pre-sequence SSU	gtt aaa cag att aaa gat tat atg
5A reverse	add nt tag SSU	gta taa gaa gga gat ata cat atg tgg tcg cac cc
5A forward	add nt tag SSU	gca gtt tga aaa agt taa aca gat taa aga tta tat g
6A reverse	add ct tag SSU	gaa ggt ccg tat ccg tat gaa tcg tca ggt cgt gaa aa
6A forward	add ct tag SSU	gca gtt tga aaa ata act cga gtc tgg taa ag
1 forward	remove nt tag and Tev cleavage site from $LSU_{construct}$	tcc cgc acc gtg atg gaa cg
H58 reverse	mutant H58x	cgg ttc gcc cat ttc acc g
H58A forward	mutant H58A	gct tcc att aag cac atc gaa gc
H58E forward	mutant H58E	gaa tcc att aag cac atc gaa gc
H58Q forward	mutant H58Q	cag tcc att ccg cac atc gaa gc
H58N forward	mutant H58N	aac tcc att ccg cac atc gaa gc
H58P forward	mutant H58P	ccg tcc att ccg cac atc gaa gc
H58S forward	mutant H58S	tct tcc att ccg cac atc gaa gc

H58F forward	mutant H58F	ttt tcc att ccg cac atc gaa gc
H58D forward	mutant H58D	gat tcc att ccg cac atc gaa gc
H58K forward	mutant H58K	aaa tcc att ccg cac atc gaa gc
S42 reverse	mutant S42A	gca ggt gtc aca gcc
S42A forward	mutant S42A	gct caa tac tgc ccg acg g
P46 reverse	mutant P46x	gca gta ttg act gca ggt gtc ac
P46G forward	mutant P46G	ggc acg gcg gcc att ttc
P46A forward	mutant P46A	gcg acg gcg gcc att ttc
T40 reverse	mutant T40x	gtc aca gcc gat gca ttt tg
T40P forward	mutant T40P	ccg tgc agt caa tac tgc ccg
T40V forward	mutant T40V	gtc tgc agt caa tac tgc ccg
P77 reverse	mutant P77x	gca atg ggt cag aca ctg g
P77G forward	mutant P77G	ggc gaa aat gcg atc tat gaa gc
P77A forward	mutant P77A	gcg gaa aat gcg atc tat gaa gc
A49P reverse	mutant A49P	ccg att ttc ggt gaa atg ggc g
A49P forward	mutant A49P	cgc cgt cgg gca gta ttg ac
C72A reverse	mutant C72A	ctg gcc gca gtt aat aca tgc
C72A forward	mutant C72A	gct ctg acc cat tgc ccg
I67P reverse	mutant I67P	aca tgc ttc gat gtg cgg
I67P forward	mutant I67P	cct aac tgc ggc cag tgt ctg
I204P reverse	mutant I204P	cgg gga ttt gca cgt act aaa gtg c
I204P forward	mutant I204P	cct ggt atg aac ggc gcg c
L73P reverse	mutant L73P	aca ctg gcc gca gtt aat aca tgc
L73P forward	mutant L73P	ccg acc cat tgc ccg g
C234A reverse	mutant C234A	cgg cat aat gga gac cgt gta aac c
C234A forward	mutant C234A	gct atc gcc aaa aaa tac gaa gg
C41A reverse	mutant C41A	ggt gtc aca gcc gat gc
C41A forward	mutant C41A	gcc agt caa tac tgc ccg
C382 reverse	mutant C382x	acc gcc cgg aca agc
C382A forward	mutant C382A	gcc gtg tgt ggc ggt gg
C382S forward	mutant C382S	tcc gtg tgt ggc ggt gg
7 forward	remove ct sequence LSU	tgg tcg cac ccg cag
7 reverse	remove ct sequence LSU	cgc ttc cag gac acc cg

2.2 Media and antibiotics

All media were autoclaved for 20 min, at 121 °C (Holzner, Nußloch) if not mentioned otherwise. All salt solutions were sterile filtered with a 0.22 µm PES filter (Minisat Injection filter, Satorius Stedim Biotech, Göttingen). For preparation of Agar-Plates 1.5% Agar was used.

2.2.1 *Desulfovibrio desulfuricans*

ATCC-medium[61]:

Solution I	5 g/L	$MgSO_4*7H_2O$
ad 400 mL	12,5 g/L	$C_6H_5Na_3O_7*2H_2O$
	2,5 g/L	$CaSO_4*2H_2O$
	2,5 g/L	NH_4Cl
Solution II	2.5 g/L	K_2HPO_4
ad 200 mL		
Solution III	17.5 g/L	L-lactate, Na-salt
ad 400 mL	2.5 g/L	Yeast extract

All solutions were adjusted to pH 7.5 and autoclaved separately. After cooling the solutions were mixed and 5 ml/L $Fe(NH_4)_2(SO_4)_2$ (20% w/v) was added.

2.2.2 *E.coli expression system*

LB-phosphate-medium:

10 g/L	Na_2HPO_4
10 g/L	K_2HPO_4
10 g/L	Peptone
5 g/L	Yeast extract

The pH was adjusted to 7.6 and the medium was autoclaved.

2.2.3 *Antibiotics*

Various antibiotics were used with the bacterial strains in this work and the following table shows the concentration of the stock solutions and the solvent used. The antibiotics were sterile filtered and stored at -20 °C in aliquots. They were added to the media immediately before use.

antibiotic	solvent	concentration
Ampicillin	water	100 mg/ml
Chloramphenicol	ethanol	40 mg/mL
Kanamycin	water	50 mg/mL

2.3 Cell growth

2.3.1 *Desulfovibrio desulfuricans*

To inoculate the 50 L fermenter it was necessary to scale the cultures up in two steps. For pre culture 1) 12 x 50 mL bottles with 50 mL of ATCC medium were inoculated anaerobically (inside a glovebox; N_2 / 2.0 % H_2, Coy, USA, MI, Grass Lake) with 150 µl of cryoculture per flask and incubated for two days at 37°C. Then for pre culture 2) 6 x 1 L bottles containing 1 L of ATCC medium were inoculated anaerobically with 100 ml / L pre culture 1) and incubated for two days at 37°C.

The fermenter (Biostad DL50, Braun Biotech, Melsungen) was filled with 43 L of MilliQ-water and the components of Solution I were added as solids. Afterwards the media was autoclaved inside the fermenter. The components of Solutions II and III were separately dissolved in 5 L of MilliQ-water and also autoclaved. After cooling these two solutions, these and the sterile-filtered $Fe(NH_4)_2(SO_4)_2$-solution were pumped into the fermenter with a peristaltic pump and the system was made anaerobic by flushing with N_2. After the pH was adjusted to 7.6 with 2 M H_2SO_4 the fermenter was inoculated with 6 L of pre culture 2). The temperature was maintained at 37 °C and the pH was maintained at 7.6 with 2 M H_2SO_4. The cultures were grown for three days. After 12 and 24 h of growth the cells were fed with 10 ml of 50 % Na-lactate. After three days of growth the cells were

harvested by centrifugation in 1 L tubes for 30 min at 4 °C and 6800x g (JLA 8.100 rotor, Beckman coulter, München). The cell pellets were stored at -80 °C until protein preparation.

2.3.2 *Overexpression of Desulfovibrio desulfuricans hydrogenase as unmaturated protein in Escherichia coli*

The protocol is based on that by Kuchenreuther et al.[62] with minor modifications. For a 2 L expression culture 50 mL of pre culture was necessary. For this, 50 mL of LB-phosphate-Medium with 50 µg/mL kanamycin and 40 µg/mL chloramphenicol were inoculated with cells from a frozen cryoculture and incubated over night with gentle shaking at 37 °C.

The next day 2 L of LB-phosphate-Medium in a baffled Erlenmeyerflask were mixed with 0.5 % glucose, 2 mM L-cysteine, 4 mM ferric ammonium citrate (FeAmCit), 50 µg/mL kanamycin and 40 µg/mL chloramphenicol. A sample for OD_{600nm} measurement was taken. The medium was then inoculated with the 50 mL pre culture (starting OD_{600nm} 0.01) and incubated at 37 °C under gentle shaking until an OD_{600nm} 0.3-0.5 was reached, thereafter the cells were transferred to a sterile 2 L bottle with a stirring bar and 25 mM Na-fumarate, 3 mM L-cysteine and 0.5 mM isopropyl-β-D-1-thiogalactopyranoside (IPTG). The bottles were closed with a septum and gassed for 1 h with argon. Protein expression was performed at room temperature overnight with gentle stirring.

The cells were harvested by centrifugation under anaerobic conditions for 30 min, at 4°C and 6800x g in 1 L tubes. (JLA 8.100 rotor, Beckman coulter) and frozen at -80 °C until protein preparation.

2.3.3 *Culture storage with cryo cultures*

For long time storage 500 µl fresh grown cells were mixed with 500 µl of LB medium containing 40 % glycerol and snap frozen in liquid nitrogen. These cultures were stored at -80 °C.

2.4 Protein purification

In the following part the final and routinely used purification methods are described. Optimization of these protocols and non-routine protocols are outlined in detail in the results chapters. All steps were performed on ice or at 4 °C if possible unless otherwise stated. For the purification of the native [FeFe]-hydrogenase from *Desulfovibrio desulfuricans* minimum exposure to light was used wherever possible. The purification of unmaturated protein was done under anaerobic conditions.

2.4.1 *Isolation of [FeFe]-hydrogenase from Desulfovibrio desulfuricans*

80-100 g of frozen cells were thawed overnight at 4 °C and resuspended in 1 L of resuspension buffer per 50 g of cells. This suspension was stirred for 30 min at RT and centrifuged for 30 min, 4 °C, 6800x g.

The supernatant was used for a two-step $(NH_4)_2SO_4$ precipitation. The first step was a 50 % saturation step: 312 g/ L $(NH_4)_2SO_4$ were slowly added and stirred for 30 min at RT followed by centrifugation (30 min, 4°C, 17600x g).

For the second precipitation step 250 g/L $(NH_4)_2SO_4$ were added and again stirred for 30 min at RT followed by centrifugation as described above.

The pellet which contains the hydrogenase was resuspended in 100 mL dialysis buffer and transferred to a dialysis tube with a molecular weight of cut off (MWCO) of 14 kDa (Visking 27/32, Carl Roth, Karlsruhe). The dialysis took place overnight at 4 °C under green light conditions against 5 L of dialysis buffer.

Resuspension-buffer	50 mM 50 mM	Tris pH 9.0 Na_2-EDTA
Dialysis-buffer	10 mM 20 mM	Tris pH 7.6 NaCl

The dialysed sample was purified with an FPLC (fast protein liquid chromatography)-system (ÄKTA basic, GE healthcare, Freiburg).

Anion-exchange chromatography (IEC)

The first column was an XK 25/50 anion-exchange-column (1 column-volume (CV) : 315 mL), DEAE-Toyo pearl 650C (GE healthcare, Freiburg).

The theoretical background of this method is the competitive interaction between ions. The protein binds to the weakly positively charged column material and can, therefore, be separated from positive or neutral components in the protein solution. Then a gradient with salt, usually NaCl is performed. The negative Cl^- ions compete with proteins for binding to the column material and, at a specific salt concentration the protein of interest will be displaced.

IEX run	column equilibration		2.0 CV buffer A
	wash out unbound sample		2.0 CV buffer A
	gradient step1	0-30%	0.1 CV buffer a + B
	gradient step2	30-80%	1.8 CV buffer A + B
	gradient step 3	80-100%	0.1 CV buffer A+B
	re-equilibration		1.0 CV buffer A

The active fractions (hydrogen-production assay with Clark-electrode) at a salt concentration of 44 - 48% buffer B (550 mL - 600 mL elution volume) were combined and concentrated in Amicon Ultra-15 Centrifugal Filter Concentrators MWCO 30 kDa (Merck-Millipore, Darmstadt) to a final volume of less than 5 mL.

Col1 IEC buffer A	10 mM	Tris pH 7.6
	50 mM	NaCl
Col1 IEC buffer B	10 mM	Tris pH 7.6
	1 M	NaCl

Size exclusion chromatography (SEC)

The second column was an XK 16/60 size exclusion column (1CV : 121 mL), Superdex 200 (GE healthcare, Freiburg).

In this chromatography method the separation is due to the different shapes and sizes of the proteins, which affects how they move through the porous column material. Larger proteins cannot enter the pores of the material and are eluted from the column quickly. Smaller proteins enter the pores and therefore see a larger column volume and hence take longer to elute.

SEC run	column equilibration	2.0 CV
	elution	2.0 CV

The active fractions, at an elution volume of 68-82 mL, were also combined and applied to the last column without any concentration step.

Col2 SEC buffer	10 mM Tris pH 7.6

Hydroxyapatite chromatography

The last column is an XK 16/10 hydroxyapatite column (1CV : 41 mL), HTP Biogel (Bio-Rad, München).

Hydroxyapatite is the crystalline form of calciumphosphate with the formula $Ca_5(PO_4)_3OH$. Proteins can adsorb to the crystalline surface. The complete mechanism is not completely understood, but the high selectivity of hydroxyapatite appears to be due to the competition for calcium ions on the crystal surface. This agrees with the finding that the content and distribution of acidic groups, in particular carboxylates on the surface of proteins, is a major determinant of protein binding to hydroxyapatite.[63] Usually the order of elution is first the basic proteins, then the neutral proteins and at last the acidic protein.

Hydroxyapatite run	column equilibration		2.0 CV buffer A
	wash out unbound sample		2.0 CV buffer A
	gradient step 1	0-100%	3.0 CV buffer A+B
	re-equilibration		1.0 CV buffer A

The active fractions, at a salt concentration of 77 - 95% (180 mL - 200 mL elution voulume), were combined and concentrated as much as possible, 20% glycerol was added and the protein was stored in aliquots at -80 °C. Routinely the concentration was measured and SDS-PAGE (sodium-dodecyl-sulfate-polyacrylamide-gel-electrophoresis) was performed to assess sample purity.

Hydroxyapatite buffer A	25mM	K-phosphate pH 7.6
Hydroxyapatite buffer B	300 mM	K-phosphate pH 7.6

2.4.2 *Purification of unmaturated [FeFe]-hydrogenase from E.coli*

The purification of unmaturated protein and all the mutants was done under anaerobic conditions in a glovebox.

Frozen cells from a 2 L expression were thawed on ice and resuspended in 25 mL wash buffer. 2 mM sodium dithionite (NaDT) and 1 mM phenylmethanesulfonylfluoride (PMSF) were added. The cells were broken by sonication (Sonopuls, Bandelin, Berlin, 3 cycles of 1 min with 1 min resting between the cycles, 50% duty, 60% amplitude). Afterwards the suspension was centrifuged, 1 h, 4 °C, 20000x g. The supernatant was filtered (0.45 µm nylon filter, Carl Roth, Karlsruhe) and applied onto a ~4 mL pre-equilibrated Streptactin column (Streptactin Superflow high capacity, IBA, Göttingen).

The affinity chromatography separates proteins on the basis of a reversible interaction between the affinity tag and the protein streptavidin attached to a column material (Sepharose). Unbound material is washed away and the protein is eluted by using the competitive ligand, desthiobiotin.[64]

After application of the supernatant, the column was washed with 5 CV (1CV : ~ 4 mL) of wash buffer to get rid of unbound proteins. For protein elution ~ 12 mL of elution buffer containing 2.5 mM desthiobiotin was applied to the column and the eluate was collected in 10 kDa-MWCO centrifugal concentrators (Merck, Millipore, Darmstadt). The protein solution was concentrated as much as possible (approximately 200 µL), mixed with 20% glycerol and stored as aliquots under anaerobic conditions (in a PCR tube, placed in a closed glass vial) at -80 °C.

The column was regenerated with 3 CV regeneration buffer A and 3 CV regeneration buffer B afterwards and stored in wash buffer at 4 °C.

Wash buffer	100 mM	Tris pH 8.0
	150 mM	NaCl
Elution buffer	100 mM	Tris pH 8.0
	150 mM	NaCl
	2.5 mM	Desthiobiotin
Regeneration buffer A	100 mM	Tris pH 8.0
	150 mM	NaCl
	1 mM	HABA
Regeneration buffer B	100 mM	Tris pH 10.5
	150 mM	NaCl

2.5 Molecular biology methods

2.5.1 *Agarose-gel electrophoresis*

DNA solutions from PCR or restriction digests were separated and the size was checked with Agarose-gel electrophoresis. For that 0.8 % Agarose gels were made in 1x TAE buffer with 0.01 % Roti safe (Carl Roth, Karlsruhe). Electrophoresis was usually performed for 45 min at 50 V (Mupid-one Electrophoresesystem, Nippon Genetics, Dueren).

For analytic gels 20 µl of sample was mixed with 5 µl sample buffer. For preparative gels 50 µl sample was mixed with 12.5 µl of sample buffer and loaded on the gel. After electrophoresis the DNA fragments were detected under black light (Mupid-one LED Illuminator, Nippon Genetics, Dueren). For size standards the GeneRuler plus (GeneRuler Plus DNA Ladder 100 bp/kb, Thermo Fisher Scientific, Schwerte) or the Gene Ruler (GeneRuler DNA Ladder 250 bp/kb, Thermo Fisher Scientific, Schwerte) were used (Figure 2-1).

50x TAE buffer	2 M	Tris/HCl
	100 mM	Na_2-EDTA pH 8.0
Sample buffer	30 %	Glycerol (w/v)
	50 mM	Na_2-EDTA pH 8.0
	0.25 %	Bromphenole blue
	0.25 %	Xylene cyanol

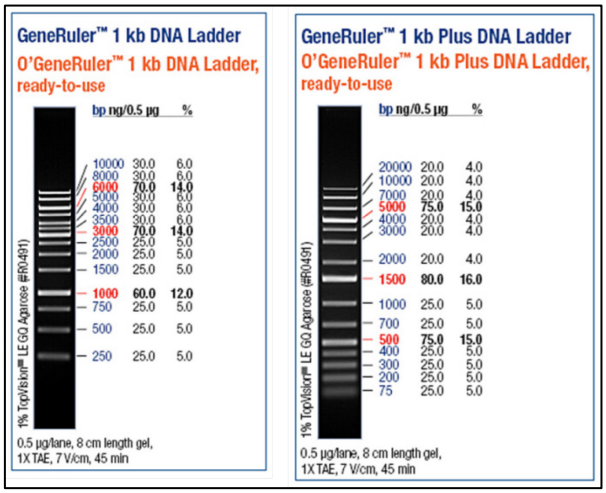

Figure 2-1 Used DNA ladders.

2.5.2 *DNA-isolation*

Isolation of plasmid DNA

For isolation of plasmid DNA the QIAprep spin Miniprep Kit (Qiagen, Hilden) was used. For that a 3 mL culture of *E.coli* in LB medium with the necessary antibiotics was grown overnight under gentle shaking at 37°C. The cells were harvested for 10 min, 4°C, 6800x g (Heraeus Biofuge, Thermo Fisher Scientific, Schwerte).

Isolation of DNA from Agarose-gels

To isolate DNA from Agarose-gels the QIAquick Gel Extraction Kit (Qiagen, Hilden) was used. The DNA fragment of interest was excised from the Agarose-gel. The DNA was eluted in 25 µL water and stored at -20 °C until use.

Concentration determination

The concentration of DNA solutions was measured with the 260 nm absorption. (Nanodrop-photometer P300, Implen, München).

Polymerase chain reaction and DpnI digest

For amplification of DNA fragments the polymerase chain reaction (PCR) was used. A typical PCR run can be divided into three different temperature steps. The first step is a temperature increasing to 92-98 °C to denature the template DNA. This is done for 5-10 min at the beginning of the PCR and then for 30 s at the beginning of each cycle. The second step is the primer annealing, the temperature of which is dependent on primer-pair melting point. This step also takes 30 s. During the third step the temperature is increased to 72 °C, the working temperature of the polymerase, allowing extension of the DNA fragments to take place. This step time is dependent upon the polymerase and the size of the amplified DNA fragment, but should be 30 s per 1 kb of template DNA. These three steps are repeated for 30 cycles followed by a 10 min extension to allow the polymerisation to complete.

For all PCR the Phusion High-Fidelity DNA Polymerase (New England Bioscience, Frankfurt am Main) was used. This is an accurate thermostable polymerase that possesses 5' → 3' polymerase activiy, 3' → 5' exonuclease activity and generates blunt-ended products. The stock concentration was 2000 units/mL.

Standard PCR approach

25 µL	Phusion Hot Start Master Mix (New England Bioscience)
20 µL	water
2 µL	template DNA (template concentration < 250 ng)
1 µL	primer forward (final concentration 0.5 µM)
1 µL	primer reverse (final concentration 0.5 µM)
1 µL	Phusion polymerase

The PCR products were digested with the DpnI restriction endonuclease, which specifically cleaves Dam-methylated DNA, to avoid contamination with wild type plasmid DNA. For that 1µL DpnI (Fast digest enzyme, Thermo Fisher Scientific, Schwerte) was mixed with 20 µL PCR solution. The following incubation was done for at least 1 h at 37 °C. Afterwards the PCR fragments were analysed with Agarose-gel electrophoresis.

2.5.3 *DNA modifications*

Digestions with restriction endonucleases

Restriction endonucleases usually recognise a palindromic sequence (depends on the enzyme) of 4-8 base pairs of DNA where they bind and hydrolyse the phosphodiester bond[65]. Depending on the restriction endonuclease blunt ended or sticky ended products are generated. For digestions usually fast digest enzymes were used (Thermo Fisher Scientific, Schwerte). The advantages of these enzymes are the short incubation times (5-30 min at 37 °C) and that double digests can be performed in the standard fast digest buffer.

Standard digest	1 µg DNA
	2 µL 10x fast digest buffer
	1 µL fast digest enzyme
	15 µL water

Ligation

For ligation usually the T4 Quick-Ligase 5000 units in the stock solution (New England Bioscience, Frankfurt am Main) was used. The ligase catalyses the formation of a phosphodiester bond between the 5’ phosphate end and the 3’ hydroxyl end of DNA molecules. Ligation was used for two main purposes, to circularize plasmids after PCR mutagenesis and to insert a DNA sequences into plasmid vectors. For circularization it was necessary to include T4 polynucleotide kinase in the reaction mixture, which allows the phosphorylation of the 5’ ends of the linear DNA molecule, facilitating ligation. Ligations were performed for 30 min at RT.

Standard ligation	50 ng plasmid-vector (excess insert) optional 5 µL Quick ligation buffer 1 µL T4 Quick ligase 2 µL PNK 5 µL PNK buffer up to 20 µL water

2.5.4 *Transformation*

Preparation of competent *E .coli* cells[66]

For amplification of ligation products transformation into competent *E.coli* cells were used. *E.coli* is naturally not competent for uptake of plasmid DNA. Several methods for making *E.coli* cells competent are known. Here calcium treatment was used. An excess of Ca^{2+} changes the permeability of the bacterial membrane which increases the ability of foreign DNA absorption.

250 mL of LB medium were inoculated with 3 mL of *E. coli* overnight culture and incubated under gentle shaking at 37 °C until an OD_{600nm} 0.3-0.5 was reached. The bacterial suspension was cooled for 30 min on ice and then harvested by centrifugation (10 min, 4 °C, 6800x g). The pellet was gently resuspended in 50 mL ice-cooled 0.1 M $CaCl_2$. The cells were again centrifuged (10 min, 4 °C, 6800x g) and again gently resuspended in cold $CaCl_2$ buffer. This suspension was incubated for 1 h on ice. After a further centrifugation step the pellet was resuspended in 2 mL of 15% glycerol (in 0.1 M $CaCl_2$) and aliquoted in 50 µL. These aliquots were frozen in liquid nitrogen and stored at -80 °C. The cells are competent for at least three months.

Heat shock transformation

50 µL competent *E.coli* cells were thawed on ice for 5 min. 2 µL purified DNA or 20 µL of a ligation reaction were added under sterile conditions and mixed. After 30 min incubation on ice the heat shock was performed for 60 s at 42 °C in a heat block. After an additional incubation on ice, for 5 min, 750 µL LB medium was added. The transformation was incubated for at least 1 h under gentle shaking at 37 °C. After that

the solution was spread onto agar plates containing the necessary antibiotics and incubated overnight at 37 °C.

2.5.5 *DNA Sequencing*

All synthesized constructs have been checked by Sanger-sequencing (LGC genomics, ready2run, Berlin). For that 10 µL of 100 ng/µl plasmid were mixed with 4 µl of 1 pM sequencing primer.

2.6 Protein analysis

2.6.1 *Concentration determination*

Concentration determination of the native [FeFe]-hydrogenase from *D. desulfuricans*

For concentration determination of the native hydrogenase UV/vis spectroscopy was used. The Beer-Lambert law describes this method. The amount of light energy which is absorbed by the sample is measured. The concentration can be calculated using the following formula:

$$A = \log\left(\frac{I_0}{I}\right) = \varepsilon * c * d$$

In this equation, A is the measured absorption, I_0 and I are the intensity of the incident light and the transmitted light, d is the pathlength of the sample and ε is the molar extinction coefficient, which is unique for each protein. For *D. desulfuricans* the molar extinction coefficient at 412 nm is known[67] to be 52500 M^{-1} cm^{-1}. For determination of the concentration an UV/vis spectrum from 250 nm - 700 nm was recorded on a nanodrop spectrophotometer (Implen, München). The [Fe-S]-cluster shows a broad absorption around 400 nm. The 412 nm absorption was used for calculation with the following equation.

$$\mathrm{c[M]} = \frac{\mathrm{A_{412nm}} * \text{dilution factor}}{52500\mathrm{M^{-1}cm^{-1}} * \mathrm{d}}$$

Concentration determination for unmaturated protein

For concentration determination of unmaturated protein a modified Lowry Assay, the DC Protein Assay (Bio-Rad, München), was used. For this assay 10 µL diluted sample were mixed with 50 µL reagent A and 400 µL reagent B. After 15 min of incubation the 750 nm absorption was measured. The protein concentration was calculated against a standard curve of BSA with known concentrations.

2.6.2 *SDS PAGE*

For purity check of the purified hydrogenase fractions the SDS PAGE (sodium dodecyl sulfate polyacrylamide gel electrophoresis) was used. SDS is an ionic detergent that denatures proteins and imparts them with a negative charge. While moving through an electric field the proteins were separated by their size.

5 µL of diluted protein sample was mixed 1:1 with sample buffer, heated up for 5 min at 99° C and loaded on a gradient gel (NuPAGE Novex 4-12% Bis-Tris Protein Gels, Life Techonolgies, Darmstadt). 60 mA (100mV) were applied to the gel for 1.5 h. The gel was stained and destained for 1 h each.

Sample buffer	10 mM	Tris / HCl pH 8.0
	1 mM	Na_2-EDTA*2H_2O
	2.5 %	Bromphenol blue
	5 %	2-Mercaptoethanol
Staining solution	120 mL	Methanol
	80 mL	H_2O
	1	Phastgel blue R tablet (Coomassie blue)
Destaining solution	10 %	CH_3COOH
	40 %	Ethanol
	50 %	H_2O

2.6.3 *Activity measurements*

Hydrogen production measured with a Clark electrode

For qualitative measurements of hydrogen production activity, for example of different fractions during purification, a modified Clark-electrode (Chlorolab II, H. Saur Laborbedarf, Reutlingen) was used. A Clark-electrode is normally used for O_2 concentration determination, but with a change of polarity the electrode can be used to detect gases like H_2 or CO_2. The electrode consists of a platinum- and a silver/silver chloride-electrode. The proceeding reactions are:

Pt (anode): $H_2 \rightarrow 2H^+ + 2e^-$ Ag/AgCl (cathode): $AgCl_{(s)} \rightarrow Ag^+ + Cl^-$

The polarisation voltage between anode and cathode is 0.6 V: For H_2 measurements the electrodes were coated as described in the user manual. For the measurements 1.4 mL of reaction buffer and 20 µL of 1 M methylviologen (gassed with argon) were placed in the reaction chamber which was closed afterwards. After starting the stirrer the measurement was started and 200 µL 1 M NaDT was added and 10 µL of diluted protein sample was injected. If there is hydrogenase activity present, an increase of the current can be observed.

Reaction buffer	100 mM	K_2HPO_4/KH_2PO_4 pH 7.0
gassed with Argon		

Hydrogen production assay with gas-chromatography

Turnover frequencies (TOF) for hydrogen production were determined with gas-chromatography (gc) measurements according to the procedure described in Winkler et al..[68] Preparation of the assay samples was performed under strict anaerobic conditions. The standard reaction volume was 150 µL, containing 100 µL of 100 mM K_2HPO_4/KH_2PO_4 buffer pH 6.8, 20 µL of 1 M NaDT, 20 µL of 100 mM MV, 100 ng of active protein (1-10 µL) and a suitable amount of water to reach the reaction

volume. After gassing the samples for 5 min with argon they were incubated for 20 min at 37 °C and immediately measured. A HP 6890 (Agilent, Santa Clara, CA, USA) gaschromatograph was used. The detector was a thermal conductivity detector (TCD) with electronic pressure control (EPC) and heated up to 200 °C for the measurements.

Column specifications:	RT-MSieve 5Å, 30 m, Ø 0.53 mm, oven temperature 30 °C
Method:	split injection at 60 °C, argon as make up gas (3 mL), reference flow 22.5 mL,
Carrier gas:	argon, 0.62 bar, 1.4 mL/min

Hydrogen oxidation assay

For calculation of turnover frequencies the hydrogen oxidation assay was used with benzylviologen (BV) as an electron acceptor in the reaction buffer. The reduction of BV leads to a colour change to dark blue which can be observed by the 600 nm absorption in UV/vis spectroscopy.

For measurements, a 1mL setup (photometer DH-mini, ocean optics, USA, FL, Winterpark) or a 200 µl setup (plate reader SpectraMax 2, Molecular Devices, Biberach) was used. All measurements were performed under anaerobic conditions inside a glovebox. All buffers were gassed with 100% H_2 for at least 20 min. For standard measurements a protein concentration around 100 nM was used for adding to the assay.

1mL setup	***200 µL setup***
1 mL gassed reaction buffer 10 µl diluted protein sample gentle stirring	190 µL gassed reaction buffer 10 µL diluted protein sample
Reaction buffer *gassed with Hydrogen*	100 mM Tris/HCl pH 8.0 1 mM benzylviologen

For calculating the specific activity the following formula was used:

$$\text{specific activity } [H_2] = \frac{\text{slope } [\text{mAU min}^{-1}] * \text{V } [\text{L}]}{\varepsilon\ [\text{mM}^{-1}\text{cm}^{-1}] * \text{d } [\text{cm}] * \text{m}_{\text{protein}}\ [\text{mg}] * 2}$$

2.6.4 *Reconstitution of unmaturated protein*

The reconstitution of unmaturated protein by inserting the azadithiolate cofactor[69] (adt) was performed inside the glovebox. A sample of unmaturated protein with a known concentration in 100 mM Tris/HCl, 150 mM NaCl pH 8.0 was mixed in a molar ratio of 1:1 with the adt complex, which is solubilized in DMSO. Due to this fact a high concentrated stock solution (4 mM) was used. Usually this mixture was incubated under gentle stirring for 1 h. The activation of the unmaturated protein was followed with the hydrogen oxidation assay mentioned above.

If the activation was done with an excess of adt, for spectroscopical measurements, removal of excess adt with a 5 mL Nap column (GE healthcare, Freiburg) was necessary. This procedure was done inside the glovebox following manufacturer instructions.

2.6.5 *Fe quantification*

To quantify the Fe content in the unmaturated protein the method developed by W.W. Fish[70] was used.

Iron releasing reagent A	0.142 M	$KMnO_4$ in 0.6 M HCl
Reducing, iron chelating reagent B	1.3 mM	ferrozine
	2.6 mM	neocuproine
	0.4 M	ascorbic acid
	1 M	ammonium acetate

To prepare the iron standards a stock solution of 1 µg Fe/mL ($FeCl_3$ in 0.01 M HCl) was used. All measurements were performed as triplets by adding 20 µL of reagent A to 40 µL of diluted protein sample (25-50 µg) or standard. After mixing, the samples were incubated for 2 h at 60 °C. Once the samples had been cooled to room temperature a centrifugation step of 1 min at 10000x g was done and 20 µL of reagent B were added. After at least 30 min at room temperature the absorption at 562 nm was measured.

2.6.6 *MALDI-TOF analysis*

To check the purity of the protein samples after each native DdH preparation a matrix-assisted laser desorption / ionization – time of flight mass spectrometry (MALDI-TOF MS) was done. The samples with concentrations around 100 µM were measured in a sinapinic acid matrix with a Voyager-DE PRO Workstation (Applied Biosystemes, Darmstadt) with an N_2 laser (338 nm, max. pulse energy 32 µJ at 10 Hz).

2.6.7 *FTIR spectroscopy*

Fourier Transformation Infrared (FTIR) spectroscopy was used to compare the native system with the reconstituted protein. For that a sample volume of 13 µL with a concentration of minimum 300 µM was used. More details are mentioned in the corresponding chapter. The measurements were performed with a Bruker Vertex 80/80v FTIR-spectrometer with MCT-detector and the related software OPUS from Bruker Optic. During the measurements the sample chamber was flushed with nitrogen to avoid CO_2 or water signals.

2.6.8 *EPR spectroscopy*

For cw-EPR measurements standard x-band tubes were filled, inside a glovebox, with 250 µL 200 µM protein samples containing 20 % glycerol. The samples were frozen in liquid nitrogen. The different sample treatments are given in respective chapters. A Bruker ELEXSYS E500 CW x-band spectrometer, equipped with an ESR 900 liquid

helium flow cryostat and an ITC 503 helium flow temperature controller (Oxford Instruments) was used. The resonator was a standard resonator ER 4102ST with a centre frequency of 9.8 GHz. Standard samples were prepared in fused quartz (Ilmasil PN) x-band tubes with a diameter of 4 mm (QSIL GmbH, Langewiesen).

2.6.9 *Protein-Film-Electrochemistry (PFE)*

For standard measurements with adsorbed or covalently attached protein 3 µL of 50 µM protein sample in 10 mM Tris pH 6.5 was used. For the native system the preparation of the electrode was performed under aerobic conditions but for the unmaturated and the reconstituted protein the electrode preparation was done inside a glovebox under N_2 atmosphere. The electrode monolayer was formed with 10 mM 4-nitro-benzene-diazoniumsalt (NBD) in acetonitrile for 5 minutes. After that the NBD was reduced by performing a cyclovoltammogram. To covalently bind the protein the pH of the electrode was adjusted with a drop of 10 mM MES buffer pH 5.8, then 2.5 µL of the protein solution was added and left for 20 min to give the protein time to orientate correctly. After that 2.2 µL of 86 mM n-hydroxysuccinimide (NHS) and 2.5 µL of 20 mM 1-ethyl-3(3-dimethylaminopropyl)-carbodiimide (EDC) were added to the electrode. The reaction took 1 h 20 min. Standard measurements were performed under 100% H_2 in the reference cell with 10 mM MES buffer pH 6.5 or buffer mix pH 6.5 with a rotation of 2000 rpm. Differences of this preparation procedure are given in the corresponding chapters.

Buffer mix		
	100 mM	NaCl
	15 mM	MES
	15 mM	HEPES
	15 mM	TAPS
	15 mM	CHES
	15 mM	Na acetate

For determination of the redox potentials for the [Fe-S]-clusters a glassy carbon electrode was used. For smoothing the CV the programme Baseline (by D. Heering)[71] was used with the Hammid method. Afterwards the interesting sections, with the weak signals, were cut. A baseline was generated using a spline curve which was then subtracted from the cut data. Finally, the peaks were fit manually using the Gaussian function:

$$f(x) = a \exp\left(-\frac{(x-b)^2}{2c^2}\right)$$

where a = peak height factor, b = potential an c = peak width factor

Table 2-3 Fitting parameters for the Gaussian curves.

	positive peak 1	positive peak 2	positive peak 3	negative peak1	negative peak 2	negative peak 3
a	9.5E-9	8.0E-9	9.5E-9	-7.0E-9	-1.08E-8	-7.0E-9
b	-0.502	-0.633	-0.452	-0.55	-0.675	-0.515
c	0.04	0.04	0.04	0.04	0.04	0.04

2.7 Theoretical section

In the following section the theoretical backgrounds of the methods used in this thesis are described to give a general overview.

2.7.1 *Theoretical background of crystallization*

To fully understand the function of an enzyme it is necessary to know its three-dimensional structure. There are three main methods for structure determination: electron microscopy, NMR-spectroscopy and X-ray crystallography, each with their own advantages and disadvantages. X-ray crystallography is generally the most widely used

technique, which gives the highest resolution, and therefore most structural information. However, not all proteins crystallize, and often it is not possible to know how well the crystal structure reflects the solution structure of the protein, which in some cases can be dramatically different. Hence, electron-microscopy and NMR are increasingly popular methods, both for studying challenging crystallographic targets and for studying more physiological conformations of proteins.[72-75] The basic principle of X-ray crystallography is that electromagnetic radiation (X-rays) are scattered in a regular way by protein crystals. This scattering is detected as a diffraction pattern of constructively and destructively interfering waves. From this diffraction patterns it is possible, through Fourier transformation, to calculate an electron density map of the unit cell in the protein crystal. From this electron density map it is possible to model the polypeptide sequence of the protein and hence a three-dimensional structural model of the protein of interest can be build.[76-78]

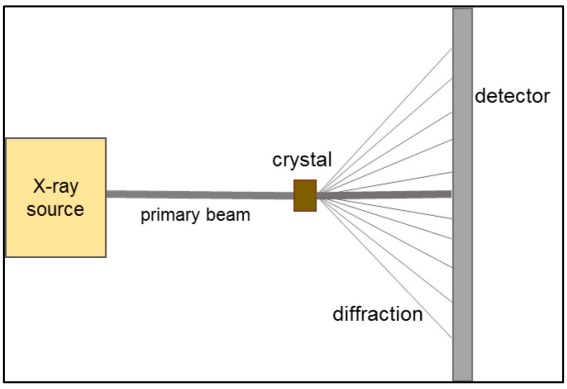

Figure 2-2 Scheme of a diffraction experiment for structure determination with X-ray crystallography.

The required electromagnetic radiation (X-rays with wavelengths between 0.1 and 100 Å, 1 pm = 0.01 Å) are formed by the acceleration of electrons. The commonly used source for this radiation in protein crystal X-ray diffraction is synchrotron radiation from electron storage rings.

The first step for X-ray crystallization is the preparation of suitable crystals. Prediction of the conditions under which a protein will crystallize is generally not possible, although there are some suggested general approaches. The growth of crystals is influenced by many factors including temperature, buffer and precipitant conditions, the presence of additives, protein concentration and purity. A typical method for protein crystallization is

vapour diffusion in sitting or hanging drop configurations. The crystallization will take place in a drop (normally a mixture of protein and crystallization buffer 1:1) above a reservoir with crystallization buffer. Due to the concentration differences of precipitants in the drop and the crystallization buffer a concentration gradient forms, and solvent evaporates from the drop and re-condenses in the reservoir. As the concentration of the precipitant approaches equilibrium the precipitant concentration in the drop increases until conditions become optimal for crystal formation. Commonly used precipitants are salts (e. g. ammonium sulfate, sodium citrate), organic compounds (e.g. polyethylene glycol) or alcohols. The following Figure 2-3 shows a scheme of both vapour diffusion techniques: sitting and hanging drop.

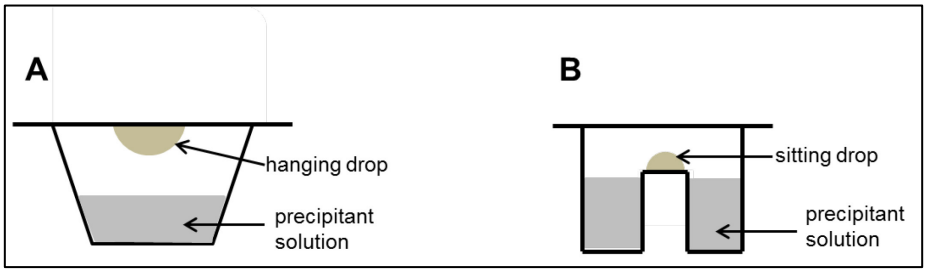

Figure 2-3 Scheme of both vapour diffusion methods for protein crystallization. A: hanging drop, B: sitting drop. Figure adapted from [78].

Protein crystals can form in different shapes and sizes, some of which are ideal for X-ray diffraction. An ideal crystal has an adequate size (normally 0.45 mm in diameter) for the X-ray beam, is homogenous with no inclusions and shows sharp and well-defined edges, can be frozen without any damage and shows well-defined diffraction spots. Such a crystal consists of many identical unit cells, each defined by three linear independent vectors (a, b, c) which span a volume with corresponding angles (α, β, γ) as shown in the following Figure 2-4. The unit cell is the smallest unit of the Bravais lattice and is characterized by its lattice constants (referred to as a, b and c).

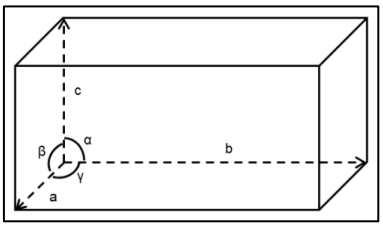

Figure 2-4 Angles and axis of a single unit cell.

For all symmetry possibilities of Bravais lattices there can be seven crystal systems.[76]

The [FeFe]-hydrogenase from the native organism has been crystallized before in either PEG 6000 or ammonium sulfate solution which also contained 100 mM acetate at pH 5.0 and 50 mM Tris pH 8.0, respectively. The enzyme was treated with 10 % hydrogen to reduce it and also the crystallization was done under anaerobic conditions.[30] But in this thesis we want to be able to look also at the aerobically isolated state and other states of the native enzyme, as well as the unmaturated enzyme and the artificially maturated enzyme. If crystals will become available EPR spectroscopy of these crystals may help to resolve the g tensor components and orientations of this enzyme in the crystal lattice.

2.7.2 *Theoretical background of EPR spectroscopy*

Electron-paramagnetic-resonance spectroscopy (EPR) is a technique for studying unpaired electron systems (spin S > 0) such as some of the reduced forms of iron-sulfur or manganese clusters, free radicals or metal-ions in macromolecules. Hence, the technique will be used extensively in this thesis and a theoretical background is advantageous to the reader.

Under the influence of an external magnetic field (B_0) paramagnetic species can absorb submitted microwave energy. There are just two possible spin orientations in the magnetic field, parallel or antiparallel to the field. Without a magnetic field both spin states (m_s = + ½, m_s = - ½) are energetically the same (degenerate).

The splitting in energy, caused by an external magnetic field is called the electron-Zeeman-splitting (see Figure 2-5) and the energy difference (ΔE) is proportional to the field (B_0) and this is what is observed in EPR spectroscopy:

$$\Delta E = g_e \beta_e B_0$$

(β_e: Bohr magneton 9.27×10^{-24} J/T, B_0: magnetic field induction,
g_e: g-value of a free electron 2.0023)

The absorption of the microwave energy is related to the electronic surrounding of the species, so information of the whole system can be generated.[79]

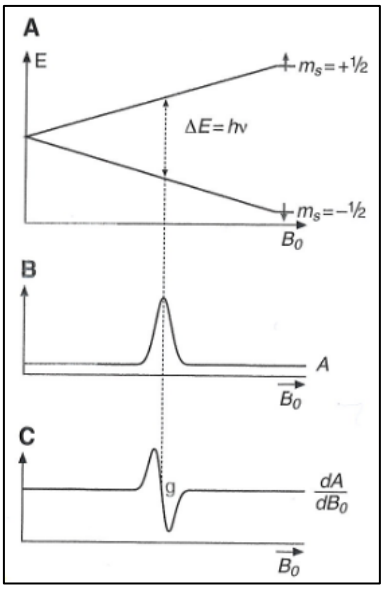

Figure 2-5 A) Electron-Zeeman-splitting for electron spin in an external magnetic field. B) Absorption spectrum under resonance conditions. C) First derivation of the absorption spectrum.[80]

Due to the instrumental setup, the magnetic field strength is varied while maintaining a fixed microwave frequency. In this thesis mostly X-band EPR was used, which uses a microwave frequency of ~9.4 GHz.

In an EPR spectrum several interactions can be observed that generate the spectrum:

- electron-Zeeman interaction (see Figure 2-5);
  Which is correlated to the g value (tensor) which represents the chemical nature of the paramagnetic centre.

- electron-electron interaction ($m_s > ½$);
  Which depends on the distribution of electrons and therefore on the interaction between those electron spins in the molecule and provides information on the structure. The zero field splitting (ZFS) ordinates from this electron-electron interaction even in the absence of an applied magnetic field.

- hyperfine interaction (for $I > 0$);
  Gives information on singly occupied molecular orbital with distances of < 1nm to the nuclei and is the coupling of unpaired electrons and magnetic nuclei, it is caused by Fermi contact (isotrop) and dipolar interactions (anisotropic).

- nuclear-Zeeman interaction ($I > 0$);
  Depends of the type of the coupled nucleus (isotope, element) but is more important in NMR spectroscopy.

- nuclear quadrupole interaction (for $I > ½$);
  This interaction is found for nuclei with a nuclear spin quantum number $I > ½$. It originates from the interaction of the electric quadrupole moment of the nuclei with the electric field gradient, which comes from uneven distributions of electric charges around the nuclei.[81]

The measured EPR spectra of magnetic moments in a crystalline or molecular environment may either depend on the orientation of the sample in the magnetic field like in single crystals or they are superpositions of many different single crystal spectra with random orientations (e. g. powder samples). In solution rotational and translational motion of the molecules often averages out the anisotropic interactions. Frozen solution EPR spectra are qualitatively identical to powder spectra.[81]

In general, due to the symmetry of the spin system three different forms for powder EPR-spectra can be observed: one isotropic ($g_z = g_y = g_x$) and two anisotropic types: axial ($g_z \neq g_y = g_x$) or rhombic ($g_z \neq g_y \neq g_x$), a scheme of them is shown in the following Figure 2-6.

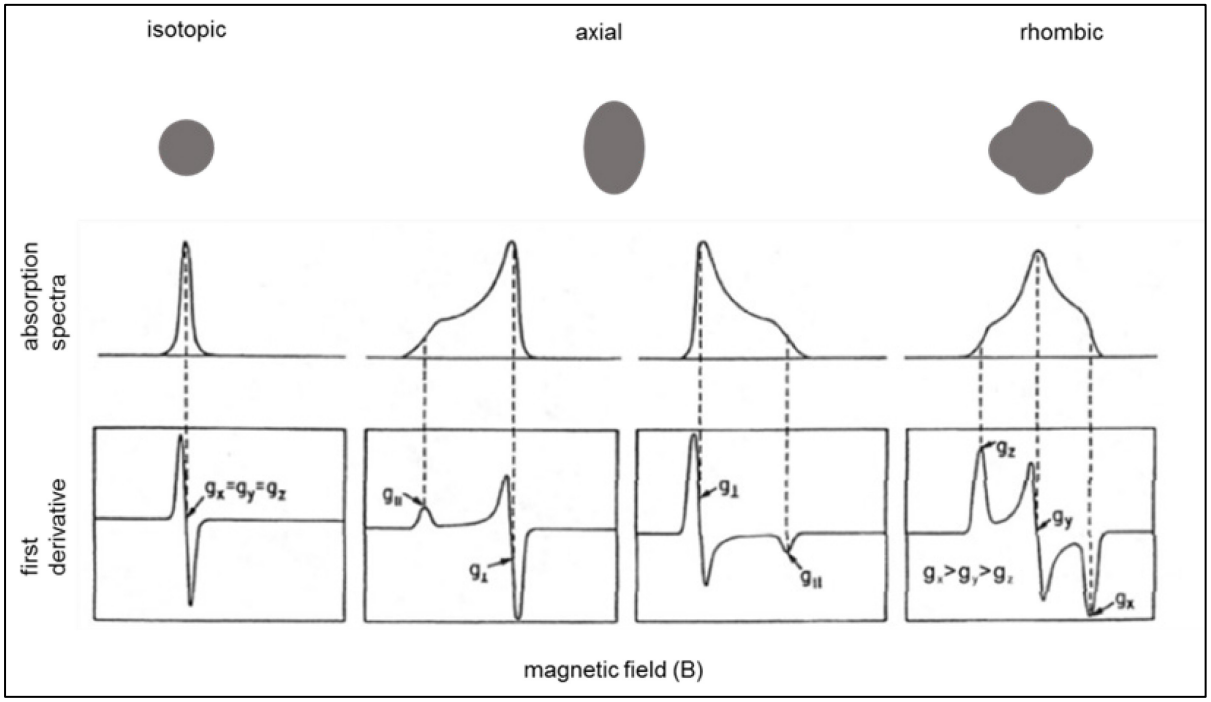

Figure 2-6 Different forms of powder EPR spectra. Figure is modified from [82]. In an isotropic spectrum all g values are identical, in an axial spectrum two g values are the same and in rhombic spectra all three are different.

All spectra, measured in this thesis are anisotropic spectra, because [Fe-S]-clusters tend to have axial or rhombic spectra because the electrons are located in non-spherical molecular orbitals. That means that, when the protein is fixed in one orientation, the electron has a different Zeeman energy to that of a protein fixed in a different orientation.

EPR on iron-sulfur clusters

As mentioned in Chapter 1 the hydrogenase of *Desulfovibrio desulfuricans* accommodates two [4Fe-4S]-cluster and an additional $[4Fe\text{-}4S]_H$-cluster in the H-cluster, which houses also the $[2Fe]_H$-active site. In the unmaturated protein the $[2Fe]_H$ active site is missing, and therefore the protein contains only three [4Fe-4S]-clusters.

Iron-sulfur clusters are often found as prosthetic groups in many different proteins where they can have different functions. For example they are involved in electron transport, in regulation of gene expression, are part of the active site of enzymes or have structural functions.[83] Three main classes of [Fe-S]-clusters are known: [2Fe]-, [3Fe]-, and [4Fe]-clusters (see Figure 2-7).

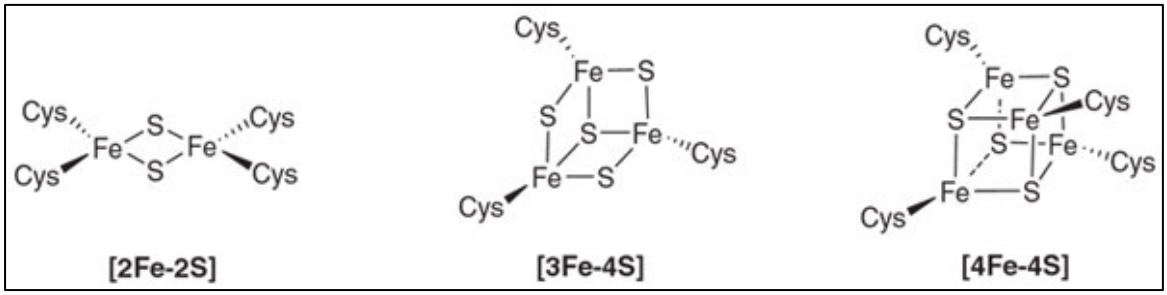

Figure 2-7 Structures of the three main types of iron-sulfur clusters.

Iron-sulfur clusters are highly amenable to study by EPR spectroscopy due to their weak anisotropy and their relatively large amplitude of their EPR signals.[44] [4Fe-4S]-clusters show mostly oxidation states of 1+ and 2+ (3+ is also possible but less common). The iron atoms in [Fe-S]-clusters show a tetrahedral coordination and are high spin. An Fe^{3+} has five electrons in its d-orbital which are all unpaired, an Fe^{2+} has six electrons in its d-orbital but only four are unpaired. As mentioned above, electrons have spins of S = ½, which means that Fe^{3+} has S = 5/2 and Fe^{2+} has S = 4/2 = 2. The oxidized $[4Fe\text{-}4S]^{3+}$-cluster (mainly observed for clusters of the HiPIP family of proteins) formally contains three Fe(III)ions and one Fe(II)ion. The one electron reduced $[4Fe\text{-}4S]^{2+}$-cluster (the typical "oxidized" form of most [Fe-4S]-clusters) contains two Fe(III)- and two Fe(II)ions. After an additional one electron reduction the $[4Fe\text{-}4S]^{1+}$ is present, which formally contains three Fe(II)- and one Fe(III)ion. Mössbauer and EPR spectroscopy show that all these clusters are better described by delocalised valence electrons.[69] Because of strong couplings between the electron spins, the $[4Fe\text{-}4S]^{3+}$-cluster and the

$[4Fe\text{-}4S]^{1+}$ have an overall spin of S = ½ . Owing to their markedly "ferrous" character, $[4Fe\text{-}4S]^{1+}$-clusters are likely to be more strongly coupled to their environment than $[4Fe\text{-}4S]^{3+}$.[44] $[4Fe4S]^{2+}$-clusters have an overall spin of S = 0 and therefore they do not show an EPR spectrum. The signal intensity of [Fe-S]-clusters is temperature dependent and follows the Curie law. Due to their general fast relaxation properties the EPR signals are quickly lost at temperatures above 20 K, in comparison [2Fe] clusters have slower relaxation and can therefore be observed also above 40 K.

For [4Fe-4S]-clusters, generally only very weak proton hyperfine couplings can be observed, because of the large distance between the electrons of the iron and the possible coupling partners (hydrogen from a cysteine or hydrogen from a hydrogen bond of an amino acid from the backbone). These couplings contribute to the linewidth of the EPR signals. In enzymes with several [Fe-S]-clusters the spin exchange interaction, which is the interaction between two unpaired clusters is quite important for the shape of the spectra. But it also needs to be considered, that even in natural [Fe-S]-cluster systems small amounts of ^{33}S, ^{57}Fe and D are present which show interactions in the spectra.

2.7.3 *Theoretical background of FTIR spectroscopy*

The basic principle of infrared spectroscopy is the absorption of low energy light (infrared light: 760 nm - 1000 nm). The main difference when compared with UV/vis- and absorption-spectroscopy, is that in UV/vis spectroscopy the transitions between electronic energy levels in molecules are measured, while in infrared spectroscopy the transitions between rotational or vibrational energy levels are measured.[84]

The active site of [FeFe]-hydrogenase contains cyanide and carbon monoxide ligands, both of which are easily detectable by FTIR due to the fact that their absorption bands are not overlapping with those from the rest of the protein, buffer and solvent. CO stretch vibration bands can be found in the 2020-1750 cm^{-1} region and the CN vibration bands can be observed in the 2110-2020 cm^{-1} region.[85] The frequencies of these vibrations act as sensitive sensors for the electron density around the active site and are, therefore, indicators for the different redox state of the hydrogenase. The following Table 2-4 gives an overview of the IR bands of some redox states from the hydrogenase of *D. desulfuricans.*[27,85-88]

Table 2-4 Overview of the different IR bands from [FeFe]-hydrogenase of *D. desulfuricans*, adapted from[85].

	H_{ox}^{air} state (as-isolated)	H_{ox} state	H_{red} state	H_{ox}-CO state
CN terminal 1	2106	2093	2093	2096
CN terminal 2	2087	2079	2079	2089
CO terminal 2	2007	1940	2041	2016 (symmetric)
			1965	1971 (asymmetric)
CO terminal 1	1983	1965	1916	1963
bridging CO	1848	1802	1894	1811

2.7.4 *Theoretical background of protein film electrochemistry*

A redox-reaction can formally be divided into two single reactions, a reduction (gain of electrons by one species) and an oxidation (loss of electrons). These reactions can take place on the surface of electrodes of an electrochemical cell, where the reduction takes place at the cathode and the oxidation takes place at the anode of the cell. It is possible to measure an electric current between those two electrodes, if the reacting system is not at thermodynamic equilibrium. The following Nernst equation describes the potential of a half cell:

$$E = E^0 + \frac{RT}{nF} \cdot \ln \frac{[Ox]}{[Red]}$$

(E: potential between both electrodes, E^0: standard electrode potential, [Ox] and [Red] concentrations of the involved species, T: temperature, n: moles of transferred electrons, R: universal gas constant 8.314 $JK^{-1}mol^{-1}$, F: Faraday constant 96485 C mol^{-1}).

In a three-electrode electrochemical cell, the electric current measured at the working electrode flows also in the opposite direction through the auxiliary or counter electrode. The setup is built in such a way that the process at the counter electrode is not rate limiting. In the experiments, reported in this thesis, a platinum wire with a higher area than the working electrode was used as a counter electrode.

There are two common methods of voltammetry experiments used in this thesis; cyclic voltammetry and chronoamperometry.

Cyclic voltammetry

In a cyclic voltammetry experiment the electrode potential is swept in a linear manner back and forth between two limits.[89] Therefore the method is also known as linear sweep voltammetry.[90] The rate at which the potential is scanned defines the time scale of the experiment and can be varied from < 1 mVs^{-1} to > 1000 Vs^{-1}, which is a very large dynamic range and makes it possible to carry out both, steady state and transient experiments on the same sample.[91] If the experiment starts at a more positive potential than the standard potential of the redox process, only a non-Faradaic current (rest current) can be measured. This current can be explained by capacitive charging and discharging of the electrode as a result of the reorganization of ions in solution at the interface electrode/electrolyte. If the potential is swept close to the standard potential of a particular species, the reduction starts and a current can be measured. This current increases until the concentration of the oxidized species close to the electrode becomes too small, then the mass transport of this species to the electrode has reached the maximum. After that the current decreases again, due to a saturation effect. This behaviour leads to a “reduction peak” of the recorded current. If the start potential is more negative than the standard potential of the redox-process and is swept to more positive potentials then the sample becomes oxidized. In this case the current curve shows a peak which is caused by the oxidation. The method is called cyclic voltammetry because the potential during a measurement is swept back and forth in cycles.

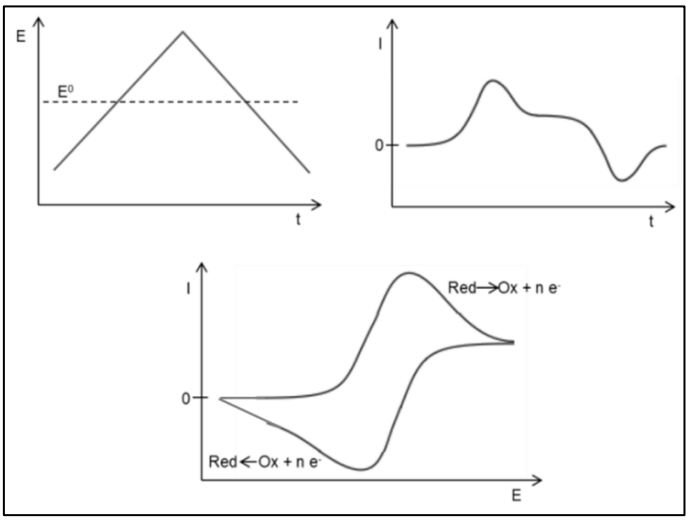

Figure 2-8 Cyclic voltammetry experiment. The upper part shows the set potential plotted against the time on the left and the corresponding current on the right. The lower part shows the typical shape of a cyclovoltammogram. Figure adapted from[92].

Chronoamperometry

In chronoamperometry the current is measured in a time dependent fashion, and the potential is maintained constant during the experiment or can be varied by different pulses. This allows a separation of the potential and the time dependency of the response.[93] The current decays with time as the reduced species accumulates and the oxidized species disposes. When measuring a catalytic process on an electrode where the catalyst is confined on the surface of the electrode the diffusion of substrate becomes relevant. Diffusion limitations can be avoided using a fast rotating electrode.

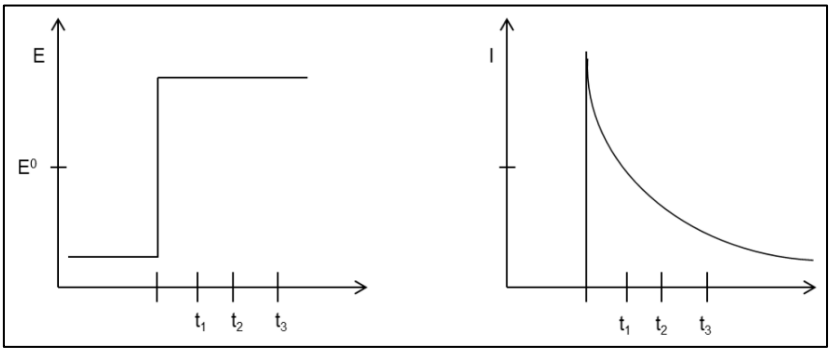

Figure 2-9 Chronoamperometry, the potential which is set during an experiment is shown on the left and the corresponding current due to diffusion processes is shown on the right. Figure adapted from[92].

Protein film electrochemistry (PFE)

In protein film electrochemistry the protein is confined on the electrode surface, forming a protein film close to a monolayer. This can be achieved by absorption of the protein or by covalent attachment. If the protein is immobilized onto the electrode, the redox process is independent of diffusion of the protein to the electrode which brings the redox driven chemistry of an active site into a sharp focus.[91,93] Due to the direct coupling of the protein onto the electrode it is not necessary to use any redox-mediators to ensure an electron transfer. It is important to make sure, that the electrode material does not change the natural conformation of the enzyme and that the electrode just reacts in a similar manner as the natural electron acceptor of the protein does. An advantage of PFE is the possibility to change the experimental conditions like buffer, pH or temperature very easily and several experiments can be done on the same sample, provided that the protein film is stable. As a tool for mechanistic enzymology, this method benefits from its sensitivity, the quantitative nature of the thermodynamic and kinetic information gained, and the extremely small sample requirements (i.e. a few picomol/cm^2 of enzyme).[91,93,94] These facts make PFE an important and useful technique to analyse redox-active proteins.

In this thesis a three electrode cell is used (see Figure 2-10). At the working electrode the redox reaction takes place, here a highly oriented pyrolytic graphite edge (HOPGE) electrode was used. Unlike a metal electrode, the surface atoms and groups have saturated valencies, so that the atomic-scale interactions with the protein are weak and non-covalent, more like the interactions that occur between proteins in solution or on a membrane.[93] On the other hand it is also possible to form a covalent bond between the enzyme and the electrode to guarantee a good electron transfer and film stability.[95] A potential disadvantage of PGE is that the surface groups include redox-active functionalities such as aldehydes and quinones that themselves undergo sluggish electron transfer reactions: these may complicate the interactions between the protein and electrode in addition to contributing signals to the voltammetry.[96,97] The second electrode is the reference, which is required because it is only possible to measure the potential in relation to a reference potential, here a saturated Calomel electrode (SCE) was used. The third electrode is the counter electrode, for that a platinum wire was used. This counter electrode, along with the working electrode, provides a circuit over which the current is either applied or measured.

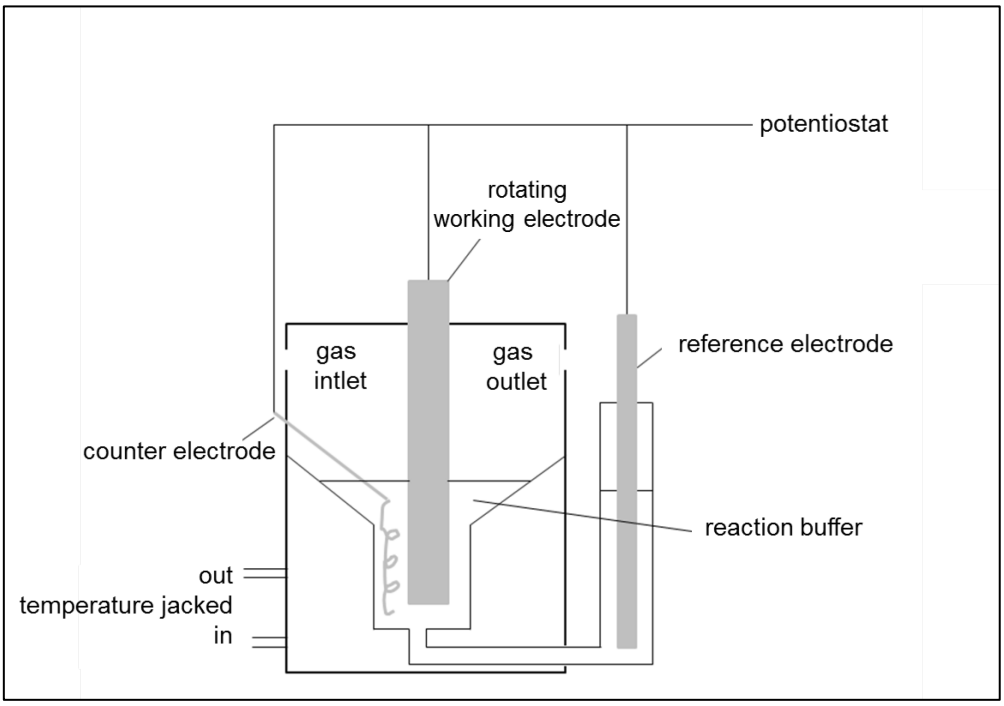

Figure 2-10 Schematic setup of an electrochemistry cell. The setup was placed in a glovebox under N_2 atmosphere. The possibility of gassing the electrochemical with H_2 is possible with this setup.

Chapter 3 Improvement in preparation of the [FeFe] hydrogenase from *D. desulfuricans* and development of a strategy for recombinant expression in *E. coli*

3.1 General Introduction

3.1.1 *Native [FeFe]-hydrogenase from Desulfovibrio desulfuricans*

As mentioned in Chapter 1, the use of hydrogenases offers a promising alternative to the currently used hydrogen production techniques. Hydrogen metabolism in *Desulfovibrio desulfuricans* and particularly, the mechanism of the [FeFe]-hydrogenase are not completely understood. In 1895 the isolation of *D. desulfuricans* was reported for the first time by Beyerinck et al.[47]. At that time the organism was named *Spirillum desulfuricans* and it was isolated from a Dutch city canal. The first isolation of the [FeFe]-hydrogenase in laboratory scale was reported by Sadana et al. in 1956.[47] A significant difference between this early purification method and more recent procedures, like the one developed by Hatchikian et al. in 1992[67], is the use of acetone to isolate the [FeFe]-hydrogenase from the organism. It is known, that acetone destroys a large amount of the protein during the exposure. Even nowadays the purification is performed based on the protocol from Hatchikian. Here the cell disruption is performed by a very gentle method: stirring the cells with EDTA-containing buffer at a high pH. Following this, the separation of the hydrogenase from the majority of other periplasmic proteins is done by ammonium sulfate precipitation. The final step, the purification by chromatography, has changed slightly during the years by further developments of new column materials (Wenk et al.).[98] The genomic sequence of *Desulfovibrio desulfuricans* was discovered in 1985 by Voordouw et al.[47] which greatly facilitates the production of genetic modifications of the enzyme, as is performed during this thesis. The work from Hatchikian et al., also refuted that the [FeFe]-hydrogenase from *D. desulfuricans* is a single subunit enzyme, which was reported in 1980 by Glick et al..[99] The first EPR spectroscopic measurements on this

enzyme were performed by Grande et al. in 1983,[100] where it was suggested that a spin-spin interaction exists between the ferredoxin-type [Fe-S]-clusters. In these first EPR studies it was supposed that the enzyme only harbours the [Fe-S]-clusters and so all spectroscopic investigation were done on the interactions between these clusters. In 1988 Patil et al.[40] showed the reductive activation of the aerobic purified enzyme by EPR spectroscopy. Until now, many further investigations on EPR spectroscopy, and especially on the active site, have been published[18,67,99,101-107], details of which are presented in Chapter 4.

Of particular interest is the fact that, under certain conditions, the hydrogenase can be purified in an oxygen resistant inactive form.[42,108] The processes by which the enzyme is converted to this inactive form, and the processes leading to reactivation are far from a detailed understanding.

A central aim of this work was to generate a strategy for heterologous expression of *Desulfovibrio desulfuricans* [FeFe]-hydrogenase. Regarding this, it was very important to have the natively purified hydrogenase as a direct comparison. Therefore, it was necessary to optimize the cell growth and hydrogenase purification for high yields with minimal preparation time.

3.1.2 *Artificial [FeFe]-hydrogenase from Desulfovibrio desulfuricans*

To develop active and cheap mimics of hydrogenases a deeper understanding of the assembly of the active site and the reaction mechanism is necessary. For this, large amounts of the protein need to be available from a highly efficient, fast and easy to handle source. One approach that has been adopted in order to enhance the amount of enzymes, is the engineering of hydrogenase either through its production in a heterologous host or through overexpression.[109-111] A promising way is the heterologous expression of the hydrogenases genes in *E.coli*. Some expression systems have already been engineered, but active enzyme yields are usually less than 1 mg/L of culture and with significantly lower activities than from their native organism, most likely because of incomplete maturation of the enzyme.[60,112-114] There are different expression methods known: with maturases or without maturases. After an expression without maturases the protein needs to be maturated afterwards, either by mixing it with the purified maturases

or with artificial maturation. Table 3-1 shows an overview of the [FeFe]-hydrogenases which are so far expressed.

Table 3-1 Expression of [FeFe]-hydrogenases in different systems. Figure adapted from[109].

[FeFe]-hydrogenase	Expression host	Year	Reference
Chlamydomonas reinhardtii	*E.coli*	2004	Posewitz et al.[45]
Clostridium acetobutylicum	*Clostridium acetobutylicum*	2005	Girbal et al.[115]
Chlamydomonas reinhardtii	*Clostridium acetobutylicum*	2005	Girbal et al.[115]
Scenedesmus obliquus	*Clostridium acetobutylicum*	2005	Girbal et al.[115]
Clostridium paraputrificum	*Clostridium paraputrificum*	2005	Morimoto[116]
Clostridium acetobutylicum	*E. coli*	2006	King et al.[117]
Chlamydomonas reinhardtii	*Shewanella oneidensis*	2008	Sybirna et al.[118]
Clostridium tyrobutyricum	*Clostridium tyrobutyricum*	2009	Jo et al.[119]
Enterobacter aerogenes	*Enterobacter aerogenes*	2010	Zhao et al.[120]
Chlamydomonas reinhardtii	*E. coli*	2010	Kuchenreuther et al.[62]
Clostridium pasteurianum	*E. coli*	2010	Kuchenreuther et al.[62]
Clamydomonas reinhardtii	*E. coli*	2012	Yacoby et al.[121]
Desulfovibrio desulfuricans	*E. coli*	2014	this thesis

Due to lower activities of the proteins expressed with maturases, the research is now more focussed on expression of an unmaturated protein (missing the $[2Fe]_H$ sub-cluster of the active site) with *in vitro* maturation after purification. This gives high yields of hydrogenases with identical activities and spectroscopic properties to those purified from the native organisms.[62,122] Details of the different types of activation are given in Chapter 4.

E. coli is a highly useful host for heterologous expression. It is one of the best characterized bacteria and due to genetic modifications (no toxins, small genome and no plasmids) most laboratory stains are safe and easy to handle. They have an extremely high doubling time (~20 min) and can therefore achieve very high cell densities within a few hours. *E.coli* does not possess a native [FeFe]-hydrogenase and, therefore, also lacks the maturation machinery. A co-expression with the native maturation machinery is possible but generates enzymes with lower activity than the native. It is also possible to produce unmaturated protein, with no active site. This makes the study of the protein in the absence of the $[2Fe]_H$ sub-cluster possible. Additionally it is possible to maturate the hydrogenase with the native and also with non-native complexes to get deeper insight into the function of the hydrogenase. Another feature of *E.coli* is that it is a facultatively anaerobic organism, which means that it can grow aerobically or anaerobically and, therefore, both types of growth can be used to find the optimum conditions for hydrogenase expression. One point, which needs to be considered, is that post-translational processing of proteins is bacteria-specific, and *E.coli* may not process the expressed protein in the same way like the native organism. For the native organism it is known, that there are two posttranslational modifications, short peptides at the amino terminal end of the small subunit and at the carboxy terminal end of the large subunit are removed after translocalisation to the periplasm. Details of this are discussed further in Section 3.3.1.

3.1.3 *Aims of the work described in this chapter*

- Improve cell growth of *Desulfovibrio desulfuricans* by increasing the fermenter volume and automate the regulation of the growth conditions.
- Increase the yield and purity of the hydrogenase by modification of the purification procedure.
- Create and optimize a construct for heterologous expression of [FeFe]-hydrogenase in *E. coli*.
- Establish and optimize an overexpression system and a purification procedure to produce high amounts of pure unmaturated protein.

3.2 Improvement in preparation of the [FeFe]-hydrogenase from *Desulfovibrio desulfuricans*

3.2.1 *Growth of Desulfovibrio desulfuricans*

D. desulfuricans was grown under completely anaerobic conditions, following procedures outlined in Chapter 2.

Prior to this work, the growth of *D. desulfuricans* was performed as reported by Wenk et al..[98] Agar-cultures (10 mL) were anaerobically inoculated from cryo-cultures and transferred after four days of growth to 50 mL pre-cultures. After two more days of growth 500 mL pre-cultures were inoculated and, after two more days, a 10 L semi-automatic fermenter was inoculated with 1 L of pre-culture. There were two of these fermenters available in the lab and therefore running in parallel. The cells from the 10 L fermenters were harvested after three days of growth. Therefore, the production of 2 x 10 L of cells took 11 days, with a yield of 50 ± 10 g cells in total from 20 L.[98]

For other hydrogenases it is known, that growth starts directly from cryo-cultures to liquid pre-cultures[123] or from liquid pre-cultures in special storage medium[92]. Therefore, it was tested if it was possible to avoid the extra step of preparing Agar-cultures, because they need a proportionally long growth time (4 d). For that 150 µL of a cryo-culture containing glycerol in the medium was directly transferred to a 50 mL pre-culture. After two days of incubation at 37 °C with occasional mixing (inverting the culture from time to time) the

culture was dark black. This black colour is caused by sulfur reduction and precipitation of Fe(II)S afterwards, this can serve as an index of growth. The 50 mL pre-culture was directly transferred to a 1 L culture. After an additional two days of growth with six of these 1 L cultures a 50 L fermenter was inoculated. The cells from a 50 L fermenter were harvested three days later. The yield of cells was 146 g ± 19 g in total from 50 L, and took just 7 days.

A comparison of the old and the newly established growth procedure is given in the following Figure 3-1.

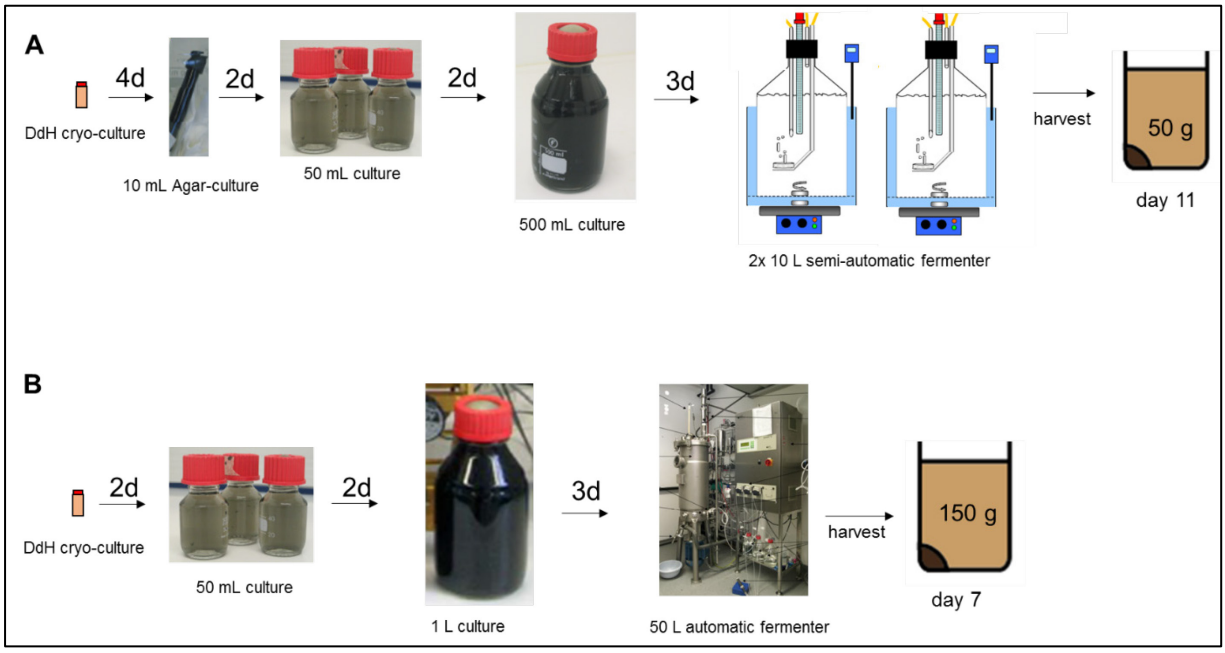

Figure 3-1 Scheme of the former growth of *Desulfovibrio desulfuricans* (A) which took 11 days until around 50 g cells could be harvested; and the improved growth of the organism (B) which takes 4 days less and yields in around 150 g per fermentation. Figure adapted from[98].

The most significant change of the growth procedure is the change from a semi-automatic 10 L fermenter to the automatic 50 L fermenter. The 10 L fermenters needed to be filled with medium and transferred to an autoclave to sterilize the setup, while the 50 L steel fermenter is directly coupled with the autoclave, this makes a more comfortable sterilization process in the vessel of the fermenter possible. Probably the most important difference between the two fermenters is the anaerobicity. The automatic fermenter monitors the oxygen concentration using an oxygen electrode and this allows

the flow of purge gas to be increased in order to remove remaining traces of oxygen. In the old setup no oxygen electrode was used and the vessel was only closed by a rubber stopper, which possibly allowed some oxygen to remain in the cultures during growth. Additionally, the temperature and pH measurement of the 50 L fermenter is more precise and these are automatically regulated, as are the additions of lactate as a carbon source and antifoam. The temperature of the old fermenter needed to be adjusted manually and the water bath, which regulated the temperature, needed to be filled every day. Likewise, acid, antifoam and lactate needed to be added manually. The automatic fermenter allows a complete monitored and regulated growth of the culture in higher volumes and is, therefore, a quite large and important improvement of the growth of *Desulfovibrio desulfuricans*.

A comparison between both fermenter setups is given in Figure 3-2.

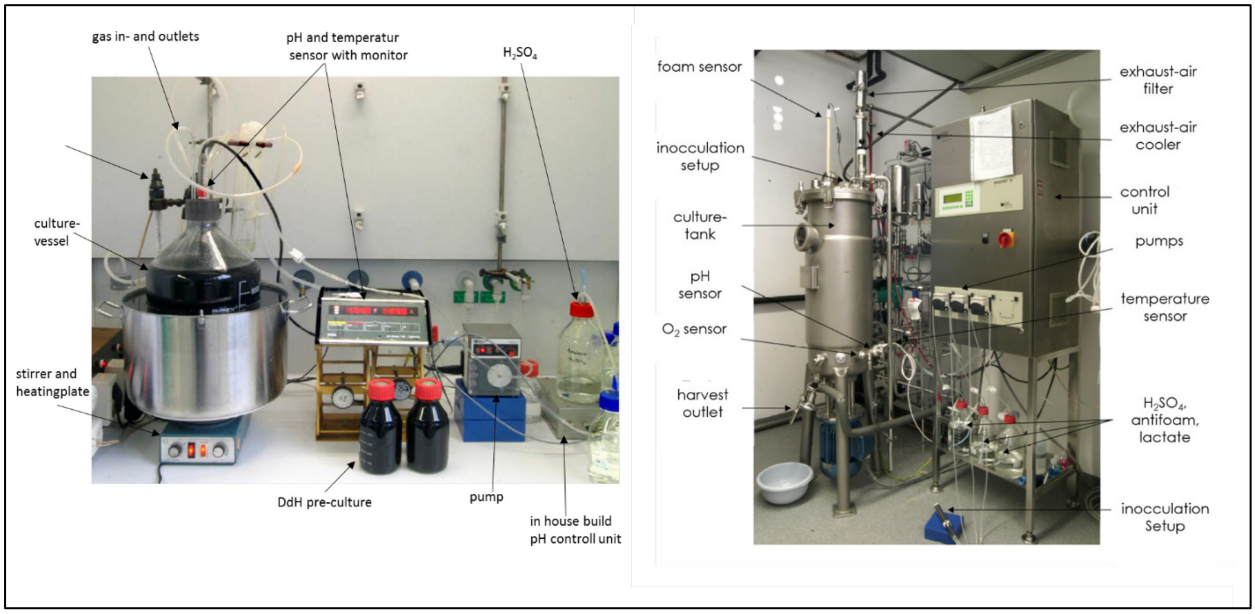

Figure 3-2 Comparison between the two fermenter systems, the old setup on the left and the new automatic fermenter on the right. Left figure adapted from[124].

The change of the fermenter system does not significant increase the cell yield per L, it increased from 2.3 ± 1.2 g/L with the semi-automated fermenter[98] to 3.4 ± 1.6 g/L with the fully automated fermenter, but the yield of purified protein increased approximately two fold from 1.5 ± 0.7 mg to 3.2 ± 0.3 mg per 100 g of cells (more details are given in the purification Section 3.2.2).

3.2.2 *Purification of [FeFe]-hydrogenase from Desulfovibrio desulfuricans*

One of the advantages of working with the hydrogenase from *D. desulfuricans* is the possibility to purify it under aerobic conditions, because the purification protocol somehow involves the conversion of the hydrogenase into the oxygen resistant H_{inact} state (see Section 1.1.3). The purification of [FeFe]-hydrogenase from *D. desulfuricans* was reported by Hatchikian et al.[67] and modified by Wenk et al.[98]. At first the established purification strategy was used in conjunction with the newly established cell growth strategy. Due to equipment constraints, no more than 80-100 g of cells were used in a single purification. For cell breaking a treatment that only permeabilises the periplasmic membrane is preferential because then the hydrogenase is purified away from the cytoplasm and the membranes in a single step. For this a treatment with EDTA at a high pH (pH 9.0) was used. The interaction of EDTA with the outer cell membrane results in a permeability of the membrane for periplasmic proteins like the [FeFe]-hydrogenase.

Cell breaking with ultrasound (sonication) resulted in a decrease of the protein yield by a factor of 5. It seems that the heat formation during this process in spite of cooling is a problem of this method. It is also known that sonication of oxygen (due to aerobic preparation) can lead to the formation of reactive oxygen species by thermal dissociation of water.[125] These reactive oxygen species may damage the [Fe-S]-clusters or other parts of the protein in spite of the H_{inact} state of the enzyme or it may also be possible, that the protein is not all converted to its H_{inact} state.

During a following centrifugation step the cell material can be separated from the hydrogenase-containing periplasmic fraction. Unwanted proteins from this supernatant are precipitated with $(NH_4)_2SO_4$ and removed by centrifugation. In a second $(NH_4)_2SO_4$ step the hydrogenase-containing fraction is precipitated and separated from remaining protein, again by centrifugation. The precipitant is solubilized in low salt buffer and dialysed to get rid of the high salt concentration from the $(NH_4)_2SO_4$.

Afterwards the purification by FPLC (fast protein liquid chromatography) starts with anion exchange chromatography (DEAE-Toyo pearl 650C). During all chromatography steps the absorption of 280 nm and 412 nm are recorded. The 280 nm absorption is formed by the delocalized π-system of the aromatic amino acids like tryptophan, phenylalanine and tyrosine and is a general protein absorption marker. The 412 nm absorption is caused by

the absorption of the [Fe-S]-clusters in proteins and gives an indication as to the presence of [Fe-S]-cluster containing proteins like the [FeFe]-hydrogenase.

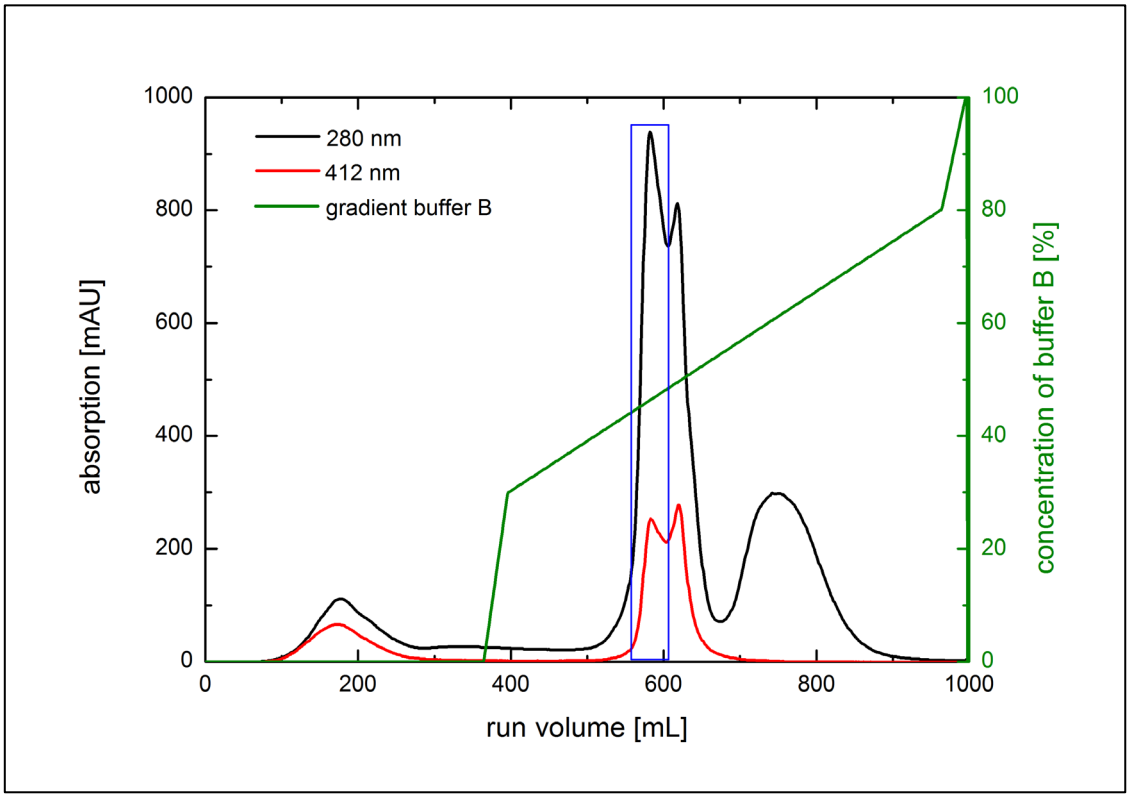

Figure 3-3 Chromatogram recorded after the first column (anion exchange column), 280 nm absorption is shown in black, 412 nm absorption in red and the gradient of buffer B is shown in green. The fractions that show hydrogenase activity are marked with the blue rectangle.

The fractions were checked for activity by measuring hydrogen production with a Clark-electrode (see Section 2.6.3) and the active fractions were combined afterwards. After a concentration step the protein sample was applied to the second column, a size exclusion column (Superdex 200).

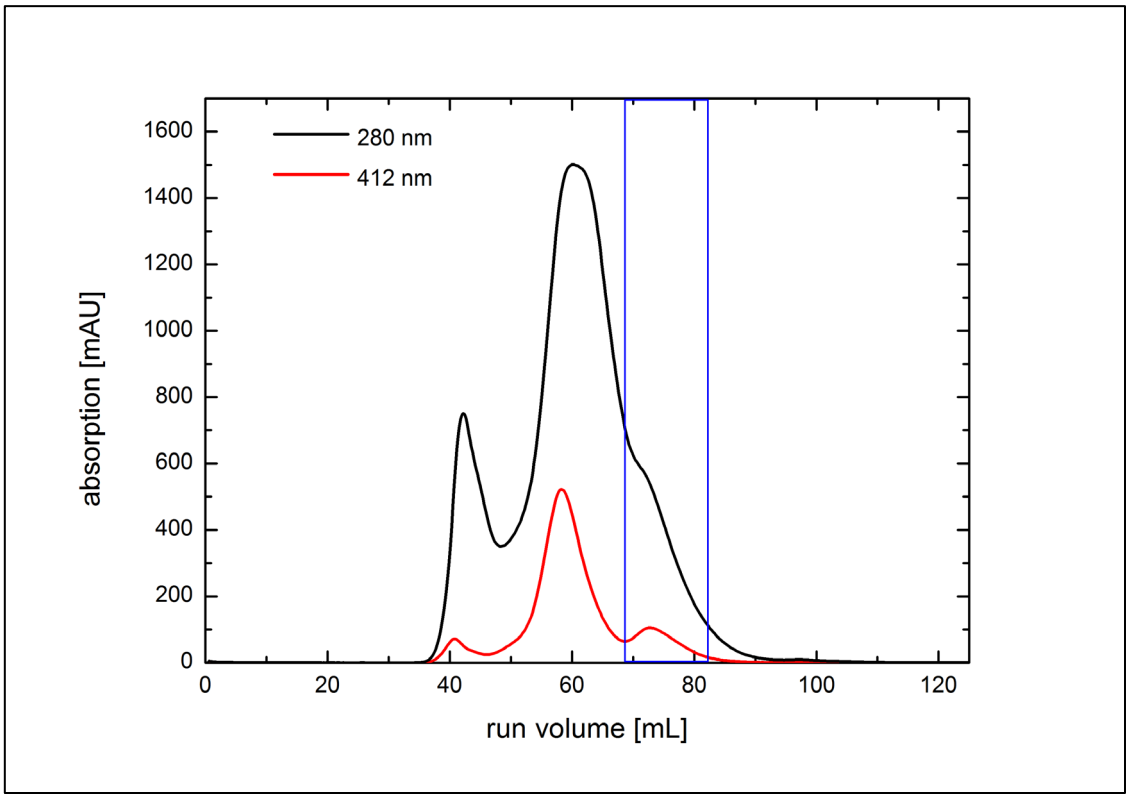

Figure 3-4 Chromatogram recorded after the second column (size exclusion), 280 nm absorption is shown in black and 412 nm absorption in red. The hydrogenase containing fractions are marked with the blue rectangle.

The third and last column is a hydroxyapatite column, after which the hydrogenase is quite pure and no further purification steps are required. The purity after each preparation is checked by SDS-PAGE and MALDI-TOF analysis.

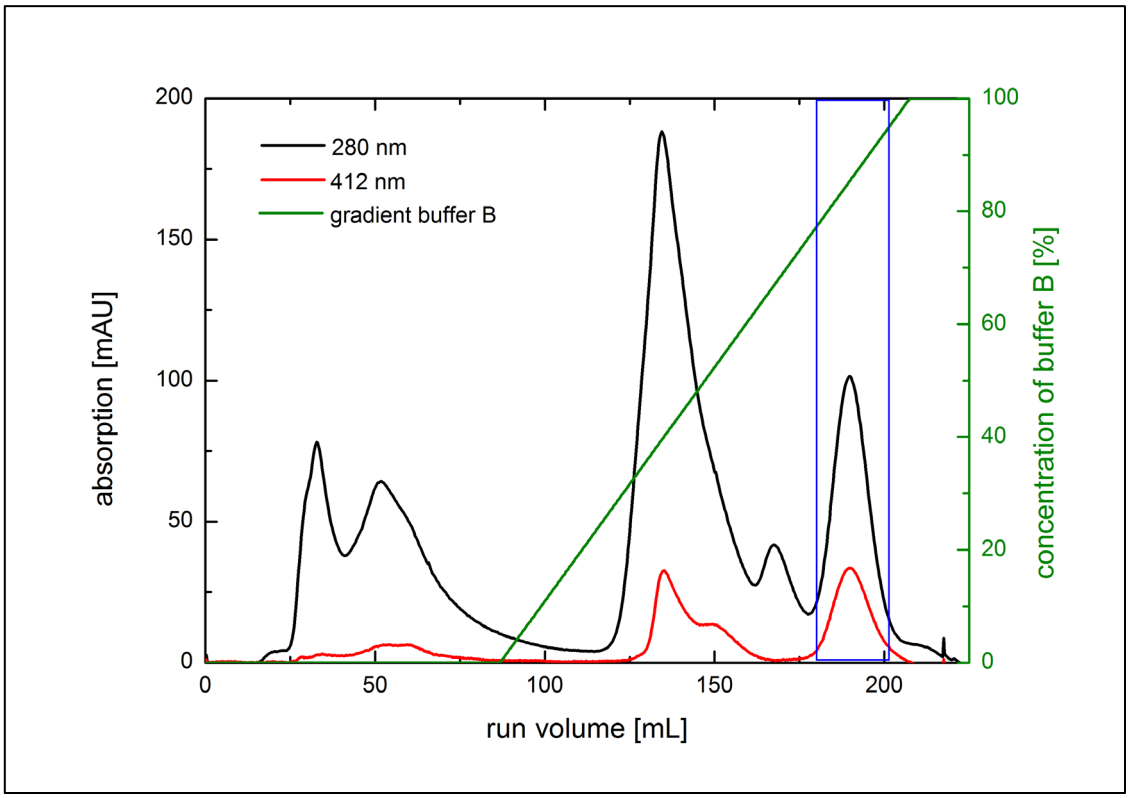

Figure 3-5 Chromatogram recorded after the third column (hydroxyapatite column), 280 nm absorption is shown in black, 412 nm absorption in red and the gradient of buffer B is shown in green. The fractions that show hydrogenase activity are marked with the blue rectangle.

After each preparation an SDS PAGE and an UV/vis spectrum were obtained to determine the sample purity and concentration, respectively. Specifically, protein concentrations were determined by measuring absorbance at 412 nm and calculated using the Beer-Lambert law and an extinction coefficient of 52500 $M^{-1}cm^{-1}$ (see Section 2.6.1).[67]

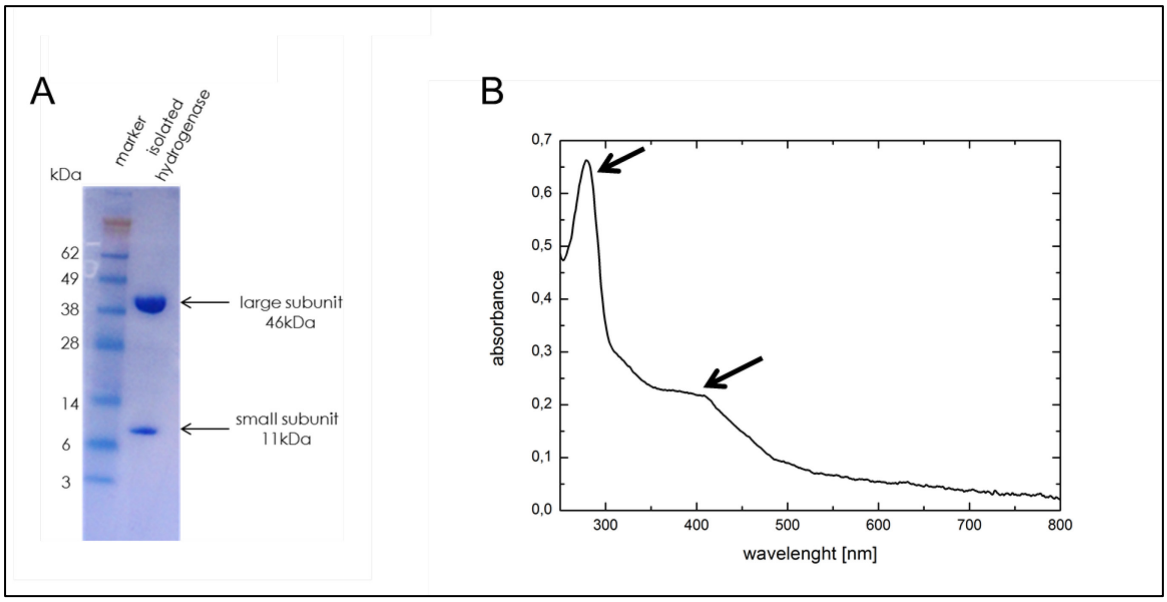

Figure 3-6 A) shows an SDS PAGE of purified *D. desulfuricans* [FeFe]-hydrogenase, the large subunit is visible at ~43 kDa and the small subunit at ~10 kDa. No other impurities are observable, which shows the high purity of the isolated protein. B) shows the UV/vis spectrum of a purified protein sample with the absorption band from the polypeptide at ~280 nm and the [Fe-S]-cluster absorption band around 412 nm. From such UV/vis spectra the sample concentrations were determined as mentioned in Chapter 2.

Routinely, a MALDI-TOF-MS spectrum was recorded in order to measure the correct sizes of both subunits of the [FeFe]-hydrogenase from *D. desulfuricans* and also to further assess the sample purity. A representative spectrum is shown in Figure 3-7.

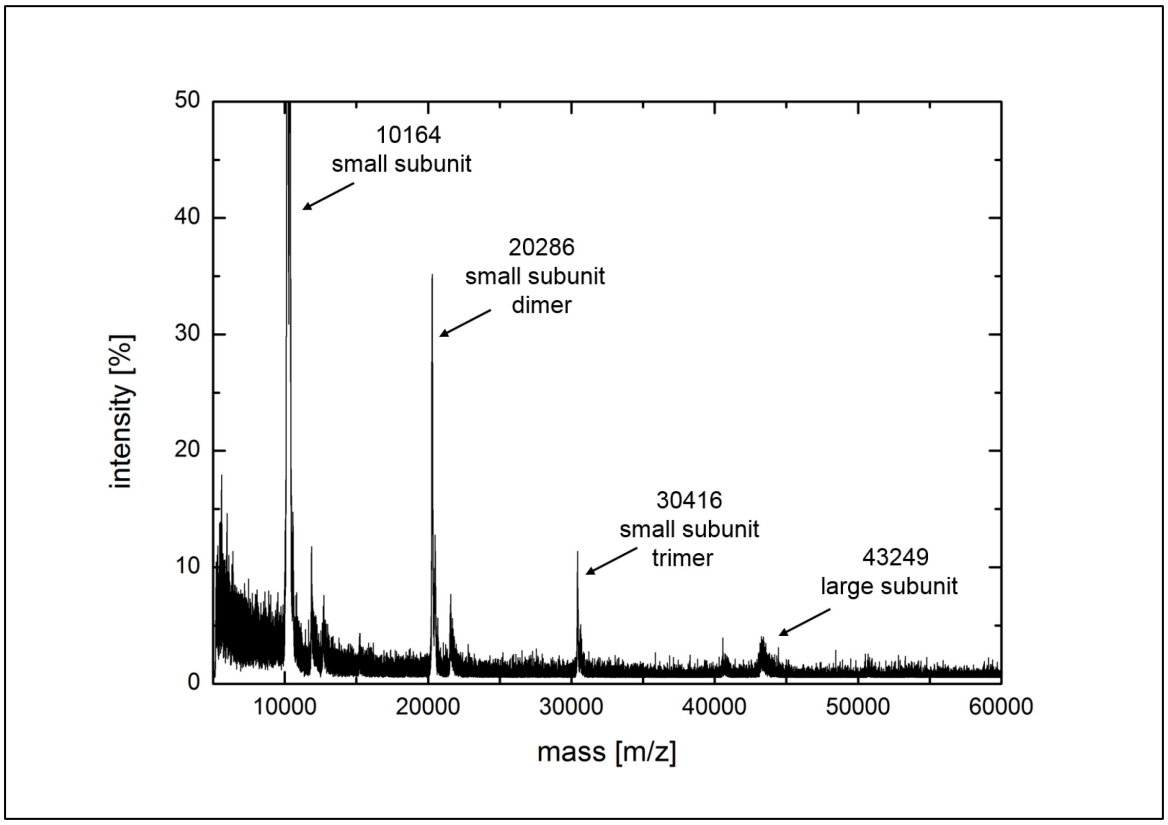

Figure 3-7 MALDI-TOF-MS spectrum of purified [FeFe]-hydrogenase from *D. desulfuricans*. The hydrogenase peaks are shown with arrows along with the masses. The measuring inaccuracy of the system is ± 150 Da. The data fit to previous reported data from literature.[30]

With these improvements in cell growth and purification, protein yields from 3.2 ± 0.3 mg/100g cells were reached. This is nearly double that reported for the old procedure (1.5 ± 0.7 mg/100g cells).[98] This could be due to the absence of oxygen during cell growth and the automatic regulation of the important growth parameters like pH or temperature. An additional, time saving advantage of establishing a larger fermentation-volume is, that now only one growth process is necessary for one preparation. (Cell yield 146 g ± 19 g/growth, 80-100 g needed for one preparation, former 50 ± 10 g cell yield/growth)

Due to the fact, that the hydrogenase activity of the resuspended pellet after precipitation is similar to the final activity it is unlikely that much enzyme is lost during preparation and the cell yield was already significantly increased simply by using the new automatic fermentation technique it was decided that the yield was unlikely to increase further by modifying the purification strategy itself.

3.3 Heterologous expression of [FeFe]-hydrogenase from *Desulfovibrio desulfuricans*

3.3.1 *Cloning strategy and design of the starting construct*

For designing a starting construct for heterologous expression of [FeFe]-hydrogenase in *E. coli,* some characteristics of the in vivo expression and maturation need to be considered. It is known, that the small subunit is preceded by an N-terminal signal peptide of 34 amino acids, while the large subunit lacks an N-terminal signal peptide.[29,126] Periplasmic hydrogenases contain a unique conserved sequence (RRXFXK) which leads to the assumption that these enzymes are exported to the periplasm via an unusual mechanism of membrane translocation.[29] But it was not clear from the sequence what the export mechanism of the large subunit is, since it lacks a leader sequence. Originally, it was proposed that a single signal peptide operates in the export of both subunits.[29,126] After the crystal structure became available it was shown, that in the electron density map beyond the amino acid Ala397 no extension of the map was possible. That shows a lack of 24 amino acids at the C-terminus of the large subunit.[30] Figure 3-8 shows the removed parts of the sequences after maturation in red.

LSU sequence	MSRTVMERIEYEMHTPDPKADPDKLHFVQIDEAKCIGCDTCSQYCPTA AIFGEMGEPHSIPHIEACINCGQCLTHCPENAIYEAQSWVPEVEKKLK DGKVKCIAMPAPAVRYALGDAFGMPVGSVTTGKMLAALQKLGFAHCWD TEFTADVTIWEEGSEFVERLTKKSDMPLPQFTSCCPGWQKYAETYYPE LLPHFSTCKSPIGMNGALAKTYGAERMKYDPKQVYTVSIMPCIAKKYE GLRPELKSSGMRDIDATLTTRELAYMIKKAGIDFAKLPDGKRDSLMGE STGGATIFGVTGGVMEAALRFAYEAVTGKKPDSWDFKAVRGLDGIKEA TVNVGGTDVKVAVVHGAKRFKQVCDDVKAGKSPYHFIEYMACPGGCVC GGGQPVMPGVLEAMDRTTTRLYAGLKKRLAMASANKA
SSU sequence	MQIASITRRGFLKVACVTTGAALIGIRMTGKAVAAVKQIKDYMLDRIN GVYGADAKFPVRASQDNTQVKALYKSYLEKPLGHKSHDLLHTHWFDKS KGVKELTTAGKLPNPRASEFEGPYPYE

Figure 3-8 Sequences of the large (LSU) and small (SSU) subunit from *Desulfovibrio desulfuricans*, the removed parts after translation are highlighted in red.

To develop a well working expression system it is necessary to generate a construct which gives high expression yields. For generating a starting construct (construct 1) the complete sequences for both subunits of the [FeFe]-hydrogenase from *Desulfovibrio vulgaris Hildenborough*, including the signal sequences was taken from the Uniprot database (LSU: P07598, SSU: P07603) because the sequences are identical to the one from *Desulfovibrio desulfuricans.*[30] Afterwards the sequences were codon optimized for *E. coli*. The codon optimization was performed by GenScript (New York, USA) and the sequences of the large and the small subunit were sent in a pUC57 vector with an amino-terminal Strep-II tag and Tev-protease cleavage site on the large subunit and restriction sites for subcloning into the pACYC-Duet-1 expression vector. The design and generating of the starting construct (1) were done by Dr. J. Birrell in our laboratory, who also supervised the whole establishment of the heterologous expression.

```
Optimized      4   ATGCAGATCGCTAGTATTACCCGTCGCGGCTTCCTGAAAGTTGCTTGTGTTACCACCGGC
Original       4   ATGCAGATAGCCAGCATCACCCGGCGCGGCTTCCTCAAGGTCGCCTGCGTCACGACGGGC

Optimized     64   GCAGCTCTGATTGGCATCCGTATGACCGGCAAAGCGGTGGCGGCCGTTAAACAGATTAAA
Original      64   GCAGCCCTCATCGGCATTCGCATGACCGGAAAGGCCGTTGCCGCCGTCAAGCAGATCAAG

Optimized    124   GATTATATGCTGGACCGTATCAACGGCGTCTACGGTGCAGATGCTAAATTTCCGGTGCGC
Original     124   GACTACATGCTTGACCGCATCAACGGCGTCTACGGGGCGGATGCCAAGTTCCCCGTTCGC

Optimized    184   GCGAGTCAGGACAATACCCAAGTTAAAGCCCTGTATAAAAGCTACCTGGAAAAACCGCTG
Original     184   GCCTCGCAGGACAACACGCAGGTCAAGGCTCTCTACAAGAGCTACCTTGAGAAGCCTCTC

Optimized    244   GGCCATAAATCTCACGATCTGCTGCATACGCACTGGTTCGACAAAAGCAAAGGTGTCAAA
Original     244   GGTCACAAGTCGCACGACCTGCTGCACACGCACTGGTTCGACAAGTCCAAGGGCGTCAAG

Optimized    304   GAACTGACCACGGCTGGTAAACTGCCGAACCCGCGTGCGTCCGAATTTGAAGGTCCGTAT
Original     304   GAACTCACCACGGCAGGCAAGTTGCCCAACCCGCGTGCTTCCGAGTTCGAAGGTCCGTAC

Optimized    364   CCGTATGAATAA
Original     364   CCCTACGAATAG
```

Figure 3-9 Alignment of the original and the codon optimized sequence from the small subunit in *D. desulfuricans*. The optimized parts are highlighted in red.

```
Optimized     6   GGTTGGTCGCACCCGCAGTTTGAAAAATCGTCAGGTCGTGAAAATCTGTACTTCCAGGGC
Original      6   GGCTGGAGCCACCCGCAGTTCGAAAAAAGCAGCGGCCGTGAAAACTTGTATTTCCAGGGC

Optimized    66   TCCCGCACCGTGATGGAACGCATTGAATATGAAATGCATACCCCGGATCCGAAAGCCGAT
Original     66   AGCCGTACCGTCATGGAGCGCATCGAATATGAGATGCACACTCCGGACCCCAAGGCCGAT

Optimized   126   CCGGACAAACTGCACTTTGTGCAGATTGATGAAGCAAAATGCATCGGCTGTGACACCTGC
Original    126   CCGGACAAGCTCCACTTCGTCCAGATCGACGAGGCAAAGTGCATAGGCTGCGACACCTGT

Optimized   186   AGTCAATACTGCCCGACGGCGGCCATTTTCGGTGAAATGGGCGAACCGCATTCCATTCCG
Original    186   TCGCAGTACTGCCCCACCGCCGCCATCTTCGGCGAAATGGGCGAACCGCACTCCATTCCC

Optimized   246   CACATCGAAGCATGTATTAACTGCGGCCAGTGTCTGACCCATTGCCCGGAAAATGCGATC
Original    246   CACATCGAGGCGTGCATCAACTGCGGCCAGTGCCTCACGCACTGCCCCGAGAACGCCATC

Optimized   306   TATGAAGCCCAATCATGGGTGCCGGAAGTTGAGAAAAAACTGAAAGATGGTAAAGTGAAA
Original    306   TACGAGGCACAGTCGTGGGTGCCTGAAGTCGAGAAGAAGCTGAAGGACGGCAAGGTGAAA

Optimized   366   TGTATTGCCATGCCGGCACCGGCTGTTCGTTACGCACTGGGTGACGCTTTTGGCATGCCG
Original    366   TGCATCGCCATGCCCGCCCCCGCCGTGCGCTATGCACTGGGCGACGCCTTCGGCATGCCC

Optimized   426   GTCGGTTCAGTGACCACGGGCAAAATGCTGGCAGCTCTGCAGAAACTGGGTTTTGCACAT
Original    426   GTCGGTTCCGTCACCACCGGCAAGATGCTCGCGGCCCTGCAGAAGCTCGGCTTCGCTCAT

Optimized   486   TGTTGGGATACCGAATTCACGGCTGACGTCACCATCTGGGAAGAAGGCTCGGAATTTGTT
Original    486   TGCTGGGACACCGAGTTCACCGCTGACGTGACCATCTGGGAAGAGGGGTCCGAGTTCGTG

Optimized   546   GAACGTCTGACCAAAAAATCTGATATGCCGCTGCCGCAGTTCACGTCTTGCTGTCCGGGT
Original    546   GAACGCCTCACCAAGAAGAGCGACATGCCGCTGCCGCAGTTCACCTCGTGCTGCCCCGGC

Optimized   606   TGGCAAAAATATGCGGAAACCTATTACCCGGAACTGCTGCCGCACTTTAGTACGTGCAAA
Original    606   TGGCAGAAGTATGCCGAGACCTACTACCCCGAACTGCTGCCGCACTTCTCCACGTGCAAG

Optimized   666   TCCCCGATTGGTATGAACGGCGCGCTGGCCAAAACCTATGGCGCGGAACGCATGAAATAT
Original    666   TCGCCCATCGGCATGAACGGCGCACTGGCGAAGACCTACGGCGCAGAGCGGATGAAGTAC

Optimized   726   GATCCGAAACAGGTTTACACGGTCTCCATTATGCCGTGTATCGCCAAAAAATACGAAGGC
Original    726   GACCCCAAGCAGGTCTACACCGTCTCCATCATGCCCTGCATCGCAAAGAAGTACGAAGGG

Optimized   786   CTGCGTCCGGAACTGAAAAGCTCTGGTATGCGCGATATCGACGCGACCCTGACCACGCGT
Original    786   TTGCGTCCCGAACTGAAGTCCAGCGGCATGCGCGACATCGACGCCACGCTGACCACCCGT

Optimized   846   GAACTGGCCTATATGATCAAAAAAGCGGGTATCGATTTTGCCAAACTGCCGGATGGCAAA
Original    846   GAGCTGGCCTACATGATCAAGAAGGCCGGTATCGACTTCGCGAAACTCCCCGACGGCAAG

Optimized   906   CGTGACTCACTGATGGGTGAATCGACCGGCGGTGCGACGATTTTTGGCGTGACCGGCGGT
Original    906   CGTGACAGCCTCATGGGTGAATCCACCGGCGGTGCCACCATCTTCGGCGTCACCGGCGGC

Optimized   966   GTTATGGAAGCGGCCCTGCGCTTCGCATACGAAGCTGTGACCGGTAAAAAACCGGATAGC
Original    966   GTCATGGAAGCGGCACTCCGCTTCGCCTACGAAGCCGTCACCGGCAAGAAGCCCGACAGC

Optimized  1026   TGGGACTTCAAAGCGGTTCGTGGTCTGGATGGCATCAAAGAAGCCACCGTCAATGTGGGC
Original   1026   TGGGACTTCAAGGCCGTGCGCGGTCTTGATGGCATCAAGGAAGCCACCGTCAACGTCGGC
```

```
Optimized  1086   GGTACGGACGTTAAAGTCGCAGTGGTTCATGGCGCTAAACGCTTTAAACAGGTCTGCGAT
Original   1086   GGTACCGACGTCAAGGTCGCCGTGGTGCACGGGGCCAAGCGGTTCAAGCAGGTCTGCGAC

Optimized  1146   GACGTGAAAGCCGGTAAATCTCCGTATCACTTCATTGAATACATGGCTTGTCCGGGCGGT
Original   1146   GATGTGAAGGCGGGCAAGTCGCCCTATCACTTCATCGAATACATGGCCTGCCCCGGCGGC

Optimized  1206   TGCGTGTGTGGCGGTGGCCAACCGGTTATGCCGGGTGTCCTGGAAGCGATGGATCGTACC
Original   1206   TGCGTCTGTGGCGGCGGTCAGCCCGTCATGCCCGGCGTGCTCGAAGCCATGGACCGCACC

Optimized  1266   ACGACCCGTCTGTATGCTGGTCTGAAAAAACGCCTGGCAATGGCCTCGGCAAATAAAGCC
Original   1266   ACCACCCGCCTTTACGCGGGCCTGAAGAAGCGCCTCGCCATGGCGAGCGCCAACAAGGCA

Optimized  1326   TAA
Original   1326   TAG
```

Figure 3-10 Alignment of the original and the codon optimized sequence from the large subunit in *D. desulfuricans*. The optimized parts are highlighted in red.

To generate the staring construct (1) with both subunits on one expression vector, both genes were cloned together into the expression vector pACYCDuet-1 (a vector card is shown in the appendix), which has a lac O promotor to overexpress the protein of interest by adding the artificial inductor Isopropyl β-D-1thiogalactopyraniside (IPTG) and a chloramphenicol resistance.

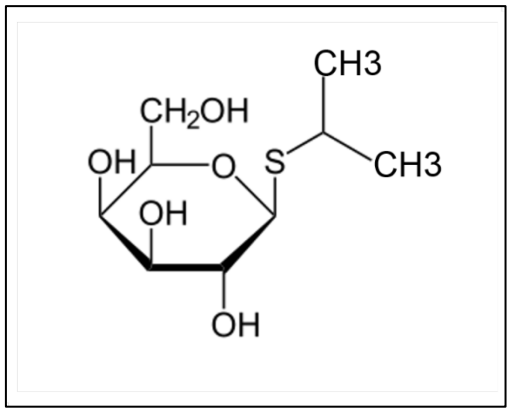

Figure 3-11 Structure of IPTG

The following Figure 3-12 shows a scheme how to generate the starting construct (1) for over-expression of the [FeFe]-hydrogenase from *D. desulfuricans* in *E. coli*. For that the pUC57 vector containing the large subunit gene and the pACYDuet-1 vector were simultaneously digested with the restriction enzymes NcoI and HindIII. Afterwards the products were run on an agarose-gel and the bands were gel purified and mixed in a ratio of five equivalents of insert to one equivalent of vector and ligated. These ligation products were transformed into *E. coli* cells and afterwards the DNA from overnight cultures were sequenced. The sequencing showed that the correct construct (pACYDuet-1 vector with the large subunit) was produced. Next the small subunit from the pUC57 vector was inserted in an analogous way. For that the pACYDuet-1 vector with the large subunit and the pUC57 vector containing the small subunit were simultaneously digested with the restriction enzymes NdeI and XhoI. The gel purification, ligation and transformation procedures were identical to the one just described. Sequencing confirmed the generating of the right product.

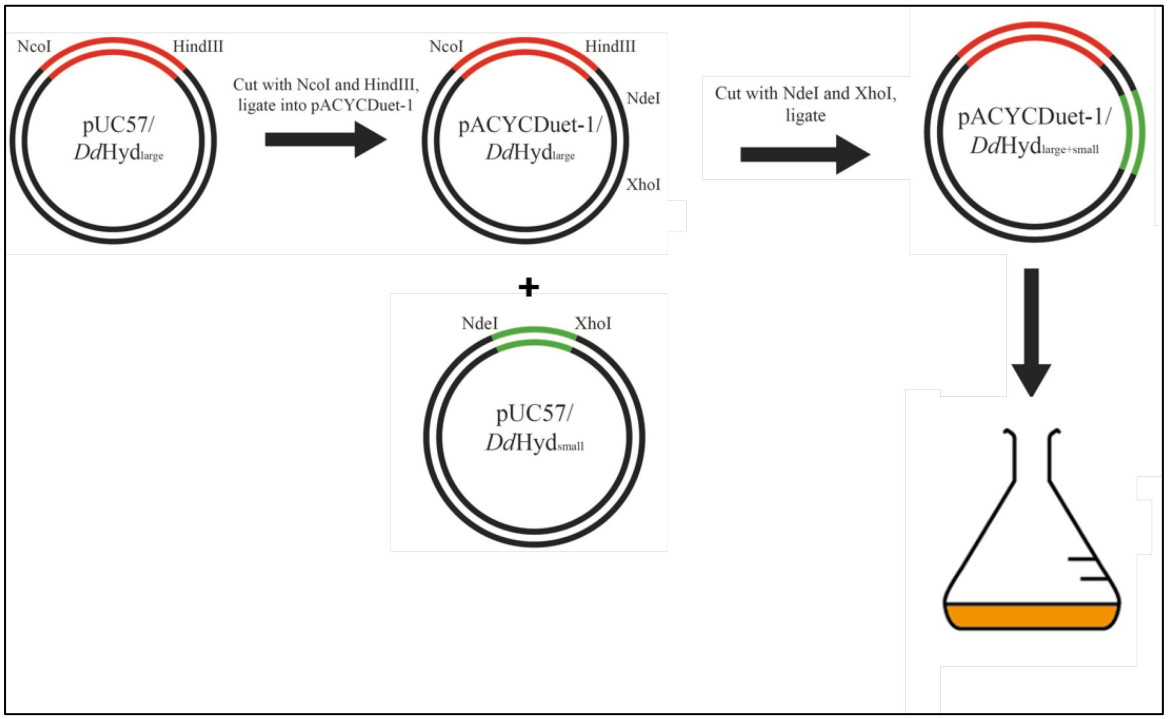

Figure 3-12 Overview of the cloning strategy to create the starting plasmid (1).

After finishing the sub-cloning, and checking the construct for correctness by sequencing, construct (1) (a scheme is given in Figure 3-14) contains:

- an N-terminal affinity tag, the Strep-tag II, which allows a fast and easy purification with a strep-tactin column. Strep-tag II is a short peptide tag, formed by eight amino acids (WSHPQFEK), the structure is given in Figure 3-13.

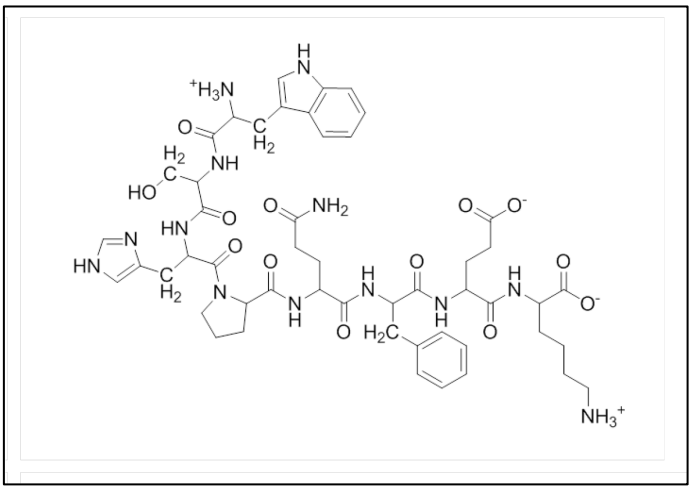

Figure 3-13 Chemical structure of the Strep-tag II.

- a TEV (Tobacco Etch Virus) protease cleavage site between the Strep-tag II and the large subunit sequence to remove the affinity tag if necessary. An advantage of this enzyme is its high specificity for the sequence ENLYFQ I S, where the “I” denotes the cleaved peptide bond.

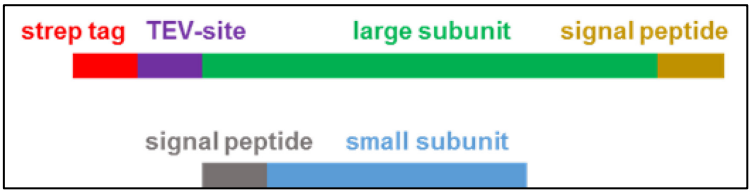

Figure 3-14 Schematic drawing of the starting construct (1) for over-expression in *E. coli*.

The correct construct 1 was transformed into *E.coli* BL21(DE3)ΔiscR for high level protein expression.[60] This strain has a knockout insertion in the iron-sulfur cluster (isc) synthesis pathway operon gene, allowing constitutive expression of the isc operon. This makes the strain particularly useful for expression of iron-sulfur cluster proteins, such as hydrogenases, and has been used previously by several different research groups.[60,62,127]

An agarose gel of the PCR products was performed after PCR and DpnI digest, the following Figure 3-15 shows representative the PCR product of construct 2 (remove of strep tag II and Tev-sequence, see Table 3-3) but since all subsequent gels looked almost identical they have been omitted.

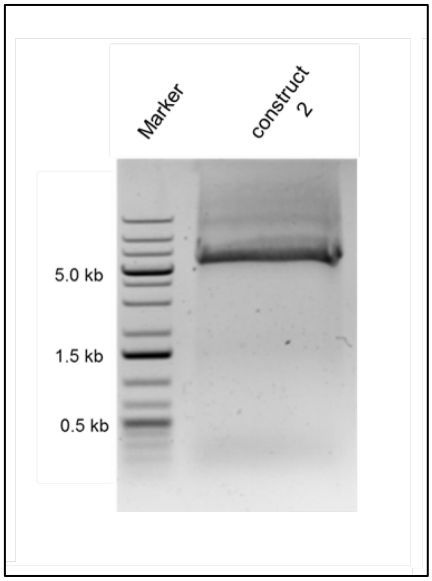

Figure 3-15 Agarose-gel of construct 2 after PCR and DpI digestion. Marker: GeneRuler 1 kb Plus DNA ladder. Size of the construct is 5498 bps.

In the beginning an expression by using the construct (1) and the expression protocol based on the one reported by Kuchenreuther et al.[62] was tested.

For that, 1L of LB-MOPS (pH 7.4) media was inocculated with 5 ml of an overnight culture. 0.5 % glucose, 2 mM ferric ammonium citrate (FeAmCit) and the antibiotics kanamycin and chloramphenicol (see Chapter 2) were added and the cells were grown at 37 °C to an optical density of 0.3-0.5 (OD_{600nm}). To the culture 25 mM sodium fumarate and 2 mM L-cysteine were added before the culture was purged with argon gas for

30 min and then the protein expression was induced with 0.5 mM IPTG. After 20 h incubation at room temperature the cells were harvested by centrifugation anaerobically and resuspended in 50 mL cold lysis buffer (25 mM Tris (pH 7.6), 25 mM KCl, 2 % glycerol, 0.1 % Tween-20, 1 mM DTT, 3 mM NaDT and 0.2 mM PMSF). Afterwards the cells were broken by sonication and the cell debris and insoluble material was removed by centrifugation. The supernatant was loaded onto a streptactin column equilibrated in lysis buffer. The bound protein was washed with lysis buffer and eluted with elution buffer (lysis buffer + 2.5 mM desthiobiotin).

Using this protocol a good protein expression level was achieved, but the protein was found to be mainly insoluble (see Figure 3-16).

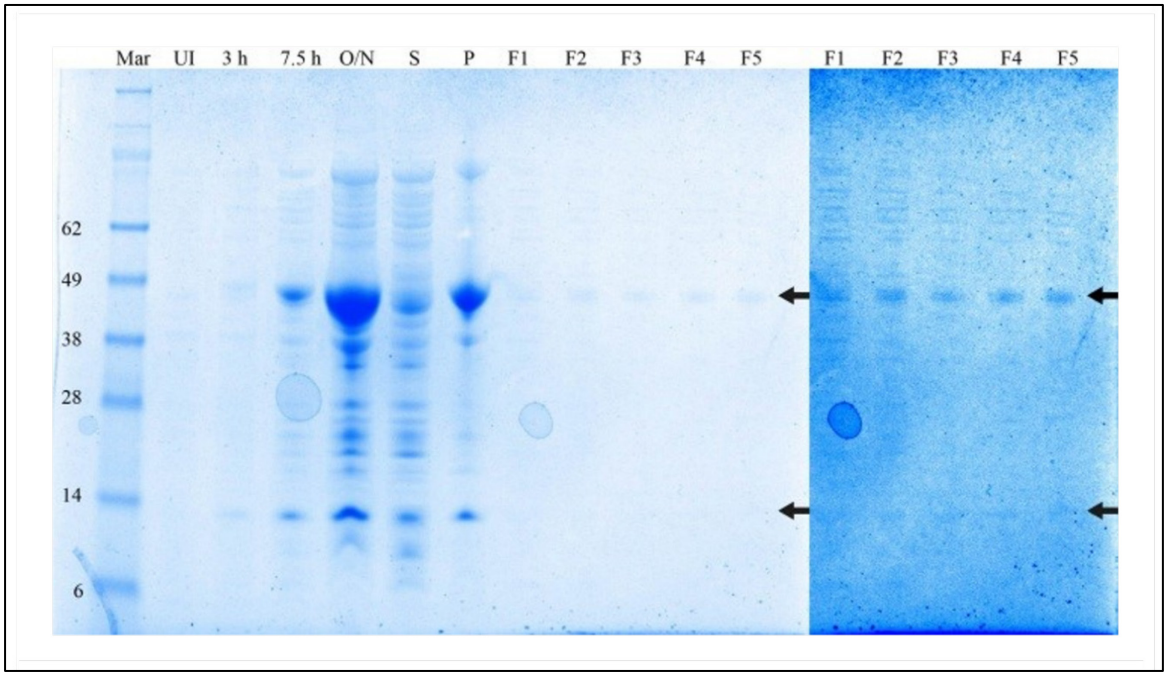

Figure 3-16 SDS PAGE of the over-expression (construct 1). Mar: molecular weight markers in kDa; Ui: uninduced cells; 3h, 7.5h O/N: cells induced for 3h, 7.5 h and overnight (20 h); S: supernatant after sonication; P: pellet after sonication; F1-F5: fractions eluted from Streptactin column. The arrows indicate the position of the hydrogenase subunits bands. The right figure is identical to the left one but with a higher contrast to make the bands better visible.

Next, screenings of different expression and purification conditions was attempted. The induction with IPTG was tested at lower and higher OD_{600nm}. It is known that these conditions are specific to each protein, but is it also known, that if the expressed protein is unstable or tends to precipitate, then an induction at lower OD might help. Additionally, different proteins are expressed at different growth states of the cell, so also a higher inducing OD might results in a better protein expression. Furthermore the optimal IPTG concentration depends on the protein, so far it is impossible to predict the optimal amount, and due to this a lower (0.1 mM) and higher (2 mM) concentration of the inducer were tested. It is known, that sometimes insoluble or precipitating proteins aggregated faster at higher temperatures due to the increased strength of hydrophobic effects. Therefore expression at different temperatures (16 °C, RT, 37 °C) were tested. Afterwards, several expression times were tested to see if shorter expression time may help to keep the hydrogenase in the soluble fraction (see Figure 3-17).

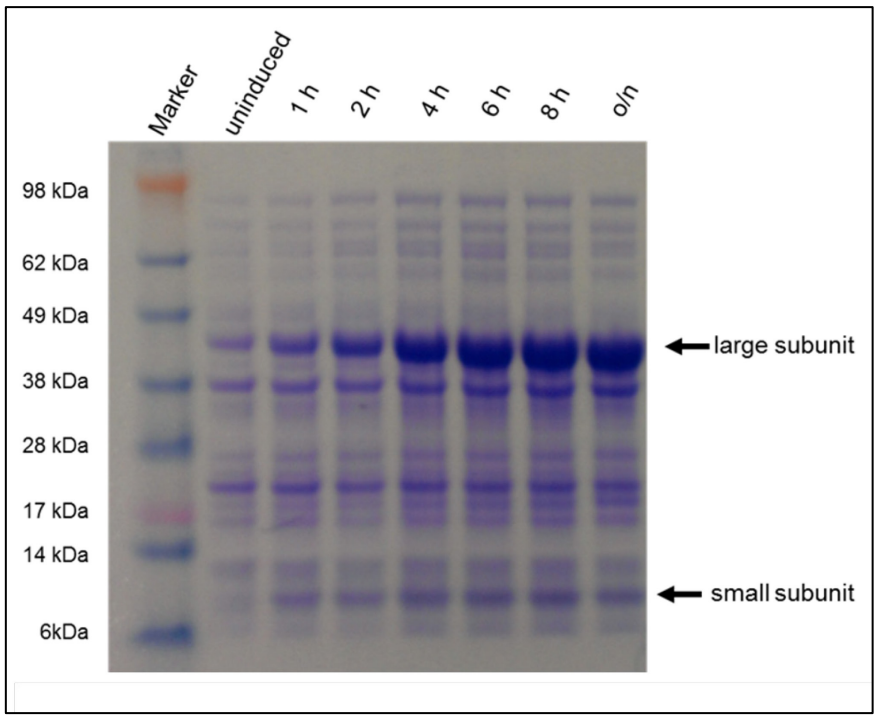

Figure 3-17 SDS-PAGE to determine the optimal expression time. Samples were adjusted to identical cell densities.

From this SDS-PAGE it can be seen, that after one hour the protein expression is only just detectable, but after that the level of expression increases steadily with time until eight hours of expression. But even overnight the expression level shows still a further increase. Because the apparent levels of protein from SDS-PAGE analysis were highest in the overnight expressed cultures and because leaving the cultures overnight rather than harvesting them after eight hours is more convenient the expression overnight was carried out in all future protein over-expression experiments.

As it was mentioned in Section 3.2.2 sonication is not a very gentle method for cell disruption and, in order to avoid potential damage by this procedure, variation in the number of sonication cycles were tested. The optimal number of sonication cycle is, when most of the cells are disrupted but the sonication does not lead to damage of the protein. For that, after each sonication a sample from the cell suspension was taken and centrifuged, afterwards the same amount was run onto a SDS-PAGE (see Figure 3-18).

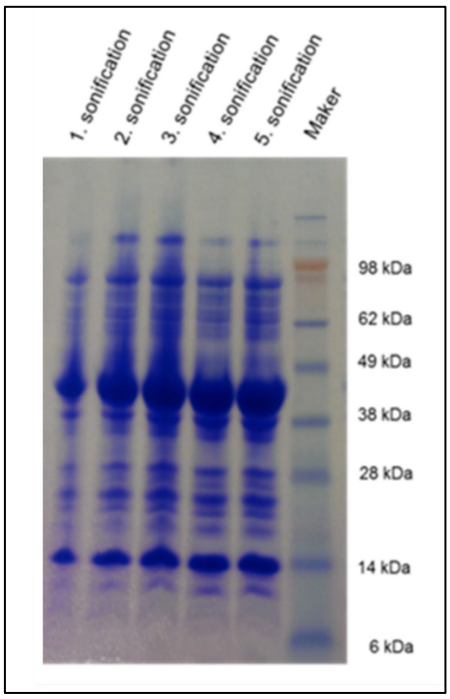

Figure 3-18 SDS PAGE to determine the optimal number of sonication cycles. Therefore, a sample of the cell suspension was centrifuged and applied onto the gel.

From this Figure 3-18 it can be seen, that in the first three sonication steps the amount of free protein increases from step to step, but after step three no further increase in protein amount can be observed. Therefore, three sonication steps of one minute with resting time in between are enough to disrupt most of the cells.

For all these attempted conditions one large culture was grown and split at regular intervals to allow induction with different amounts of IPTG at specific OD. Only one culture was used to avoid differences in protein expression caused by different batches of pre-culture.

An essential part of the expression system is the expression media which can also lead to different protein yields, therefore different standard media like LB, 2xYT, TB, SOB and M63 were tested in additional test-expressions. Here the other conditions were kept the same.

Unfortunately none of the tested conditions improved the solubility of the [FeFe]-hydrogenase significantly, this was tested by SDS PAGE. The following Table 3-2 summarizes the tested conditions.

Table 3-2 Summary of the tested expression conditions to achieve a high yield of soluble protein.

tested conditions
Induction at higher and lower OD_{600nm}
Induction with lower (0.1 mM) and higher (2 mM) IPTG
Different expression times (2h, 5h, 20h)
Different expression temperatures (RT, 16 °C)
Different expression media (LB, 2xYT, TB, SOB, M63)
Different number of sonication cycles (1-5)

Because changing of the expression conditions did not lead to higher amounts of soluble protein it was decided to change the construct (1) to see if it is possible to increase the solubility. The modifications of the construct (1) and the optimization of the over-expression and purification are discussed in the following Section 3.3.2.

3.3.2 *Modifications of the construct*

It has been shown previously, that the position of affinity purification tags can affect protein folding and, therefore, the Strep-tag II was moved to the C-terminus of the large subunit and to either the end of the small subunit. It was also decided that a C-terminal TEV-cleavage site was not necessary, because cleavage would still leave a polypeptide extension as long as the Strep-tag II itself. As reported in Section 3.3.1, both the large and the small subunit have signal peptides at their C-terminal end (large subunit) and their N-terminal (small subunit). Constructs, in which these sequences were removed were also tested.

The Strep-tag II and the TEV sequence were removed by PCR using the primers reported in Chapter 2. A scheme for the cloning construct 6 (via construct 2) is shown in Figure 3-19. In a first step it was necessary to remove the Strep tag II and Tev-sequence from the starting product by PCR. After DpnI digestion and gel purification (from an agarose gel) the linear PCR product was ligated and transformed into *E. coli.* Purified DNA from overnight cultures was checked for correctness by sequencing. From this construct 2 other constructs can be generated by the same procedure: PCR to insert the Strep tag II at a defined position, DpnI digestion and gel purification. Afterwards, ligation, transformation into *E. coli* and sequencing to check the construct were performed.

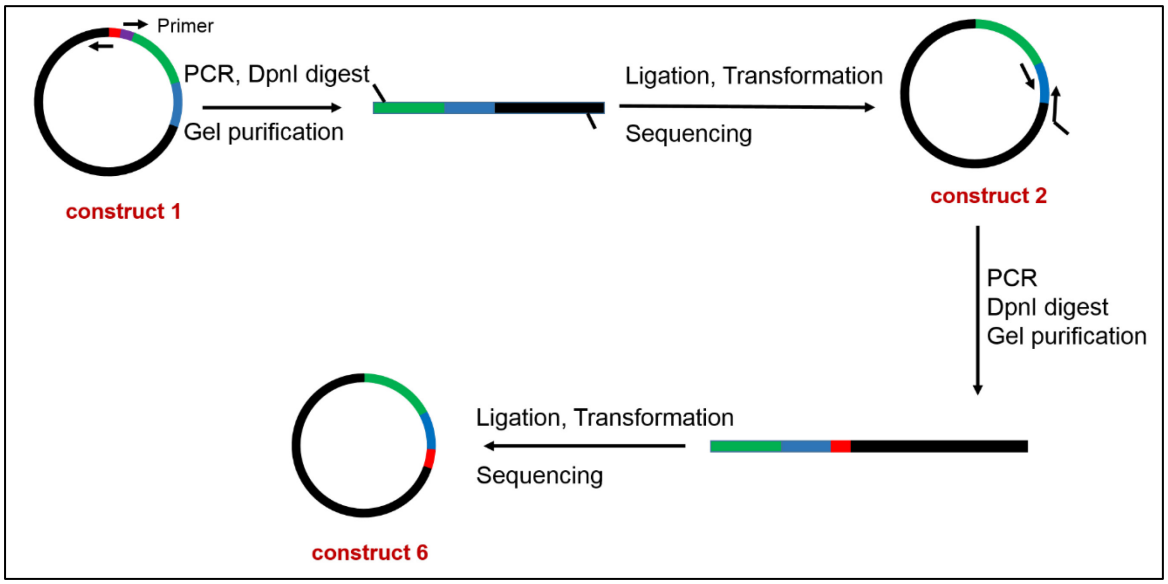

Figure 3-19 Cloning scheme for generating construct 6 starting from construct 1. For generating other mutants, the Step tag II and the Tev-sequence need to be removed in the first step via PCR. After DpnI digest and gel purification this product was ligated and transformed into *E. coli*. Afterwards, overnight cultures were checked for correctness with sequencing. From the right construct the DNA was purified and a second PCR for insertion of the Strep tag II at a certain position was performed. Also here DpnI digest, gel purification, ligation and transformation was done and the final construct 6 was checked for correctness by sequencing. In this scheme the signal peptides at the large- and small subunit are not marked, for a better lucidity.

DNA sequencing confirmed that the construct (2) was correct. Next, the Strep-tag II was introduced at the C-terminus of the large subunit (construct 3,5), small subunit (construct 6,7) and the N-terminus of the small subunit (construct 8), also by PCR. The sequences of the final constructs are shown in Table 3-3. All constructs were checked by DNA sequencing. Afterwards the correct plasmids were transformed into *E. coli* BL21(DE)ΔiscR cells and tested for expression of soluble protein.

Table 3-3 Overview of different modifications of the starting plasmid 1, done by PCR.

generated construct	modification	template	primer	scheme
construct **2**	remove nt tag and TEV site from LSU	construct 1 (Figure 3-14)	1A forward 1A reverse	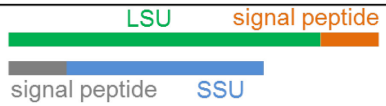
construct **3**	add ct tag to LSU	construct 2	2A forward 2A reverse	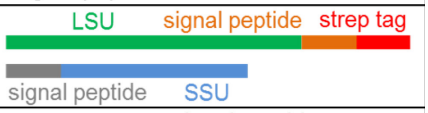
construct **4**	remove preseq.from SSU	construct 1	4 forward 4 reverse	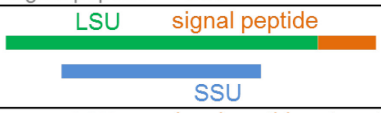
construct **5**	add ct tag to LSU no preseq. at SSU	construct 4	2A forward 2A reverse	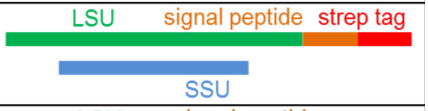
construct **6**	add ct tag to SSU	construct 2	6A forward 6A reverse	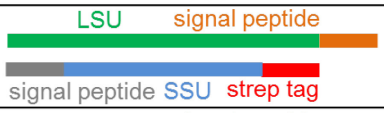
construct **7**	add ct tag to SSU no preseq. at SSU	construct 4	6A forward 6A reverse	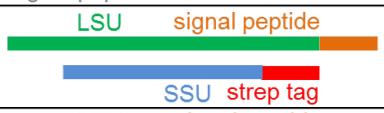
construct **8**	add nt tag to SSU no preseq. at SSU	construct 4	5A forward 5A reverse	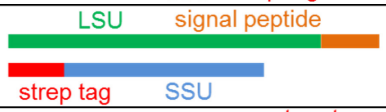
construct **9**	remove ct signal seq. from LSU, no preseq. at SSU	construct 5	7 forward 7 reverse	

After checking the constructs by sequencing the right plasmids were transformed into ΔiscR cells and protein expression tests were performed using the protocol described in Section 2.3.2 and 2.4.2; an SDS PAGE was done to see the different expression levels. The gel is shown in Figure 3-20.

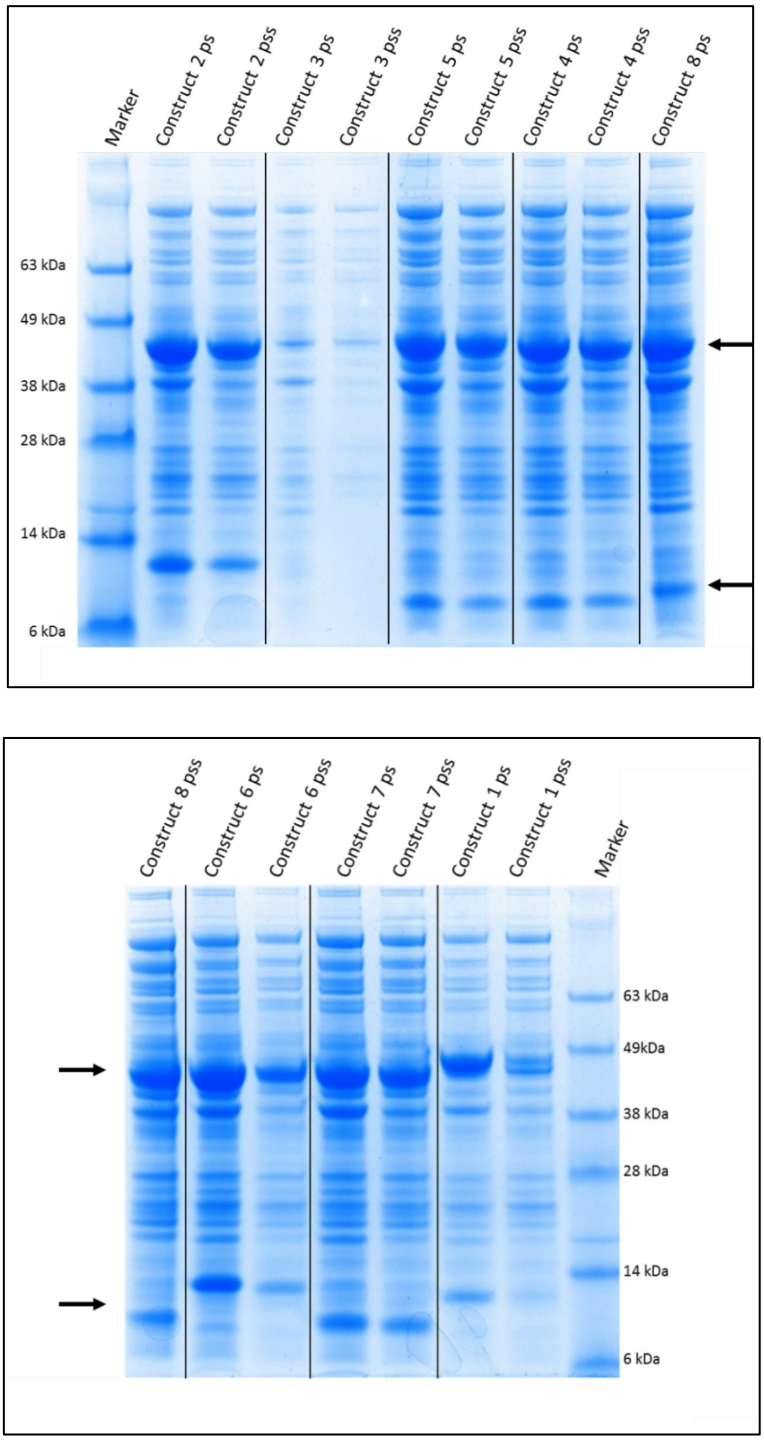

Figure 3-20 SDS-PAGE of expressed constructs. ps: post sonication, pss: post sonication supernatant (after ultracentrifugation), construct 2: no tag, no TEV site, construct 3: ct tag at large subunit, no TEV site, construct 5: same as construct 3 but without pre-sequence at small subunit, construct 4: no tag, no TEV site, no pre-sequence at small subunit, construct 8: nt tag at small subunit, no pre-sequence at small subunit, no TEV site, construct 6: ct tag at small subunit, no TEV site, construct 7: same as construct 6 but without pre-sequence at small subunit, construct 1: nt tag at large subunit, with TEV site at large subunit.

From this Figure 3-20 it can be seen, that constructs 1 and 3 show in general a low expression level, so that they are not considered to become the “standard construct”. Constructs 2 and 6 show a good expression level but yield only poor soluble protein. As it is obvious from this figure the other constructs (4, 5, 7, 8) show not much difference between each other, so the strep tag II on the large subunit (construct 5) was chosen because than it is possible to test whether a good expression of the large subunit in the absence of the small subunit can be achieved.

Also the carboxy-terminal truncation of the large subunit (see Section 3.3.1) with a carboxy-terminal Strep-tag II at the large subunit and no pre-sequence at the amino-terminal end of the small subunit was generated (construct 9). In the beginning this sequence was not removed, because the earlier generated construct 5 worked well and we were not aware that there is also a pre-sequence at the small subunit. That means, early experiments of this thesis were done with construct 5 but after construct 9 was available, we checked the behaviour of this construct and found, that construct 5 and 9 behave identical (activity measurements and spectroscopic experiments) except for crystallization, which worked only with construct 9 (see Section 4.2.1).

From the expression tests of the different constructs it can be concluded that the pre-sequence of the small subunit needs to be removed to be able to generate high yields of soluble protein. It seems like, that the large subunit is also stable with the pre-sequence while the small subunit is not. Or another possibility is, that the small subunit can only bind to the large subunit in a proper way, if the pre-sequence at the small subunit is removed.

During this thesis it was also tested if it is possible to only express the large subunit and if this construct can be activated. Therefore, the construct was generated by PCR as reported for the other mutants. After checking the construct by sequencing the expression was tested, as reported in Section 2.3.2 and 2.4.2. As it is visible from Figure 3-21 which shows the SDS-PAGE for this expression, it is clear that no soluble protein is expressed. That also confirms the assumption, that a correct folding of the large subunit is only possible in the presence of the small subunit.

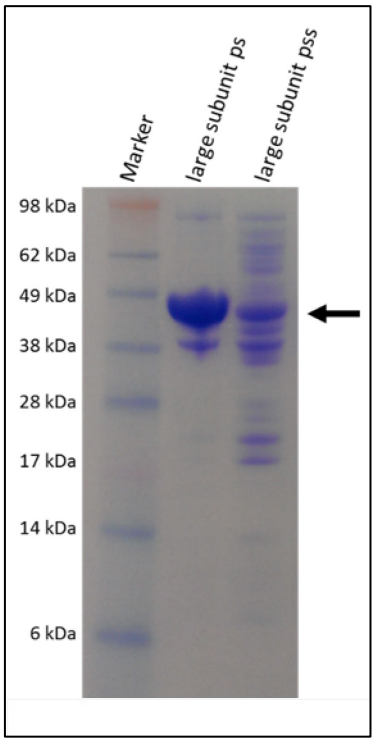

Figure 3-21 SDS PAGE of the over-expressed large subunit only. As it is visible, there is almost no soluble protein expressed. ps: post sonication, pss: post sonication supernatant (after ultracentrifugation)

3.3.3 *Optimization of the over-expression and purification procedure for [FeFe]-hydrogenase from D. desulfuricans*

All optimization steps of the previous reported overexpression were re-tested with construct 5.

During the first test-expressions samples at different time points have been collected and the pH was checked. It was shown, that the pH during expression changes in an irreproducible way. Therefore, LB media with additional phosphate (see Section 2.2.2) was tested. In the beginning a LB-MOPS medium was used, but it was decided to change to phosphate, because it is possible to add more phosphate to stabilize the pH than in case of MOPS. An additional advantage of phosphate is that it is cheap and can be autoclaved.

[FeFe]-hydrogenases are [Fe-S]-proteins, therefore the iron and the sulfate in the growth media were expected to play a major role for protein expression. For that, different

concentrations of cysteine and FeAmCit (iron ammonium citrate) were tested. This yields to an overall amount of 5 mM of L-cysteine.

The same expression tests were performed to determine the optimal concentration of FeAmCit and also here an increase of the amount in the culture by two fold gave the best expression yields of [FeFe]-hydrogenase. Therefore, an increased amount from 2 mM of FeAmCit to 4 mM in the culture was used for further expressions. Due to the fact, that optimization of the expression method and the optimization of the construct were done simultaneously, no exact values for protein yield with different FeAmCit and cysteine concentrations can be given.

It is reported for hydrogenases, that a heterologous expression works best under anaerobic conditions[62], to confirm this also for the [FeFe]-hydrogenase from *D. desulfuricans* an aerobic expression was tested. The expression under aerobic conditions gave nearly the same amount of cells, but after purification (aerobic and anaerobic purification were tested) under both conditions the yield of unmaturated protein was ten times less than after anaerobic expression and anaerobic purification.

After the development of construct 5 and optimization of the construct, the over-expression procedure and the purification method a new, reproducible standard preparation for [FeFe]-hydrogenase was established. Standard yields from this modified procedure are 200 µL of 1 mM unmaturated protein from 2 L of culture, the concentration was quantified by the DC protein assay (see Chapter 2). This yield is a bit less, than the yields which are reported for other over-expressed [FeFe]-hydrogenases.[62] For comparison, HydA1 from *Chlamydomonas reinhardtii* gives yields of 30 ± 11 mg L^{-1} of culture and the one from *Clostridium pasteurianum* (CpI) 7.9 ± 0.8 mg L^{-1} of culture, while the expression of 5.2 ± 1.2 mg L^{-1} of culture was reached for *D. desulfuricans.* Maybe this can be explained by the different amount of inserted [Fe-S]-clusters, because the expression yields for *D. desulfuricans* and *Clostridium pasteurianum* are quite similar. Both of them harbour additional [4Fe-4S]-clusters, while the hydrogenase from *C. reinhardtii* has no additional F-clusters (see Figure 3-22).

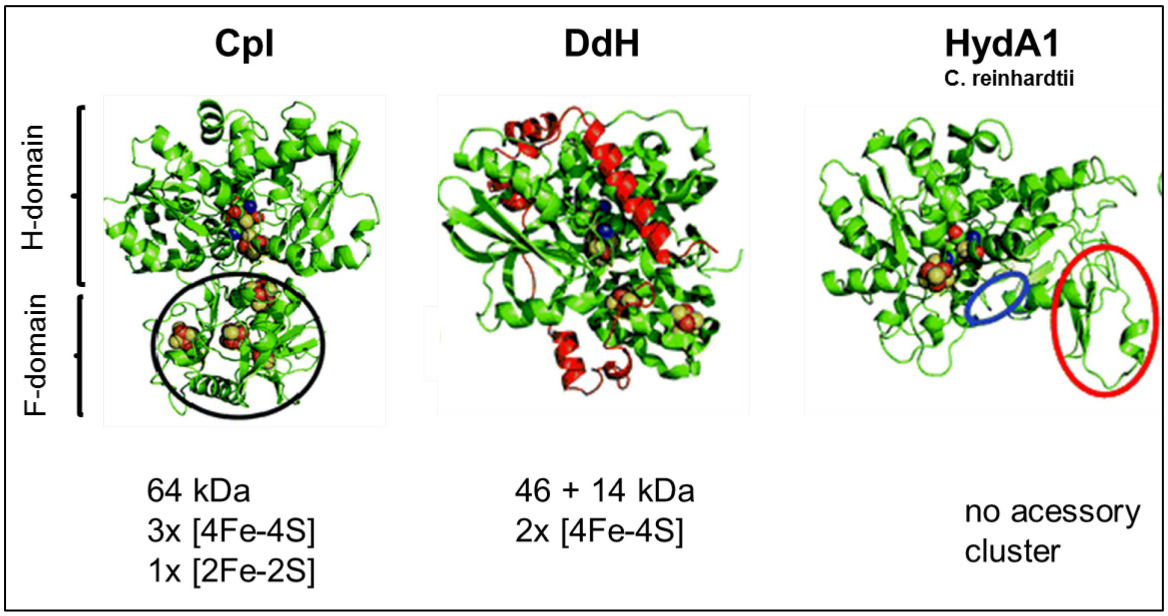

Figure 3-22 Comparison of [FeFe]-hydrogenases with their F-cluster regions. The structures are shown as cartoons. The model of HydA1 has been designed by homology modelling. For CpI the F-domain in marked black and contains 4 clusters. In DdH the small subunit is shown in red and the two accessory clusters are harboured in the large subunit. HydA1 has no acessory clusters but shows an algal-specific "insertion" which is marked in red. In blue a positively charged binding niche for interaction with ferredoxin is marked. Figure adapted from[128]

For checking the purity of the sample SDS-PAGE (see Figure 3-23) was done during all purification steps. An additional method to check the purity and determine iron-sulfur cluster content in the protein is UV/vis spectroscopy. An example spectrum of the unmaturated protein is shown below in Figure 3-23.

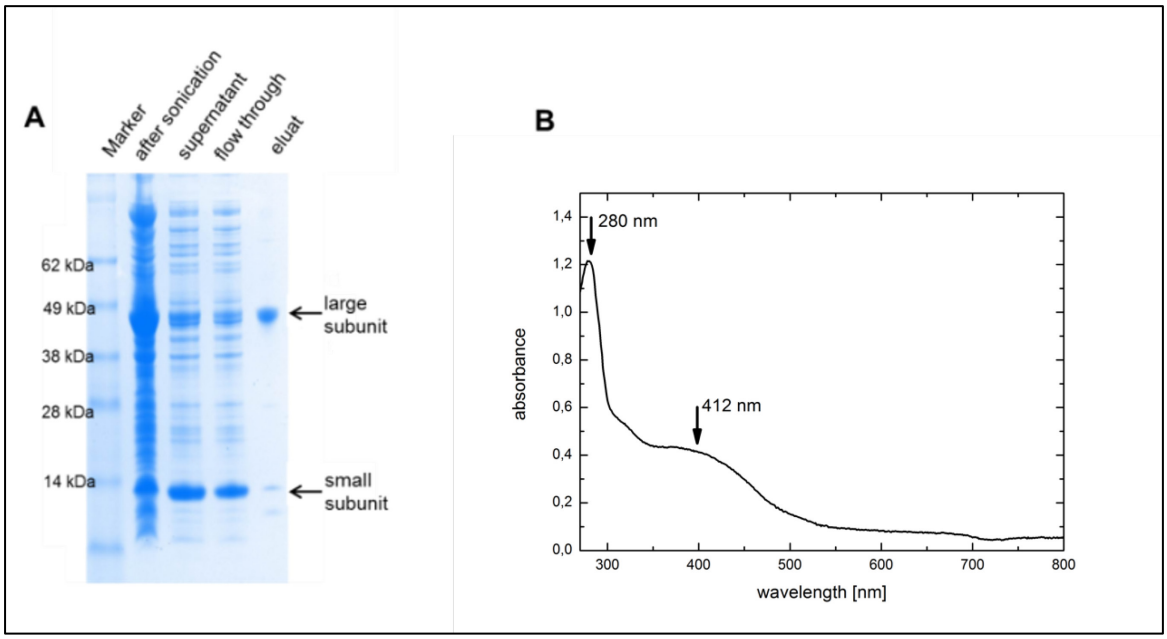

Figure 3-23 A shows an SDS PAGE from a "standard" expression of construct 5. The first lane next to the marker shows the suspension after sonication; the supernatant after ultracentrifugation and the flow through after loading onto a strep tactin column are shown. In the last lane the purified protein is shown with its two subunits. B shows the UV/vis spectrum of a purified protein sample with the 280 nm protein absorption and the 412 nm [Fe-S]-cluster absorption.

To be able to make a quantitative statement about the iron content of the produced, unmaturated protein iron quantification (see Chapter 2) was used. As mentioned in the introduction the unmaturated protein lacks the $[2Fe]_H$ sub-cluster of the active site, which results in a protein that houses only the three [4Fe-4S]-clusters, the distal and the medial accessory clusters (F-clusters) and the [4Fe-4S]-cluster of the H-cluster. Therefore, with a sensitive method, 12 irons per protein should be determined if all clusters are present in all proteins, otherwise this number will be an average of the iron content in the sample. With the used iron quantification, 10.83 – 12.24 ± 1.4 irons per molecule protein could be detected. This result is in good agreement with the expected number of irons and suggests that most of the unmaturated proteins contain the correct number of irons per protein. The iron quantification is not very precise for a number of reasons: the method relies on both a precise measurement of the protein concentration and the iron content of the samples, both of which are subject to experimental errors. In addition the protein samples may contain small amounts of contaminants leading to overestimation of the hydrogenase content of the sample.

To verify the correct sizes of both subunits from the over-expressed protein MALDI-TOF analysis was performed. A representative spectrum is shown in Figure 3-24.

Unfortunately it was not possible to detect both subunits together, even though several matrices were tested (the best results were achieved with sinapinic acid). However, the mass of the small subunit (10128 Da) fits well to its expected mass (10146 Da) and the experimentally measured mass (10164 Da) for the native subunit (Section 3.2.2). Therefore, it can be conclude that both proteins are identical and that it is possible to produce unmaturated [FeFe]-hydrogenase from *D. desulfuricans*. The large subunit (43249 Da measured for the native enzyme) was also difficult to detect with the native hydrogenase, and it is possible that the increased difficulty here is due to subtle differences in the sample preparation or in the post-translational modification of the subunit in *D. desulfuricans* compared with *E. coli*.

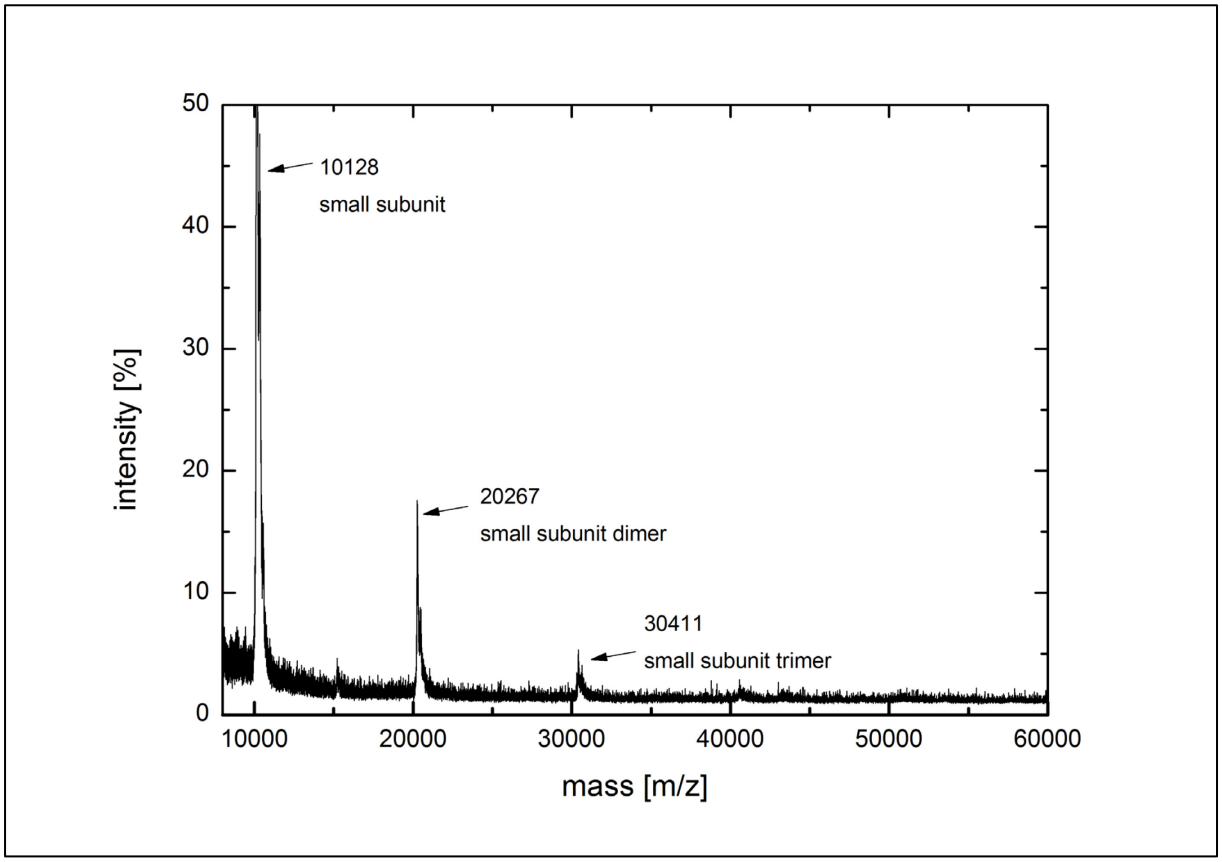

Figure 3-24 MALDI-TOF-MS spectrum of purified, unmaturated [FeFe]-hydrogenase. The measuring inaccuracy of the system is ± 150 Da. The data fit to the one measured from the native system.

3.4 Summary

In this work it has been demonstrated that the growth of *Desulfovibrio desulfuricans* can be scaled up to a 50 L automated fermenter. This increased the total cell yield from one growth by a factor of three, which corresponds to an increase in cell yield per litre culture of 0.5 g. In addition, the number of pre-culture steps was reduced in order to save time so that one growth can be achieved in 7 days compared with 10 days previously. Finally, the hydrogenase yield from the preparation was also increased from 1.5 mg per 100 g of cells to 3 mg per 100 g cells. Due to the fact that the purification method was not changed it is assumed that the better control of the growth conditions (pH, O_2 level) in the 50 L fermenter leads to higher levels of protein expression. This will allow further characterization of this interesting hydrogenase by techniques such as NMR spectroscopy (nuclear magnetic resonance), Mößbauer spectroscopy or spectro-electrochemistry, which require very large quantities of protein. In connection with the heterologous expression of [FeFe]-hydrogenase from *D. desulfuricans* it is important to produce high amounts of pure protein allowing comparisons between both systems. The native enzyme and the heterologously expressed enzyme will be studied by electrochemistry in Chapter 6.

An important step to get closer insight into the *D. desulfuricans* metabolism and pathway is the generation of a well working construct and an overexpression system with a purification method which leads to very high yields of pure unmaturated [FeFe]-hydrogenase. During this thesis a well working overexpression system was developed. This protein production method has lots of advantages in comparison to preparation of native proteins. The whole preparation of unmaturated protein with heterologous expression takes, including cell growth and single step purification, only three days. Furthermore, the yield of protein from the recombinant expression system is far superior to the native organism. With the native system only 0.1 ± 0.07 mg L^{-1} of culture can be achieved compared with 5.2 ± 1.2 mg L^{-1} of culture for the over-expression system, an increase by factor of 50. It should be noted, however, that the maturation of the hydrogenase required further time-investment as the synthesis of the $[2Fe]_H$ complex does (see Chapter 4).

With the unmaturated protein, there is also the possibility to study the [Fe-S]-clusters in the absence of the active site by e.g. EPR (see Chapter 4) and electrochemistry (see

Chapter 6). This would be an enlargement of the studies from 2 [4Fe-4S]-cluster proteins, like the well-studied ferredoxin. A further discussion about this will be given in Chapter 4.

Furthermore, the maturation of the protein is an important and interesting process, which is possible to analyse by the in vitro maturation of the heterologously expressed protein. It is shown in literature, that the nature of the inserted active site is important for protein function and activity.[127,129] Kinetic studies of activation can be explored and there is also the possibility to test several different $[2Fe]_H$-complexes which can help to generate a higher active hydrogenase or leads to the development of efficient catalysts.

The use of a quite simple medium gives the possibility to isotopically label the protein e.g. with ^{57}Fe for EPR and Mößbauer studies or ^{13}C and ^{15}N for NMR in a more convenient (and cheap) way as would be possible for a growth in the 50 L fermenter.

A method which becomes available by generating plasmids from the protein of interest for expression in *E.coli* is mutagenesis. This is a powerful method for analysing protein properties. As it is mentioned in Chapter 5 this allows to change the redox-potentials of the different [Fe-S]-clusters and study their influence on catalysis.

In summary, improvement of the hydrogenase preparation of the native organism and the establishment of a well working over-expression system are powerful tools to get closer insight into the reaction pathways of the enzyme. Due to the high amounts of protein achieved methods, which require large sample concentrations, like NMR, Mößbauer spectroscopy, spectro-electrochemistry or crystallization experiments become possible.

A small disadvantage of the heterologously expressed enzyme is maybe the absence of the oxygen tolerant “as isolated” state as it is known from the native enzyme. But it might be possible, that this state can be generated under certain conditions which would allow to study the properties of this oxygen tolerant state. Further investigations on this need to be performed in the future.

Chapter 4 Characterization of native and recombinant [FeFe]-hydrogenase from *D. desulfuricans*

4.1 Introduction

4.1.1 *Artificial maturation*

As reported in Section 1.1.4, the *in vivo* maturation of [FeFe]-hydrogenases requires three specific maturases in the cell. With the heterologous expression system developed in Chapter 3, unmaturated protein is produced; to get catalytically active protein, reconstitution of the active site is necessary.

As reported in Table 3-1 (see Chapter 3) the first overexpression of [FeFe]-hydrogenase was reported in 2004.[45,117] Kuchenreuther et al. reported in 2010 a better expression system of unmaturated [FeFe]-hydrogenase from *Chlamydomonas reinhardtii* (HydA1) and *Clostridium pasteurianum* with co-expression of the maturases.[62] This method yields hydrogenase samples with comparable activities to those purified from the native organisms. Isolated HydA1 from the native system shows rates of 741 s^{-1} for hydrogen evolution, the maturated hydrogenase by co-expression with the maturases give similar rates of 641 s^{-1}. This shows, that this maturation method works and active [FeFe]-hydrogenase can be achieved. In 2007 Mc Glynn et al.[130] reported an over-expression of unmaturated protein, followed by *in vitro* maturation with cell extracts (containing maturases). This method also led to fully active protein.

It was assumed (see Section 1.1.4), that the maturase HydF is necessary to insert the $[2Fe]_H$-site into the protein. In vivo this $[2Fe]_H$ sub-site is first assembled on the maturation enzyme HydF and then delivered to the unmaturated hydrogenase for activation.[43] Therefore, several synthetic mimics of this $[2Fe]_H$-site were synthesized to test their ability to maturate the overexpressed enzyme. Berggren et al. tested in 2013 three different mimics of the $[2Fe]_H$-sub-site (see Figure 4-1).[127] All mimics contain 4 CO, 2 CN and the bridging dithiolate but they differ in the nature of their bridgeheads (see Figure 4.1). All three were loaded onto HydF from *Thermotoga maritima*, which was also

heterologously expressed in *E. coli,* and afterwards the mimic was transferred to unmaturated HydA1. A fully active hydrogenase was received only by using the azadithiolate (adt) bridge. For the CH_2 and O bridgehead containing complexes, the hydrogenase could be maturated but no activity could be observed. Nevertheless, it was shown, that a controlled activation of metalloenzymes with helper proteins, like HydF, is possible. Insertion of the NH_2 bridgehead complex leads to formation of the native $[2Fe]_H$-cluster, this implies an isomerisation of one CN-ligand in HydF (reversion in HydA1). The CO moves into a bridging position and one CO is released from the distal iron. A conformational rearrangement adopt the inverted square pyramid structure required for opening a substrate binding site on the distal iron.[131]

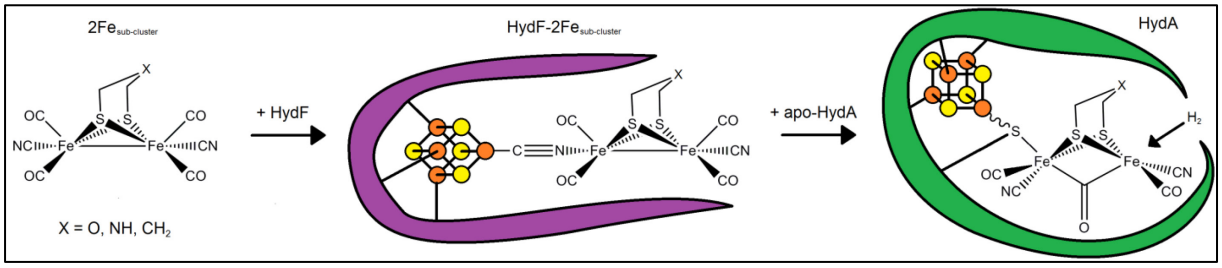

Figure 4-1 Scheme for artificial maturation by the helper protein HydF. In the first stage a synthetic binuclear iron complex is transferred to HydF (purple) and in the second step the complex is transferred from HydF to HydA1 (green). The binding of HydF is associated with inversion of the orientation of one CN-ligand on the $[2Fe]_H$ sub-cluster. The transfer from HydF to HydA is associated with the loss of one CO-ligand, reversion of the CN-ligand and movement of one CO-ligand into a bridging position, with the result that the configuration of the proximal iron becomes inverted. Figure adapted from[127].

This provides a unique, simple and straightforward tool for producing active, recombinant hydrogenases, with no requirement for co-expression with the still incompletely characterized complex maturation machinery.[127]

In 2013 Esselborn et al.[122] reported the reconstitution of unmaturated HydA1 to full activity without HydF. Only the adt, which also gave the highest activity in earlier reports[127] was able to fully activate the hydrogenase. This method offers a very simple way of *in vitro* maturation by simply mixing the unmaturated protein with the $[2Fe]_H$-mimic adt under anaerobic conditions. A scheme of the described method is given in the following Figure 4-2.

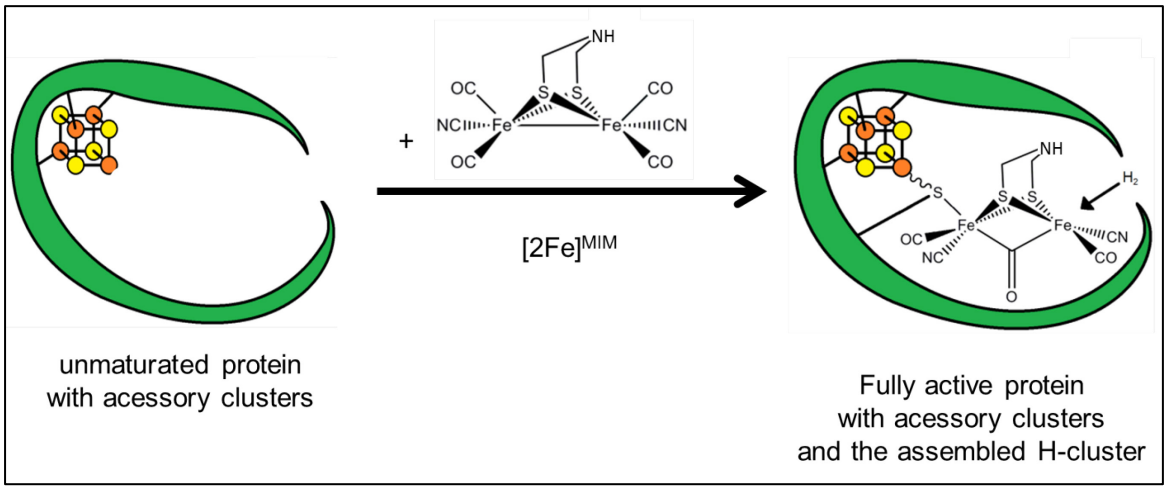

Figure 4-2 The H-cluster is assembled from a regular [4Fe4S]-cluster and a unique $[2Fe]_H$-subcluster. The synthetic mimic $[2Fe]^{MIM}$ differs from the binuclear active site by an additional CO group.

So far the [FeFe]-hydrogenase from *D. desulfuricans* has not been artificially maturated. The intention of this chapter is to apply the direct insertion method with the $[2Fe]_H$-mimic adt to generate active hydrogenase samples, which can be studied by EPR, FTIR and crystallography to further study the structure and function of this protein.

4.1.2 *Aims of the work described in this chapter*

- Find crystallization conditions for native and heterologously expressed [FeFe]-hydrogenase from *Desulfovibrio desulfuricans.*
- Establish activity assays for hydrogen oxidation and production by the purified native hydrogenase.
- Characterization of the unmaturated protein by EPR spectroscopy.
- Try to generate fully active hydrogenase by reaction with the $[2Fe]_H$-mimic adt and compare it to the native enzyme by measuring the activity with the established assays.
- Characterize the maturated enzyme by EPR and FTIR spectroscopy and compare it to the native enzyme.

4.2 Characterization of unmaturated [FeFe]-hydrogenase from *Desulfovibrio desulfuricans*

4.2.1 *Crystallization of [FeFe]-hydrogenase from D. desulfuricans*

To set up crystal trials large amounts of highly purified native enzyme are needed. Unfortunately no crystals grew by testing the reported conditions[30] (2.5 M $(NH_4)_2SO_4$, 100 mM Tris/HCl pH 8.0, 2.1 M DDAO or 20 % PEG 6000, 100 mM acetate-buffer pH 5.0, 2.1 M DDAO) neither with the hanging drop nor with the sitting drop vapour diffusion methods under anaerobic conditions. After several tries with different protein concentrations (10-30 mg/ml) it was decided to test other crystallization conditions using a range of crystallisation screening kits (see Table 4-1), which were already available in the lab. Because the native enzyme is not sensitive to oxygen and it is more comfortable it was decided to set up these trials with the crystallization robot (Crystal Phoenix Liquid Handling System, Art Robbins Instruments, CA, USA) under aerobic conditions in micro-crystallization plates (INTELLI-PLATE 96-3, Art Robbins Instruments, CA, USA), the plates were stored in a fridge at 4 °C. This would lead to crystals in the H_{ox}^{air}-state, which would also allow the nature of this state to be studied. If crystals can be generated under aerobic conditions it can be further tested, whether the same conditions might work under anaerobic conditions to have the enzyme in a defined H_{red} state.

Unfortunately none of the tested conditions led to crystals of the native enzyme. A list of the tested commercial kits is given in the following table.

Table 4-1 Overview of the tested crystallization screening kits.

Screening Kit	Company
PEG/Tacsimate pH 5.8 with Silver bullets	Hampton Research
JBScreen Wizzard 3+4	Jena Bioscience
PEG/Ion Screen	Hampton Research
PEG/Ion 2 Screen	Hampton Research
PEGRx^{TM}1	Hampton Research
JBScreen Basic1+2+3+4	Jena Bioscience
JBScreen Classic 1+2	Jena Bioscience
JBScreen PEG/Salt	Jena Bioscience

With the establishment of the heterologous expression system, large amounts of pure, unmaturated enzyme became available, and crystallization was tried. A structure of unmaturated hydrogenase is not reported so far and would also give useful information about the protein. Furthermore, if crystallization conditions are found, they could also be tested for the native or the artificially maturated enzyme as well. In the beginning construct 5 (see Section 3.3.2) with a Strep tag II at the carboxy-terminal (CT) end of the large subunit and no pre-sequence at the amino-terminal (NT) end of the small subunit was used to test the screening kits from Table 4-1 under aerobic conditions with different protein concentrations, but also for this enzyme no crystals were formed.

Afterwards construct 9 (see Section 3.3.2) was tested, which also has the CT Strep tag II at the large subunit and no pre-sequence at the NT of the small subunit, but additionally here the signal peptide at the CT end of the large subunit was removed, which is also the case after translation in the native enzyme. Due to the fact, that the protein from the Streptactin column contained some impurities like desthiobiotin a method for further purification was added before crystallization. The unmaturated protein was run over a size-exclusion column (Superdex 200, GE Healthcare, Freiburg). After this the protein was concentrated to 13.6 mg/ml and used for crystallization. Only two conditions from the reported screening kits (Table 4-2) gave well defined crystals.

The first crystals appeared after three days and the conditions are summarised in the following Table 4-2.

Table 4-2 Crystallization conditions for the first crystal, which appears after three days.

crystallization buffer (0.2 µL)	25 % w/v PEG 3350
(PEG/Tacsimate pH 5.8 Crystallization reagent, Hampton Research, CA, USA)	0.1 M MES pH 5.8
additives (0.2 µL)	0.005 M Gadolinium(III)chloride hexahydrate
(Silver Bullets Screening Kit, D4	0.005 M Samarium(III)chloride hexahydrate
Hampton Research, CA, USA)	0.05 M Benzamidine hydrochloride
	0.25 % w/v Salicin
	0.02 M HEPES sodium pH 6.8
protein concentration (0.4µL)	13.6 mg/ml
crystallization method	sitting drop

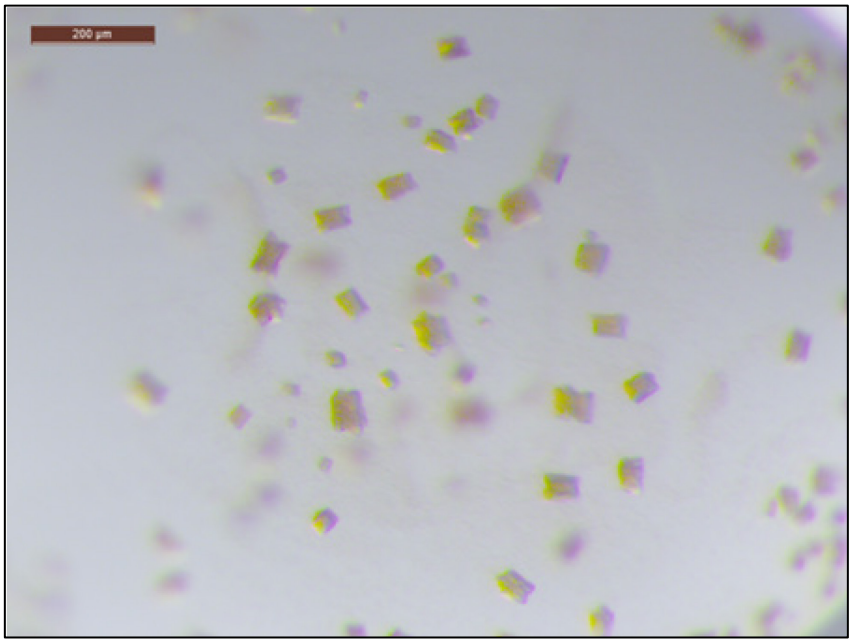

Figure 4-3 Picture of crystals of unmaturated [FeFe]-hydrogenase from *D. desulfuricans*, conditions are given in the text above. This crystals appeared after three days.

The X-ray diffraction experiments were performed by Dr. H. Ogata at the synchrotron source BESSY II (Helmholtz Zentrum, Berlin). A diffraction pattern of a crystal is shown in the following Figure 4-4.

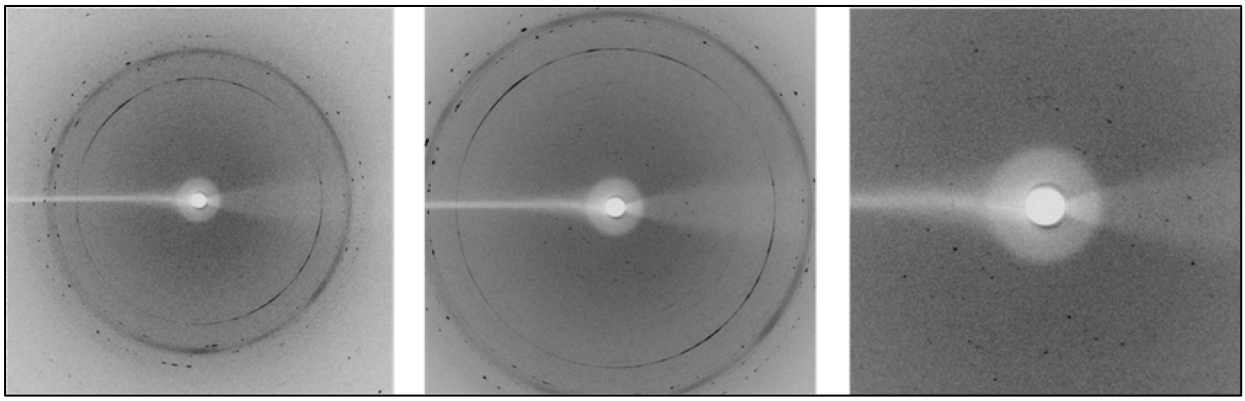

Figure 4-4 Diffraction pattern of one unmaturated [FeFe]-hydrogenase crystal from *D. desulfuricans*, the images are all from one crystal but with different enlargements.

Based on the collected data set, it was possible to calculate several values for the crystal parameters of the unmaturated [FeFe]-hydrogenase from *Desulfovibrio desulfuricans* which are summarized in the following Table 4-3. There are two molecules in the asymmetric unit. It was possible to determine the space group and the parameters of the unit cell. The crystal shows an orthorhombic unit cell with the space group $P2_12_12_1$ (No. 19 of the International Table for Crystallography[132]) and the corresponding length of a = 49.61 Å, b = 87.95 Å and c = 88.94 Å.

Table 4-3 Data collection and refinement statistics of unmaturated [FeFe]-hydrogenase from *D. desulfuricans*. The highest resolution shell is shown in parenthesis.

Data collection	
X-ray source	BESSY II (BL 14.)
Wavelength	0.91841 Å
Space group	$P2_12_12_1$
Unit cell parameters:	
A	49.61 Å
B	87.95 Å
C	88.94 Å
Resolution	44.5 -5.02 Å (5.32.-.5.02 Å)
No. of observed reflections	12506
No. of unique reflections	1838
R_{merge}	0.68 (1.29)
Completeness	99.2 % (96.1 %)
I/σ	2.8 I (1.5 I)
Refinement	
Resolution	30.00 – 5.02
R	25.5 %
R_{free}	42.6 %
No. of residues	485
No. of water	0
Rmsd bond length	0.007 Å
Rmsd bond angle	1.795°

After four month the set up crystallization plates were checked again and additional crystals of unmaturated *D. desulfuricans* were found, which appeared to be larger than the first reported ones. Unfortunately there was also some precipitate in the wells, nevertheless they will be tested for diffraction. The crystallization conditions are given in the following Table 4-4.

Table 4-4 Crystallization conditions for [FeFe]-hydrogenase from *D. desulfuricans.* Crystals appeared after four month.

crystallization buffer (0.2 µL)	6 % PEG 20000
(PEGRX™1, Hampton Research, CA, USA, E13)	0.1 M citric acid pH 3.5
	5 % v/v 2-propanol
protein concentration (0.4µL)	13.6 mg/ml
crystallization method	sitting drop

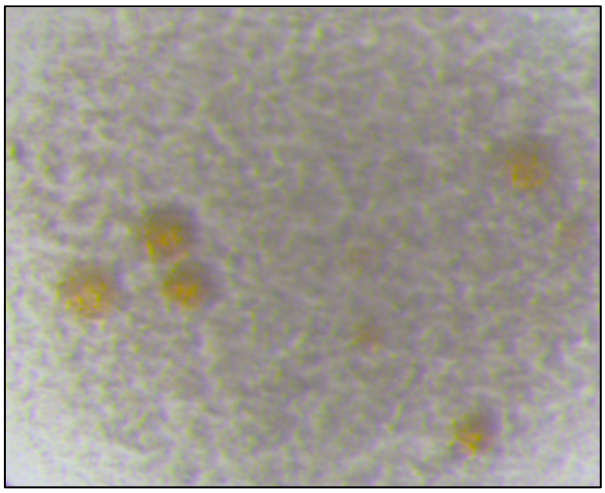

Figure 4-5 Picture of the crystals from *D. desulfuricans* which appeared after four month. Crystallization conditions are given in Table 4-5.

The space group found for the unmaturated protein is identical to the one which is reported by Nicolet et al.[30] in 1999 for a reduced crystal of native *D. Desulfuricans* [FeFe]-hydrogenase. It was decided, that it was not possible to calculate an electron density map from the data because of the low resolution. The next step is to improve the resolution of the diffracting crystals to solve the structure of the unmaturated protein. A crystallization under anaerobic conditions needs to be also tested and afterwards these crystallization conditions can be tested for activated protein. With maturated protein crystallization of the different redox-states becomes available which can help to solve the structure of these states. An additional challenge will be to generate larger crystals of the native and the heterologously expressed enzyme and try crystal EPR. It is also possible to try the activation of unmaturated, crystallized protein by soaking the $[2Fe]_H$-mimic adt into the crystal and see difference in the structure.

4.2.2 *EPR spectroscopy of unmaturated [FeFe]-hydrogenase*

The unmaturated protein of [FeFe]-hydrogenase from *D. desulfuricans* is an interesting system for EPR spectroscopy, because it is a relatively simple 3 [4Fe-4S] system. A 2 [4Fe-4S]-system, which has been extensively studied is that of the 8 Fe ferredoxins.[133-135] Ferredoxin serves as a natural electron donor for key enzymes of anaerobic metabolism, for example in *Thauera aromatica*[136] But the [Fe-S]-cluster interaction in this 2-cluster system is still not fully understood. EPR spectra of the partially reduced and fully reduced form of ferredoxin from *Clostridium acetobutylicum* are given in Figure 4-6. The unmaturated protein from *D. desulfuricans* also has this ferredoxin-like 2 [4Fe-4S] domain and an additional [4Fe-4S]-cluster. The interaction of this cluster is an interesting topic to study by EPR spectroscopy; in the unmaturated protein (construct 5) maybe not all clusters are reduced. Studying the iron-sulfur clusters of the active enzyme is complicated by the presence of the active site. Without the $[2Fe]_H$-sub-cluster, it is possible to study the clusters by EPR redox titrations. Also the $[4Fe\text{-}4S]_H$-cluster of the H-cluster is likely influenced by its connection to the $[2Fe]_H$-site. It will be interesting to study this cluster in the unmaturated protein. Furthermore, mutations of these clusters, reported in Chapter 5 of this thesis, can influence the redox-properties of the clusters and therefore also the interactions between the clusters. This can be studied by EPR spectroscopy in the unmaturated proteins.

In general [Fe-S]-clusters are an important subject to study, because they seem to be involved in the catalytic directionality of hydrogenases or in their oxygen stability as mentioned in Chapter 1. Furthermore they are prominent co-factors in biological systems and are found in all types of organisms.

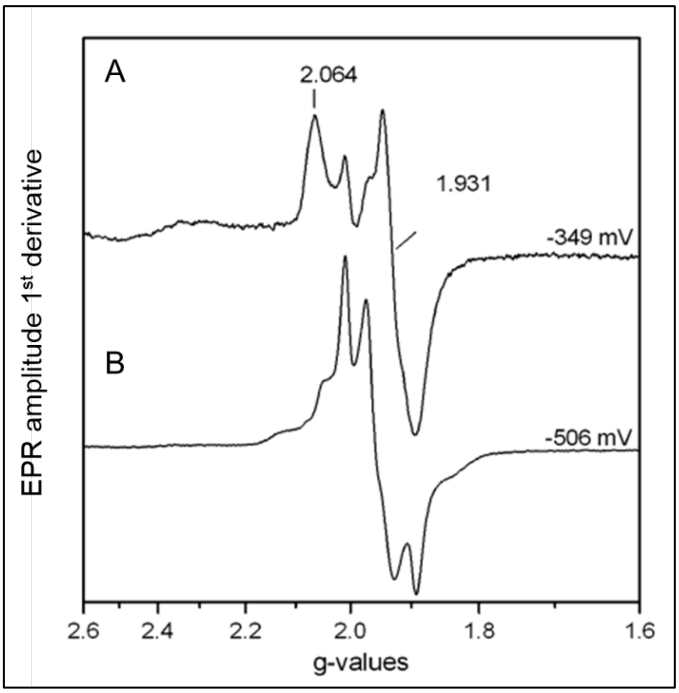

Figure 4-6 *Clostridium acetobutylicum* Ferredoxin EPR spectra of its oxidized form (A) and its reduced form (B). Figure adapted from[137]

For studying the unmaturated [FeFe]-hydrogenase continuous wave (cw) X-band EPR spectroscopy was used. As mentioned above, the unmaturated enzyme does not host the $[2Fe]_H$-cluster from the active site. That means, that all observed EPR signals belong to the [4Fe-4S]-clusters. For a basic introduction to EPR spectroscopy itself and for EPR spectroscopy of [Fe-S]-cluster see Section 2.7.2. The standard sample prepared inside an anaerobic glovebox contains 1 mM NaDT to reduce the protein.

In Figure 4-7 two EPR spectra of the unmaturated protein are shown. As is obvious from this figure, the protein shows an unusual behaviour at different temperatures.

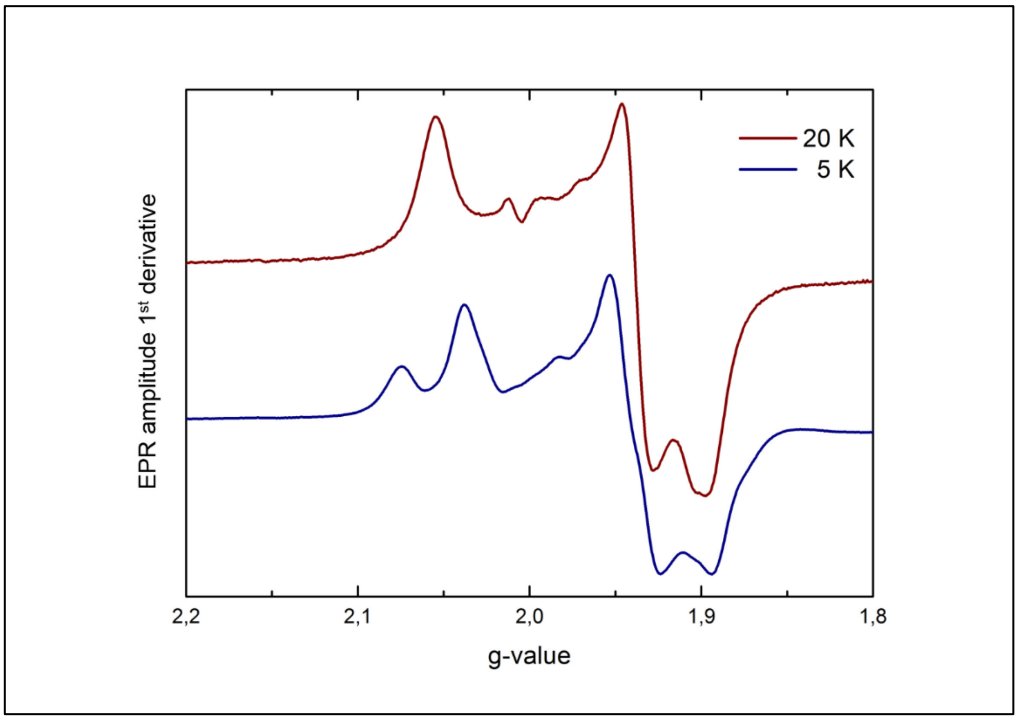

Figure 4-7 X-Band cw EPR spectra of unmaturated [FeFe]-hydrogenase, anaerobically prepared with 1 mM NaDT. The red trace is at 20 K and the blue one at 5 K with a spliting at g = 2.05 with a distance of 5.8 mT.

At 20 K, a reasonably simple rhombic [4Fe-4S]-cluster spectrum can be observed, with g-values of 2.05, 1.93 and 1.90, with evidence for more than one component apparent at g = 1.9. This suggests that at least two clusters are reduced with very similar overlapping spectra. At lower temperatures the signal around g = 2.05 splits into two signals with a separation of 5.8 mT. Also, the other g-values show more complicated features. For further characterization of this behaviour a temperature dependency (at 33 dB power attenuation) was determined (see Figure 4-8). It is possible that the signal at low temperature comes from two different clusters that relax much more quickly than the cluster observed at higher temperature. However, the more likely explanation is that there is a spin-spin interaction that is only observed at low temperature. If the former is the case, both signals at low temperature may change differently with temperature, but if it is the latter case, then the low temperature spectrum should change to the high temperature spectrum in a symmetrical manner. It is known, that the amplitude of an EPR signal is inversely proportional to the measurement temperature,[138] this is described by the Curie law and it originates from the statistical difference between spin populations in the initial and final energy levels producing the EPR transition. Boltzmann statistics states that this population difference is exponentially dependent on the temperature and

the energy difference between the spin-up and spin-down states. The temperature dependence may often be approximated as 1/T.[139] To compensate for the Curie behaviour of the signals, in the following Figure 4-8, the spectra have been normalized to temperature.

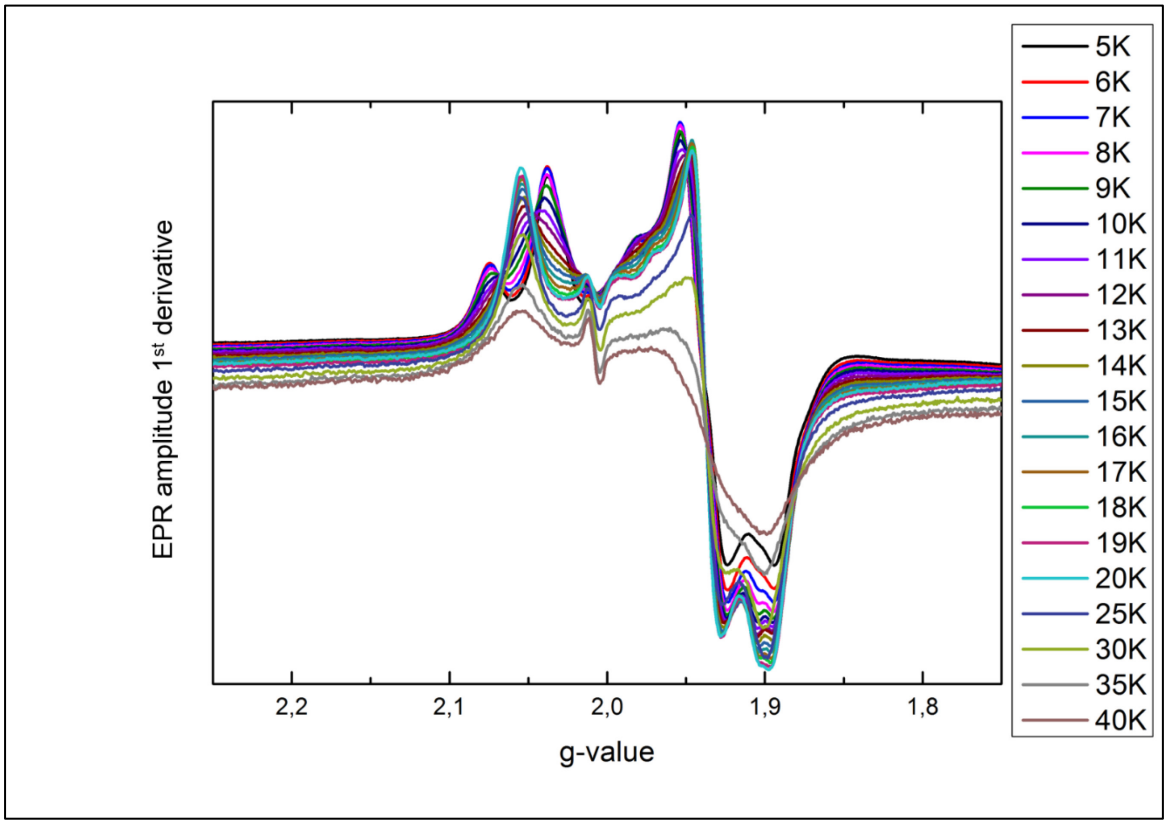

Figure 4-8 X-Band cw EPR spectra for determination of the temperature dependency of the split signal at 33 dB. All spectra were normalised by temperature.

For a better visualization of the unsplit and the split signal, the next Figure 4-9 shows the same spectra as Figure 4-8 but without the temperature normalization. It is clear, from inspection of these two figures that the “split-signal” collapses to the “unsplit-signal” symmetrically, and, therefore, the individual components of the spectra do not follow the Curie law. Particularly, the “unsplit” signal at g = 2.05 increases.

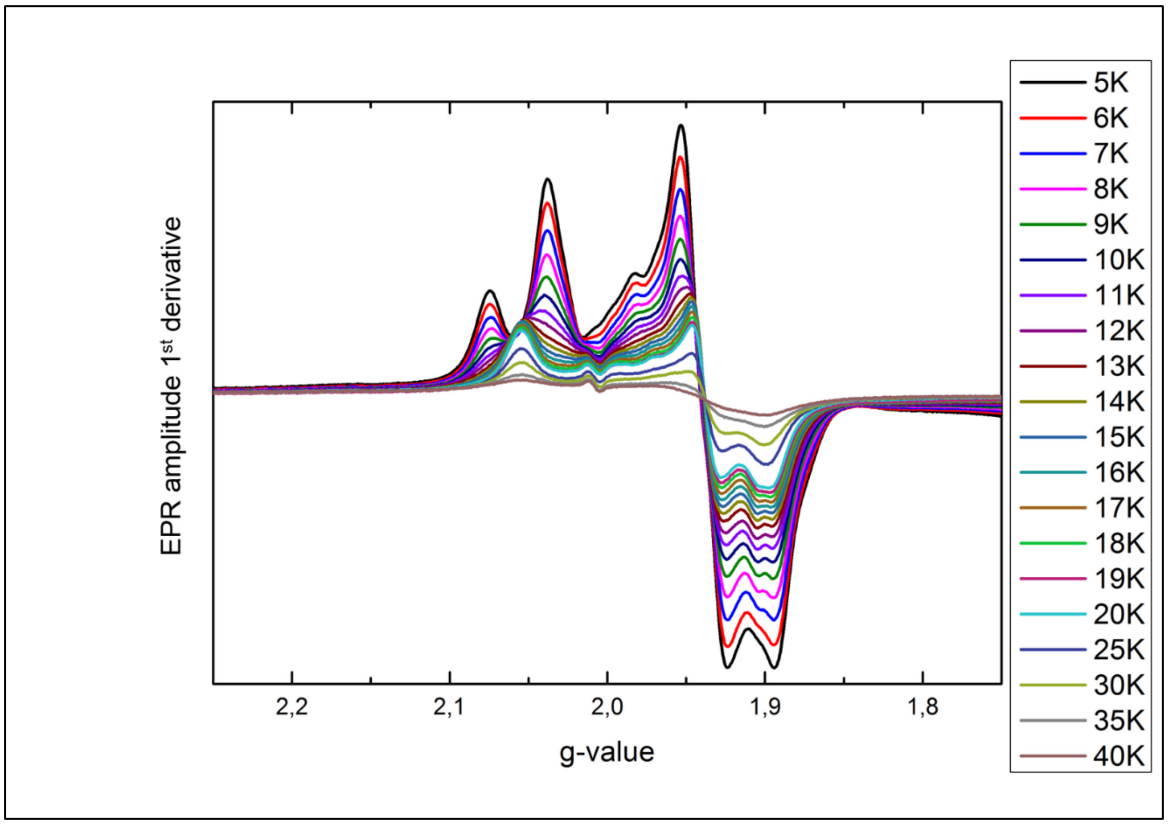

Figure 4-9 X-Band cw EPR spectra for determination of the temperature dependency of the split signal at 33 dB.

The spectra, shown in Figure 4-8 and 4-9 are modulated spectra, which are automatically produced by the cw-EPR technique. These modulated spectra represent the first derivative of the absorbance spectrum, which therefore can be obtained by integration (see Figure 4-10).

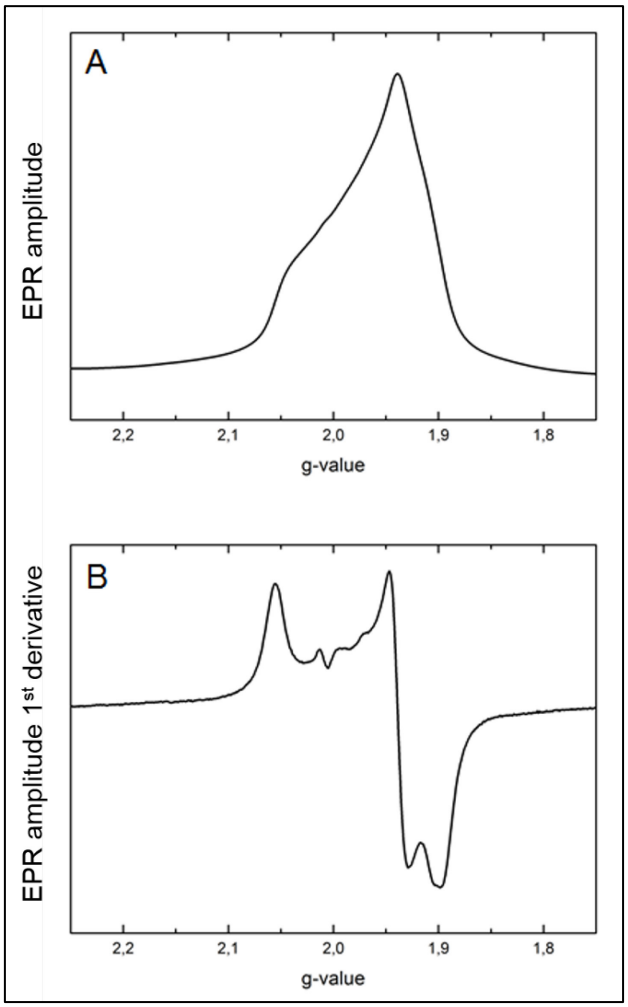

Figure 4-10 A) Absorbance spectrum of unmaturated protein at 20 K and 33 dB B) first derivative of A) to receive the modulated EPR spectrum.

A further integration of the absorbance spectrum yields the area under the curve which is proportional to the number of the spins. In Figure 4-11 this area is plotted against the inverted temperature. As expected the system appears to show Curie behaviour as the total signal intensity is inversely proportional to the temperature with a slope of 5.8. Due to the fact, that no standard measurement with copper was done, this slope can be considered as proportional to the Curie constant for this system.

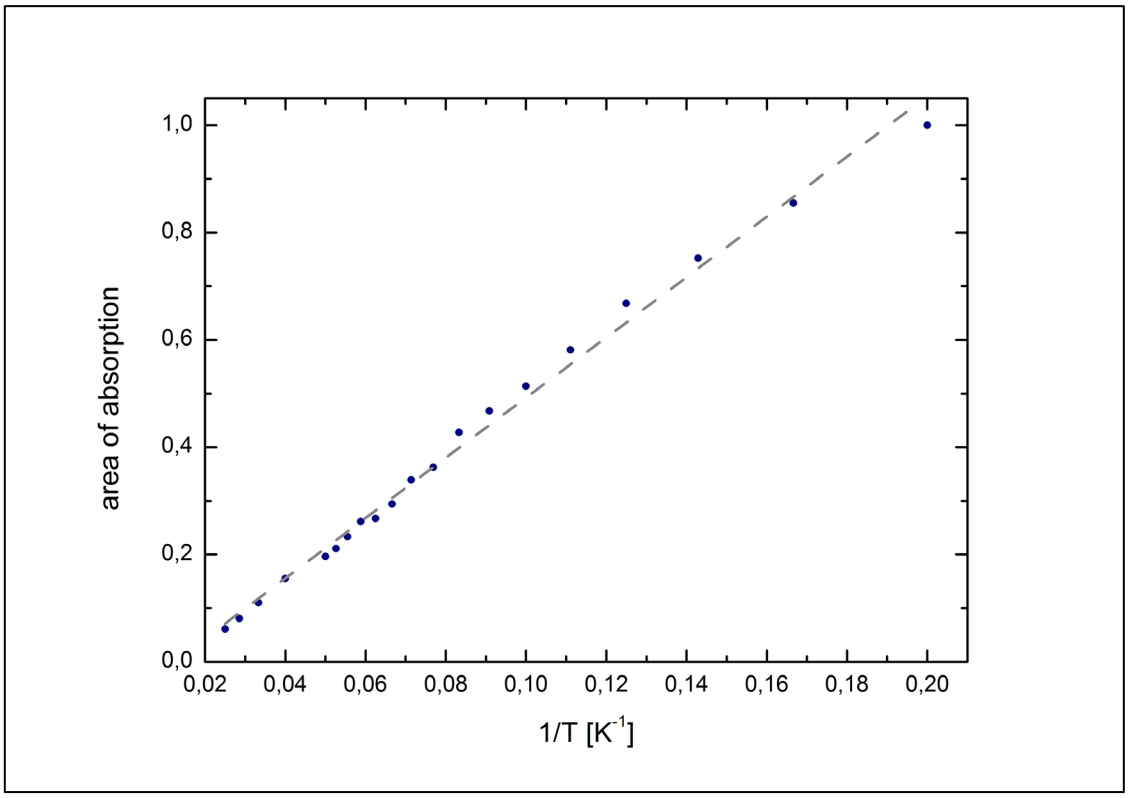

Figure 4-11 Plotted data of the temperature dependency of the EPR signal from figure 4-15 as area of the absorption against the inverted temperature to analyse the Curie behaviour of the sample. A linear fit of the data points is shown by the grey dashed line.

Figure 4-9 shows that at temperatures below 12 K the single signal at g = 2.05 starts to split. A similar behaviour is reported in the literature[136] for the 2 [4Fe-4S]-cluster ferredoxin of *Thauera aromatica*. It is suggested, that the splitting originates from a dipole-dipole interaction between the two clusters, because the authors observe an interaction of a high spin state species at high g values (g_z = 4.35, g_y = 4.26 and g_x = 4.19). But for the unmaturated hydrogenase of *D. desulfuricans* no high spin species can be observed. Therefore it can be concluded that this splitting belongs to a dipolar coupling of two S = ½ spin systems.

Also, power saturation experiments were performed to get an idea of the contribution of different paramagnetic species in the sample. From the recorded EPR spectra of the unmaturated protein (Figure 4-9) it is clear, that there is more in the sample than a single [4Fe-4S]-cluster. At different powers different species behave in a different way, which means that if there is another species in the sample the saturation of both species should be different. The results are given in the following Figure 4-12. From this figure it

is visible, that at 20 K no splitting of the signal during power saturation can be observed. At 15 K the beginning of the splitting can be observed and at 7 K the peak splitting can be observed but the splitting of the signal does not change by power saturation. The relaxation properties of the species in this sample are characteristic for [4Fe-4S]-clusters as expected.

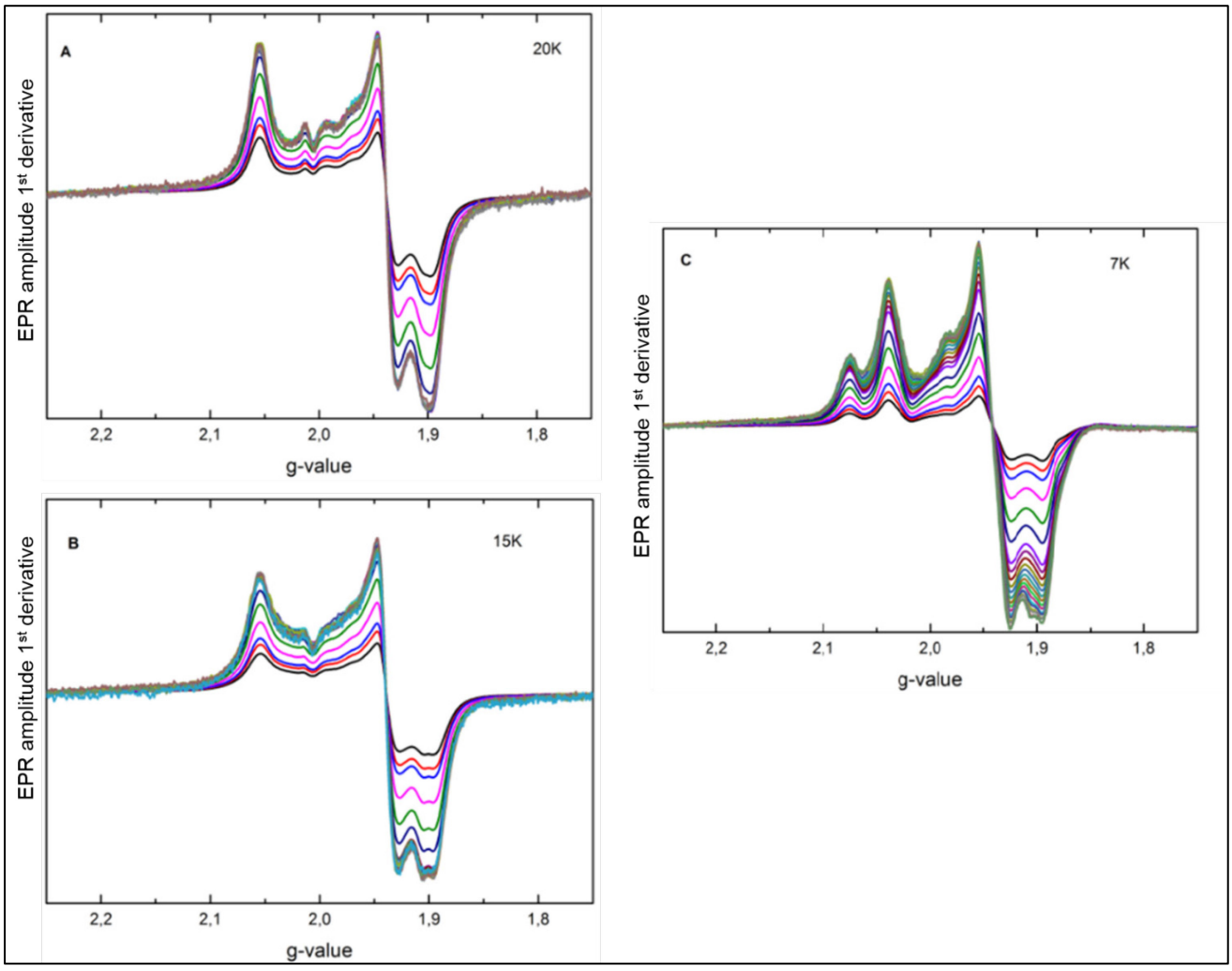

Figure 4-12 X-Band cw EPR experiments, power saturation experiments of unmaturated protein at different temperatures. A) power saturation at 20 K, no peak splitting is observable. B) power saturation at 15 K, the beginning of the splitting. C) power saturation at 7 K a complete peak splitting is visible.

The ferredoxin from *T. aromatica* belongs to the *Chromatium vinosum* type of ferredoxins (CvFd), which differ from the clostridial ferredoxin by a six amino acid insertion between cysteines of the binding motive CXXCXXC…CP. It was mentioned, that this insertion may have an influence of the different redox-potential.

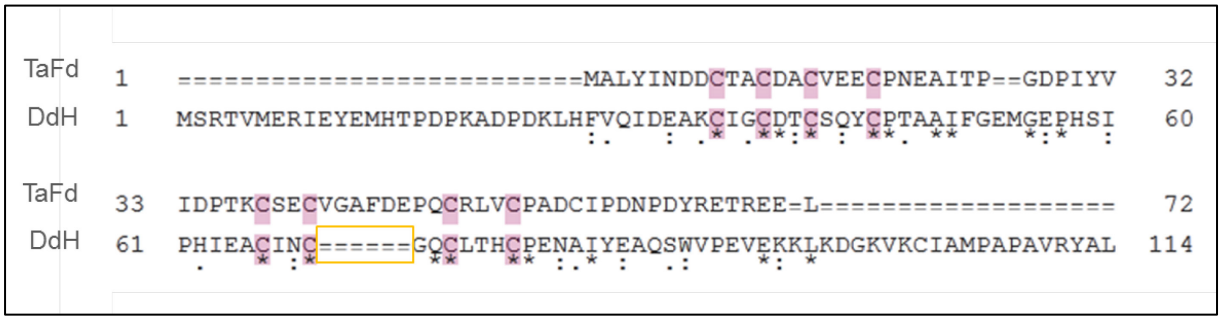

Figure 4-13 Sequence alignment of parts of the large subunit from *Desulfovibrio desulfuricans* (DdH; Uniprot P07598) and *Thauera aromatica* ferredoxin (TaFd; Uniprot O88151). The metal binding sites are highlighted in pink and the instertion of six amino acids in the TaFd is marked with a yellow rectangle.

Due to the fact that the unmaturated protein of *D. desulfuricans* does not have this specific insertion but shows a similar behaviour, the structural environment cannot explain the splitting of the peak. Considering that the protein has 3 [4Fe-4S]-clusters it is possible that the splitting is caused by the interaction between the other pair of these clusters. Such a peak splitting has not been observed previously for the native [FeFe]-hydrogenase from *D. desulfuricans* in the H_{red} state.[103] Therefore, it had to be verified, that the peak splitting is not observable in the native system (see Figure 4-14).

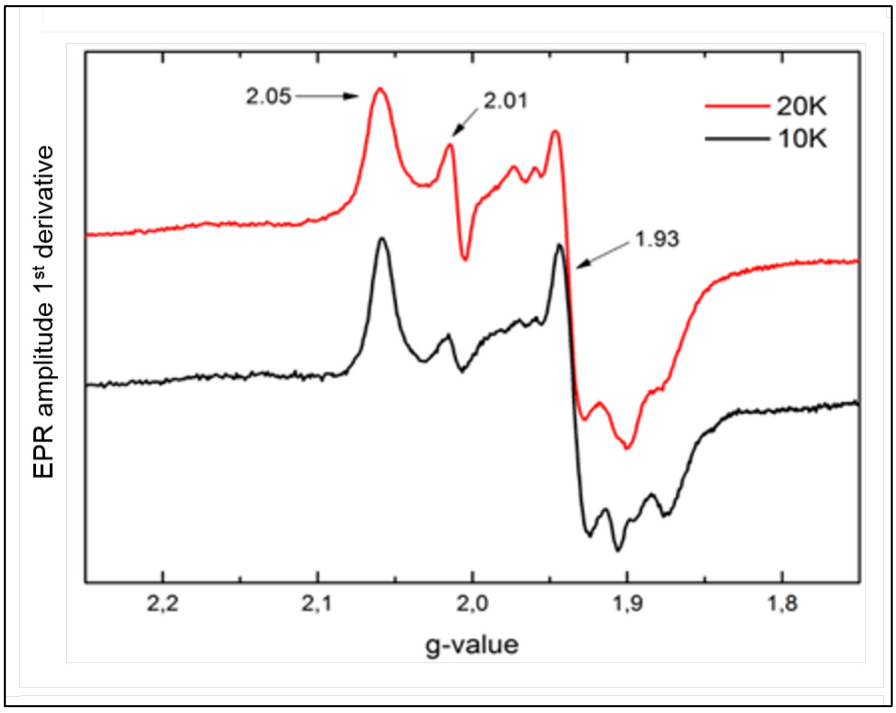

Figure 4-14 X-Band EPR spectra of reduced, native [FeFe]-hydrogenase after reduction with hydrogen overnight at 23 dB, 20 K (red trace) and 10 K (black trace).

In the spectra of the hydrogen reduced native system (Figure 4-14) there are no big differences between the shown temperatures 20 K and 10 K. What is observable is that at lower temperature the signals are narrower and the signals at lower g-values become more distinguishable. It is known for [Fe-S]-clusters to show a relaxation broadening at higher temperatures, so the differences in these temperature spectra were expected.

Normally the reduction of native [FeFe]-hydrogenase is done by gassing the sample with 2 % hydrogen instead of reduction with NaDT, which is necessary for the unmaturated protein. The reduction potential set by hydrogen is more positive than that set by NaDT, so maybe the [4Fe-4S]-cluster which is part of the H-cluster is only fully reducible in the presence of NaDT. That would lead to the assumption that the splitting is caused by an interaction between the medial [4Fe-4S]-cluster and the $[4Fe\text{-}4S]_H$-cluster which is part of the H-cluster. Therefore the native system was also reduced by NaDT to see if different reductants show different EPR spectra (see Figure 4-16). 2 % hydrogen at a pH of 7.6 should set the reduction potential of the sample to approximately -400 mV, whereas reduction with dithionite should exert a potential much more negative than that, probably around -600 mV. However, adding a large amount of dithionite to the sample may decrease the pH, which could increase the potential slightly. Also, it is possible that

dithionite is contaminated with a small amount of its oxidation product (bisulphite), increasing the potential still further.

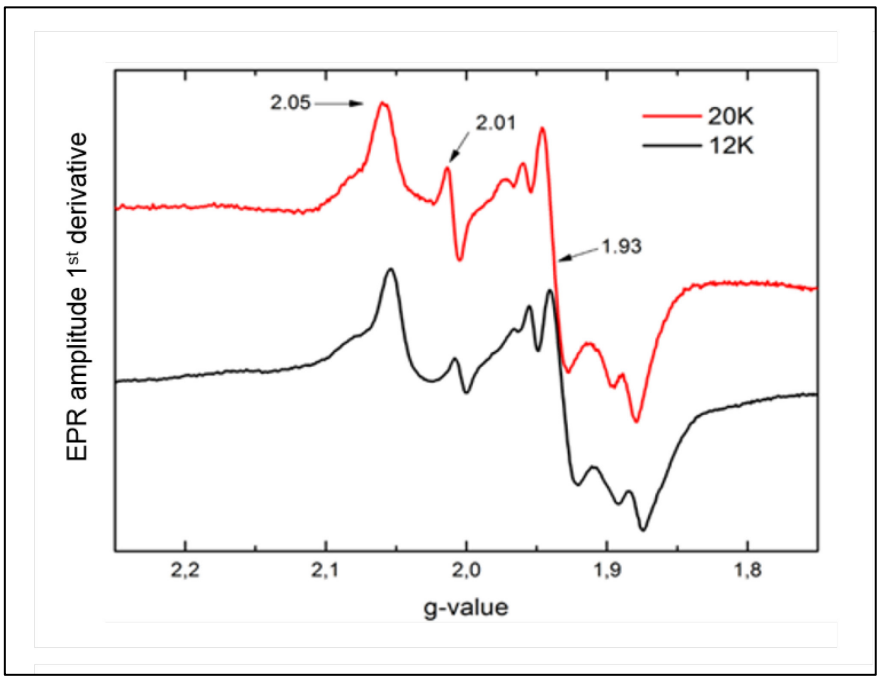

Figure 4-15 X-Band EPR spectra of reduced, native [FeFe]-hydrogenase after reduction with NaDT at 23 dB at 20 K (red trace) and 12 K (black trace).

There are some differences between the NaDT reduction and the hydrogen reduction spectra. A comparison of both reductants is shown in the following Figure 4-16.

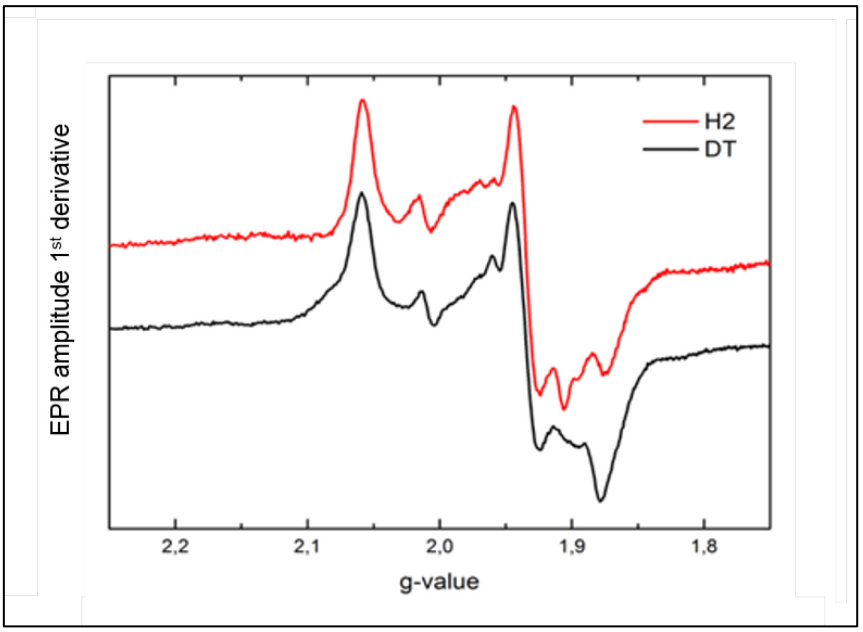

Figure 4-16 Comparison of the X-Band EPR spectra after reduction of the native enzyme by hydrogen (red trace) and reduction by NaDT (black trace) at 10 K and 23 dB.

Some small differences between the H_2 and the NaDT spectra can be observed in Figure 4-16. In the NaDT reduced spectrum a shoulder in front of the g = 2.05 peak appears, as well as a dip in front of the g = 1.93 peak and a signal increase of the g = 1.88 signal. However, these are most likely not significant differences and it is clear that we do not observe such a spectrum as that observed for the unmaturated protein at low temperature.

To further confirm that the temperature dependence of the split signal in the spectra of the unmaturated protein are due to a spin-spin interaction the samples were measured at different frequencies (X-Band = 9.8 GHz, Q-Band = 34 GHz, see Figure 4-17).

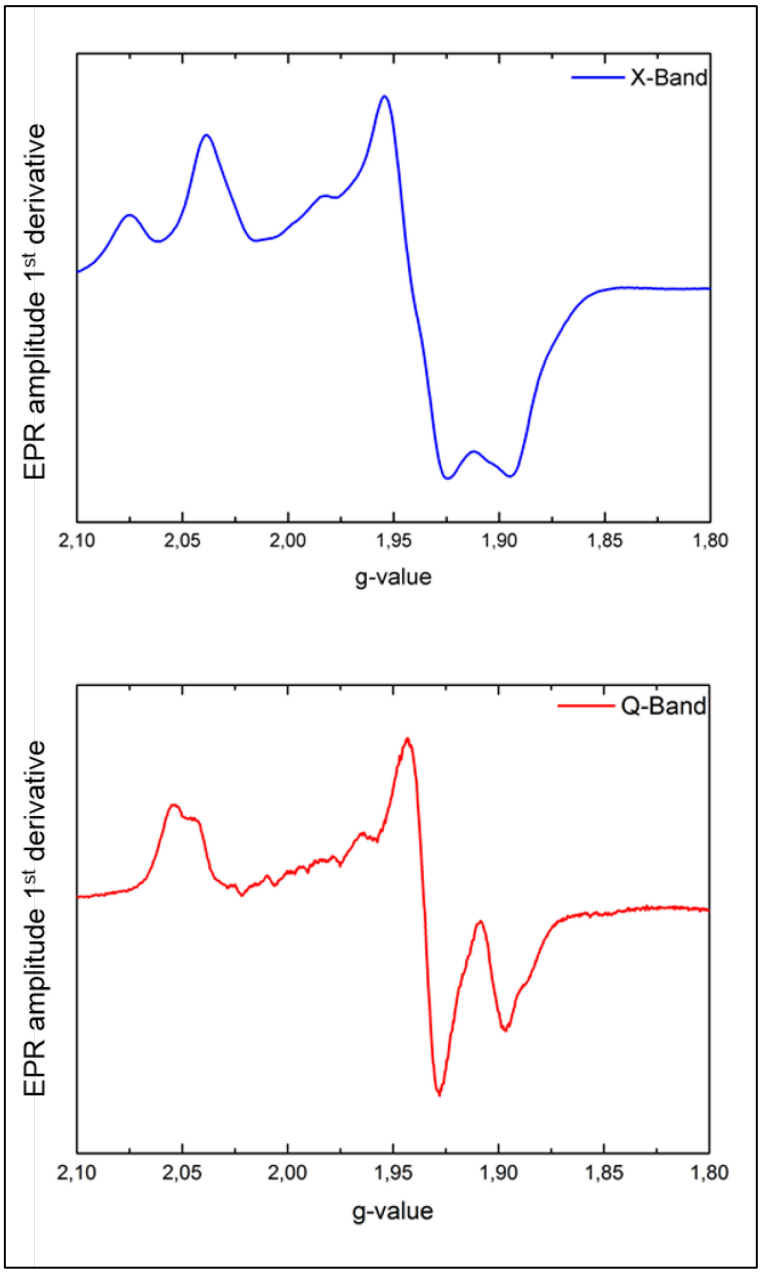

Figure 4-17 Summary of unmaturated [FeFe]-hydrogenase measured at different microwave frequencies at 6 K. Details of the measurement are given in the text above.

From this Figure 4-17 it can be seen, that the spectra at Q-Band becomes more simple than in X-Band, which means that the signal splitting is constant in terms of the microwave frequency, which is typical for spin-spin interactions. From this comparison it can be concluded, that the split signal is due to a spin-spin interaction between two S = ½ species.

It might be possible, that the split signal is not only showing a temperature dependency but also a pH dependency. For that a pH titration was done (see Figure 4-18).

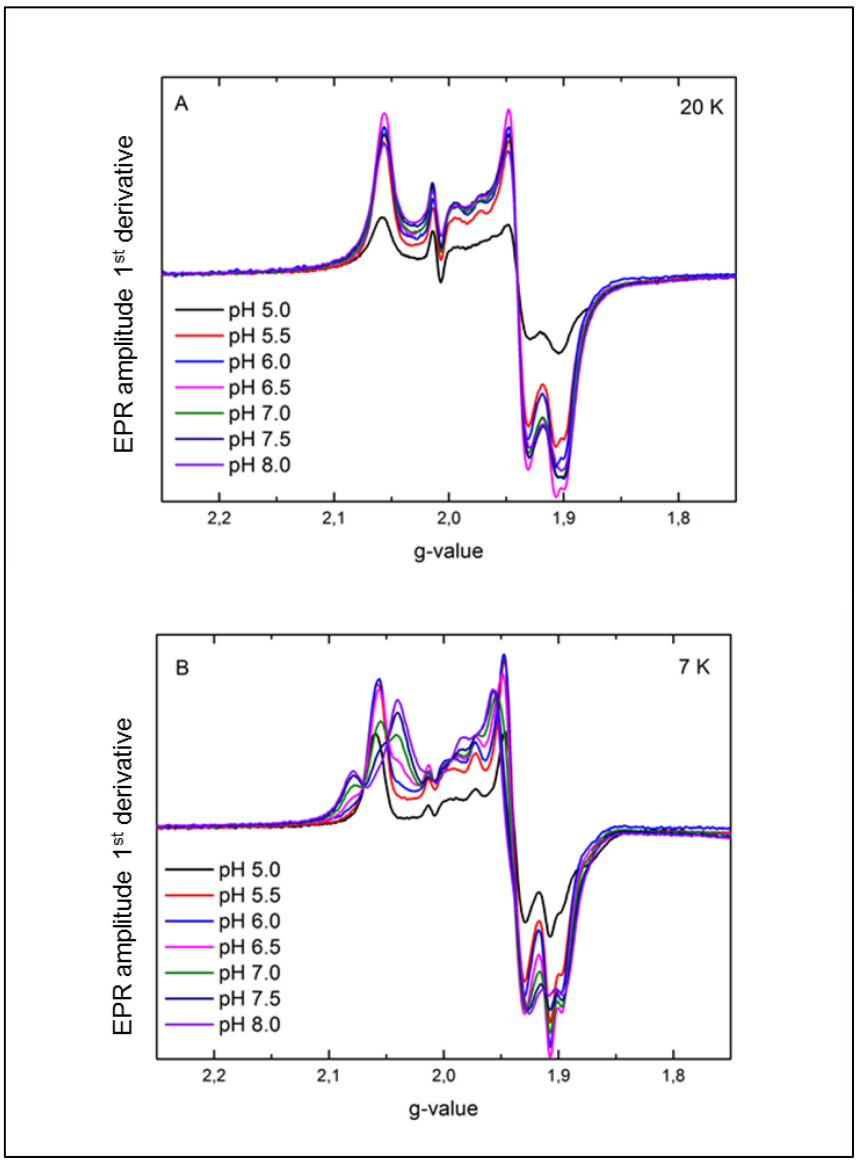

Figure 4-18 X-Band pH titrations at A) 20 K and 33 dB, where no split signal is observed and B) at 7 K and 33 dB, where the formations of the split signal can be observed. All spectra are normalized and background subtracted.

It can be seen, that at 20 K no split signal is observed, as expected from further experiments. At 7 K the formation of the split signal is visible, but it disappears between a pH of 6.0 and 8.0. At pH 5.0 a loss of signal can be observed. The changes are likely to be due to a change in the reduction potential of NaDT, becoming more positive at

lower pH values. It appears that the spin-spin interaction is dependent on the set reduction potential. This is likely due to a change in the reduction state of one of the iron-sulfur clusters. As the most negative potential cluster becomes oxidized, the spin-spin interaction between this cluster and its neighbour disappears.

To more precisely investigate the potential dependence of the EPR signals in the unmaturated enzyme an EPR redox potential titration was done. To set the potentials, a mediator mix of anthraquinone-1,5-disulfonate, neutral-red, phenosafranine, benzylviologen and methylviologen was used. Spectra of some characteristic potentials are shown in Figure 4-19, all spectra are background subtracted, normalized by the number of scans, temperature and receiver gain.

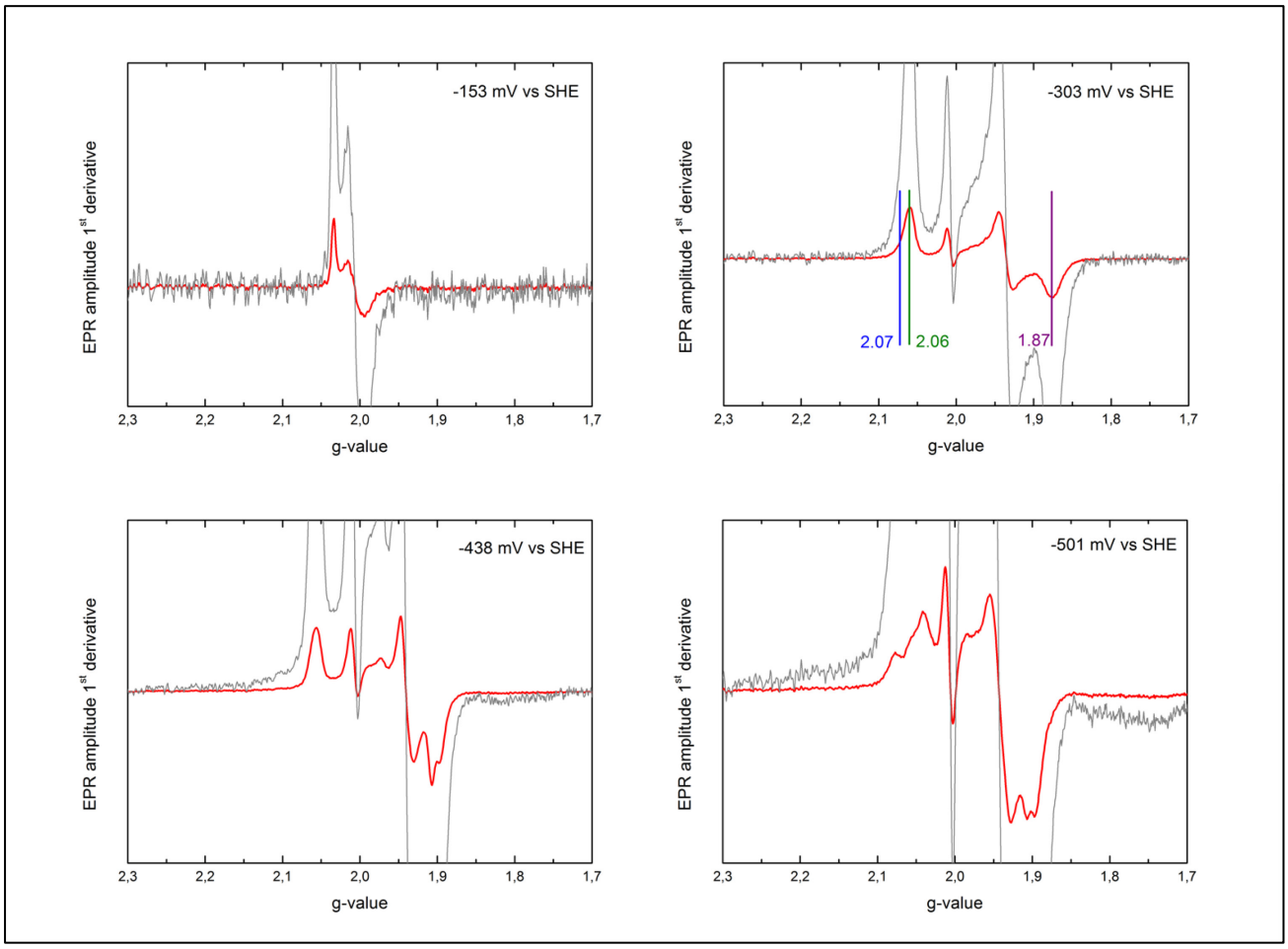

Figure 4-19 EPR spectra of different potential steps at 43 dB and 10K. All spectra are background corrected and normalized to the number of scans, temperature and receiver gain. The red lines represent the original data and the grey trace is a ten time zoom to see more details of the spectra. The coloured labels in the -303 mV vs SHE spectrum mark the chosen peak positions for the integration in Figure 4-20.

From Figure 4-19 the formation of the split signal can be observed. At the highest potential (-153 mV) only a [3Fe]-cluster signal is visible, which might comes from degeneration of the protein, during the experiment. That means, that all [4Fe-4S]-clusters of the protein are oxidized and therefore EPR silent at this potential. The -303 mV spectra shows a characteristic rhombic spectrum for a reduced [4Fe-4S]-cluster without any further interactions, so it can be conclude, that only one cluster is reduced at this potential. An assignment of this spectrum to a particular cluster in the protein is not yet possible. At -438 mV the second cluster becomes reduced and around g = 1.8 (grey trace of the spectra) an additional, broad signal appears. Earlier, we suggested that this spectrum (seen in the native hydrogenase and the high temperature spectrum of the unmaturated hydrogenase) was due to two overlapping spectra with

similar g-values but no spin-spin interaction. It is clear from a comparison of the -438 mV and -303 mV spectra that the peak at g = 1.87 disappears at lower potential, and a broad signal at g = 1.8 appears. This means that the two clusters reduced at -438 mV must be interacting. When setting a more negative potential of -501 mV also the third [Fe-S]-cluster gets reduced and the split signal, discussed earlier at g = 2.05, becomes observable. Surprisingly, this spectrum does not appear to have much greater signal intensity than that at -438 mV, but this might be due to relaxation broadening. Now there are two interactions visible which would fit for a three electron reduced state of the cluster. By visual comparison between the pH titration and the potential titration it can be concluded, that the change in the EPR signals in the pH titration is due to the potential change of NaDT.

To determine the redox-transitions the intensities of the absorbance spectra were plotted against the potentials (see Figure 4-20 D), as it was described earlier for the temperature dependency. However, the potentials of the three transitions seem to be quite close together in value. Therefore, a second approach was used, namely comparing how the EPR signal intensity at three different positions in the EPR spectrum changes over the range of potentials. For this, three different peak positions, g = 1.87, g = 2.05 and g = 2.06 (see coloured marks in Figure 2-19) were chosen. The following Figure 2-20 shows the behaviour for these three g-values and the overall plot against the potential.

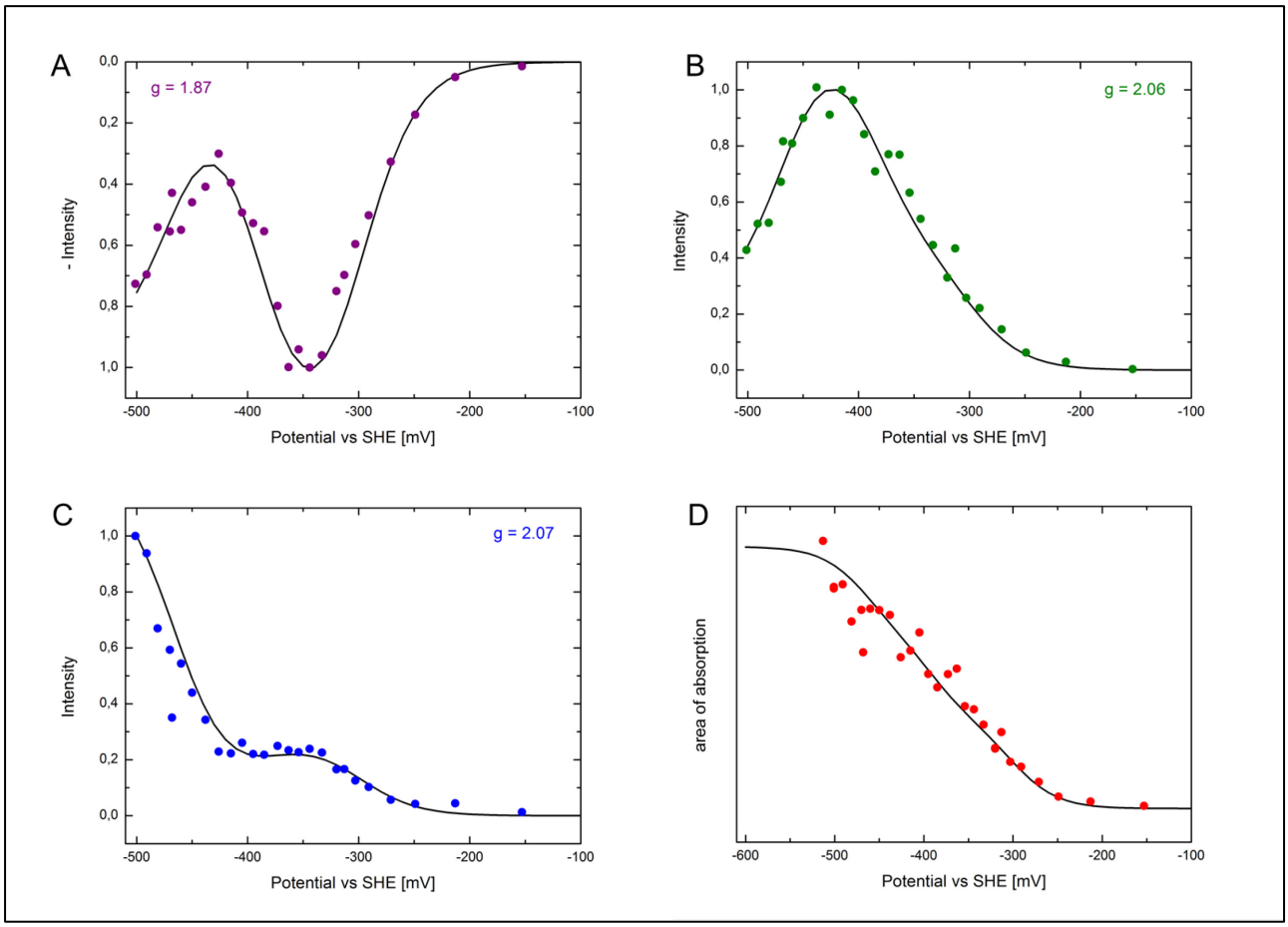

Figure 4-20 Plotted data from the redox-titration at different g-values against the potential vs SHE and the overall plot. All data were measured at X-Band, 43 dB, 10 K and are normalized. The dots are the measured data and the black trace is the simulation with a Nernst equation.

By following the intensities of three g-values from Figure 4-19 (g = 1.87, g = 2.06 and g = 2.07) the redox transitions can be observed. For the g = 1.87 signal (Figure 4-20 A) first an increase (with a negative intensity) is observed followed by a decrease. Afterwards, around -350 mV a second increase can be observed, this is caused by a formation of an additional species in the spectrum. For the g = 2.06 signal (Figure 4-20 B) an intensity increase from both species can be observed followed by a decrease of intensity due to signal splitting. For the g = 2.07 signal (Figure 4-20 C) there are two different increases observable, the first one is due to the chosen position of this signal on the shoulder of the g = 2.06 signal. The second, more significant increase is due to the formation of the spilt signal. Figure 4-20 D shows the integral of the whole EPR spectrum at different potentials.

From this Figure 4-20 above, three redox transitions can be observed, around **-300 mV**, around **-390 mV** and around **-465 mV** (inflection points of the curves). Due to the inaccuracy of the integrals, these values are only approximate numbers. The dots are the measured data and the black line is the so far best fit to determine the redox-transitions. These transitions represent the different reduction potential of the three [4Fe-4S]-clusters in the enzyme.

4.3 Artificial maturation of heterologously expressed [FeFe]-hydrogenase and activity comparison with the native enzyme

As described in Section 4.1.1 several methods for artificial maturation of [FeFe]-hydrogenases are known. In this thesis the activation by simple mixing of the unmaturated protein with the cofactor was tested. For that, the unmaturated hydrogenase from *D. desulfuricans* was activated with the azadithiolate cofactor (adt)[140] by mixing them together under strictly anaerobic conditions in 20 mM Tris/HCl pH 7.6. All measurements were done with hydrogen saturated buffer, it needs to be mentioned that hydrogen is not very soluble in aqueous solutions. Even if the buffers are gassed with 100 % hydrogen the rate of the reaction might be limited by the hydrogen concentration in the reaction. At the beginning a ten time excess of the cofactor was used to see if activation is possible. Afterwards the H_2/benzylviologen oxidoreductase activity was measured as described in Section 2.6.3. As expected the adt and the unmaturated enzyme alone do not have any activity, whereas a 1:10 mixture of protein to adt shows already after 20 s clearly hydrogen oxidation activity. (see Figure 4-21)

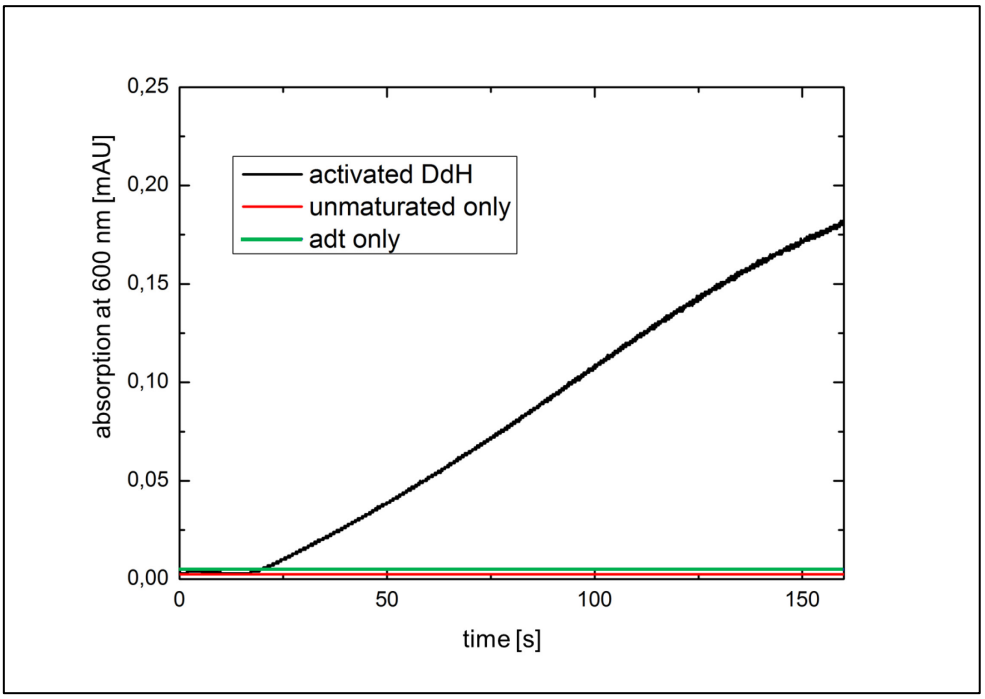

Figure 4-21 Artificial maturation of unmaturated protein by mixing with adt (black). Experiments of only adt (green) and unmaturated protein (red) are shown in the same graph.

It was decided to test different maturation conditions to see which gives optimal results. It is possible that the optimal conditions differ slightly from those reported for other hydrogenases. To determine the reaction time between the unmaturated protein and adt it is important to consider some characteristics of the ongoing reaction: one important issue is the stability of adt itself in aqueous solutions, after diluting the adt (normally dissolved in DMSO) in water the activation needs to take place within a few hours otherwise no activation of the unmaturated enzyme is observed, maybe caused by degradation of the adt in water (decrease of the 347 nm band in UV/vis spectroscopy over time, Figure is shown in the appendix). The second, more important issue is the necessary release of a CO group from the adt. After binding of the cofactor to the protein CO is released to generate active protein (see Section 4.1.1). If the CO concentration in solution increases, also the possibility of forming the stable H_{ox}-CO state increases. This is problematic because in this state one substrate binding site of the distal iron atom is occupied by the CO atom, this leads to a loss of hydrogenase activity. The release of CO from the maturated protein was followed by measuring the change in the position of the Soret band of haemoglobin. CO has a very high binding affinity to haemoglobin, therefore the absorption change in UV/vis spectroscopy for this reaction can be used for observing this release. The oxidized form of haemoglobin (Hb_{ox}) shows a Soret peak at

406 nm and the deoxygenated form (Hb_{deoxy}, generated by reduction with NaDT) at 430 nm, if CO binds to this reduced form, the Soret peak shifts to 419 nm (Hb_{CO}). The Soret positions for these different species are shown in the following Figure 4-22.

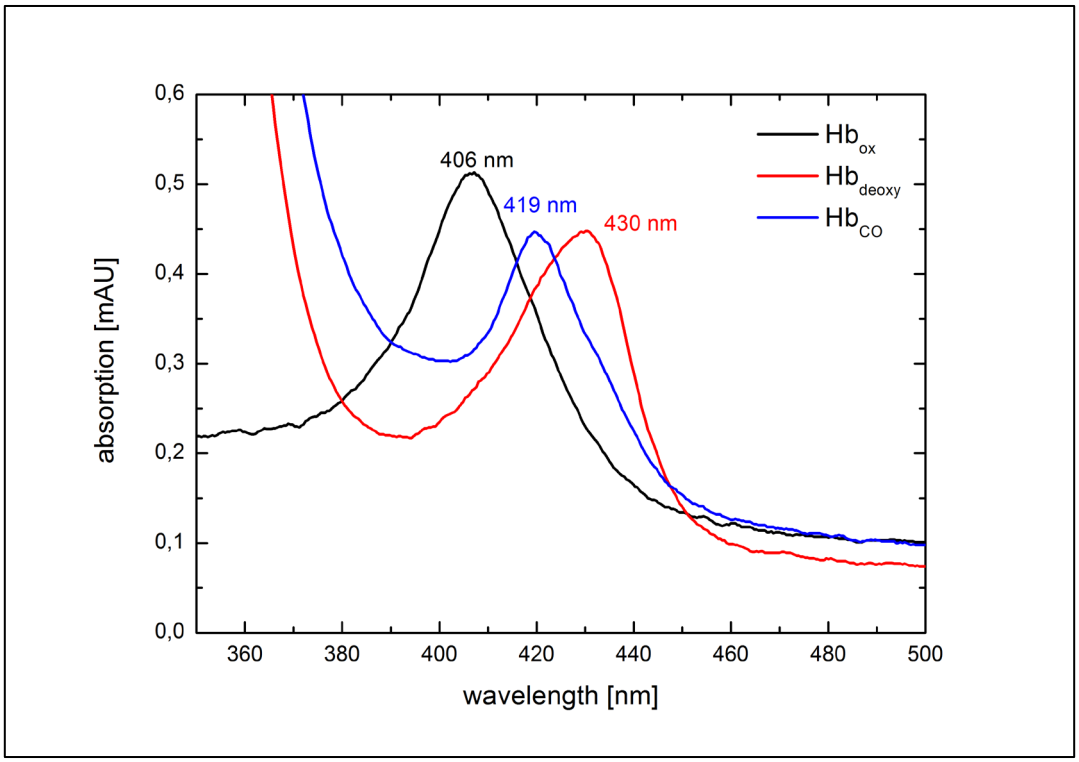

Figure 4-22 Shifts of the Soret peaks from 1 mM haemoglobin. The oxidized form is shown as a black line. The deoxygenated form, generated by adding NaDT to a final concentration of 12 µM, is shown as red line. After adding a final concentration of 20µM adt and 20µM unmaturated protein to the deoxygenated form the Hb_{CO} is generated (blue line).

The changes of the 430 nm and the 419 nm Soret peak is shown as a function of time in the following Figure 4-23. It can be observed, that if the 430 nm peak decreases because of the released CO from the maturated protein the 419 nm peak increases due to the formation of the Hb_{CO} state.

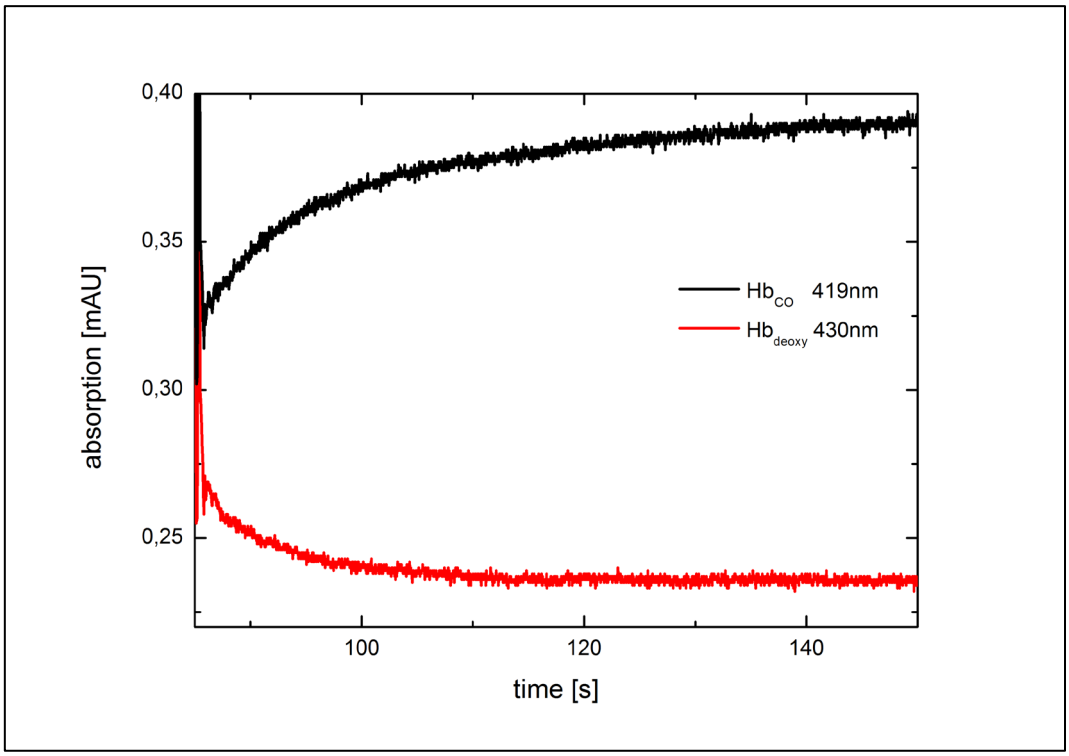

Figure 4-23 Kinetics of the reaction of deoxygenated haemoglobin with adt and maturated protein.

For determining the optimal activation time, unmaturated protein was mixed under anaerobic conditions with an equimolar ratio of adt. At different time points the hydrogen oxidation activity was measured by using the benzylviologen assay as described in Section 2.6.3. (see Figure 4-24)

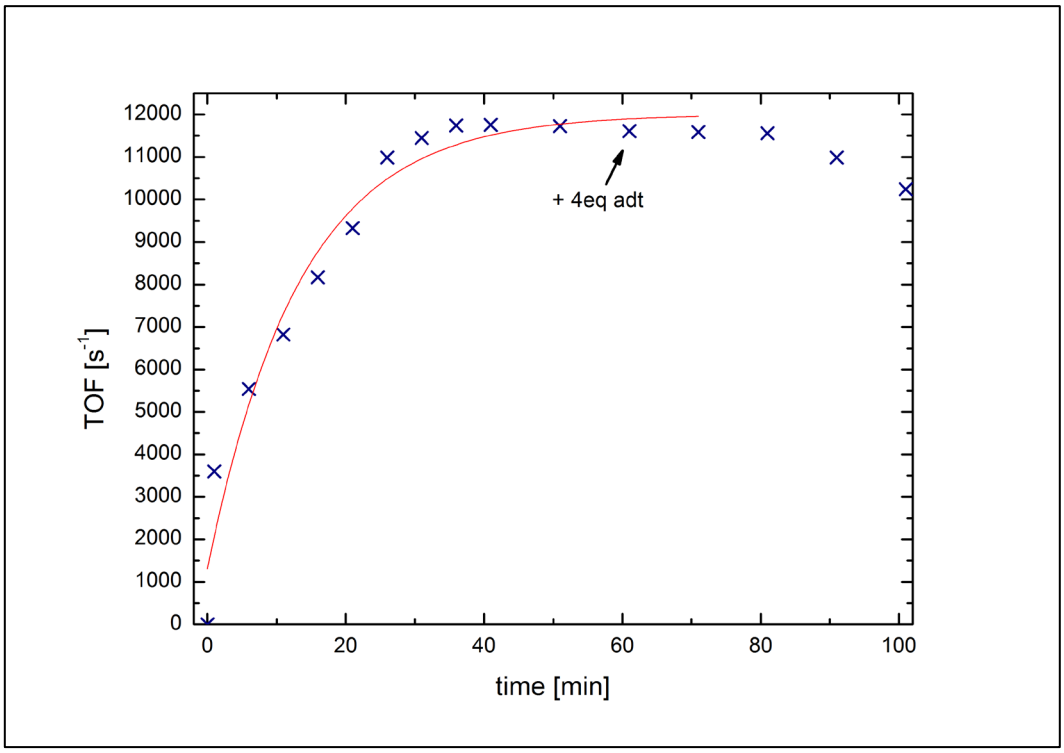

Figure 4-24 Hydrogen oxidation activity during activation, measured at different time points (t=0: unmaturated protein in the absence of adt. Unmaturated protein was mixed with adt in a 1:1 ratio at the beginning. As marked in the figure after a stagnation of the activity additional 4 equivalents of adt were added to see if the stagnation is due to substrate limitation. The red curve is the best exponential fit for these data points.

After mixing the unmaturated protein in a 1:1 ratio with the adt under anaerobic conditions 1 µL of this solution was taken and measured using the hydrogen oxidation assay as mentioned above. The activity increases nearly linearly up to 30 min, after this time the activity levels off. To be sure, that this is not caused by substrate limitation (adt) additional 4 equivalents of adt were added to see, if a further increase of the activity can be observed, which was not the case. 20 minutes after the second addition of adt the activity starts to decrease drastically, this is likely due to the destruction of the H-cluster and to the inhibition of other H-clusters by CO. From this experiment the optimal incubation time for activating the unmaturated [FeFe]-hydrogenase from *D. desulfuricans* was set to 30 minutes. The data points were fitted with an exponential function in the program origin 8.5. From this fit a half-life time of 7.6 min can be calculated.

In the benzylviologen assay it might be possible that the reaction is limited by the redox partner benzylviologen. To determine the optimal amount of benzylviologen, several different concentrations have been tested (Figure 4-25) in the hydrogen oxidation assay.

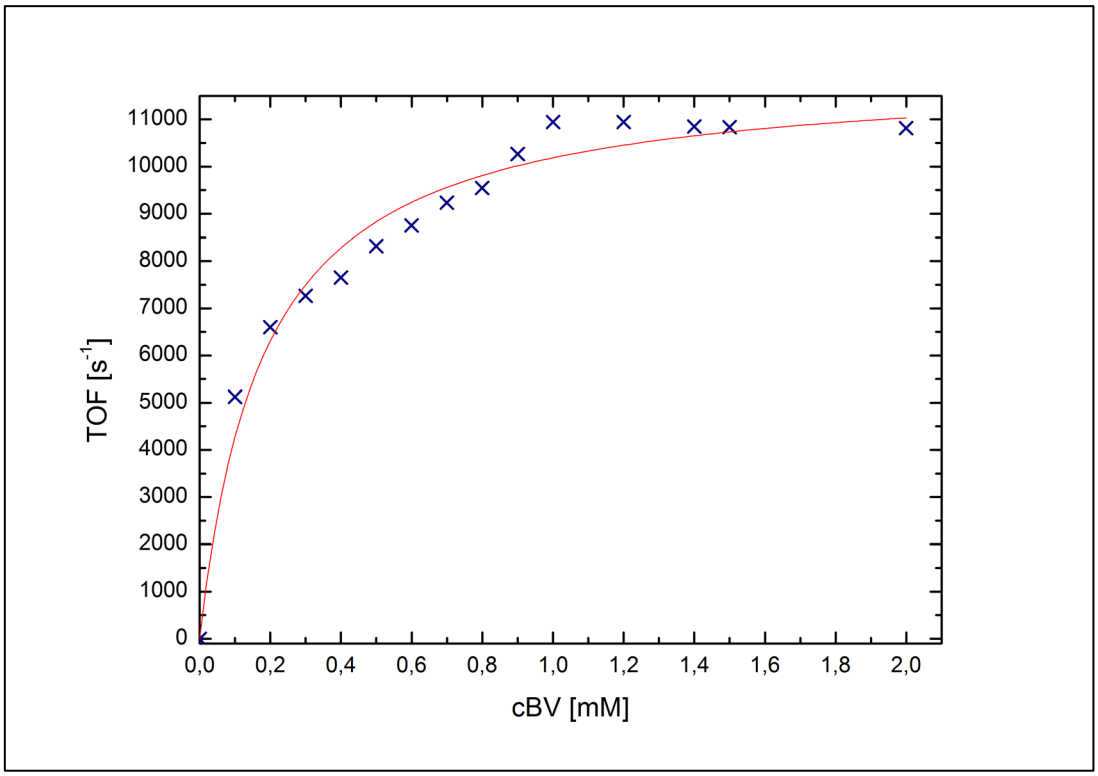

Figure 4-25 Determination of the optimal benzylviologen concentration in the hydrogen production assay. Protein to adt ratio was 1:1 and the activation time was 30 min, after that the maturated enzyme was purified via gel filtration to get rid of free complex. The red trace shows the best fit of a Hill equation in origin with n=1.

The Figure 4-25 shows that with increasing t benzylviologen concentration the measured activity also increases up to 1 mM. A further increase of the benzylviologen concentration does not result in an additional increase of activity. Every data point was measured with a freshly incubated sample (incubation with adt for 30 min). From this figure a benzylviologen concentration of 1 mM was chosen as standard concentration for hydrogen oxidation assays. The data points were fitted with a Hill equation ($y= V_{max}*x^n/(k^n+x^n)$) in origin 8.5, where n was set to 1 for modelling the easiest form of the Michaelis Menten function. As is obvious, the fit is not very good so it is not possible to give values for V_{max} and K. Maybe the mechanism of the reaction is not a Michaelis Menten kinetic; however, it is more likely that the data points show large errors. That means that the data points are no averages and an additional problem might be that the hydrogen saturation of the reaction buffer was not constant during the different measurements, which limits the substrate.

To provide insights into whether any particular buffers or pH has a significant influence on the measurement, several buffers were tested (see Figure 4-26). For this experiment the maturation of the enzyme was done in Tris/HCl pH 7.6 buffer for 30 minutes with a 1:1 ratio of protein and adt to be sure that the protein maturates. 1 µL of this solution was used for the hydrogen oxidation assay which contains 1 mM benzylviologen. Commonly used biological buffers were used at different pH.

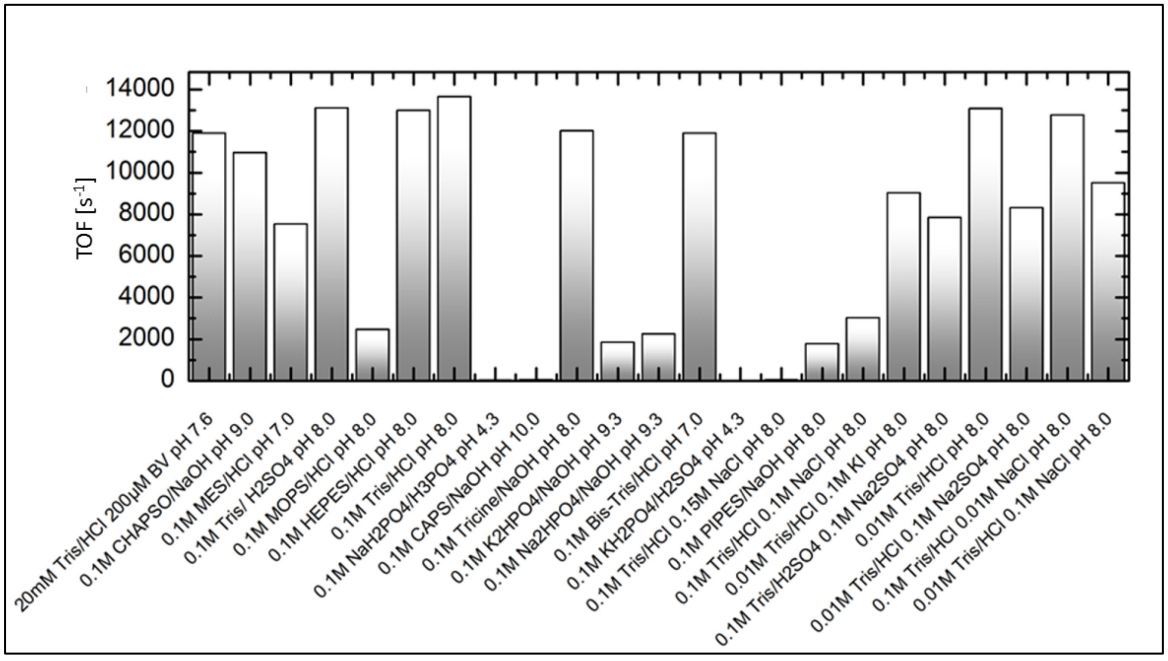

Figure 4-26 Overview of the hydrogen production assay in various buffer systems. Parameters for protein concentration and assay conditions are given in Section 2.6.3, all buffers contained 1 mM BV.

From this Figure 4-26 three groups of buffers can be determined: the buffers which gave almost no activity (0.1 M MOPS pH 8, 0.1 M K_2HPO_4 pH 4.3, 0.1 M CAPS pH 10, 0.1 M K_2HPO_4 pH 9.3, 0.1 M Na_2PO_4 pH 9.3, 0.1 M KH_2PO_4 pH 4.3, 0.1 M Tris/HCl pH 8 with 0.15 M NaCl and 0.1 M PIPES pH 8), buffers with high activities (20 mM Tris/HCl pH 7.6 with only 20 mM benzylviologen, 0.1 M CHAPSO, 0.1 M Tris/SO_4 pH 8, 0.1 M HEPES pH 8, 0.1 M Tris/HCl pH8, 0.1 M Tricine pH 8, 0.1 M Bis-Tris pH 7, 0.01 M Tris/HCl pH 8 and 0.1 M Tris/HCl pH 8 with 0.01 M NaCl) and buffers with lower activity (0.1 M MES pH 7, and 0.1 M Tris/HCl pH 8 with 1 M KI, 0.1 M Tris/HCl pH 8 with 0.1 M $NaSO_4$, 0.01 M Tris/HCl pH 8 with 0.1 M Na_2SO_4 and 0.01 M Tris/HCl pH 8 with 0.1 M NaCl). Except the buffers with extreme pH, where no activity was expected due to

protein damage no prediction of activity can be done. But based on this experiment 100 mM Tris/HCl pH 8.0 was set as standard buffer.

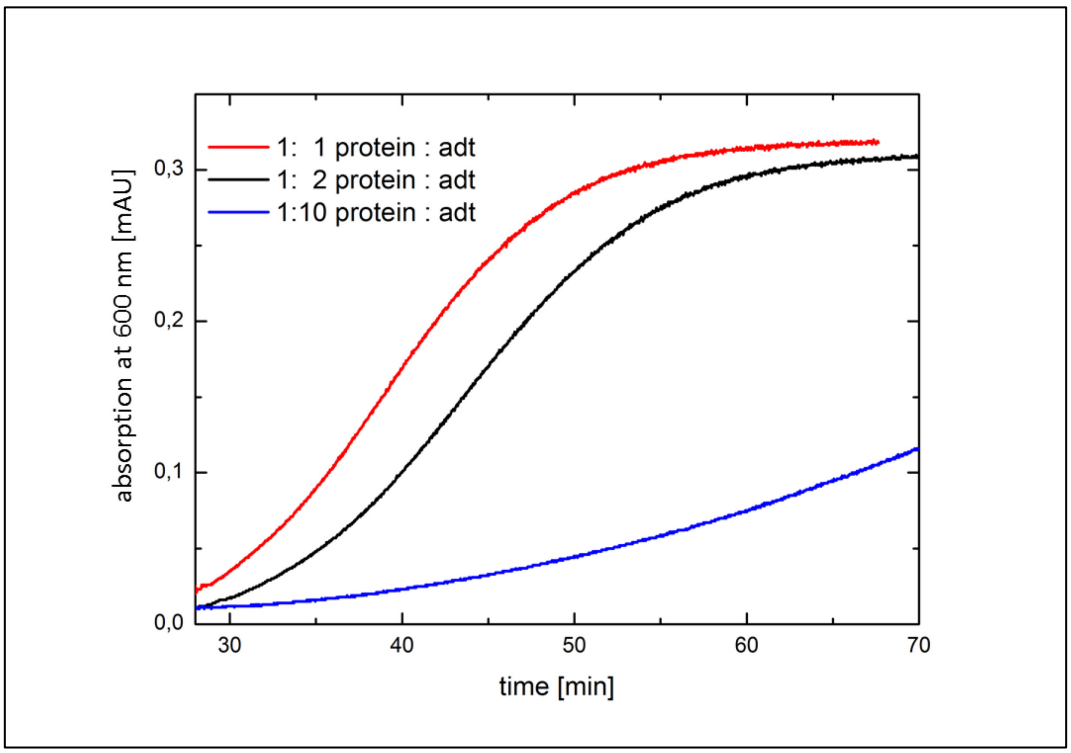

Figure 4-27 Hydrogen oxidation assay with different ratios of protein to adt, incubation time 1h in non-saturated 0.1 M Tris/HCl pH 8.0 buffer with 20 mM BV. The slopes of the linear parts are 0.015 for the 1:1 ratio, 0.013 for the 1:2 ratio and 0.004 for the 1:10 ratio.

This Figure 4-27 shows, that the slopes of the linear parts of the 1:1 ratio curve of protein to adt shows the highest activity. It was expected to see the fastest activation with an excess of adt but a ratio of 1:10 shows a significant decrease of the slope is observed. This is likely caused by a higher free CO concentration in the solution than for lower ratios, which leads to the inactive H_{ox}-CO state. From this result a 1:1 ratio was set as the standard activation ratio. For other protein activation (HydA1 from *C. reinhardtii*) in our laboratory it is knows, that an excess of adt in the solution does not results in a slower activation or in less active protein. Maybe the [FeFe]-hydrogenase from *C. reinhardtii* is less CO sensitive than the [FeFe]-hydrogenase from *D. desulfuricans*.

Based on all these reported experiments a standard protocol for the hydrogen oxidation assay can be summarized as:

- ratio of 1 : 1 protein to adt for activation
- activation time 30-40 minutes under anaerobic conditions
- hydrogen saturated 0.1 M Tris/HCl pH 8.0 buffer with 1 mM benzylviologen

By following these conditions a H_2:benzylviologen oxidoreductase turnover frequency of **10073 ± 500 [s^{-1}]** was measured for the artificially maturated [FeFe]-hydrogenase expressed in *E. coli* with adt.

To compare this number with the native [FeFe]-hydrogenase from *D. desulfuricans*, the same assay was used to measure the activity. Due to the fact, that the hydrogenase from the native system is purified under aerobic conditions, the activation curve shows a very unique sigmoidal form. After purification the protein is in its oxygen tolerant but inactive state (see Section 1.1.3). If the measurement was started immediately after taking the sample inside the glovebox it took a while to receive fully active protein (see Figure 4-35 A). Partly this is due to oxygen removal from the sample (remaining oxygen will re-oxidize the reduced benzylviologen) and then the protein needs to be converted from the H_{inact} state to the active H_{ox} state. If the protein was incubated for 30 minutes inside the glovebox before starting the measurement the lag phase is no longer visible (see Figure 4-28).

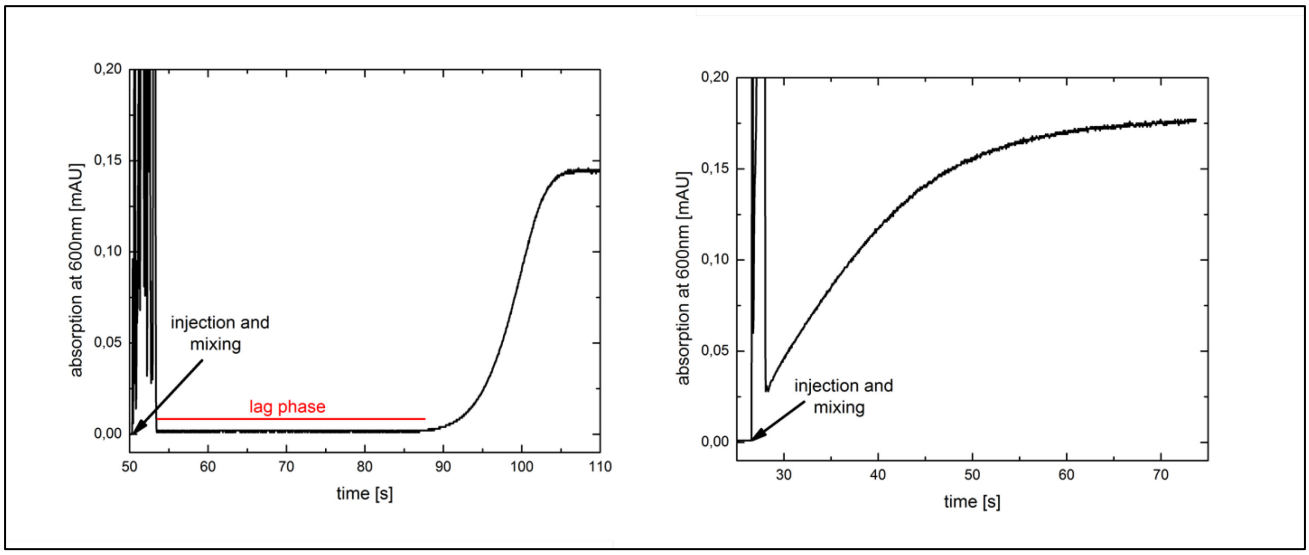

Figure 4-28 Kinetic trace of the hydrogen oxidation coupled to benzylviologen reduction by [FeFe]-hydrogenase from *D. desulfuricans*. A) without pre-incubation in the glovebox and B) after 30 min incubation in the glovebox (2 % hydrogen). The lag phase is marked in red. The points of injection and the mixing with the pipet are marked by the arrow.

To determine the specific activity for the native system, the sample was activated for 30 minutes inside the glovebox before measurement. Following the protocol for the maturated enzyme a turnover frequency of **11420 ± 200 s^{-1}** was calculated for hydrogen oxidation.

Since hydrogenases are bidirectional enzymes also the opposite direction (the production of hydrogen) was analysed by gaschromatography for both systems as reported in Section 2.6.3. A summary of the measured activities for both setups is shown in the following Table 4-5.

Table 4-5 Comparison of the activities from the native and artificially maturated enzme.

[FeFe]-hydrogenase from:	hydrogen oxidation activity TOF [s^{-1}]	hydrogen production activity TOF [s^{-1}]
native system	11420 ± 200	9667 ± 350
artificial maturated	10073 ± 500	10647 ± 350
% of the native system	88 %	110 %

As is visible from Table 4-5 the maturated enzyme from the heterologous expression system shows nearly the same turnover numbers as the native system. It can be assumed that the differences are due to measurement or system errors. From this data it can be shown that the heterologous expression system followed by activation with adt leads to fully active hydrogenase and that a 1:1 ratio of protein : adt is sufficient for complete activation.

No specific turnover numbers for the [FeFe]-hydrogenase from *D. desulfuricans* are reported in literature, therefore it was very important to measure the native system for getting these values as a comparison to the maturated protein and to compare the activity of the [FeFe]-hydrogenase from *D. desulfuricans* with other [FeFe]-hydrogenases. It is known from the literature that [FeFe]-hydrogenases show higher activities than [NiFe]-hydrogenases in both directions (see Table 4-6).

Table 4-6 Hydrogenases catalytic activities[141]

	[FeFe]-hydrogenase	**[NiFe]-hydrogenase**
hydrogen oxidation	28000 s^{-1}	700 s^{-1}
hydrogen production	6000-9000 s^{-1}	700s^{-1}

The measured values of 9967 [s^{-1}] for hydrogen production and 11420 s^{-1} for hydrogen oxidation for the native system fit nicely to this general overview. Not many turnover numbers for [FeFe]-hydrogenases are reported in literature and normally they are measured in different ways, which makes is hard to directly compare these data. For the [FeFe]-hydrogenase *Ca*HydA from *C. acetobutylicum* a turnover number for hydrogen production of 21000 s^{-1} was reported.[142] Also in our laboratory other [FeFe]-hydrogenases are studied, the [FeFe]-hydrogenase from *C. reinhardtii* shows turnover frequencies of 450 s^{-1} for hydrogen production and 150 s^{-1} for hydrogen oxidation. Although if these activities are much lower than the one measured for the [FeFe]-hydrogenase from *D. desulfuricans* the measured activities for *C. reinhardtii* fit well to the turnover frequencies reported in literature.[127,129]

Iron determination:

Routinely, the iron content of unmaturated and maturated protein was measured as described in Section 2.6.5. The maturated protein shows an iron content of 12.64 - 13.94 ± 1.4 irons/protein while the unmaturated protein only show 10.83 - 12.24 ± 1.4 irons/protein. These values are in agreement with the expected 14 irons/protein for the maturated and 12 irons/protein for the unmaturated enzyme.

4.4 Spectroscopic characterization of maturated [FeFe]-hydrogenase from *D. desulfuricans* and comparison to the native enzyme

To compare the artificially maturated enzyme to the native one, two spectroscopic techniques were used in this thesis, Fourier Transformation Infrared (FTIR) spectroscopy and Electron Paramagnetic Resonance (EPR) spectroscopy.

4.4.1 *FTIR Spectroscopy*

To analyse the native system in comparison to the maturated enzyme first an as isolated spectrum was measured. Figure 4-29 shows an FTIR-spectrum of the as isolated enzyme.

In this as isolated state the terminally-bound CN^- groups show bands at 2106 cm^{-1} and 2087 cm^{-1}, the two terminally bound COs can be observed at 2007 cm^{-1} and 1983 cm^{-1}, finally the bridging CO shows a signal at 1848 cm^{-1}.

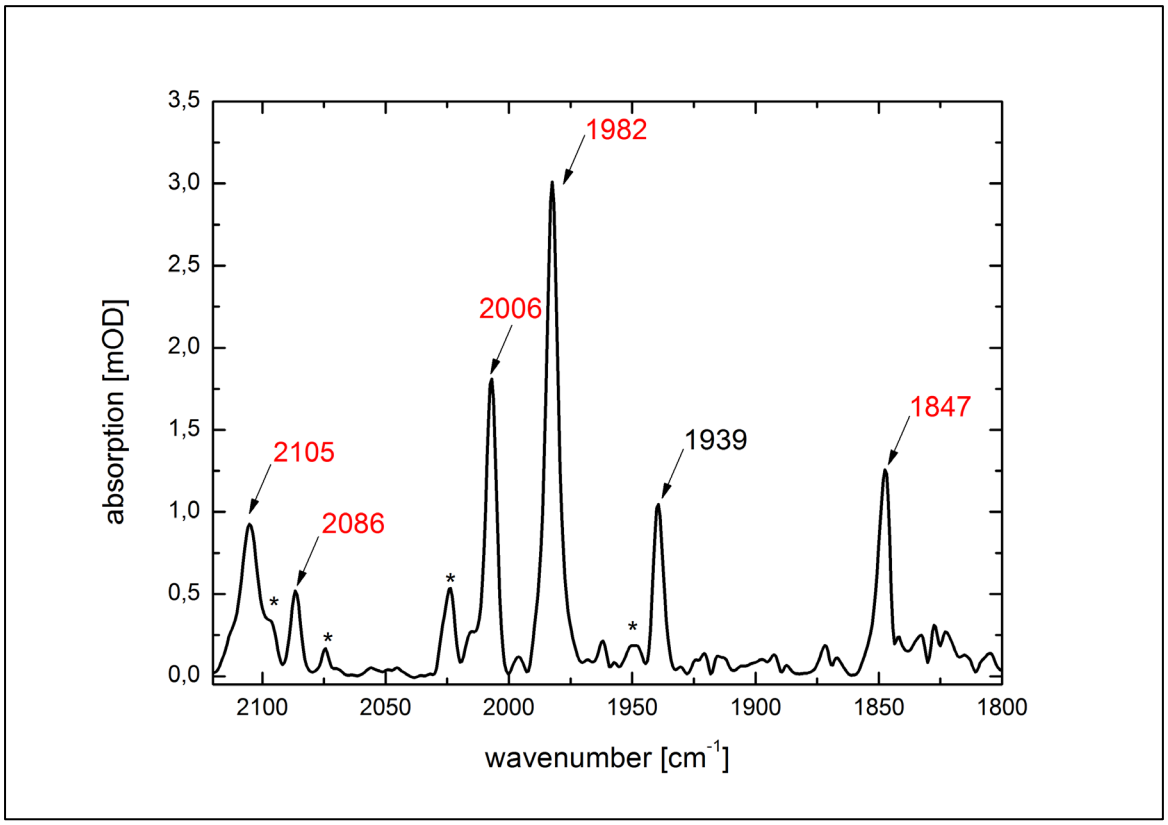

Figure 4-29 FTIR spectrum of the as isolated state of [FeFe]-hydrogenase from *D. desulfuricans*. The red indicated signals belong to the reported as isolated state. The black labelled signal is known from former preparations[98] but does not belong to a known redox state. The unlabelled signals are maybe caused by contamination of the sample and marked with asterisks.

The measured signals (labelled in red) fit nicely to the reported values in the literature. The black labelled peak at 1939 cm^{-1} is known from former purifications of this enzyme but does not fit to any known redox-state.[98] The unlabelled peaks are maybe caused by some contamination in the sample.

To generate the reduced state from the as isolated enzyme, which should be the same redox state as for the maturated enzyme without further treatment, a protein solution was incubated for 30 min anaerobically on ice inside the glovebox, containing 2 % of hydrogen in the surrounding, also the FTIR cell was filled inside the glovebox to avoid oxygen damage to the protein. A measured spectrum of the reduced state hydrogenase is shown in Figure 4-30.

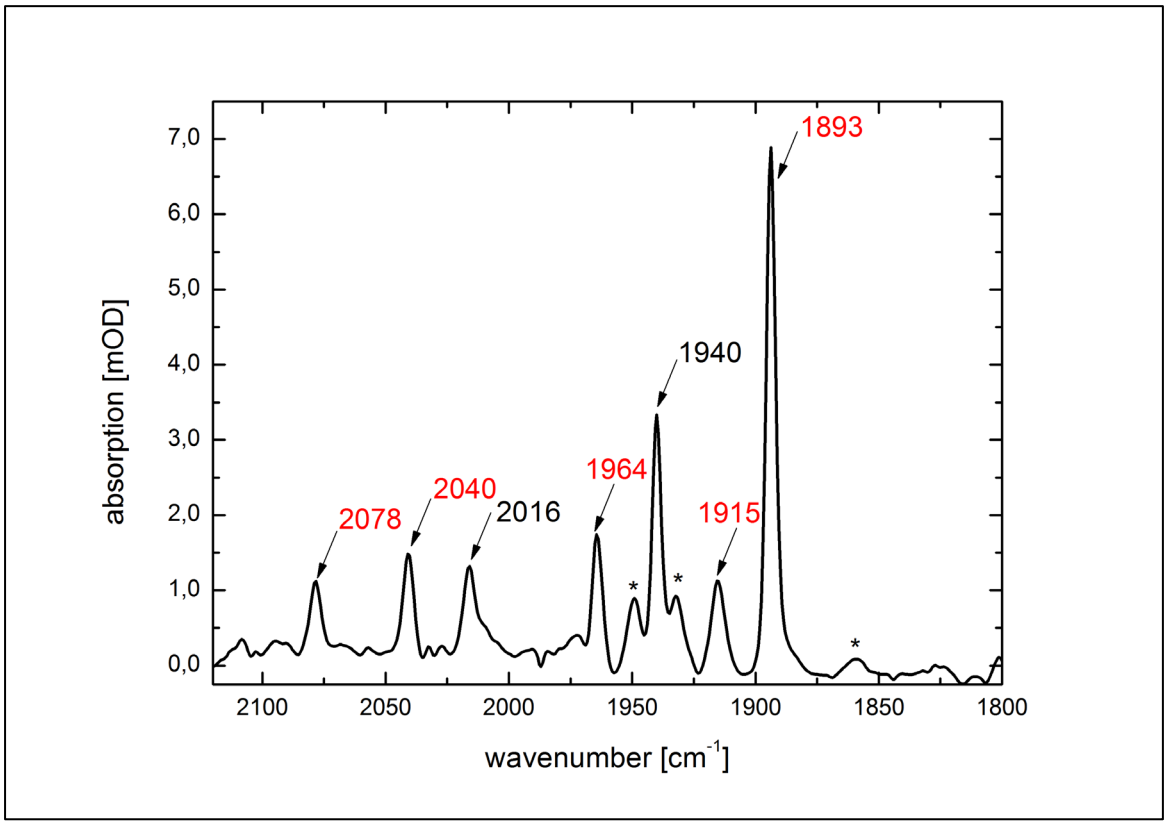

Figure 4-30 FTIR spectrum of the reduced state, formed by incubation under hydrogen. The red indicated signals belong to the reduced state. The black labelled peak at 1940 cm^{-1} is similar to the one reported in Figure 4-29 and the peak at 2016 cm^{-1} is the most prominent signal of the $H_{ox\text{-}CO}$ state and is maybe caused by a slow degradation of the protein.

As for the as isolated state, the measurement fits quite well to the reported spectra in the literature. Also in this spectrum the peak at 1940 cm^{-1} is observable, due to the fact, that both samples are not from the same batch no statement of the signal intensity can be done. The signal at 2016 cm^{-1} is the most prominent signal of the $H_{ox\text{-}CO}$ state and maybe due to slow degradation of the protein.

It was planned to compare the reduced state of the native enzyme with the artificially maturated enzyme because it was expected, that after maturation in the glovebox the enzyme will be in the reduced state. Unfortunately, until now it was only possible to record an FTIR-spectrum of the maturated enzyme in its CO inhibited state (H_{ox}-CO). From the activity measurements (Section 4.3) it is clear, that after maturation the enzyme is in its active form, but for FTIR measurements higher sample concentrations are needed. It is possible that after maturation, predominantly the H_{ox}-CO state is formed, which upon dilution into the assay buffer is converted to H_{ox} by dissociation of the CO,

whereas in the more concentrated FTIR samples the CO exchange is not fast enough. It is also possible that the generation of the CO-inhibited state is due to cannibalism effects, reported previously.[85] If a protein gets damaged by light, CO is released from the damaged H-cluster and this free CO can bind to other intact H-clusters. This leads to an enrichment of the H_{ox}-CO state in the sample. A spectrum of the maturated enzyme in the CO-inhibited state is shown in Figure 4-31.

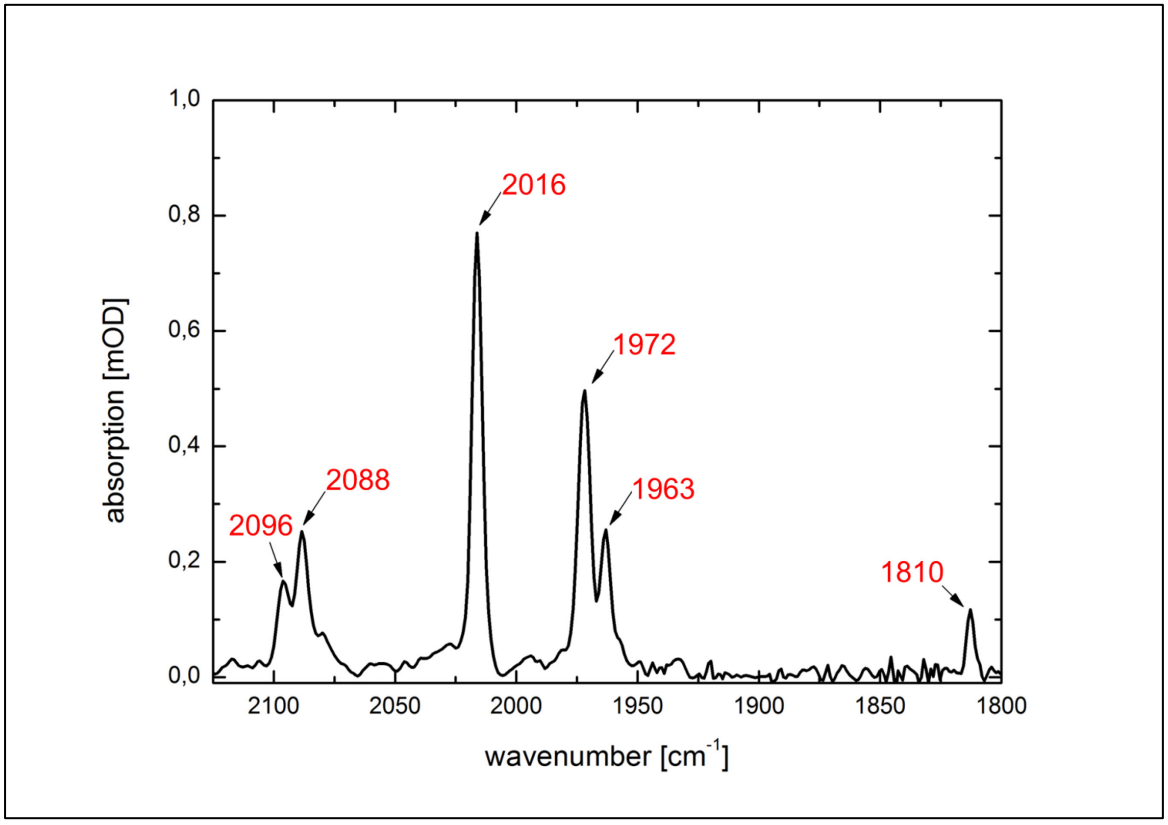

Figure 4-31 FTIR spectrum of the $H_{ox\text{-}CO}$ state of maturated [FeFe]-hydrogenase from *Desulfovibrio desulfuricans*. The red indicated bands belong to the reported H_{ox}-CO state.

Also the measured signals from the maturated enzyme fit very well with the signals of the native enzyme, reported in the literature. A difference to the native system is that the unknown peak at 1940 cm^{-1} is not observable in these samples. Even if the maturated hydrogenase could not be converted in the reduce state, this spectrum demonstrates at least, that the H_{ox}-CO state in the artificially maturated enzyme is identical to that in the native enzyme.

4.4.2 *EPR spectroscopy*

An additional method for analyzing the maturated and the native [FeFe]-hydrogenase is EPR spectroscopy. A theoretical introduction of EPR spectroscopy is given in Section 2.7.2. In the as isolated, oxygen tolerant state of the native system, the H-cluster is in a diamagnetic (and therefore EPR silent) state. The relatively isotropic signal (see Figure 4-32) observed close to g = 2 is caused by a small amount of $[3Fe\text{-}4S]^{+}$ cluster, presumably generated by oxygen damage during aerobic purification, which has also been reported previously in the literature.[103]

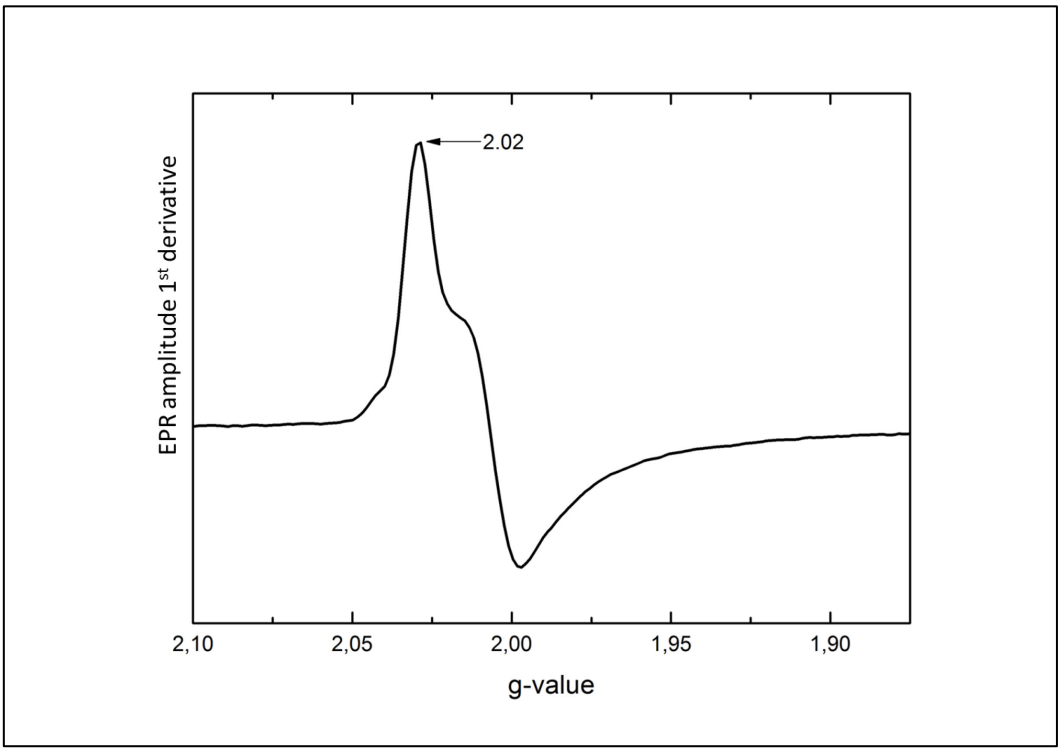

Figure 4-32 X-Band EPR spectrum of "as-isolated" [FeFe]-hydrogenase from *Desulfovibrio desulfuricans.* Spectrum was recorded at 20dB and 10K.

During activation in the presence of hydrogen the as-isolated hydrogenase forms a transition state, the so called H_{trans} state. This state is characterized by a rhombic S = ½ EPR signal with g-values of 2.06, 1.96 and 1.89. It is assumed that these signals belong to a reduced [4Fe-4S]-cluster, most likely the $[4Fe\text{-}4S]_H$-sub-cluster of the H-cluster.[103]

Further reduction of the enzyme yields the H_{ox} state, which is the active state of the enzyme, and which can be reduced to the H_{red} state by electrons or hydrogen.

$$H_{ox} + H_2 \rightleftharpoons H_{red}$$

Details about the reduced spectra of native [FeFe]-hydrogenase are given in Figures 4-14, 4-15 and 4-16 in Section 4.2.2, where also the differences between hydrogen and dithionite reduction are described. For completeness Figure 4-33 shows again the dithionite reduced spectra.

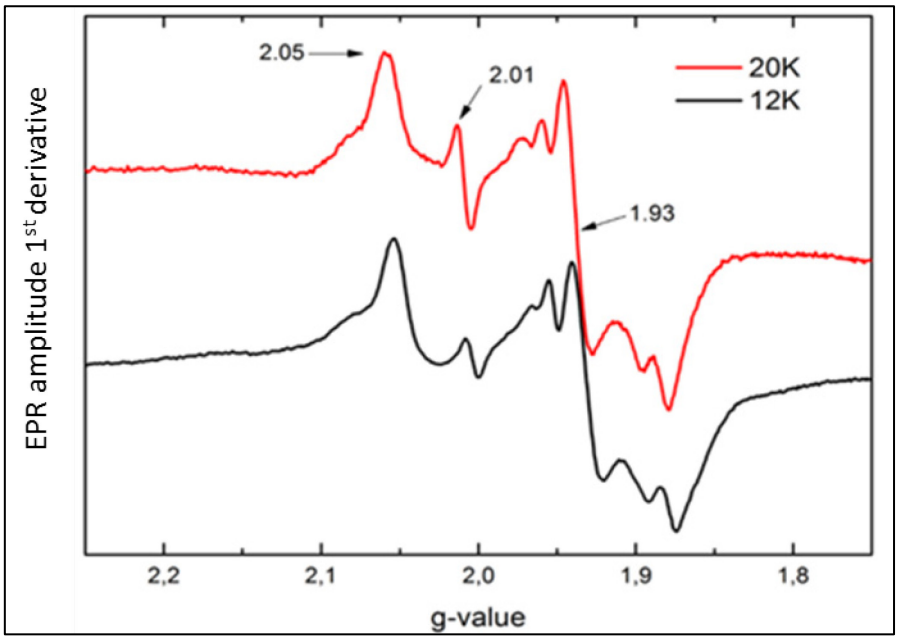

Figure 4-33 X-Band EPR spectra of reduced [FeFe]-hydrogenase after reduction with NaDT at 23 dB at 20 K (red trace) and 12 K (black trace).

The H_{ox} state shows a rhombic S = ½ signal with g values of 2.10, 2.04 and 1.99, which fit well to the spectra reported in the literature. A spectrum of the oxidized state is shown in Figure 4-34 for two different temperatures. It is known, that the H_{ox} becomes more clearly observable at higher temperature, this is also shown in this Figure. The signals become clearer at 40 K than at 10 K.

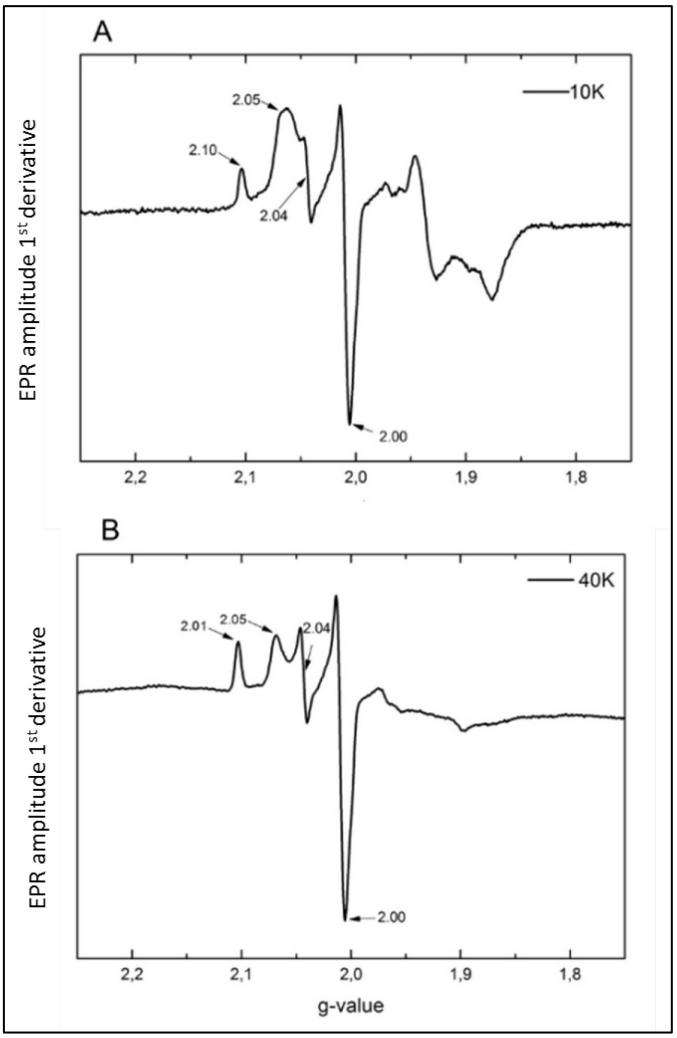

Figure 4-34 X-Band EPR spectra of the *D. desulfuricans* [FeFe]-hydrogenase oxidized under N_2/Ar. The spectra were recorded with a power of 1 mW and at a temperature of A) 10 K and B) 40 K. the g-values of the H_{ox} state and $H_{ox\text{-}CO}$ states are indicated. This is caused by the assumption, the the H-cluster is in the H_{red} state and one of the F-cluster is reduced.

To compare the native system with the maturated enzyme and with the unmaturated enzyme the same experiments were performed with the artificial maturated enzyme, if not stated otherwise all samples contain 1 mM NaDT. The following Figure 4-35 shows the NaDT reduced X-Band spectra of the reconstituted protein at different temperatures, also here a split signal is observed as reported for the unmaturated protein, earlier in this chapter.

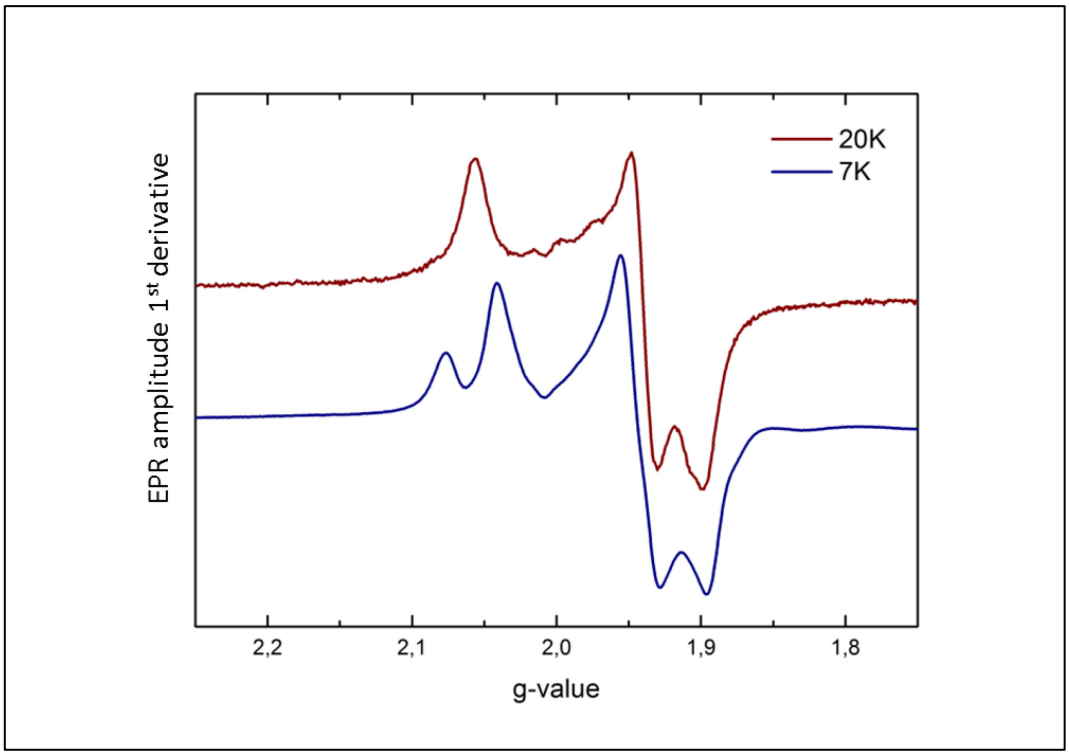

Figure 4-35 X-band EPR spectra of maturated protein at different temperatures (20K in red, 7K in blue), 23 dB.

The maturated protein was also measured after reduction with hydrogen only (no NaDT in the sample). These spectra differ from the NaDT reduced form as shown in Figure 4-36, hence there is no peak splitting is observed.

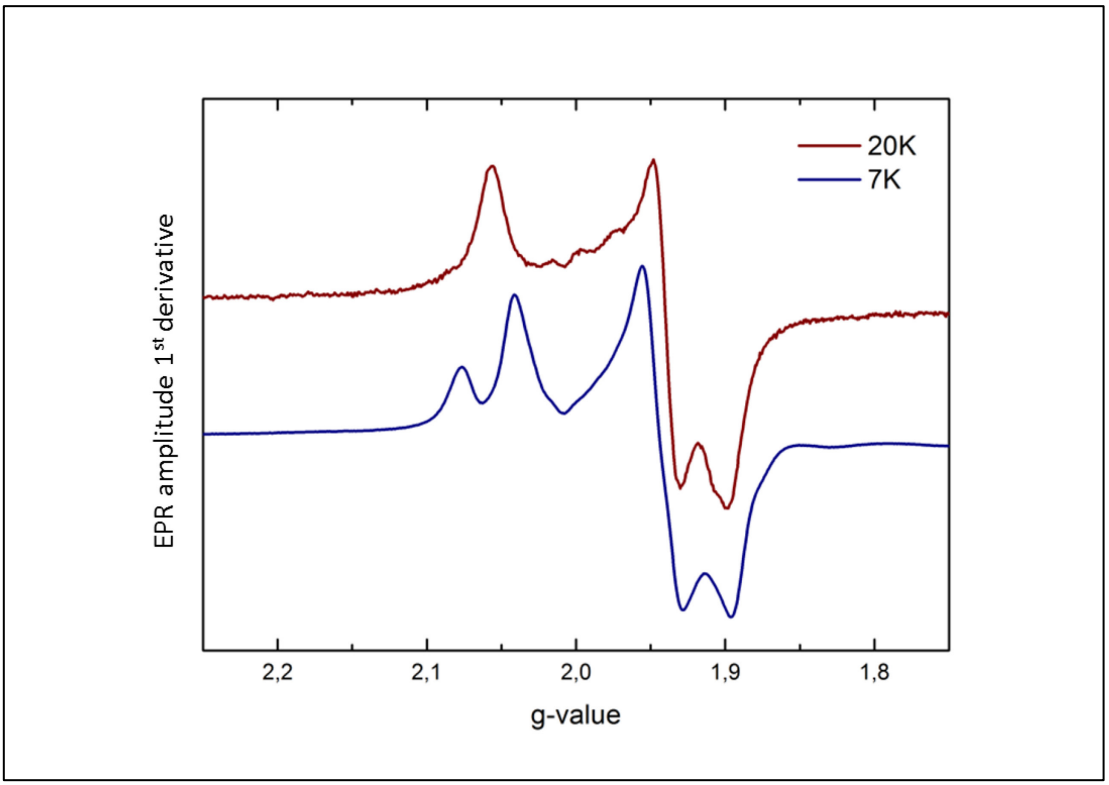

Figure 4-36 X-band EPR spectra of maturated enzyme after reduction with hydrogen (no NaDT) at different temperatures (20K in red, 7K in blue), 23 dB.

For a better comparison between the recorded spectra, the next figure 4-37 show the unmaturated protein, reduced with NaDT, and the maturated protein reduced either with NaDT or with hydrogen at two temperatures.

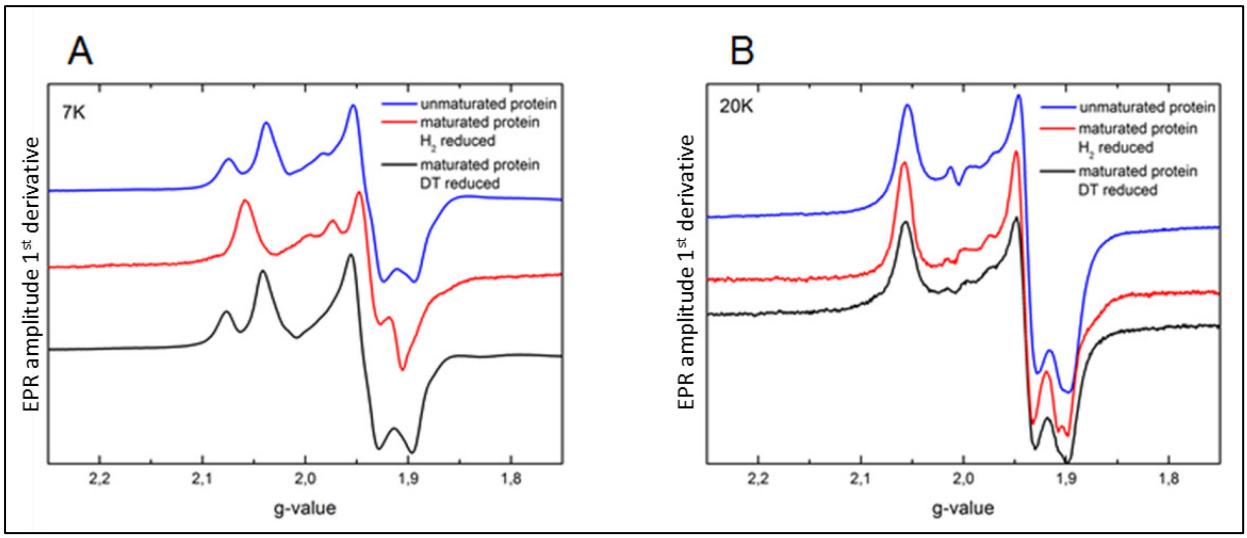

Figure 4-37 Comparison of the X-band EPR spectra from NaDT reduced unmaturated protein (blue) and maturated protein reduced with NaDT (black) or hydrogen (red) at 7K (A) and 20K (B), 23 dB.

As it is obvious from the preceding figures at low temperatures the maturated protein reduced with NaDT behaves like the unmaturated form and shows a splitting like described in Section 4.2.2 and at high temperatures the split signal disappeared and all spectra look the same. But several considerations need to be in mind while thinking about these spectra:

- It is not clear if 100 % of the protein is maturated after the treatment with adt, so it is possible, that the observed split signal in the NaDT reduced sample derives from still unmaturated protein in the sample.
- If the split signal is caused by an interaction as described in Section 4.2.2 a reduction with only hydrogen does not decrease the potential enough to have a fully reduced sample and therefore it is not possible to observe a signal splitting. A reduction with hydrogen for the unmaturated protein is not possible, so a comparison for that is not feasible.

So far, there is no splitting for the signal known for the native sample, also not after reduction with NaDT but there are also some points to mention in this context. NaDT can influence the pH of the system, and so far for the native system a buffer with a lower buffer concentration was used, this could lead to a noticable change of pH and this can

also change the behaviour of the protein and it was shown for the unmaturated protein that the splitting of the signal is pH dependent. But it seems to be clear that the maturation of the protein leads to an active hydrogenase.

Also for the reconstituted protein power saturation experiments at 10K and 40K were performed and are shown in the following figure 4-38.

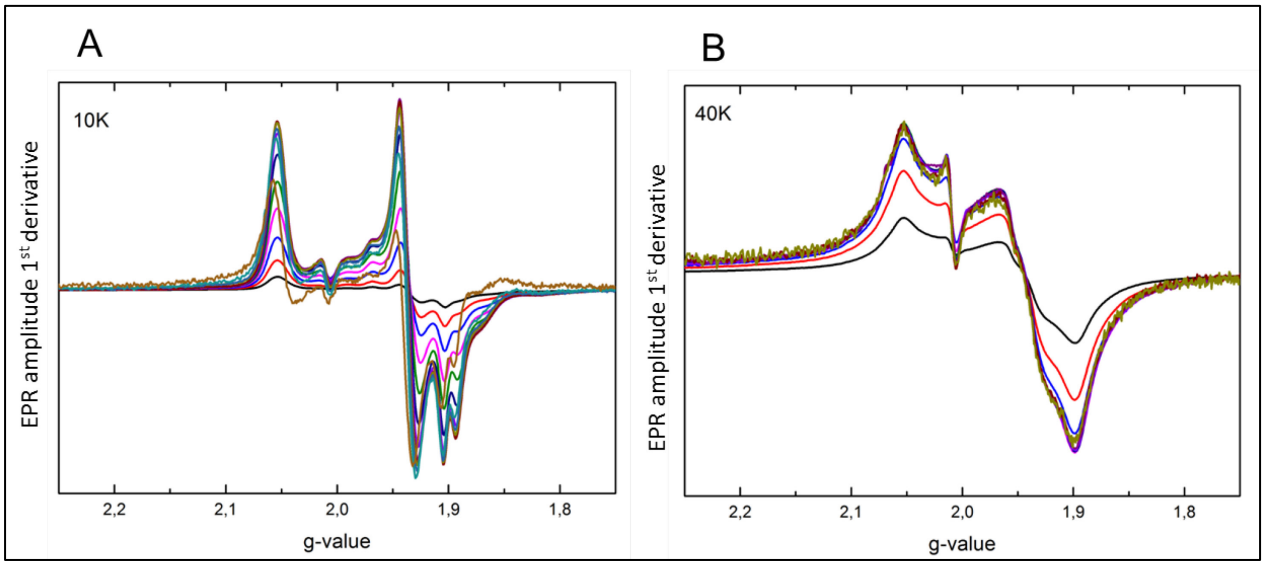

Figure 4-38 X-Band EPR, power saturation experiments for maturated protein, at 10K (A) and 40K (B).

The following Figure 4-39 shows a comparison of the native protein and the unmaturated enzyme, each reduced with NaDT. It is obvious from this Figure 4-39 that there are some small differences between both spectra. The artificially maturated spectra shows less of the peak at g = 1.86 and a shift in the g-value of the g1 peak from 2.005 to 2.05. Nevertheless, it can be concluded that the enzyme from the heterologous expression is identical to the native enzyme. Still it is unclear where the split signal comes from, even when it is observable in the maturated enzyme.

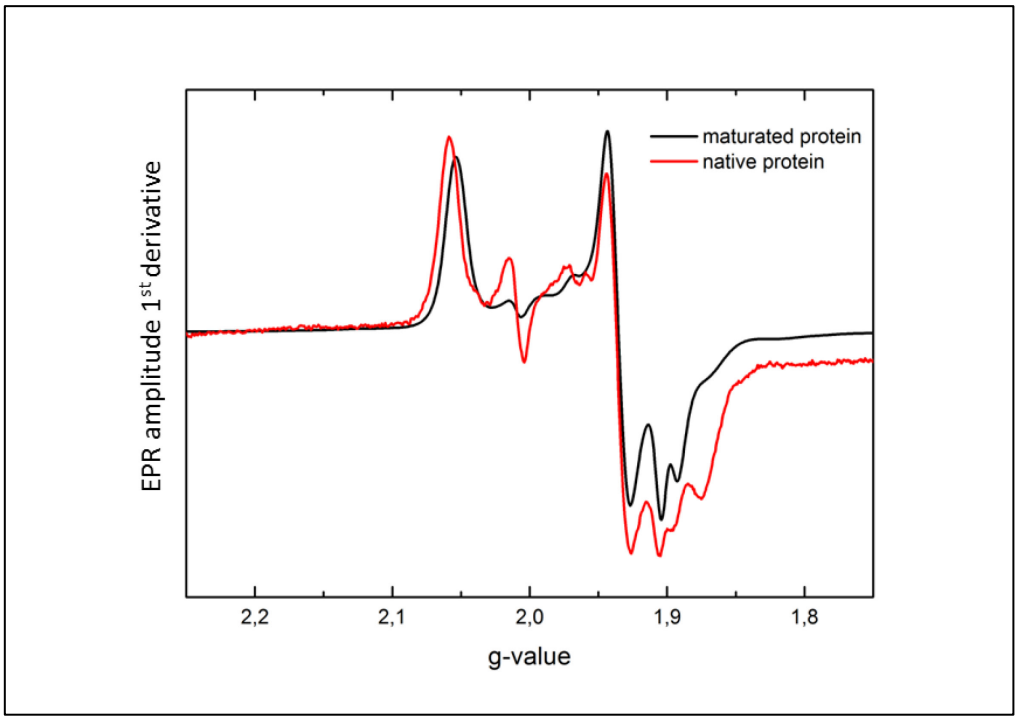

Figure 4-39 Comparison of X-band EPR spectra of the native [FeFe]-hydrogenase (red trace) and the maturated hydrogenase from the over-expression system (black trace).

4.5 Summary

After successful expression of unmaturated protein (see Chapter 3), the unmaturated enzyme was characterized with EPR spectroscopy where it shows unusual behaviour by showing a split signal around g = 2.05. This splitting disappears at higher temperatures and the total signal intensity follows the Curie law. In further experiments three redox potentials at **-300 mV**, **-390 mV** and **-465 mV** were determined, which correspond to the successive reduction of the [Fe-S]-clusters.

It was also possible to find crystallization conditions to receive a crystal of unmaturated protein which shows X-ray diffraction to around 5 Å. From this diffraction pattern the space group $P2_12_12_1$ which is the same space group as reported for the native protein[30] was calculated. This means, that the insertion of the $[2Fe]_H$-sub-cluster does not change the space group of the crystal, so it is unlikely that there are large conformational changes involved in maturation. Further investigations in optimizing the crystal conditions are necessary to improve the resolution to be able to calculate an electron density map.

These conditions might offer a possibility for crystallization of maturated enzyme to also characterize this.

It was also possible to activate the unmaturated enzyme with the $[2Fe]_H$-sub-cluster mimic adt to fully active hydrogenase. For this the activation procedure was optimized and turnover frequencies of 10073 ± 500 s^{-1} for hydrogen oxidation and 10647 ± 350 s^{-1} for hydrogen production could be measured. Unfortunately there were no turnover frequencies known in literature for the native enzyme, therefore the turnover numbers for the native protein were also measured for the first time. The native enzyme gave activities of 11420 ± 200 s^{-1} for hydrogen oxidation and 9667 ± 350 s^{-1} for hydrogen production.

The maturated enzyme was also characterized by EPR and FTIR and compared with the native protein. Also the maturated enzyme shows the signal splitting in EPR, while the native enzyme does not. So far it was only possible to get FTIR spectra of the unmaturated enzyme in its CO-inhibited state, further investigations are planned to fully characterize the heterologous expressed enzyme.

Chapter 5 Site-directed mutagenesis of the [Fe-S]-cluster surrounding to change redox-properties

5.1 General Introduction

The active site of the [FeFe]-hydrogenase from *Desulfovibrio desulfuricans* is connected via two [4Fe-4S]-clusters to the surface of the protein. All of them are separated by distances over which direct electron transfer can take place. For a better differentiation of maturated/unmaturated and native enzyme in this chapter the standard nomenclature of these clusters is changed to proximal ($[4Fe\text{-}4S]_H$), medial and distal as shown in Figure 5-1.

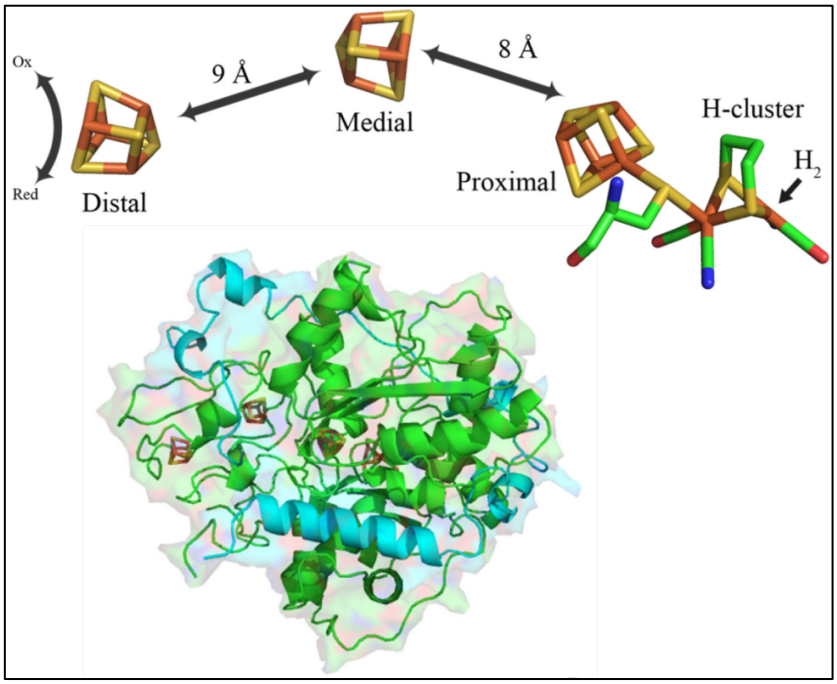

Figure 5-1 Scheme of the [Fe-S]-cluster distribution in the [FeFe]-hydrogenase from *Desulfovibrio desulfuricans* including the nomenclature used in this chapter. This figure was made with the pymol program and the pdb coordinates from 1HFE.

These clusters can be separated into two types, the proximal cluster which is part of the H-cluster, together with the $[2Fe]_H$-sub-cluster and the distal and the medial cluster, which are bound in an 8Fe ferredoxin-like domain. All of these [Fe-S]-clusters are coordinated by four cysteine residues, which are highly conserved in different [FeFe]-hydrogenases. Figure 5-2 shows an alignment of three highly divergent hydrogenases: the periplasmic hydrogenase from *Desulfovibrio desulfuricans*, the cytoplasmic hydrogenase from *Clostridium pasteurianum* I (CpI), and the hydrogenosomal hydrogenase from *Trichomonas vaginalis* (TvH). The figure shows clearly that despite the sequence divergence of the hydrogenases, all three show the same cysteine residues for binding the [Fe-S]-clusters.

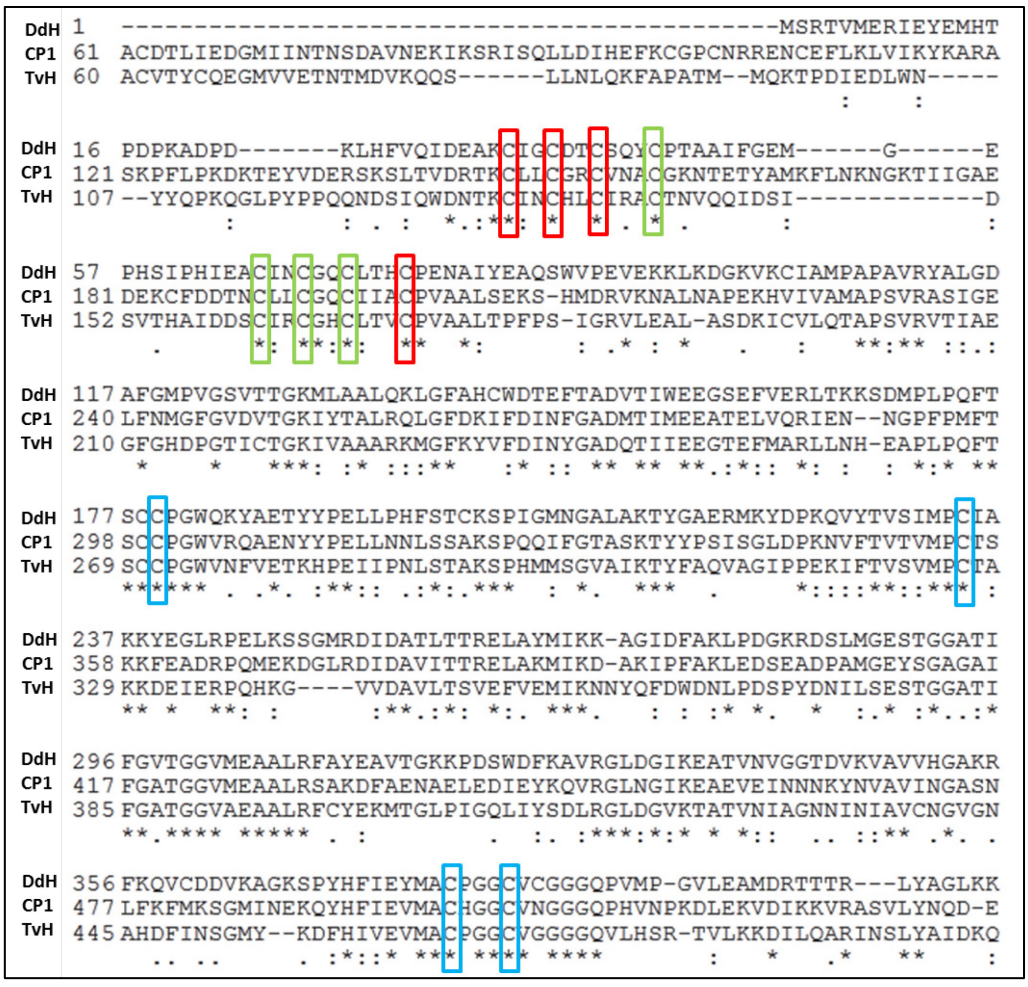

Figure 5-2 Sequence alignment of three different [FeFe]-hydrogenases, the periplasmic hydrogenase from *Desulfovibrio desulfuricans* (DdH, Uniprot P07598), the cytoplasmic hydrogenase from *Clostridium pasteurianum I* (CP1, Uniprot P29166) and the hydrogenosomal hydrogenase from *Trichomonas vaginalis* (TvH, Uniprot A2DJT6). The cysteine binding sites for the distal cluster is marked in red, the binding sites for the medial cluster in green and the cysteine residues for the proximal cluster are marked in blue. Figure adapted from Y. Nicolet et al..[30]

Despite the conservation of the cysteines the rest of the amino acid sequence is very divergent. This could have large consequences on the iron-sulfur cluster properties. But not only the sequences of hydrogenases are very divergent, they also have different activities, directionalities and oxygen sensitivities; a reason for this might bethe different numbers of accessory clusters. For example it is clear that comparison of the oxygen sensitive and tolerant [NiFe]-hydrogenase (*Aquifex aeolicus*) reveals that the coordination of the proximal F-cluster can alter it from a normal [4Fe-4S]-cluster to the [4Fe-3S]-cluster connected by six cysteine residues, which can easily access two reduction potentials for electron transfer to the active site, where the oxygen is reduced to water.[143] Also the clusters in [FeFe]-hydrogenases influence the behavior of the protein. There is a clear correlation between the high potential inactivation (see Chapter 6) and the number of F-clusters.[37] From these examples it is obvious, that iron-sulfur clusters play an important role in the enzyme. As it is reported in Chapter 1 their main function is electron transfer. Therefore, it was considered to change the redox potential of the different clusters to see changes in their activity. It might be possible to increase the enzyme activity or change the directionality.

There are several interactions in the protein which should play a role in determining [Fe-S]-cluster potentials:

1. The nature of the cluster and its first coordination sphere ligands. (i.e. is the cluster a [2Fe], [3Fe] or [4Fe]-cluster and does it have cysteine ligands or other ligands around)
2. The second coordination sphere, which effects may be due to hydrogen bonding or also due to electrostatic effects, hydrophobic effects or strain on the cluster and its ligands.
3. Amino acids that do not make direct contact to the cluster but that interact with the second coordination sphere ligands and may also have effects.

So far, modifications on the first coordination sphere (the cluster itself) are not straight forward. It is not known so far, how to change a [2Fe] to a [4Fe]. It has been shown that a [4Fe] can be changed to a [3Fe] by mutation[144] but these effects are rather large and not always applicable. So far this change is only successful when two related proteins show the two different clusters suggesting that the sites here may be adapted to accommodate both types of cluster. It is also possible to substitute cysteine for histidine

or other ligands but again these are quite drastic effects and may not work or may give too large changes.

Modifications of the second coordination sphere are known to be easier because they usually do not have a large effect on the cluster structure but can still cause reasonably large changes of the potentials. It is mentioned that charged amino acids can have an influence on the reduction potentials of metal cofactors. However, [Fe-S]-clusters generally show large numbers of hydrogen bonds both from backbone amide protons and from side chain, amides, hydroxyls, carboxylic acids and amines. The hydrophobic effects are perhaps less easy to predict and there is not a commonly used method known how to induce strain on the clusters. Therefore, manipulation of hydrogen bonds seems to be the most straightforward approach to change the potentials of the clusters.

For changing single amino acids in the clusters surrounding the technique of site-directed mutagenesis was used. This is a method to create specific and targeted changes in plasmid DNA. For that specific primers were designed to change an amino acid, all primers are given in Chapter 2.

5.1.1 *Aims of the work described in this chapter*

- Design and clone different mutants of the [FeFe]-hydrogenase to change the properties of the [Fe-S]-clusters.
- Express and purify the different mutants and characterize them by EPR spectroscopy.
- Try to activate the mutant proteins and compare their activities with the wild type protein.

5.2 Cloning and expression of the different mutants

5.2.1 *Planned mutations on the [FeFe]-hydrogenase from D. desulfuricans*

For understanding the importance of a residue in a protein usually the amino acid of interest is changed to alanine which ensures that the mutation does not disrupt the secondary structure due to steric hindrance and has no reactive groups to interact with the clusters. A change of proline may influence the secondary structure of the enzyme, because proline usually interrupts the secondary structure of a protein and there is no possibility to form any hydrogen bonds to interact with the surrounding amino acids.

Proximal cluster ($[4Fe]_H$)*:*

The proximal cluster is here defined as [4Fe]-sub-cluster of the H-cluster ($[4Fe]_H$) in the maturated enzyme. Only three mutations were planned on this cluster. Due to the fact that this cluster forms part of the H-cluster, the mutations should have a large influence on the activity.

The planned mutations were:

- C234A
- C382A and C382S

The mutation of C234 to alanine is predicted to change the 4Fe-cluster to a 3Fe-cluster. Such a change has been previously observed with similar mutations in other enzymes but there the cloning site was not directly attached to the H-cluster.[144,145] The change of cysteine 382 to alanine and to serine removes the bond between the $[4Fe]_H$-cluster and $[2Fe]_H$ sub-clusters of the H-cluster. This may prevent maturation, or may lead to a maturated protein with a disconnected H-cluster, perhaps with altered activity. Additionally, the C382A mutation may lead to formation of a [3Fe] cluster. Figure 5-3 shows the proximal cluster with the labelled amino acids for mutation.

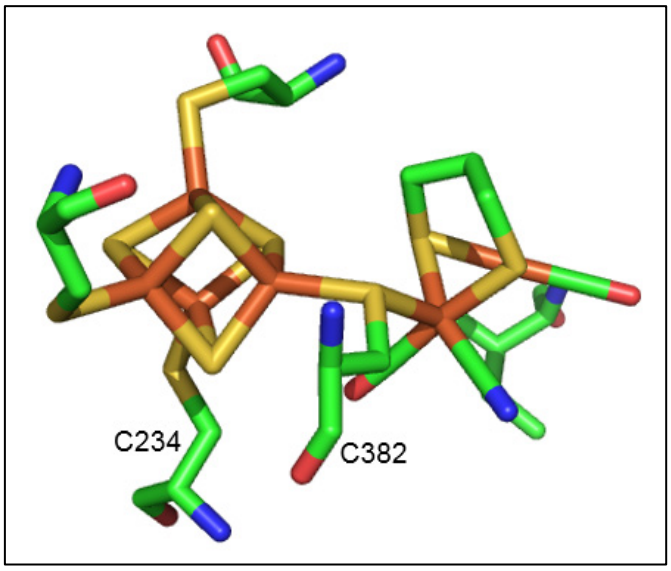

Figure 5-3 Scheme of the proximal cluster of the [FeFe]-hydrogenase from *D. desulfuricans* with the labelled C234 and C382 for planned mutations to C234A and C382A, C382S. The figure was constructed with pymol.

Medial cluster:

Five amino acids were chosen for the mutations of the medial cluster:

- P46G and P46A
- A49P
- I67P
- C72A
- L73P

The changes to proline (A, I, L) should remove hydrogen bonds to the medial cluster, which might influence the properties of the cluster, for example the potential of the cluster, while the change of proline 46 to glycine or alanine should allow the formation of a new hydrogen bond to the cluster. The cysteine mutant again was designed to alter the [4Fe] to a [3Fe] cluster. The following Figure 5-4 shows the medial cluster with the labelled amino acids for mutation.

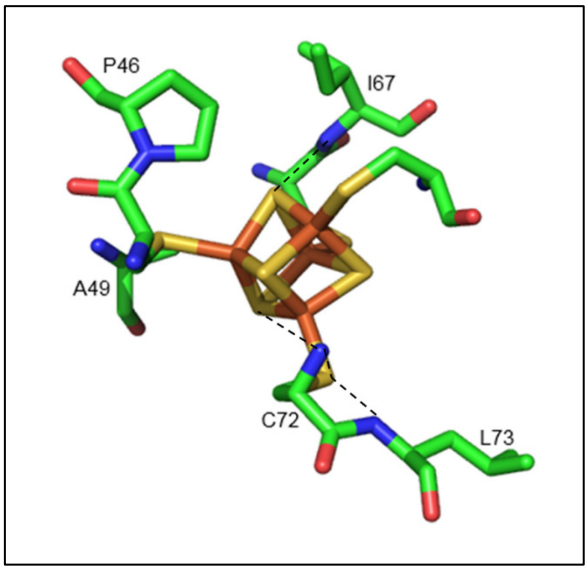

Figure 5-4 Scheme of the medial cluster of the [FeFe]-hydrogenase from *D. desulfuricans* with the labelled amino acids for mutation (P46G/A, P49P, I67P, C72A and L73P). Hydrogen bonds to the cluster are indicated by dashed lines. The figure was constructed with pymol.

Distal cluster:

Most mutations were planned for the distal cluster, where the exchange of electrons with the redox-partner takes place (see Figure 5-1). The following Figure 5-5 shows a scheme of the distal cluster with the marked amino acids. The following mutations were planned:

- T40P and T40V
- C41A
- S42A
- H58F, H58D, H58K, H58A, H58E, H58Q, H58N, H58P and H58S
- P77A and P77G

The mutation from threonine to valine should remove a hydrogen bond to the cluster from the hydroxyl group of the threonine while the mutation to proline additionally removes the backbone amide hydrogen bond. S42A again removes a hydroxyl hydrogen bond and C41A may allow formation of a [3Fe]-cluster. The mutations of proline (P77A and P77G) should allow formation of backbone hydrogen bonds. The majority of mutations were planned for the histidine to see the influence of this amino acid on the cluster. With histidine two different effects were predicted. Form the structure, it can be seen that H58 lies with its ring facing the cluster perhaps exerting a π-electrostatic

interaction. Histidines become positively charged upon protonation, and so it is possible that this amino acid affects the potential of the cluster in a pH dependent manner. Furthermore, it is also possible that under certain conditions (e.g. protonation at low pH) H58 can rotate and form hydrogen bonding interactions with the cluster. Finally, it appears that the backbone amide of H58 forms a hydrogen bond to CXX, a ligand of the cluster. As such this amino acid was mutated to alanine to check whether H58 plays any role at all; to phenylalanine to check the effect of the π-interaction; to aspartic acid, lysine and glutamic acid to check charge effects; to asparagine, glutamine and serine to check whether they could form hydrogen bonds to the cluster from their side chain amides. The mutation to proline was done to check whether the backbone amide hydrogen bond can influence the cluster potential.

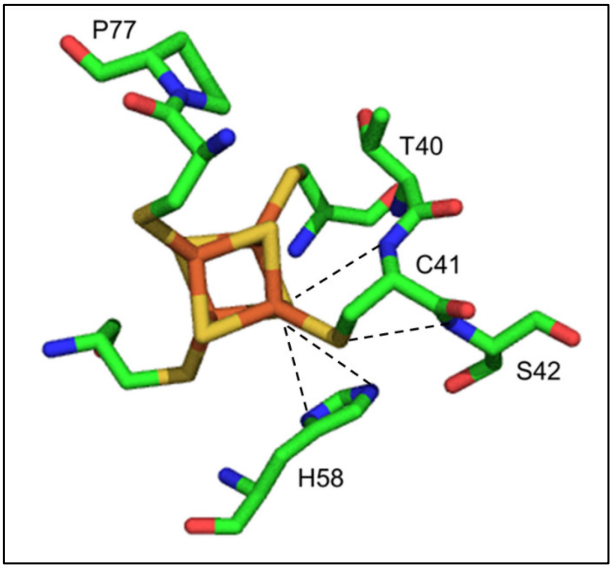

Figure 5-5 Scheme of the medial cluster of the [FeFe]-hydrogenase from *D. desulfuricans* with the labelled amino acids for mutation (T40P/V, C41A, S42A, P77G/A and H58F/D/K/A/E/Q/N/P/S). The figure was constructed with pymol; hydrogen bonds to the cluster are indicated by dashed lines.

5.2.2 *Cloning strategy*

The mutagenesis was done by PCR with construct 9 (see Section 3.3.2) which has the Strep tag II at the C-terminal end of the large subunit. The signal sequence of the large subunit and the pre-sequence of the small subunit are removed. The used primers are given in Table 2-2 in Section 2.1. The cloning strategy is identical to the one reported in

Section 3.3.1. After performing PCR with the reported primers a DpnI digest was done and the PCR products were checked by agarose gel. An example of an agarose gel for cloning the mutants is shown in Figure 5-6. All PCR products have identical size of around 5 kbp and all gels therefore looked basically identical and are not shown in this thesis.

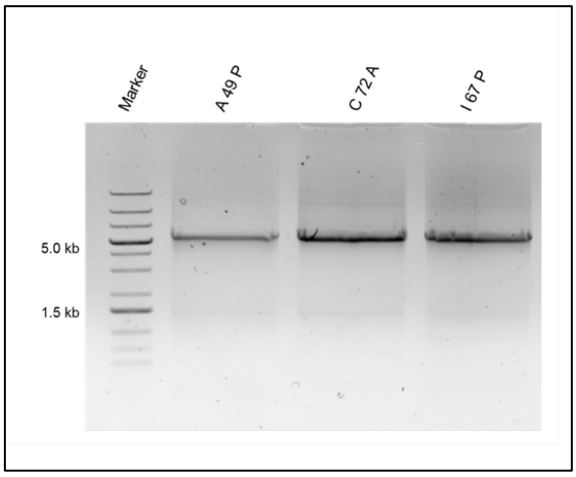

Figure 5-6 Agarose-gel of three mutants (A49P, C72A, I67P) with a size of ~ 5.0 kb.

Afterwards the required band was excised and purified, followed by ligation and transformation into *E. coli* BL21(DE3) cells. The DNA from overnight cultures was checked by sequencing and a correct plasmid was transformed into the expression strain. A scheme of the mutagenesis is shown in the following Figure 5-7.

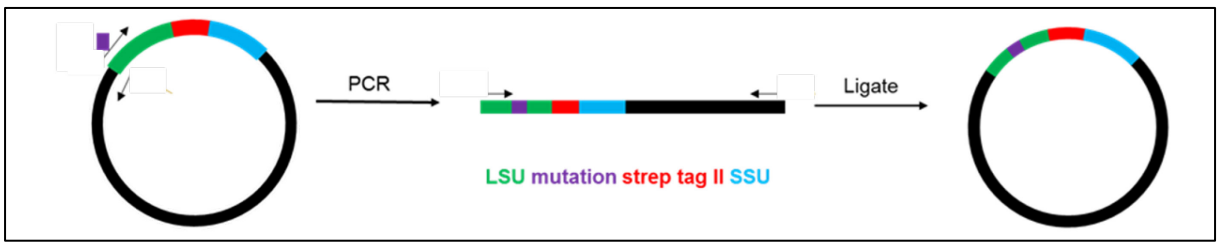

Figure 5-7 Scheme of the cloning strategy to generate the mutants. Black part correspond to the cloning plasmid, where the coloured parts belong to the [FeFe]-hydrogenase part of the vector (green: large subunit, blue: small subunit, red: Strep tag II). The purple part indicates a mutation which was inserted with PCR by the corresponding primer pair.

5.2.3 *Expression of the mutants*

All mutants were expressed as described in Section 2.3 and purified as described in Section 2.4. After all preparations an SDS-PAGE was done for checking the purity. For some mutations it was obvious from the colour of the sample, that the expression level was low. Nevertheless concentrations were determined with the Lowry assay (Section 2.6.1) for comparison. A summary of this is given in the following Table 5-1.

Table 5-1 Summary of the expression of the mutants compared to construct 9 (wild type), the typical volume after expression was 0.2 mL and the values are given for that.

mutant	expression yield [mg]	% yield relative to "wild type"
wild type	11.2 ± 1.3	
H58A	5.4 ± 2.2	48
H58E	2.6 ± 2.0	23
H58Q	5 ± 1.3	45
H58N	2.6 ± 0.2	23
H58P	3.4 ± 0.6	30
H58S	4.6 ± 1.3	41
H58F	6.4 ± 2.2	57
H58D	7.6 ± 1.9	68
H58K	12 ± 1.2	107
S42A	5.8 ± 1.3	52
P46A	4.4 ±1.2	39
P46G	3.8 ±1.2	34
T40P	2.6 ±0.4	23
T40V	6.8 ±1.1	61
P77G	6.4 ±1.2	57
P77A	9.2 ± 2.7	82
A49P	1.2 ± 0.4	11
C72A	0.4 ± 0.09	4
I67P	3.4 ± 0.4	30
I204P	10.8 ±2.8	96

L73P	1.6 ± 0.3	15
C41A	1.2 ± 0.1	11
C382S	10.6 ± 2.1	95
C382A	no expression	
C234A	no expression	

Table 5-1 shows, that some mutants like C382A and C234A are not expressed while others, like I204P, C382S, P77A or H58K show nearly identical expression levels to the wild type. A prediction of the expression is not possible and the received results do not show a relation between the mutation and the expression level.

All mutants were tested with the $[2Fe]_H$ mimic adt for hydrogen production and oxidation activity, the results are shown in Section 5.4 of this chapter.

5.3 EPR spectroscopy of the unmaturated mutants

Most spectroscopic investigations on the mutants were done by EPR spectroscopy. For that samples of unmaturated protein were treated like the wild type as described in Section 2.6.8 and measured in a cw X-Band spectrometer. As discussed later in Section 5.4 the H58 mutants are of special interest and are, therefore, considered separately from the other mutants in Section 5.3.

All shown EPR spectra were measured at 7 K. At this temperature a splitting of the g = 2.05 signal is expected as reported in Section 4.2.2. For an easier comparison the wild type spectrum is shown in each figure as a black trace on the top.

Proximal cluster mutations:

Unfortunately two of the mutants with changes at the proximal cluster (C382A and C234A) could not be expressed in *E. coli*. Mutant C382 was successfully expressed but shows no activity (see Section 5.4). After maturation a FTIR spectrum was measured to see if the adt was inserted into the protein. However, there were no signals observed in

FTIR spectroscopy therefore it shown, that the adt cannot be inserted into the protein which leads to no activity.

Medial cluster mutations:

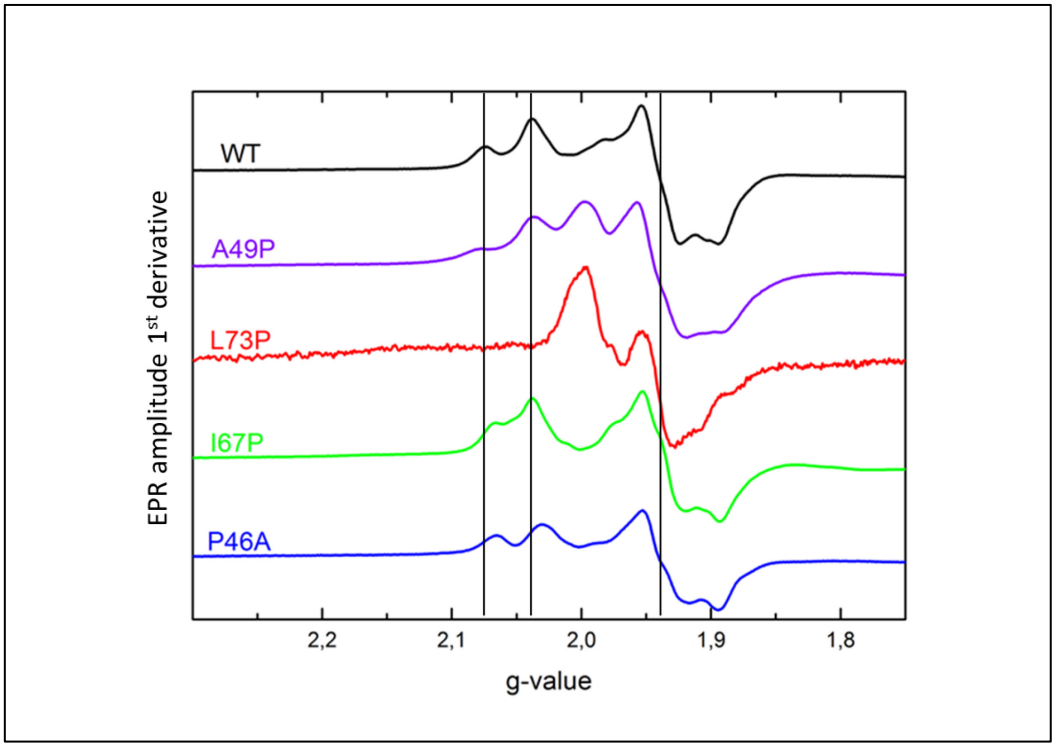

Figure 5-8 X-Band cw EPR spectrum of the mutations at the medial cluster. All measurements were done at 7K and 23 dB. All other parameters are given in Section 2.6.8.

Here it is obvious, that mutations at the medial cluster of the unmaturated protein change the EPR spectra in part drastically. It is clear that with A49P and L73P mutants that should lower the potential of the medial cluster a new EPR signal is observed around g = 2.0. This signal looks very similar to the fully reduced ferredoxin from CpI. The mutation from proline to alanine (P46A) is almost without effect on the EPR spectrum but perhaps with subtle changes of the g-values from the medial cluster. The I67P mutant spectrum looks like there is slightly less “split signal” (see Section 4.2.2) and a change in the g-values, so perhaps the interaction between this cluster and the $[4Fe\text{-}4S]_H$-cluster of the H-cluster is perturbed.

Distal cluster mutations:

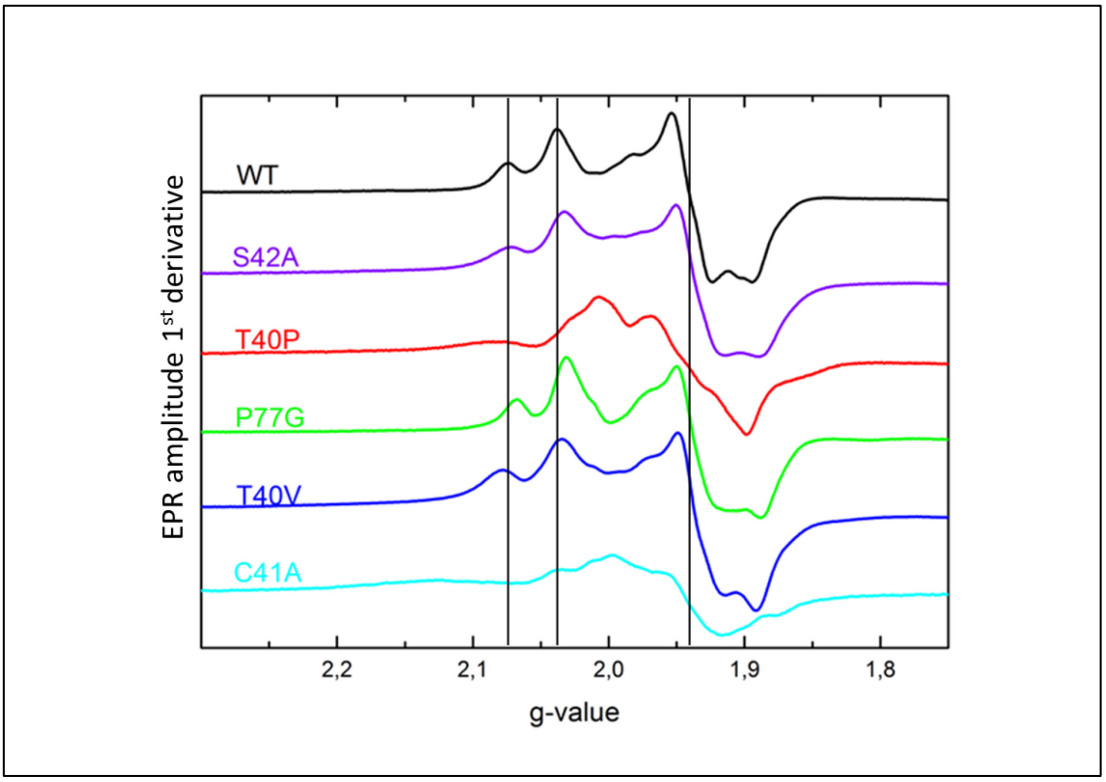

Figure 5-9 X-Band cw EPR spectrum of the mutations at the distal cluster. All measurements were done at 7K and 23 dB. All other parameters are given in Section 2.6.8.

From this Figure 5-9 it can be seen, that some mutations of the distal cluster do not influence the EPR spectra very much, but there are small changes in the g-values. The spectra of S42A, P77G and T40V look similar to the spectrum of the wild type protein, with a small signal broadening in the S42A and T40V mutants. The T40P spectrum changes again drastically as it was observed for the proline mutant in the medial cluster (see Figure 5-8). Also here this could be caused by a change in the secondary structure of the protein. Mutant C41A shows a broadening of the signals; here it could be caused by concentration problems with the sample.

H58 mutants of the distal cluster:

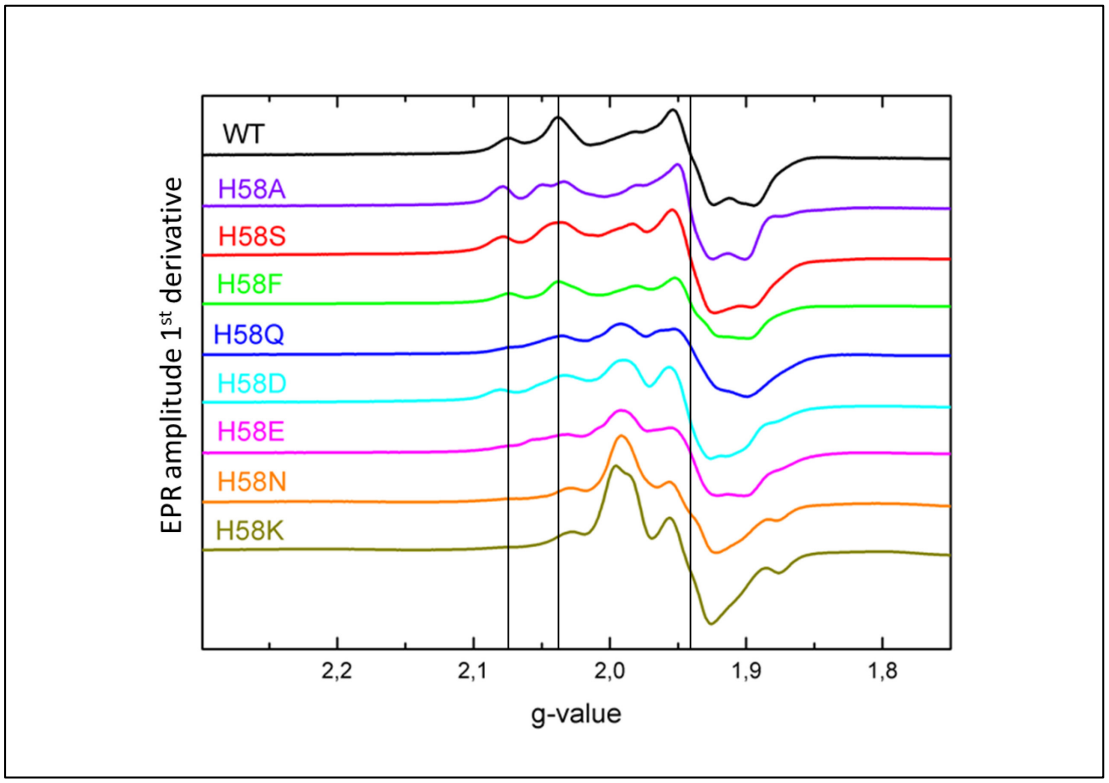

Figure 5-10 X-Band cw EPR spectrum of H58 mutations at the distal cluster. All measurements were done at 7K and 23 dB. All other parameter are given in Section 2.6.8.

Initially it was not expected that the histidine 58 mutations would show particularly large effects. However, a drastic change in the EPR spectrum is observable for the H58K and H58N mutants, were the split signal around g = 2.05 diminishes and a signal at g = 2.0 appears. Mutations to Q, E and D show smaller amounts of this new signal. The H58A, H58S and H58F mutants show only slight alterations of the g-values.

Most likely, therefore, H58 does provide an interaction between the imidazole ring and the cluster but that introduction of large amino acids with amine, amino or carboxyl groups drastically alter the properties of the cluster such that the spin-spin interaction between the distal and medial clusters changes, giving an EPR signal that is very similar to that observed in the 8Fe ferredoxins. It is, presently, not possible to fully explain the changes which are caused by the mutations. Further characterization of the unmaturated mutants is, therefore, necessary, through for example redox potential titrations like for

the wild type protein may help to discover changes in the redox behaviour of the mutants.

5.4 Maturation and activity measurements of the mutants

The maturation with adt was tested for all mutants under anaerobic conditions as described in Section 4.3. For most of the mutants their hydrogen oxidation activity was measured with the benzylviologen assay and their hydrogen production activity was measured with gas chromatography. A comparison between the mutants and the wild type is given in the following tables. The activity values for the wild type enzyme are set to 100 % and the activities for the different mutants are given as a percentage of the wild type enzyme.

Even, if hydrogen oxidation and production turnover frequencies of the wild type enzyme are both set to 100 % they show a slightly difference in their absolute values (see Section 4.3).

Table 5-2 Overview of the TOF for hydrogen oxidation and production of the wildtype enzyme

wildtype hydrogen oxidation s^{-1}	wildtype hydrogen production s^{-1}	difference between them
10073 ± 500	10647 ± 350	5 %

Proximal cluster mutations:

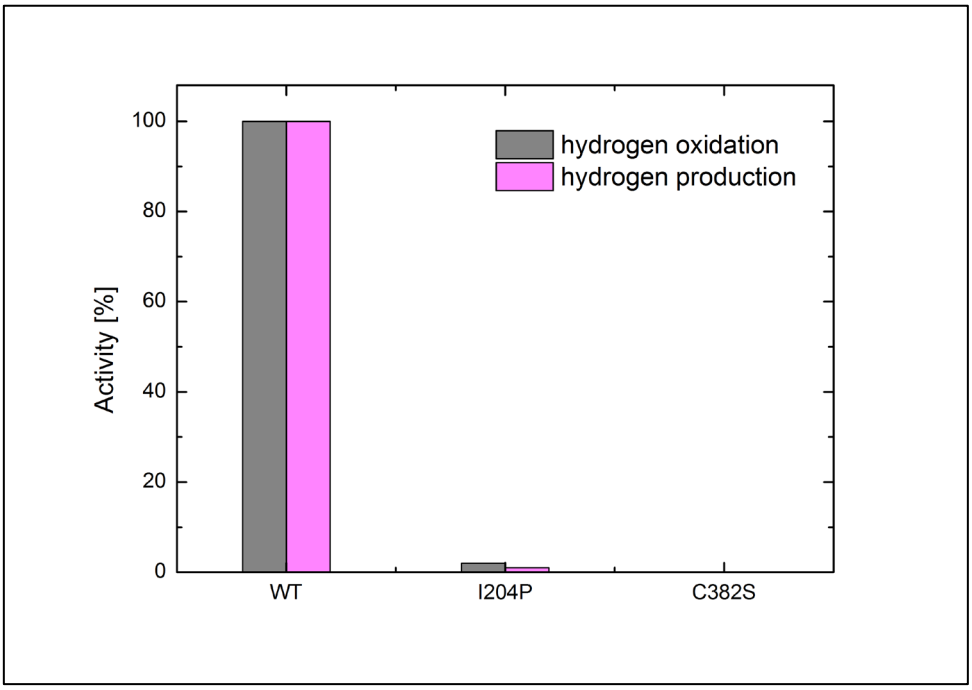

Figure 5-11 Comparison of the maturated wild type enzyme with the maturated mutants of the proximal cluster. Hydrogen oxidation is marked in grey and hydrogen production in pink.

From this Figure 5-11 it is obvious, that the mutations of the proximal cluster decrease the activity of the enzyme drastically for the change from isoleucine to proline. The change of the cysteine to a serine shows no activity because the $[2Fe]_H$ mimic adt is inserted (tested by FTIR spectroscopy).

Medial cluster mutations:

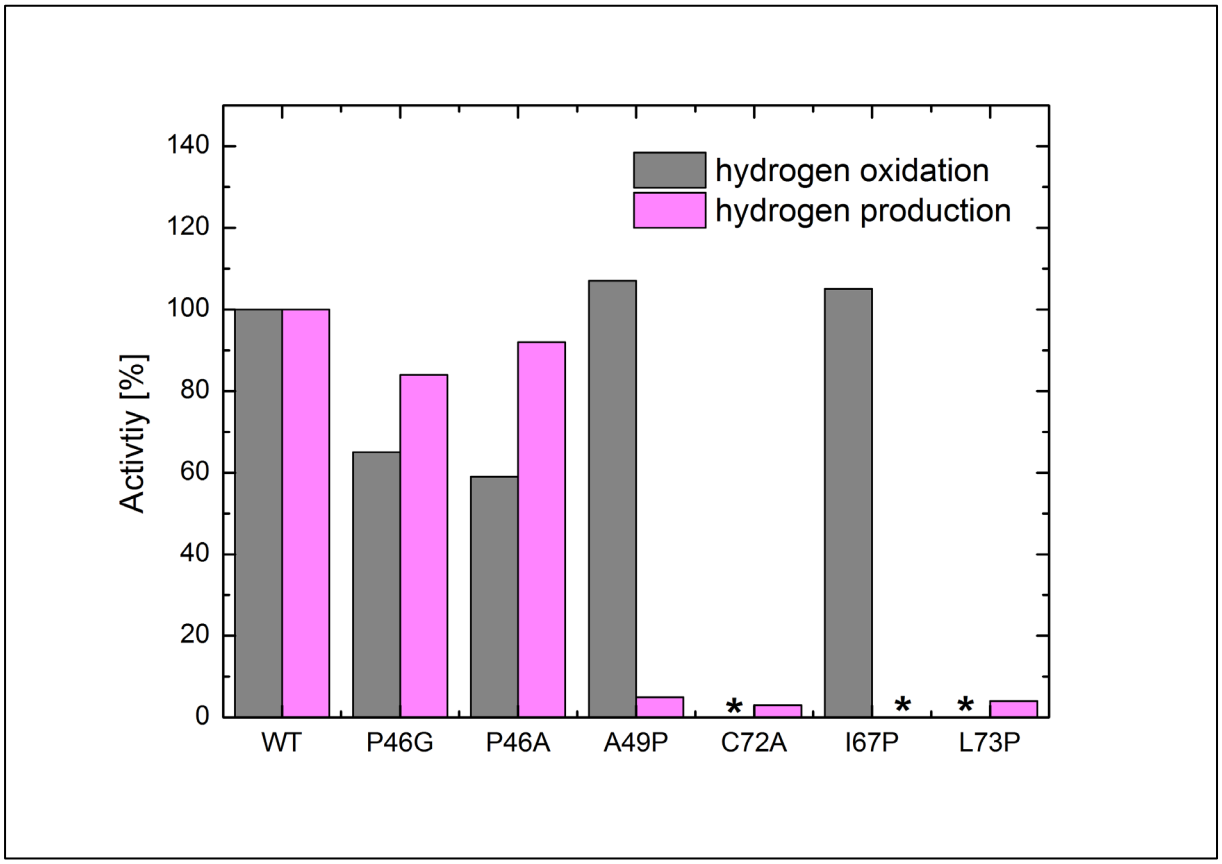

Figure 5-12 Comparison of the maturated wild type enzyme with the maturated mutants of the medial cluster. Hydrogen oxidation is marked in grey and hydrogen production in pink. * indicates assays which were not done so far (low expression yields) for the corresponding mutants.

From Figure 5-12 it is obvious, that a change of proline 46 decreases slightly both hydrogen oxidation and hydrogen production activities. The A49P mutant shows an a typical behaviour; the hydrogen production activity shows a drastic decrease, while the hydrogen oxidation activity slightly increases, which means that this mutation changes the directionality of the enzyme to only hydrogen oxidation. For C72A and L72P a similar decrease of the hydrogen production activity is observed. I67P shows a similar increase of hydrogen oxidation activity. But also these are mutations to proline it might be expected that this mutant shows similar results as the A49P.

Distal cluster mutations:

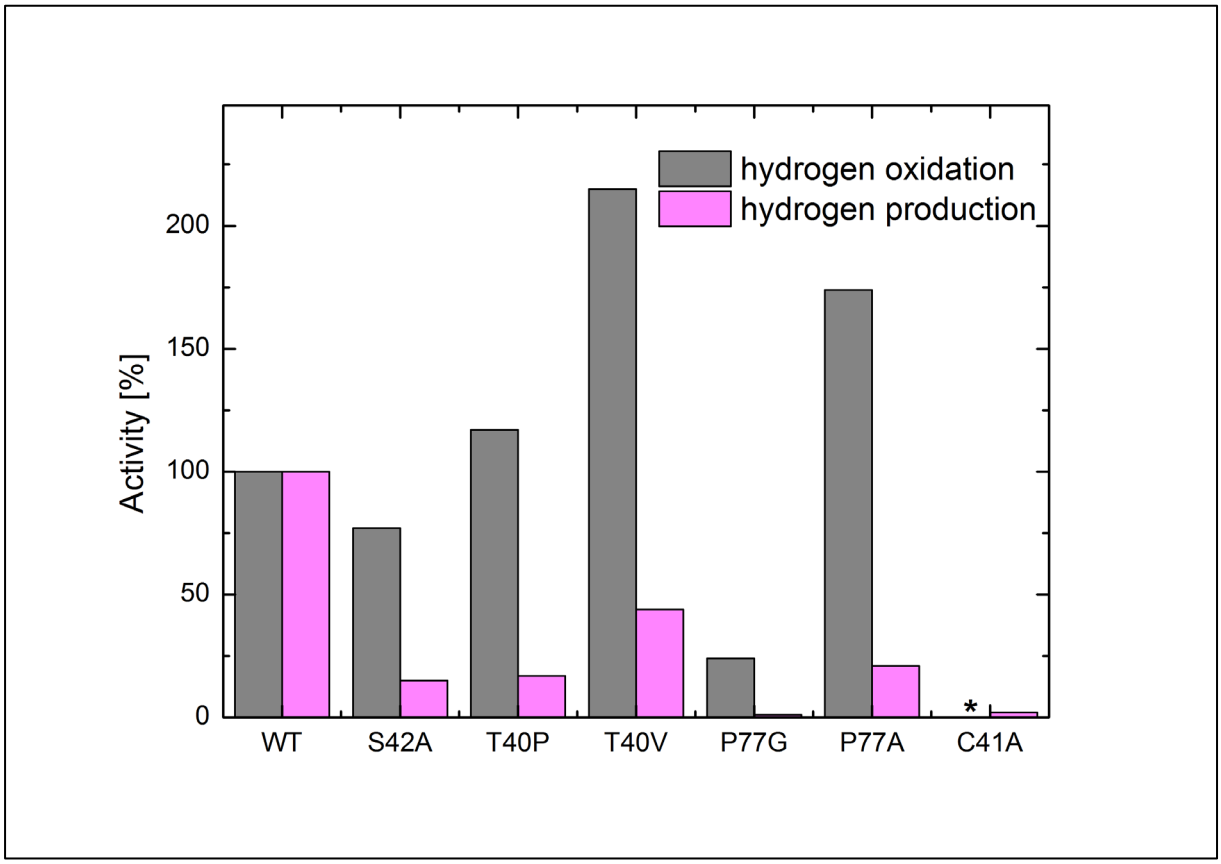

Figure 5-13 Comparison of the maturated wild type enzyme with the maturated mutants of the distal cluster. Hydrogen oxidation is marked in grey and hydrogen production in pink. * indicates assays which were not done so far for the corresponding mutants.

As is obvious from Figure 5-13 all mutations of the distal cluster decrease the hydrogen production activity of the enzyme. This tendency cannot be seen for hydrogen production activity, S42A and P77G decrease the hydrogen production activity while T40P, T40V and P77A increase the hydrogen oxidation activity.

H58 mutants of the distal cluster:

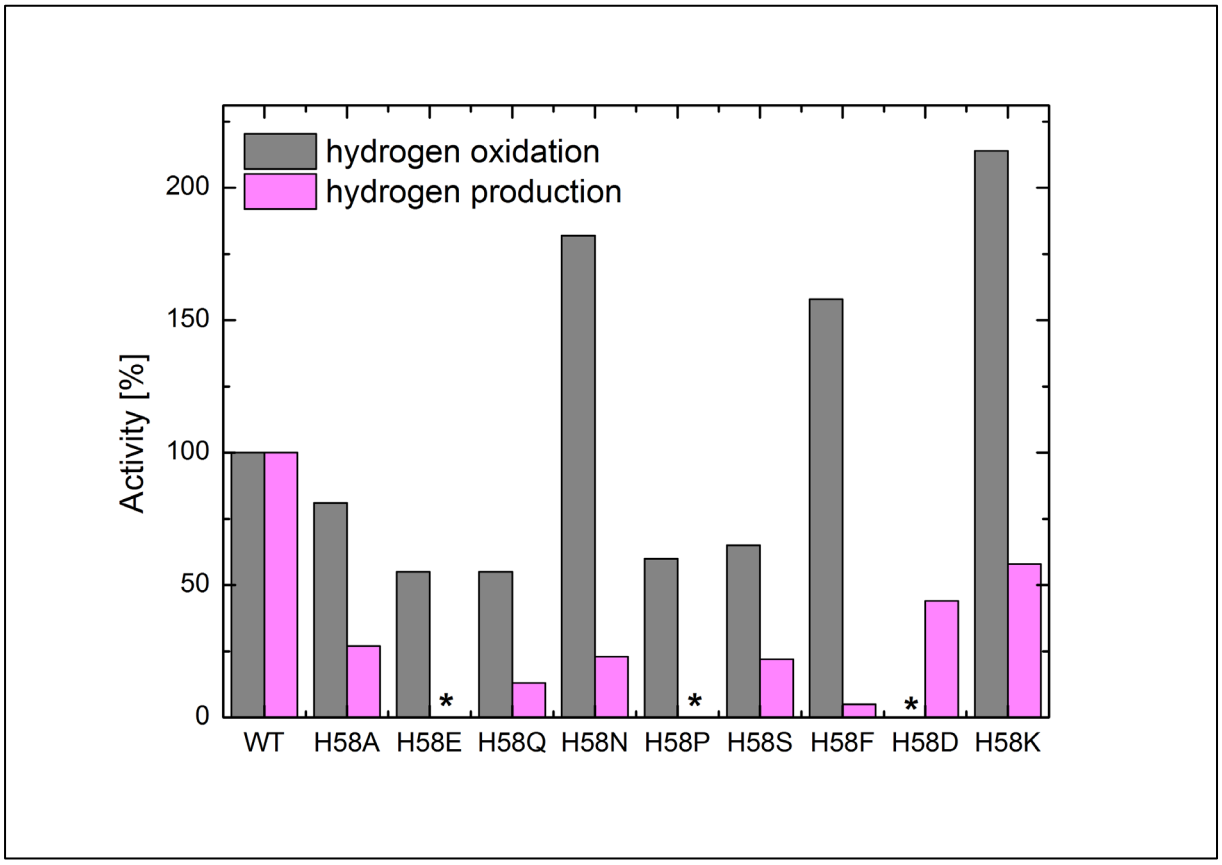

Figure 5-14 Comparison of the maturated wild type enzyme with the maturated H 58 mutants of the distal cluster. Hydrogen oxidation is marked in grey and hydrogen production in pink. * indicates assays which were not done so far for the corresponding mutants.

From this Figure 5-14 it is obvious that mutations of this histidine change the directionality of the enzyme. In all mutants the hydrogen oxidation is preferred. A change to asparagine, phenylalanine and lysine drastically increase the hydrogen oxidation activity. The other mutants show lower hydrogen oxidation activities. Three of these mutants (H58N, H58F and H58K) show a significant increase in hydrogen oxidation which is maybe caused by a change of the cluster potentials due to mutagenesis.

5.5 Summary

In this chapter it could be shown that it is possible to clone and express different mutants of the [FeFe]-hydrogenase from *D. desulfuricans*. Some of these unmaturated enzymes show similar EPR spectra to the wild type enzyme, but some of them show strong differences. This can be also seen for activity of the maturated enzymes.

A special set of mutations are those of H58, which change the directionality of the enzyme. In the native system and in the wild type of the heterologously expressed enzyme the hydrogen oxidation and hydrogen production activities show similar turn-over frequencies but with the H58 mutations the hydrogen oxidation activity is clearly preferred. Also, the EPR spectra of H58N, F and K show drastic differences, they show typical ferredoxin like signals while other mutation causes line broadening in the spectra.

The significant increase of the H58K and H58N mutant correlates to a drastic change in the EPR spectrum of the unmaturated protein (a weaker or at least no split signal can be observed). If this is related to the change in activity and directionality of the enzyme is not clear at the moment. For the other mutants no correlation between the activities and the EPR spectra can be seen.

Further characterizations of these mutants are necessary to study the electron transfer in these enzymes to get closer insight into the catalytic cycle of the hydrogenases. It might be possible to generate enzymes with higher hydrogen production rates to produce more hydrogen. It might also be possible to design an enzyme which shows oxygen tolerance.

The possibility for generating mutants is a powerful tool in the research of [FeFe]-hydrogenase from *D. desulfuricans*. An important experiment for the future will be the determination of the cluster potentials by PFE (protein film electrochemistry, see Chapter 6) or by EPR redox titration (see Chapter 4). The expected changes in the potentials will help to further understand the hydrogen reaction cycle of the native enzyme by comparison.

Chapter 6 Electrochemistry on [FeFe]-hydrogenase from *D. desulfuricans*

6.1 Protein Film Electrochemistry

6.1.1 *Electrochemistry of hydrogenases*

It is known, that most hydrogenases inactivate reversibly at high potentials under anaerobic conditions, but for the [FeFe]-hydrogenase from *D. desulfuricans* it is a very fast process.[146] This oxidized, inactive form of the enzyme is inert towards reaction with CO and O_2 but it rapidly reactivates upon one-electron reduction.[39] For the [FeFe]-hydrogenase from *D. desulfuricans* Albracht et al.[103] and De Lacey[88] showed that the enzyme in its inactive, as isolated state can be reversibly reduced to the also inactive H_{trans} state. After another irreversible reduction, the active H_{ox} state appears.[103] Armstrong et al. found a reversible, anaerobic one-electron oxidative inactivation, which he assigned to the H_{ox}^{inact} state.[39] Even, if not all publications use the same terminology, it was suggested that the isolated state H_{inact} is identical to the H_{ox}^{inact} state which is received under anaerobic and high potential conditions (see Figure 1-9 and 6-1). But a recent publication from Léger and co-workers[108], as well as some experiments at our department (not published) suggest that this is not the case. Further investigation is therefore necessary to characterize this oxidized state.

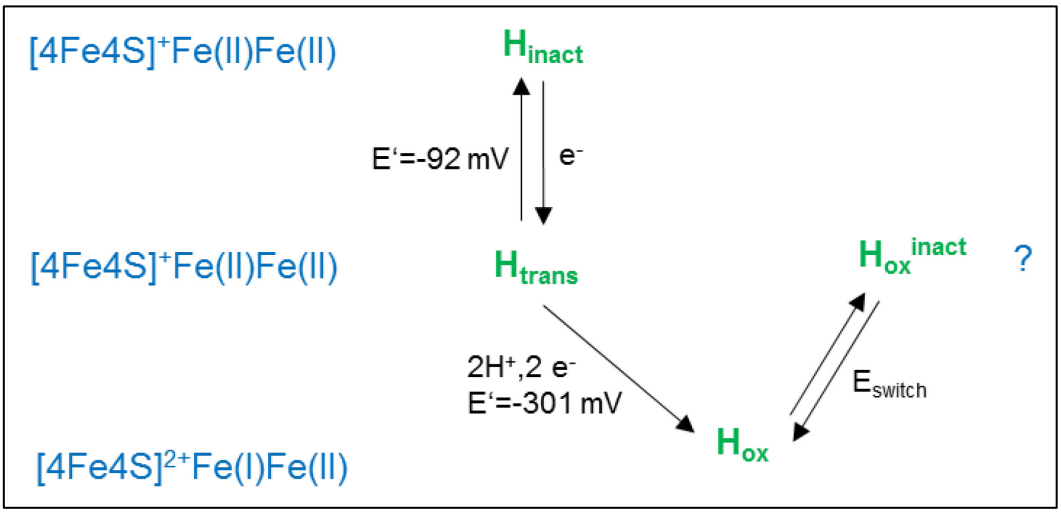

Figure 6-1 Scheme of some of the different redox states of the [FeFe]-hydrogenase from *D. desulfuricans*. It is still under discussion, if the as isolated H_{inact} state is identical to the H_{ox}^{inact} state, which occurs under anaerobic and high potential conditions.

6.1.2 *Aims of the work described in this chapter*

- Measure the catalytic current of [FeFe]-hydrogenase from the native system to have a comparison to the heterologously expressed hydrogenase.
- Try to get further information about the redox-cycle of the native enzyme and the high potential inactivation. (HPI)
- Measure the catalytic current of heterologously expressed [FeFe]-hydrogenase and compare to the native enzyme.
- Try to insert the $[2Fe]_H$-subcluster mimic to an already immobilized unmaturated protein to observe kinetic activation processes.

6.2 PFE experiments on the native [FeFe]-hydrogenase from *D. desulfuricans*

6.2.1 *Immobilization of the [FeFe]-hydrogenase onto a HOPGE electrode*

More than 30 % of all enzymes are oxidoreductases, like the hydrogenases, which catalyse redox-reactions. Many of them carry out electron transfer processes and couple these processes to discrete transformations of a substrate at the catalytic site, to conformational changes or to transmembrane ion/proton pumping. The detection of these processes by electrochemistry is a powerful tool to study the enzyme activity.[93]

As it is shown in Figure 6-2 the H-cluster of the hydrogenase from *D. desulfuricans* is connected via two additional [4Fe-4S]-clusters to the surface of the enzyme. The hydrogenase is orientated so that the negatively charged patch of the enzyme (see Figure 6-2 B, red regions) is facing the electrode surface. This is done by modifying the electrode surface with a positively charged molecule for covalent attachment.

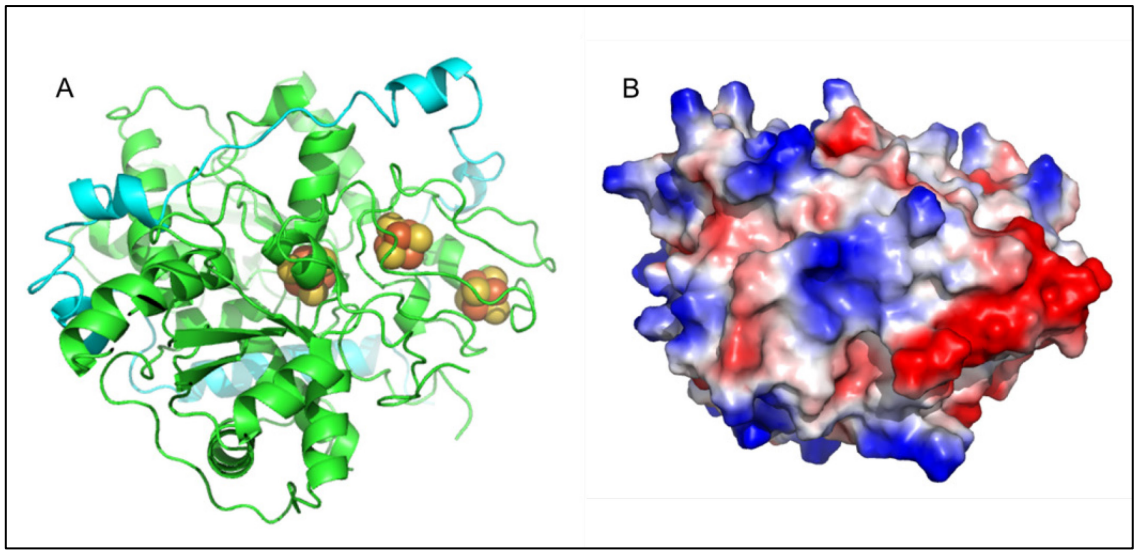

Figure 6-2 [FeFe]-hydrogenase from *Desulfovibrio desufuricans*. A) Protein structure showing the connection to the surface via [Fe-S]-clusters. B) Charge distribution on the protein surface. Negative areas are indicated red and positive areas are indicated blue.

Prior to protein immobilization the surface of the HOPGE has to be modified to induce the right protein orientation on the electrode (see Chapter 2).[95,98] In the first step the electrode is incubated with 4-nitrobenzenediazonium salt (NBD) which reacts with the electrode surface through formation of a radical intermediate to form a carbon-carbon bond. In the presence of H_2SO_4 at -650 mV vs SHE (standard hydrogen electrode) the nitro group is reduced to an amine (Figure 6-3 A). Afterwards a mixture of protein, N-hydroxysuccinimide (NHS) and 1-ethyl-3-(3-dimethylaminopropyl)-carbodiimide (EDC) is incubated on the electrode surface at pH 6.5, close to the determined pKa of the monolayer (6.9).[147] The carboxyl-groups of the acidic amino acids (glutamic acids and aspartic acids) from the protein form unstable intermediates with the EDC. The EDC is replaced by NHS (Figure 6-3 B) and in the last step the NHS-activated carboxylic acids react with the amine groups from the electrode to form an amide bond (Figure 6-3 C).

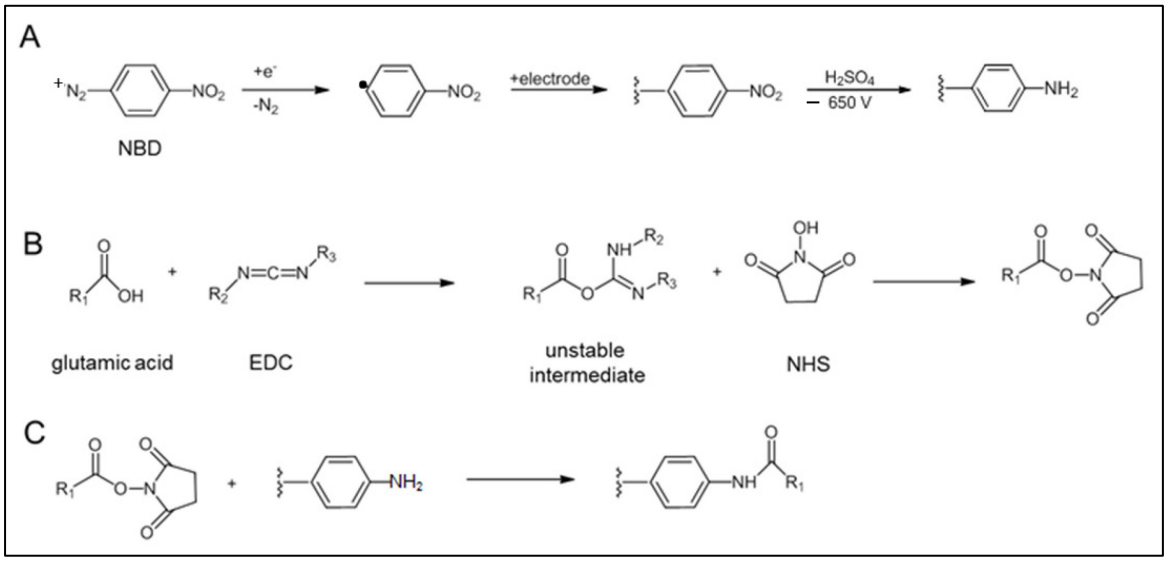

Figure 6-3 Reaction mechanism of the coupling process of hydrogenases to the electrode surface. A) electrochemical reduction of NBD to couple it to the electrode. B) Forming an instable intermediate of EDC, protein and the electrode. C) Transfer of the protein to the bonded NBD.

For simply adsorbing the protein onto the electrode surface (rather than covalent attachment), the electrode was first polished with cotton wool and alumina slurry. After rinsing the electrode with water 5 µL of the protein (30 µM in 50 mM MES buffer pH 6.5) were pipetted on the electrode surface. After 5 minutes the electrode was rinsed with water and transferred to the electrochemical cell.

6.2.2 *Cyclic voltammetry and high potential inactivation*

Due to the fact that [FeFe]-hydrogenases are bidirectional enzymes an advantage of electrochemical experiments is the possibility to control the driving force of the reaction by changing the potential. This means that applying potentials more positive than the thermodynamic H^+ reduction potential the enzyme oxidizes H_2 while at lower potentials H_2 is produced from H^+. During hydrogen oxidation electrons from hydrogen are transferred to the electrode, which leads to a positive current. Conversely, at low set potentials electrons from the electrode are transferred to the hydrogenase and protons are reduced, this leads to a formal negative current.

After the covalent attachment of the protein onto the electrode surface the electrode was transferred to the electrochemical cell inside an anaerobic glovebox and was gassed with hydrogen. To limit diffusion effects the electrode is rotating during measurements.

For all experiments a saturated Calomel electrode (SCE) was used as reference electrode. All potentials have been corrected to the potential of a standard hydrogen electrode (SHE) using the following formula:

$$\mathrm{E_0\ (SHE) = E_0\ (SCE) + 241\ mV}$$

A standard cyclic voltammogram of the covalently attached [FeFe]-hydrogenase from *D. desulfuricans* in buffer mix, pH 6.0 under hydrogen saturation, is shown in the following Figure 6-4. This voltammogram fits very well to those previously reported in the literature.[39,146] There are three defined regions: H^+ reduction (low potential, negative current), H_2 oxidation (medium potential, positive current) and a potential region where the enzyme undergoes inactivation (high potential, positive current but decreasing). At the point between the H^+ reduction and the H_2 oxidation regions, the two processes are balanced such that there is no overall current. At higher potentials, it is noticeable that the current drops: this has been previously suggested to be due to the formation of an oxidatively inactivated enzyme state.[108,146,148] Normally this behaviour is called anaerobic inactivation or high potential inactivation (HPI).

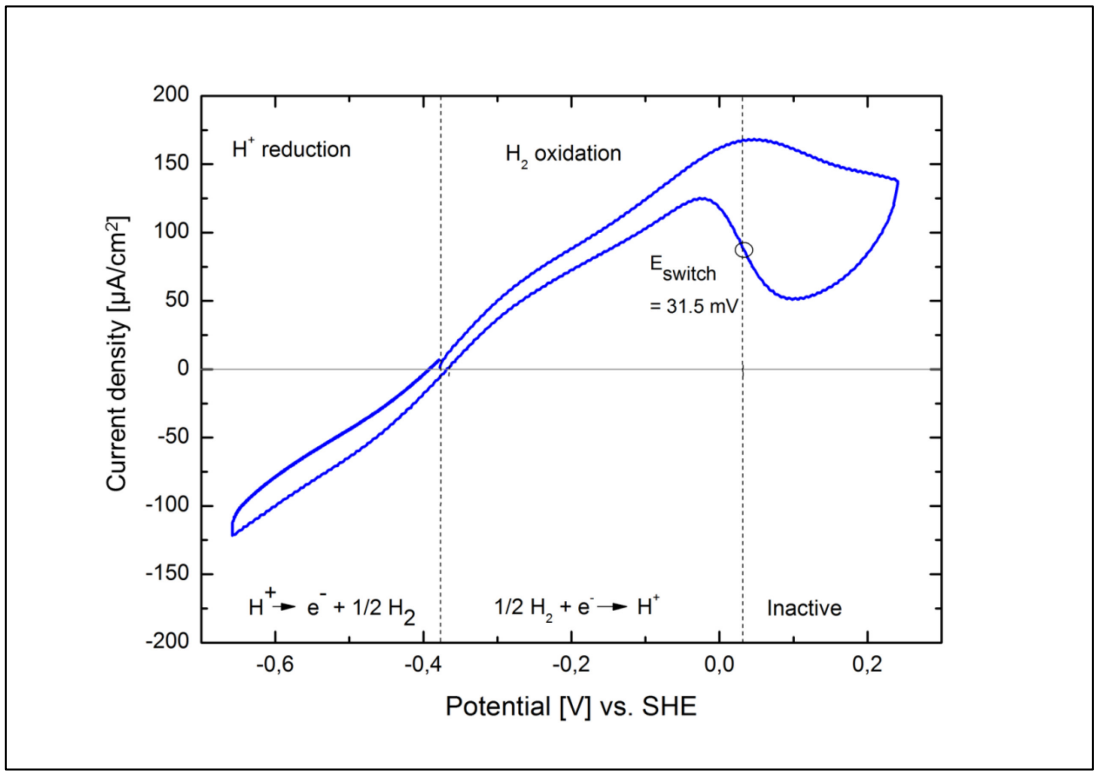

Figure 6-4 Cyclic voltammogram of [FeFe]-hydrogenase from *Desulfovibrio desulfuricans*. Electrode rotation: 2000 rpm, 1 bar H_2, in buffer mix pH 6.0, scan speed 200 mV/s, 10 °C.

High potential inactivation is characterized by an enzyme specific switch potential. This potential is the midpoint potential for reactivation that means, at this potential 50 % of the enzyme molecules are reactivated. The switch potential can be calculated from the first derivative dI/dE of the voltammogram, where the minimum corresponds to the E_{switch} potential (see Figure 6-5).

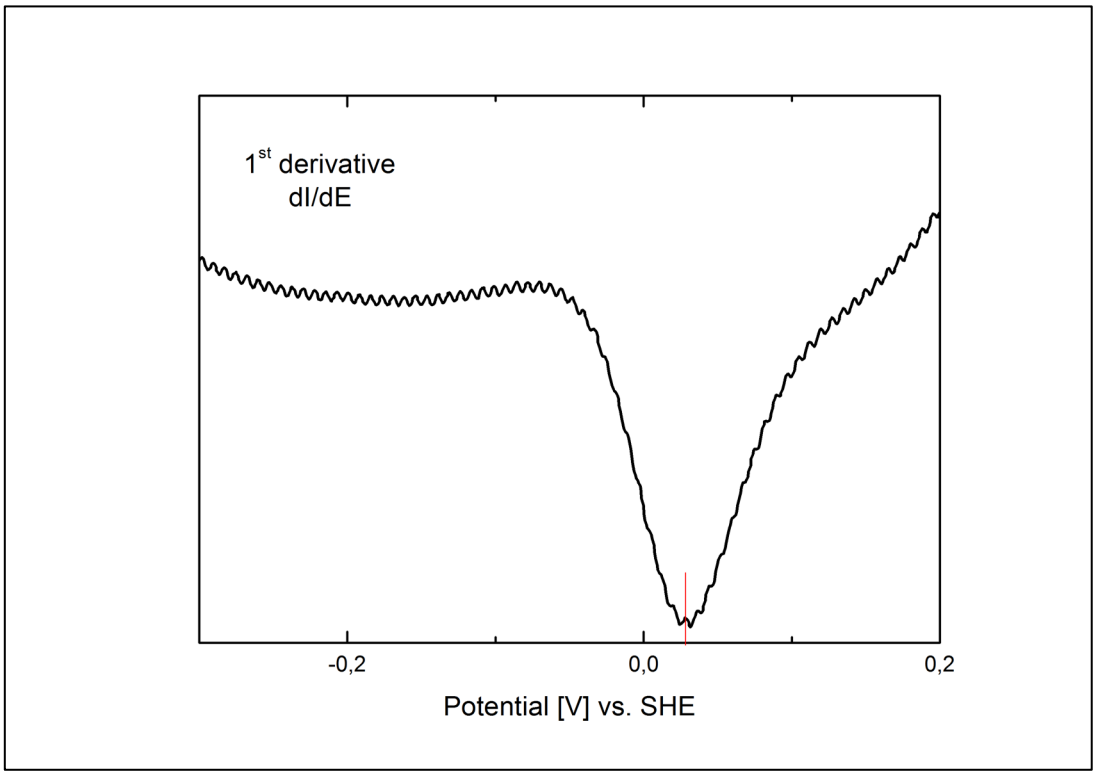

Figure 6-5 First derivative of the recorded voltammogram from 6-4 in reduced direction. The switch potential is marked as a red line in the minimum of the curve.

High potential inactivation in the [FeFe]-hydrogenases is still not fully understood. It is known for some [FeFe]-hydrogenases (*D. desulfuricans, C. reinhardtii*)[108,146] and [NiFe]-hydrogenases (*A. vinosum, D. vulgaris)*[146] that under anaerobic conditions and positive potentials they are oxidised to an inactive form, which is inert towards reaction with CO and oxygen. This oxidation is reversible so that the enzyme reactivates upon one-electron reduction under hydrogen atmosphere. But not all [FeFe]-hydrogenases show this high potential inactivation, the [FeFe]-hydrogenase from *Clostridium acetobutylicum* does not show HPI under identical conditions. For the [NiFe]-hydrogenases this oxidized state corresponds to the Ni-B “ready state”, also formed in the presence of oxygen, which is well-characterized spectroscopically and structurally.[146,149] For *D. desulfuricans* the formed inactive state is still not fully understood. One commonality between some [NiFe]-hydrogenases and the [FeFe]-hydrogenase from *D. desulfuricans* is the purification under aerobic conditions. It is still discussed if the state which is formed during the high potential inactivation of *D. desulfuricans* is the same H_{inact} state in which the enzyme is purified (and is therefore oxygen tolerant).[88,103,103,150]

To get some closer insights into the mechanism of the high potential inactivation the same cyclic voltammetry experiment was performed at two different temperatures. (Figure 6-6)

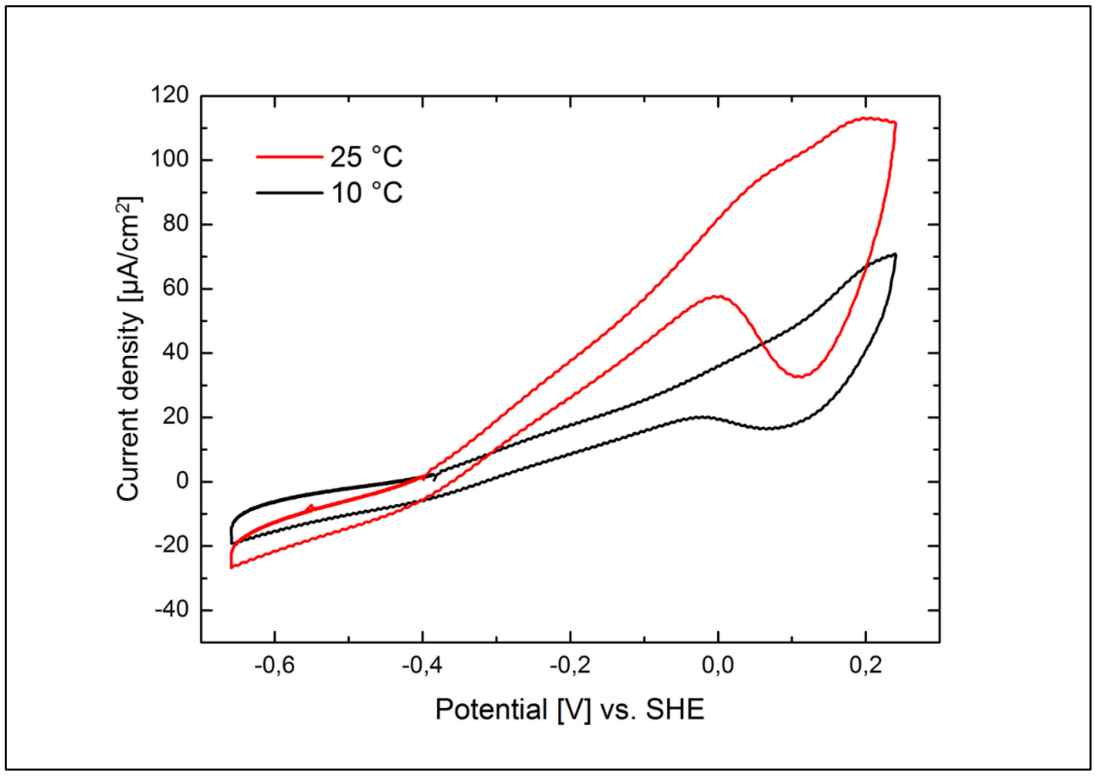

Figure 6-6 Cyclic voltammogram of [FeFe]-hydrogenase at different temperatures. Rotation speed of the electrode 2000 rpm, 1 bar H_2, in buffer mix pH 6.0, scan speed 100 mV/s.

Figure 6-6 shows, that as expected the rates of catalysis are quicker at higher temperature. In general, the high potential inactivation is due to removal of electrons from the active site of the enzyme. An increased rate of electron transfer from the H-cluster is theoretically possible at higher temperatures, but it may also be the case that some other process is limiting that is faster at higher temperatures.

It was noticed during this work that high potential inactivation could not be observed in some experiments. This different behaviour resulted from changing from a multi-component mixed buffer system to using a more simple 10 mM MES/HEPES buffer mix. When using a buffer mixture of 10 mM MES/HEPES the high potential inactivation was lost (see Figure 6-7). This result suggested, that the HPI is dependent on the buffer

composition used (see Chapter 2), and that either some component of the mixed buffer facilitated HPI or some component of the MES/HEPES buffer protects against it.

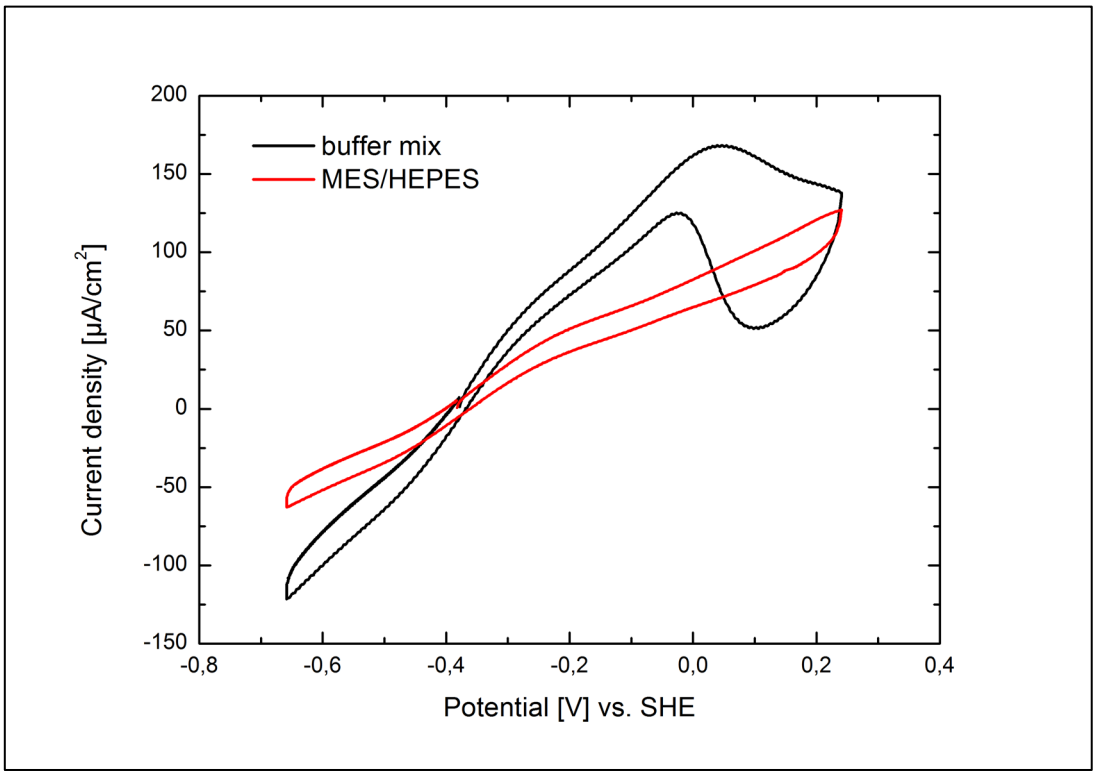

Figure 6-7 Cyclic voltammograms of [FeFe]-hydrogenase in buffer mix (black trace) and in MES/HEPES buffer (red trace). 10 °C, pH 6.0, scan speed: 200 mV/s rotation of the electrode 2000 rpm and 1 bar H_2.

As it is obvious from this Figure 6-7 there is a clear difference in the HPI of the protein in these two buffer systems which were further studied in this thesis.

To test, if there is a change in the time dependency of HPI in MES/HEPES buffer, the same experiment was performed at lower scan rates (Figure 6-8) which exposes the enzyme for longer at the applied potentials.

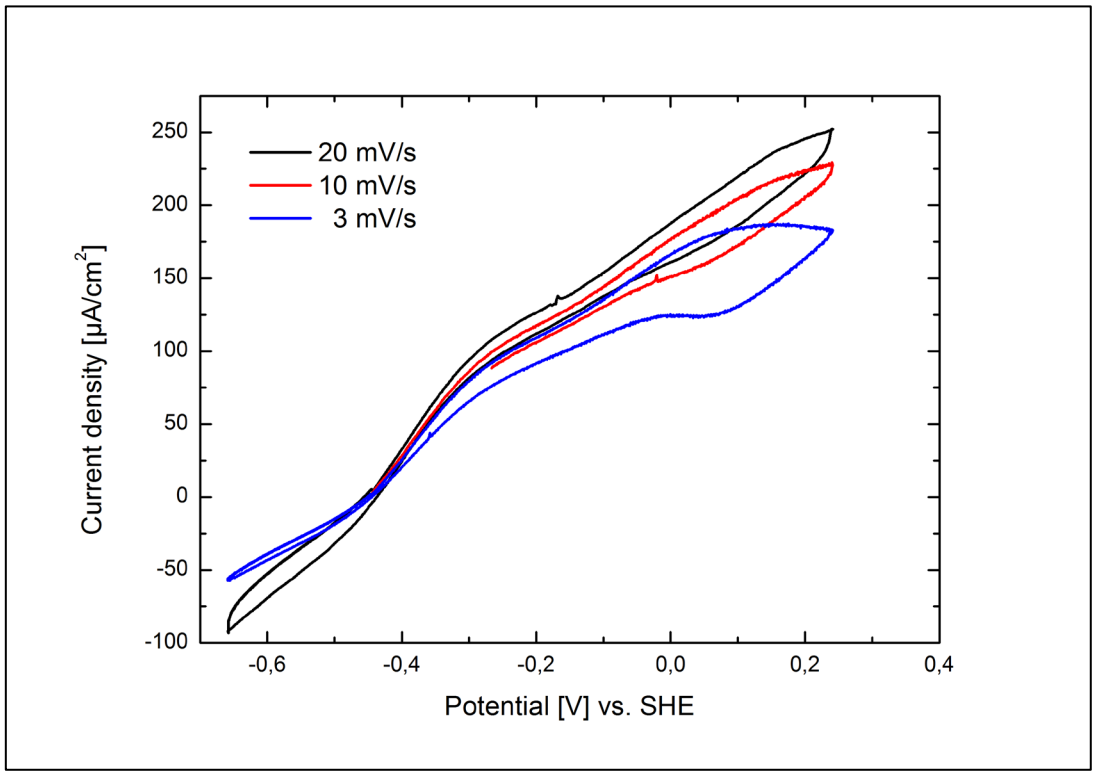

Figure 6-8 Cyclic voltammograms of [FeFe]-hydrogenase at different scan rates. Rotation of the electrode: 2000 rpm, MES/HEPES buffer pH 7.0, 10 °C and 1 bar H_2.

At a scan rate of 10 mV/s, there is no noticeable difference to the cyclic voltammogram other than a slight decrease to the rate of H_2 oxidation. At 3 mV/s, a small HPI can be observed, but to a much lesser extent that seen with the buffer mix. This suggests a change in the kinetics of HPI, being one of the components of the buffer mix responsible for a faster HPI.

For getting closer insights into the conditions required for forming the high potential inactive state the ingredients of both buffer systems were compared. For detailed buffer recipes see Chapter 2.

The first consideration was, that the high potential inactivation in buffer mix is caused by the higher ionic strength of this buffer compared to the MES/HEPES buffer, mainly due to the presence of 100 mM NaCl in the buffer mix. To test this idea, an additional experiment was performed in 100 mM MES/HEPES buffer, to see if a high potential inactivation can be observed. (Figure 6-9)

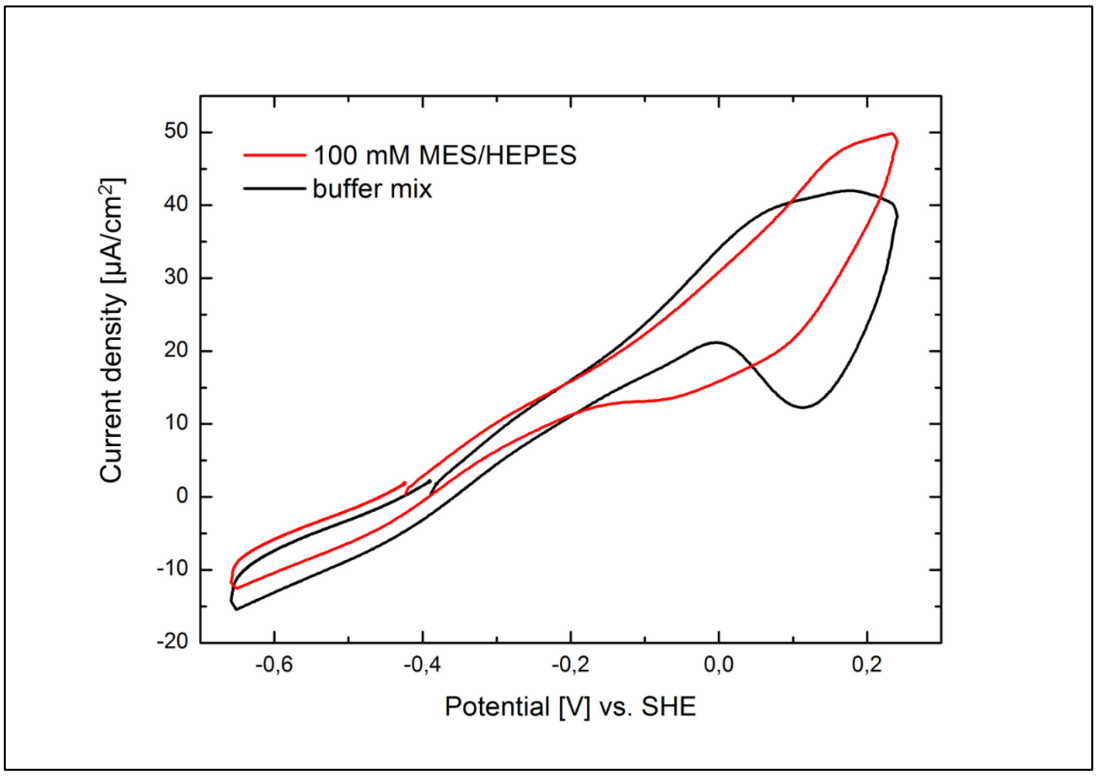

Figure 6-9 Cyclic voltammograms of [FeFe]-hydrogenase, comparison between two buffer systems, electrode rotation 2000 rpm, 10 °C, pH 7.0, scan speed: 200 mV/s and 1 bar H_2.

As it is observed from Figure 6-9, an increase of the ionic strength of the buffer system does not show HPI to the same degree as the buffer mix.

So it was considered that the sodium chloride may play an important role in the formation of this state. Therefore an addition of 100 mM NaCl to the MES/HEPES buffer was tested in cyclic voltammetry experiments. To maintain the total ionic strength the concentration of MES/HEPES was lowered to 10 mM. The result is shown in Figure 6-10.

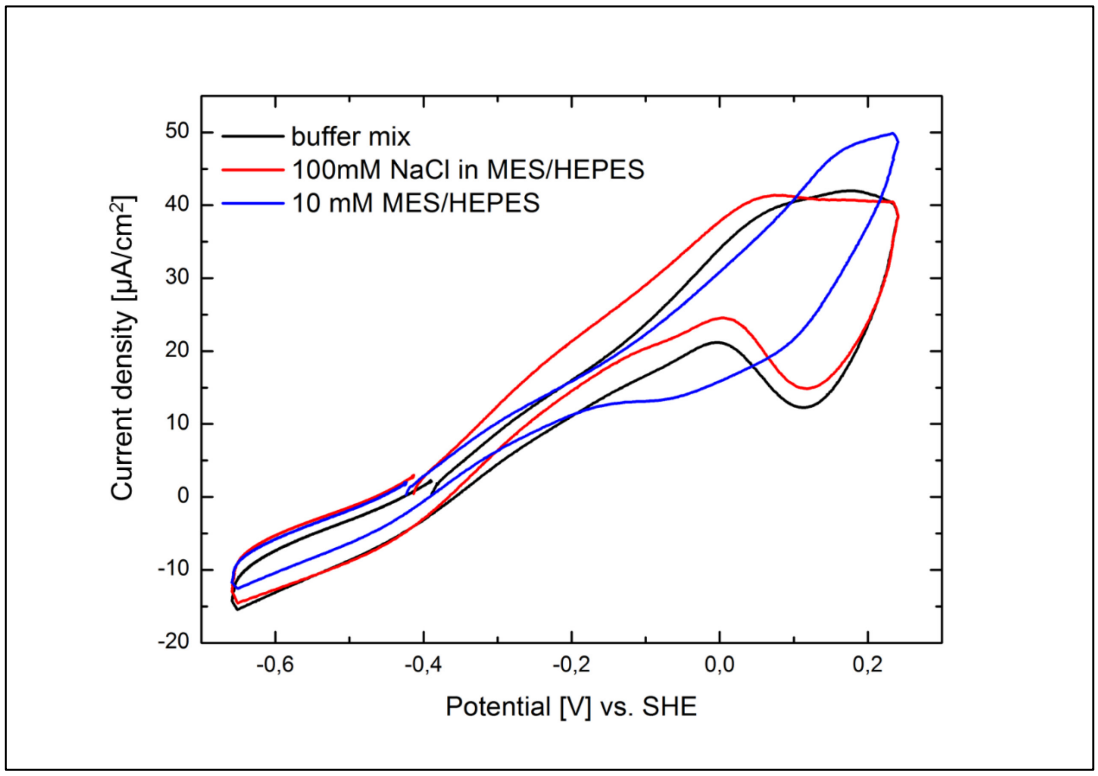

Figure 6-10 Cyclic voltammograms of [FeFe]-hydrogenases in different buffer systems. Electrode rotation: 2000 rpm, pH 7.0, scan speed: 200 mV/s and 1 bar H_2.

The cyclic voltammogram of [FeFe]-hydrogenase in 10 mM MES/HEPES buffer with the addition of 100 mM NaCl shows the same degree of HPI as for the mixed buffer system. With 10 mM MES/HEPES buffer but no NaCl, no high potential inactivation was observed. This indicates that NaCl has a dramatic effect on the formation of this inactive state.

To elucidate if the Na^+ or the Cl^- is responsible of the HPI or if it is the mixture of both, different electrolytes were tested. First the cation was switched from sodium to potassium. (Figure 6-11)

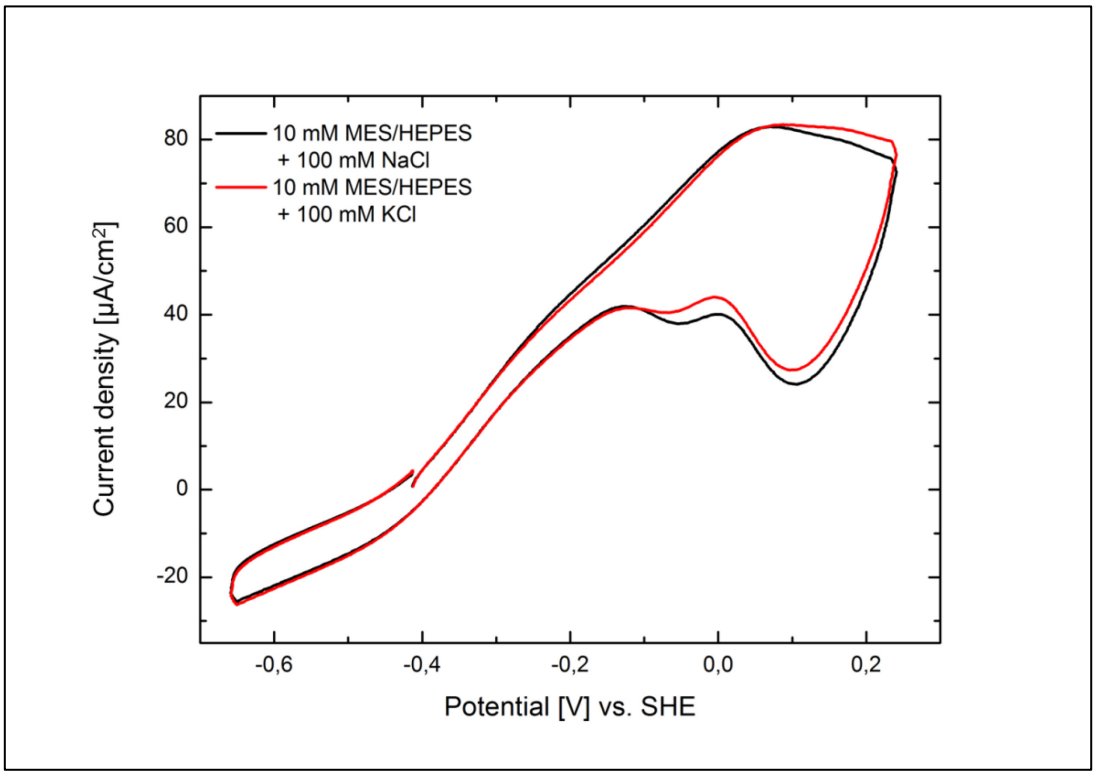

Figure 6-11 Cyclic voltammogram of [FeFe]-hydrogenase with NaCl (black trace) or KCl (red trace) in 10 mM MES/HEPES buffer pH 7.0. Electrode rotation: 2000 rpm, scan speed 200 mV/s and 1 bar H_2. The signal at -0.1 V seem to be contamination in the sample.

There is no difference between the experiment in the presence of 100 mM NaCl or 100 mM KCl: in both cases a high potential inactivation of the protein can be observed. It is most likely, that the nature of the cation does not play an important role regarding this phenomenon but there are some more tests which need to be done to be sure e.g. testing other monovalent cations like Li^+ or NH_4Cl and divalent cations like Ca^{2+} or Mg^{2+}.

Next, the influence of the anion was tested. First, SO_4^{2-}-and the ClO_4^- anions were tested because they are quite common in electrolyte systems. The results are shown in the following Figure 6-12.

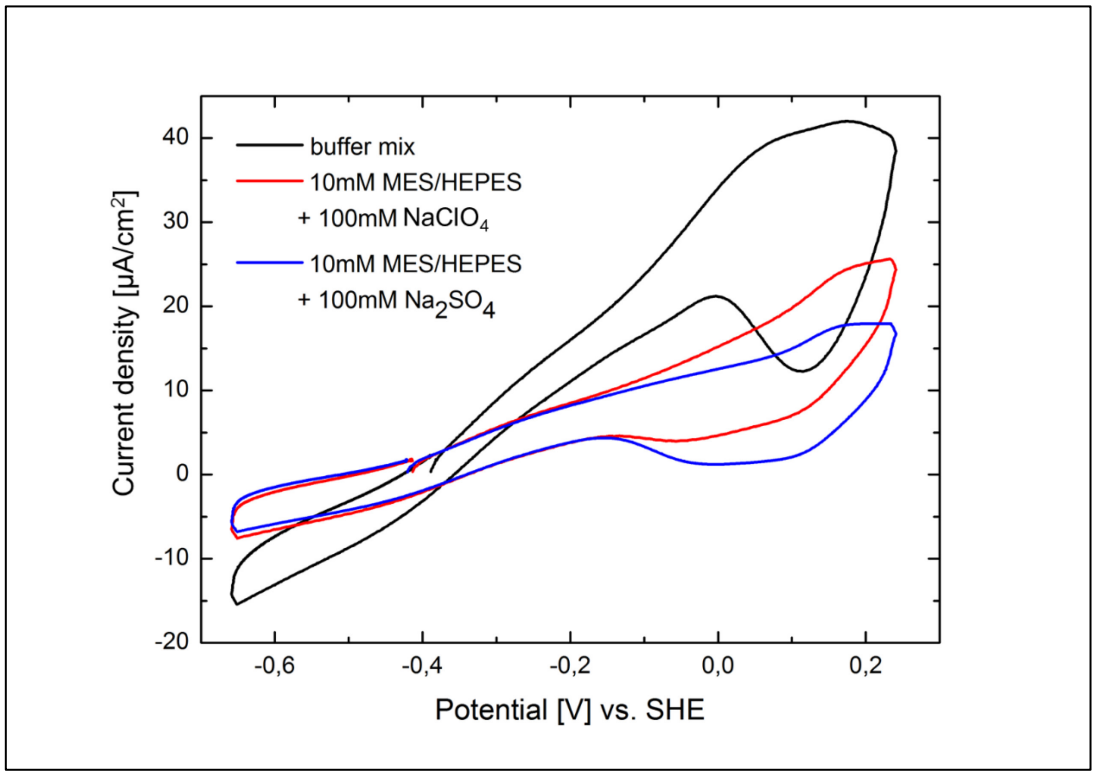

Figure 6-12 Cyclic voltammogram in buffer mix (black trace) and in 10 mM MES/HEPES with 100 mM $NaClO_4$ (red trace) or 100 mM Na_2SO_4. Electrode rotation: 2000 rpm, pH 7.0, scan speed 200 mV/s and 1 bar H_2.

As it is seen from this Figure 6-12 the enzyme does not show high potential inactivation in the presence of sulfate or chlorate. These measurements were performed on different days with different protein films; this is the reason for the differences in the hydrogen oxidation and reductions rates. Nevertheless, from these experiments it can be concluded, that the high potential inactivation of [FeFe]-hydrogenase from *Desulfovibrio desulfuricans* is dependent on the presence of chloride (or possibly more generally on halides). To confirm this, other halides like the larger iodide and the smaller fluoride, both as sodium salts, were tested. (Figure 6-13)

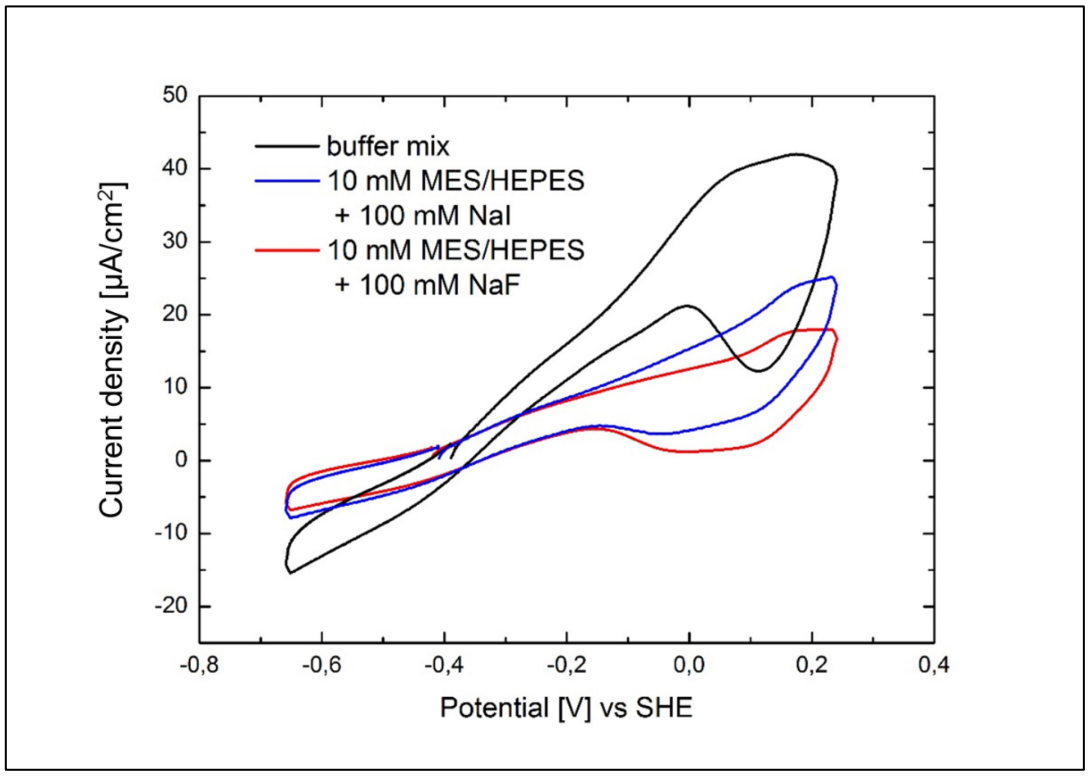

Figure 6-13 Cyclic voltammogram in buffer mix (black trace) and in 10 mM MES/HEPES with 100 mM NaF (red trace) or 100 mM NaI (blue trace). Electrode rotation: 2000 rpm, pH 7.0, scan speed 200 mV/s and 1 bar H_2.

As is deduced from this Figure 6-13 neither the presence of NaI or NaF gave high potential inactivation, and so this phenomenon is highly likely to be specific to chloride. All these experiments show a so far unknown contribution of chloride to the generation of the high potential inactivated hydrogenase state. It is not clear from electrochemistry experiments how chloride facilitates HPI. It might be possible, that chloride binds somewhere to the protein, but due to the fact that chloride is quite inert a chemical reaction with the amino acids or with the iron-sulfur clusters is unlikely. More likely, chloride blocks a substrate channel. There are two possibilities for that, the first is the proton channel, where a blocking might stops the evolution of H^+ from the active site, but this should affect the hydrogen production and oxidation activities of the enzyme, which is not observed in the electrochemical experiment. Additionally, it is not obvious how this would contribute to enzyme inactivation. A second and more likely channel is the hydrogen channel: blocking this would slow down diffusion of hydrogen to the active site. This would lead to slower electron input into the active site, while at high potentials, the electron removal would be quite quick and could lead to over-oxidation. Again, however, this should also show up as a slower rate of hydrogen oxidation in the presence of

chloride, which is not seen. A related idea is that chloride might bind allosterically, inducing a conformational change of the protein, leading to closing of proton or gas channels or affecting the structure and properties of the active site itself. The possibility that chloride binds directly at the active site seems unlikely. However, all these ideas require that chloride behaves in a way that only affects the protein at high potentials. A full understanding will require knowledge of how potentials affect the protein in the absence of chloride.

6.2.3 *Chronoamperometric experiments*

In the following section chronoamperometric experiments on the [FeFe]-hydrogenase are shown. As described in the theoretical introduction (Section 2.7.4) in these experiments the corresponding current is detected and plotted against the time.

From the reported experiments above and from the literature it is still not certain, what the high potential inactivation really is. Therefore further investigations to characterize this state were done by chronoamperometric experiments.

The experiments of the following section were motivated by a result of the work which was published in 2014 by Léger et al., in which the high potential inactivation of [FeFe]-hydrogenases for *Chlamydomonas reinhardtii* was described.[108] Léger and his group studied the enzyme by electrochemistry and found out, with the support of theoretical calculations, that the coordination sphere of the distal iron, where the open coordination site for hydrogen or the inhibitor CO binding is located (Figure 6-14), is more flexible than was initially anticipated.

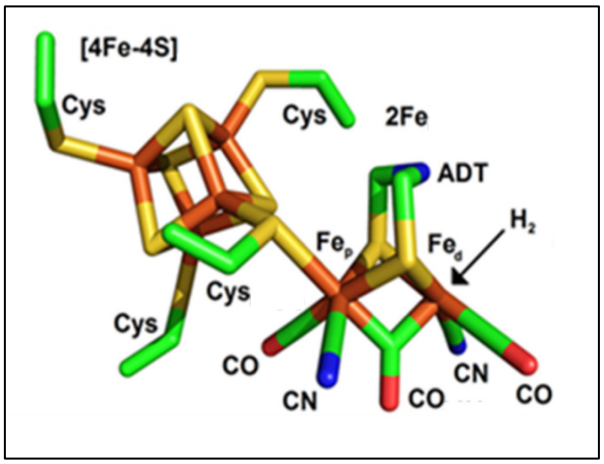

Figure 6-14 Structure of the H-cluster of the [FeFe]-hydrogenase, the open coordination side at the distal iron is marked with an arrow.

This flexibility is supposed to prevent the oxidative damage of the H-cluster during high potential inactivation. These results are based on chronoamperometric experiments which will be discussed later with the corresponding experiments of this thesis. To summarize the experiments of the Léger group: the reversible high potential inactivation of the enzyme results from binding of hydrogen to coordination positions that are normally blocked by intrinsic CO-ligands and that hydrogen is, therefore, necessary to protect the enzyme from oxidative damage.

In order to verify that the [FeFe]-hydrogenase from *D.* desulfuricans shows the same behaviour as that from *C. reinhardtii* a test experiment was performed to see the behaviour of [FeFe]-hydrogenase from *D. desulfuricans* in our setup. In the first experiment (Figure 6-15) the high potential inactivation under a hydrogen feed for *D. desulfuricans* in buffer mix is shown.

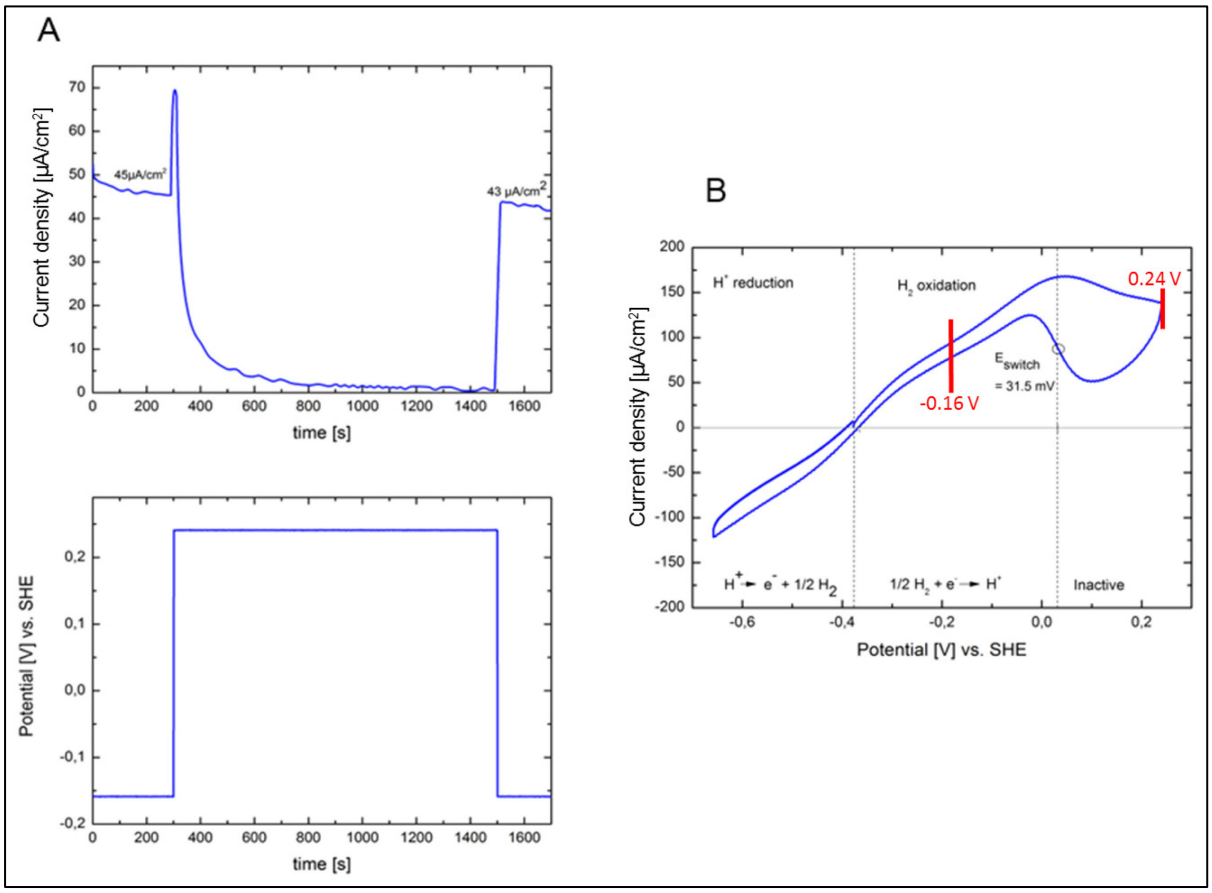

Figure 6-15 A) Chronoamperogram of [FeFe]-hydrogenase. After an initial potential of -0.16 V the potential is increased to 0.24 V which induced a high potential inactivation. After 20 min the potential is decreased to the initial potential to see a recovery of the enzyme activity. Electrode rotation: 2000 rpm, buffer mix pH 7.0, 1 bar H_2. B) For better understanding of the redox process of the enzyme, during chronoamperometry, a cyclic voltammogram (from a different experiment, see Figure 6-7) is shown.

For this chronoamperometric experiment, the covalently attached protein was exposed, under a hydrogen atmosphere, to an initial potential of – 0.16 V where a catalytic current of 45 µA/cm^2 was measured. Afterwards the potential was increased to 0.24 V where a higher hydrogen oxidation rate is measured as a result of increased driving force. This is visible as a drastic increase of the current to 69 µA/cm^2. Immediately after this, the current drops to nearly zero, caused by high potential inactivation of the protein. After 20 minutes when the current was zero, the potential was lowered back to the initial potential of -0.16 V to reduce the enzyme and observe a recovery of the catalytic current to 43 µA/cm^2.

This experiment shows that under hydrogen the enzyme activity can be recovered after an inactivation at higher potential by more than 90 %.

In Section 6.2.2 the influence of chloride on the high potential inactivation was shown and reported for the first time. Due to these results, the chronoamperometric experiment from Figure 6-15A was repeated in 100 mM MES/HEPES buffer pH 7.0 to compare both buffer systems. The result in shown in Figure 6-16.

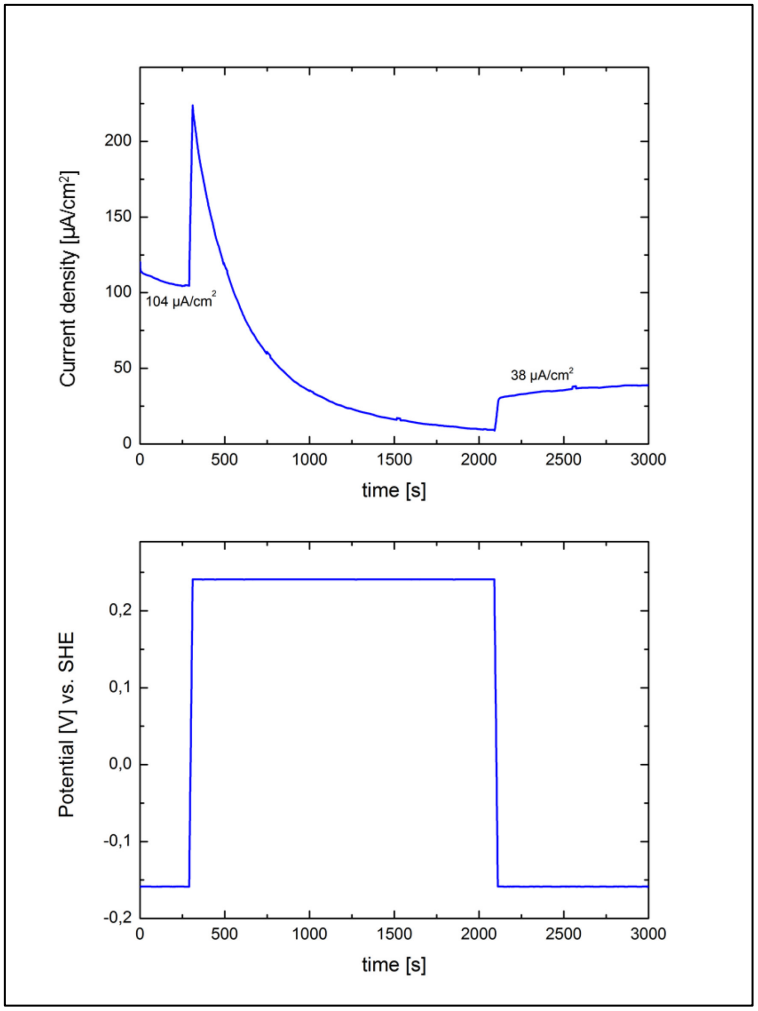

Figure 6-16 Chronoamperogram of [FeFe]-hydrogenase. After an initial potential of -0.16 V the potential is increased to 0.24 V which induced a potential inactivation. After 30 min the potential is decreased to the initial potential to see a recovery of the enzyme activity. Electrode rotation: 2000 rpm, 100 mM MES/HEPES buffer, pH 7.0, 1 bar H_2.

The conditions used for this experiment were the same as in that previously reported. After an initial potential of -0.16 V with a measured catalytic current of 104 µA/cm^2 the potential was increased to a higher potential of 0.24 V where, as it was also seen in Figure 6-15. It is obvious from comparison of both experiments, that the high potential inactivation in MES/HEPES buffer is lower than in buffer mix. The half-life time in buffer

mix is 7 s, while in MES/HEPES buffer it is 97 s. The half-life time was here defined as the time it takes to lose half the activity of the enzyme. The activity for MES/HEPES buffer recovers only to 37 μA/cm^2, which corresponds to 30% of the initial current. This result could mean, that chloride might protect the enzyme from permanent damage by facilitating formation of an inactive state more rapidly than the permanent inactivation process. But due to the fact, that the catalytic current at the beginning of this experiment (at -0.16 V) decreases continuously it is not possible to be sure that the lower recovery rate is really caused by the different buffer, it might be a general loss of protein activity during the experiment, caused by film loss.

To later test the reported influence of hydrogen on the high potential inactivation, an analogous chronoamperometric experiment to the one reported in the paper of the Léger group[108] was performed to see if the behaviour of the [FeFe]-hydrogenase from *D. desulfuricans* in our setup is identical to the reported behaviour for *C. reinhardtii*. In the experiment of Léger a rotating disc graphite electrode in hydrogen saturated mix buffer was stepped from a 65 mV potential to 165 mV which results in an increase of the hydrogen oxidation current followed by a decrease caused by the inactivation of the enzyme. After the potential is stepped back to 65 mV a slow recovery of the activity is observed, which shows that the inactivation is reversible.

For the experiment with *D. desulfuricans* the protein was also covalently attached to the electrode and rotated in hydrogen saturated buffer mix. At an initial potential of -158 mV a catalytic hydrogen oxidation current of 39 μA/cm^2 was measured. Afterwards, the potential was increased in two steps, first to 59 mV and second to 116 mV. This potential increase leads to an increase of the catalytic current, which is immediately followed by a rapid decrease at 116 mV caused by inactivation of the enzyme. After the potential is stepped back to 59 mV, a recovery of the enzyme activity is observed. At the initial potential of -158 mV a catalytic current of 37 μA/cm^2 was measured, this is a recovery of the enzyme activity under hydrogen conditions of 95 %. This result is identical to the experiment performed by Léger. Also here the small decrease of the catalytic current during the experiment can be explained by a slow, irreversible inactivation of the enzyme, as described above. The experimental data are shown in the following Figure 6-17.

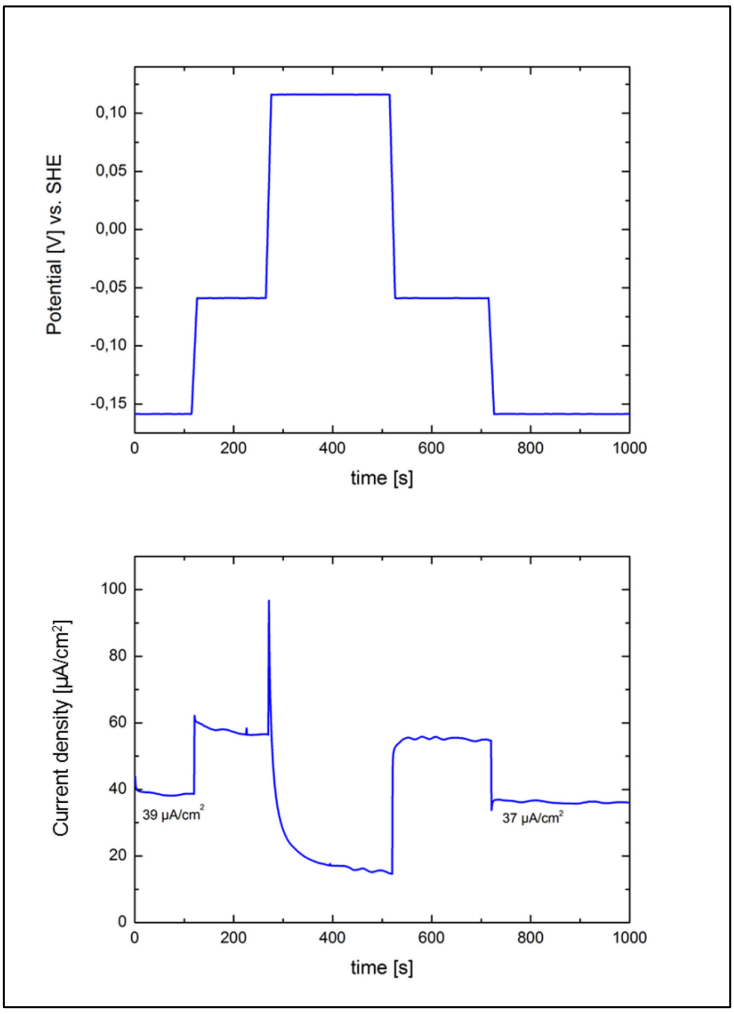

Figure 6-17 Chronoamperometric experiment of [FeFe]-hydrogenase to compare the used setup with the results, published in Léger's paper.[108] The potential steps are shown in the upper part of the figure. The electrode was rotated with 2000 rpm, in hydrogen saturated buffer mix pH 7.0.

Léger postulated that two inactive states are reversibly formed under oxidizing conditions in the presence of hydrogen, where hydrogen blocks the free reaction site at the distal iron preventing the binding of oxygen. A scheme of the proposed intermediates by Léger is given in the following Figure 6-18. The open coordination site can be blocked in two possible ways (left or right arm of the scheme) by hydrogen, from Léger's DFT calculations it is not possible to decide which arm is the most likely one. There is spectroscopic evidence for one of these intermediates. Also the fact, that the bridging NH group is not included into the postulated mechanisms is a problem of this calculation. It is known, that the bridge-head is important in the catalytic cycle of the hydrogenases, also the pH dependency of the HPI (pk_A ~ 6.5 same as for amines) indicates an involvement of this group in the HPI.

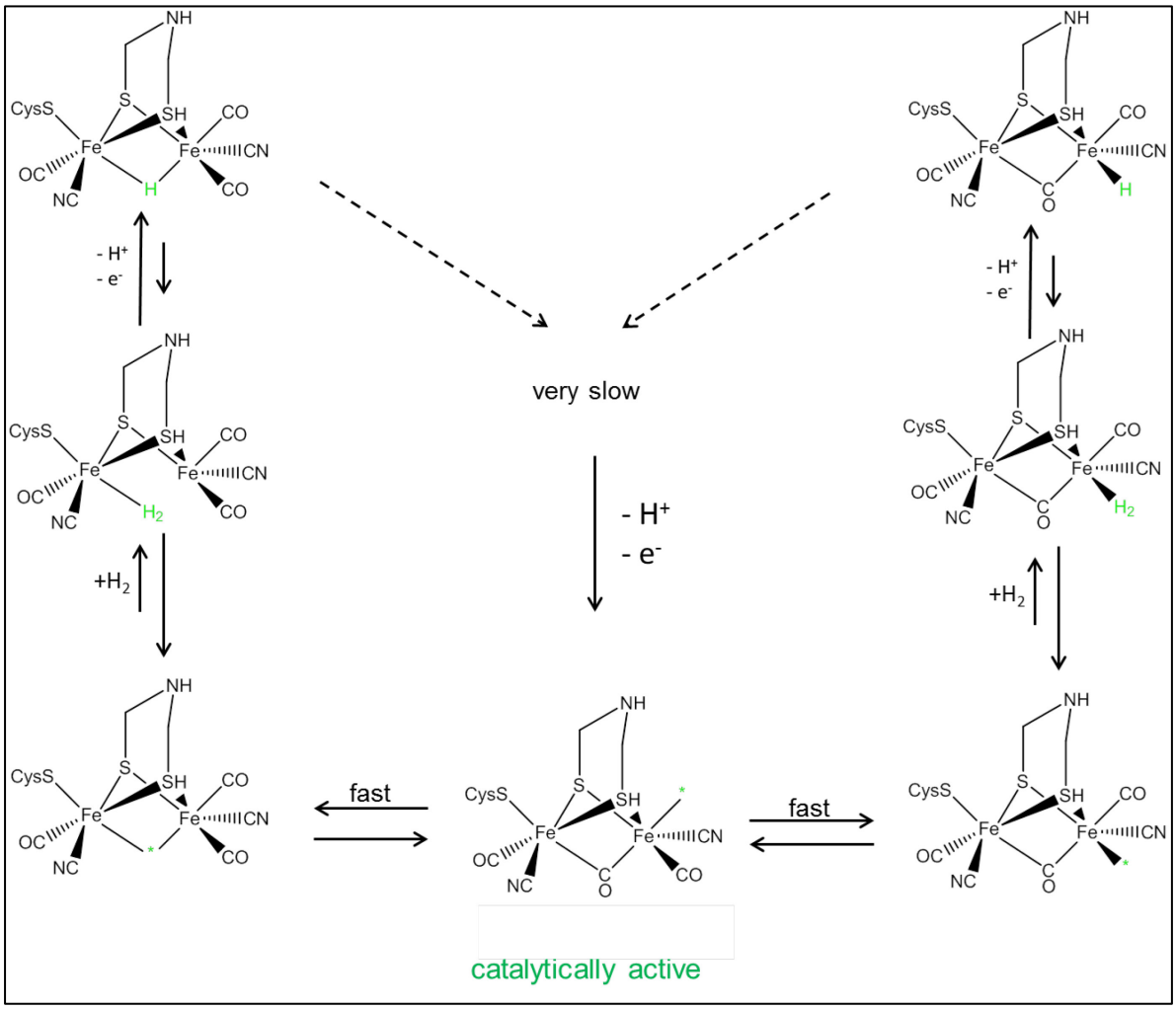

Figure 6-18 Scheme of the postulated intermediates during the formation of the oxygen tolerant state by high potential inactivation. Figure adapted from[108]. The open coordination site, labelled with a green asterisk, is blocked in two possible ways (left or right arm of the scheme) by hydrogen.

In this thesis it was tested, if hydrogen is really necessary to protect the enzyme for oxidative damage during high potential inactivation, as postulated by Léger. For that, an additional chronoamperometric experiment was designed. Since under N_2 it is not possible to measure H_2 oxidation currents, it is difficult to evaluate the inactivation of the enzyme at high potential using only PFE. Therefore an indirect measurement was used. At the beginning of the experiment the electrochemical cell is saturated with hydrogen and after an initial potential of -159 mV the potential is increased to 241 mV to oxidize the protein to its inactive state (high potential inactivation). When the current drops, as a result of HPI, 1 mL of oxygen saturated buffer is injected to the cell – to estimate the amount of inactivated enzyme. If the enzyme is not in the oxygen resistant inactive oxidized state[39] oxygen would cause irreversible damage of the protein, which would

prevent a recovery of the catalytic current when the potential is stepped back to the initial potential of -159 mV. An anaerobic control was always measured before the O_2 experiment was done to test the stability of the electrode. The first part of the experiment is performed under a hydrogen atmosphere to show the high potential inactivation as reported previously[39], the second part of the experiment is performed as in the first part but under a nitrogen atmosphere. If hydrogen is really necessary for the conversion of the enzyme to its oxygen tolerant state, then in the second part of the experiment no recovery of activity should occur.

As is clear from the first part of the experiment (see Figure 6-19) the catalytic current can be recovered by 85 % under hydrogen, both in the experiment with oxygen and in the anaerobic control. From this part two things can be concluded. First, under a hydrogen atmosphere the enzyme activity can be recovered after high potential inactivation and second, that the high potential inactivated state is oxygen tolerant.

After the enzyme is allowed to recover at -159 mV, the hydrogen gas is changed to nitrogen. Immediately a drop of the current is observable caused by a lack of substrate (hydrogen). Afterwards, the potential was increased to 241 mV, as in the first part of the experiment. Based on the proposed inactivation mechanism[108], high potential inactivation should not occur under these conditions. In the same way as in the first part of the experiment 1 mL of oxygen saturated buffer is injected to cause irreversible damage if the enzyme is not in an oxygen tolerant state. To reduce the enzyme again, and to show hydrogen oxidation activity, the gas is switched back to hydrogen. After the cell was saturated with hydrogen, the potential is stepped back to the initial potential of -159 mV. A recovery of the catalytic activity of 65 % was observed.

For a better comparison of both experiments, the currents in Figure 6-19 were normalized.

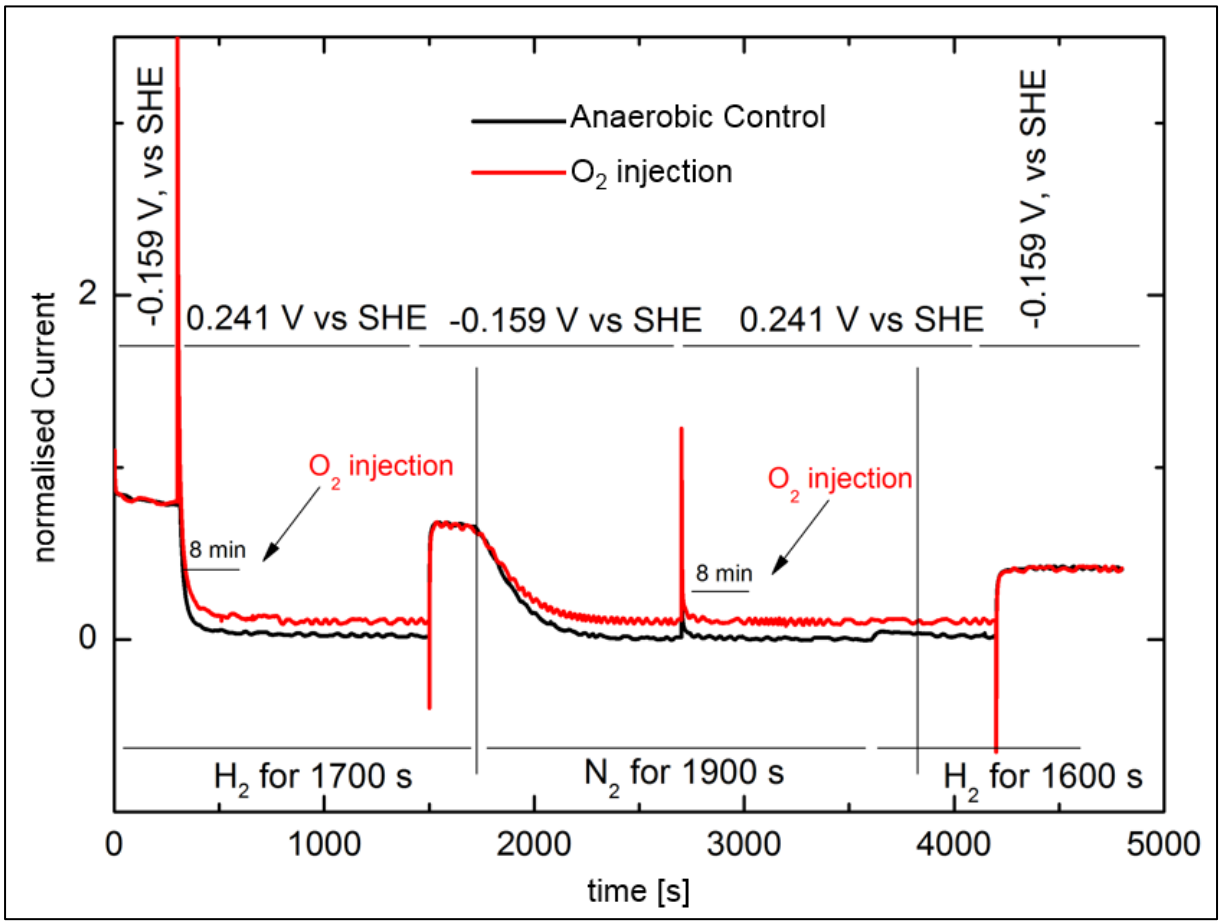

Figure 6-19 Chronoamperogram of the experiment to show if hydrogen is necessary for generate the oxygen tolerant state. Electrode rotation: 2000 rpm, buffer mix pH 7.0, scan speed 0.2 V/s. The anaerobic control and the oxygen measurement were performed on the same protein film, one after another. For a better comparison the currents were normalised.

These experiments show that also under a nitrogen atmosphere the enzyme can generate the oxygen tolerant state by high potential inactivation, which means that hydrogen is not a requirement necessary to form the oxidized inactive state. Maybe the chloride from the mixed buffer system plays also a role in protecting the enzyme from oxygen corresponding to the results from Section 6.2.2.

The experiment can be summarized to the conclusion that hydrogen is not absolutely necessary for the enzyme to generate the oxygen tolerant state and that the open coordination site can be also protected by other substances. So far it is not possible to make any assumptions about the nature of the blocking substance. It might be also possible, that the high potential inactivation does not involve blocking the active site of the protein with anything. So far there are no experimental results that suggest that oxygen is blocked from the active site.

6.3 PFE experiments on [FeFe]-hydrogenase from heterologous expression

After the heterologous expression system was established (see Section 3.3) and the maturation of the resultant protein was achieved (see Section 4.3), it was tried to measure catalytic current with the electrochemical setup as it was done for the native system.

6.3.1 *Immobilization of [FeFe]-hydrogenase onto HOPGE electrode*

The covalently attachment of the maturated enzyme was performed as described in Section 6.2.1 for the native enzyme but with one major difference. Once the enzyme is maturated it is sensitive to oxygen, therefore the covalent attachment was performed under anaerobic conditions inside a nitrogen filled glovebox. The additives NHS, EDC and NBD were also dissolved in degassed buffer inside the glovebox.

Alternatively, the protein was also simply adsorbed on the surface of a HOPGE as follows, the HOPGE electrode was polished with alumina powder and water, after rinsing the electrode with water a protein solution (50 µM) was pipetted on the top of the electrode. After 20 minutes the electrode is rinsed with water to remove non adsorbed protein.

6.3.2 *Electrochemical experiments on the maturated [FeFe]-hydrogenase*

In the first experiment it was tested, if it is possible to covalently attach the maturated enzyme under anaerobic conditions to the electrode, following the protocol mentioned above (Section 6.3.1).

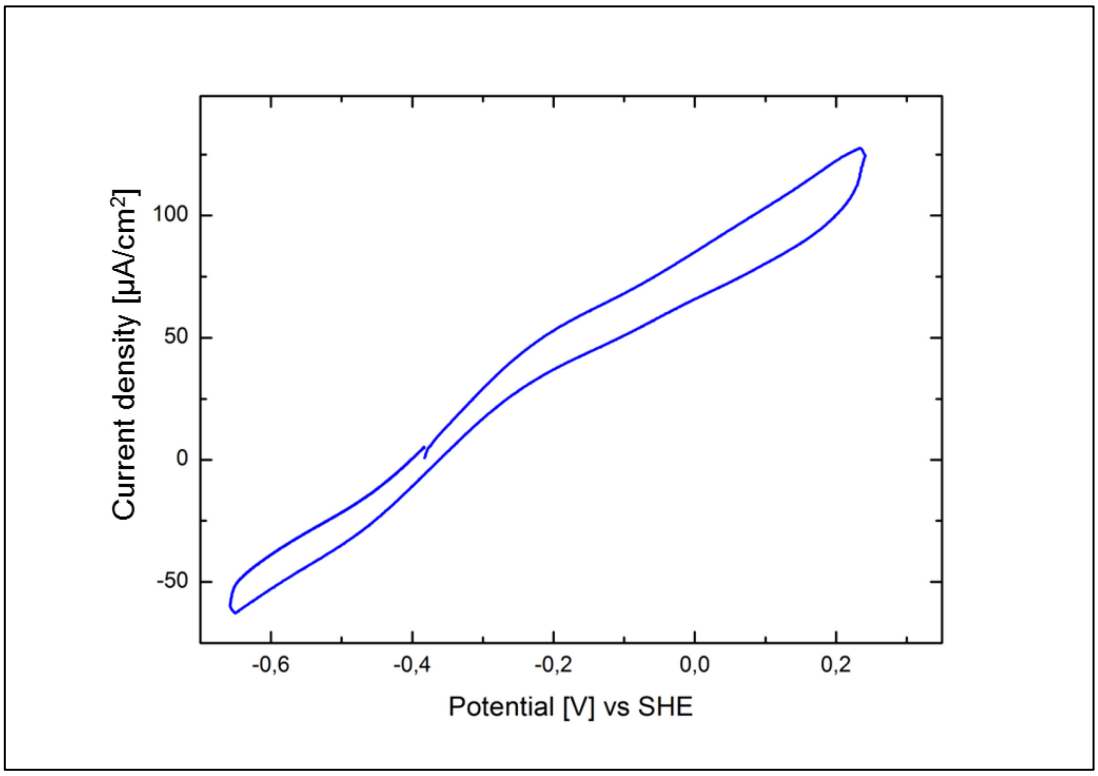

Figure 6-20 Cyclic voltammogram of maturated [FeFe]-hydrogenase. Electrode rotation: 2000 rpm, MES/HEPES buffer pH 7.0, scan speed 0.02 V/s, 1 bar H_2.

Figure 6-20 shows the cyclic voltammogram of covalently attached maturated [FeFe]-hydrogenase. It is visible, that there is catalytic current, which means, that the same protocol for covalent attachment also works under anaerobic conditions for maturated enzyme from heterologous expression systems. In the tested MES/HEPES buffer system there is, like for the native system, no high potential inactivation visible. Since the influence of chloride was discovered at the end of this thesis, all experiments with the maturated enzyme were performed with the MES/HEPES system.

For a comparison of both enzymes the following Figure 6-21 shows both enzymes under the same conditions.

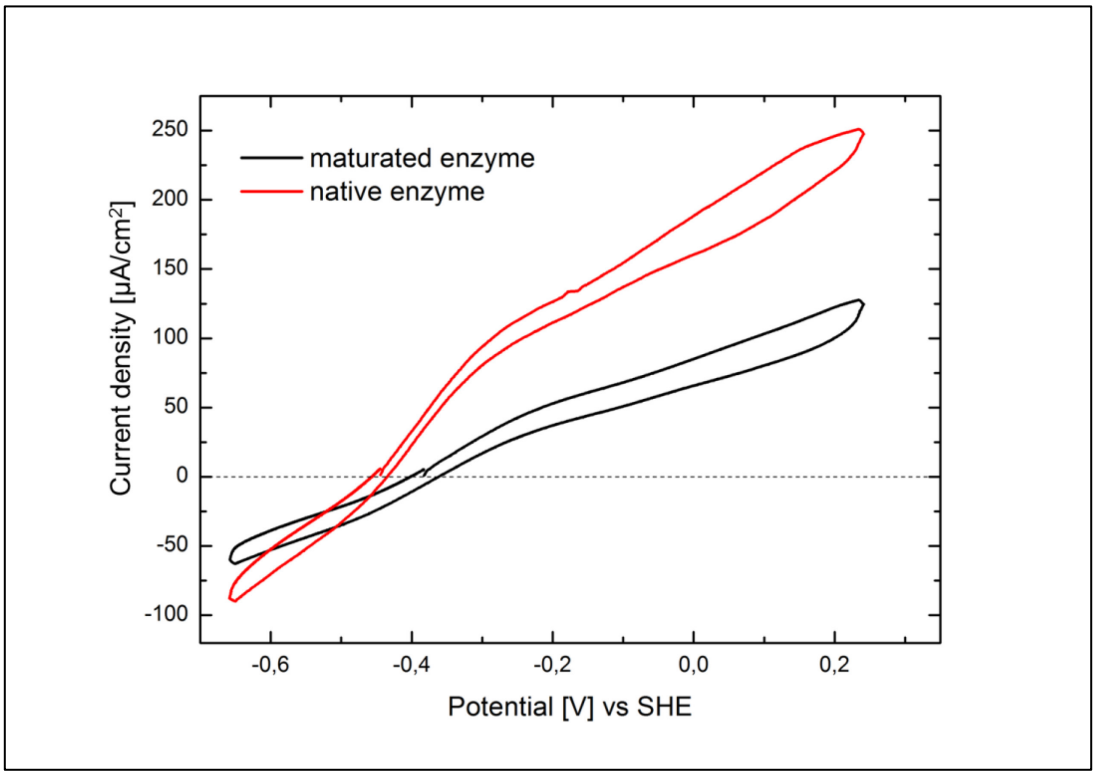

Figure 6-21 Comparison cyclic voltammograms of native (red trace) and maturated (black trace) [FeFe]-hydrogenase. Electrode rotation: 2000 rpm, MES/HEPES buffer pH 7.0, scan speed 200 mV/s, 1 bar H_2.

The native system shows consistently higher activities than the recombinant enzyme, which is probably to do with incomplete maturation of the unmaturated enzyme. Both electrodes had been prepared with a protein solution of the same concentration, which means that the coverage of the electrode should be the same for both experiment but it is not clear if the covalent attachment under anaerobic conditions shows the same efficiency than under aerobic conditions. The measurements were performed on different days, and also for different electrode preparations of the native enzyme not always the same maximum current was measured. Nevertheless, the overall shape of the cyclic voltammogram is similar for both systems, as it was expected.

To test the influence of the buffer pH several pHs were tested by changing the buffer in the electrochemical cell. The results are shown in the following Figure 6-22.

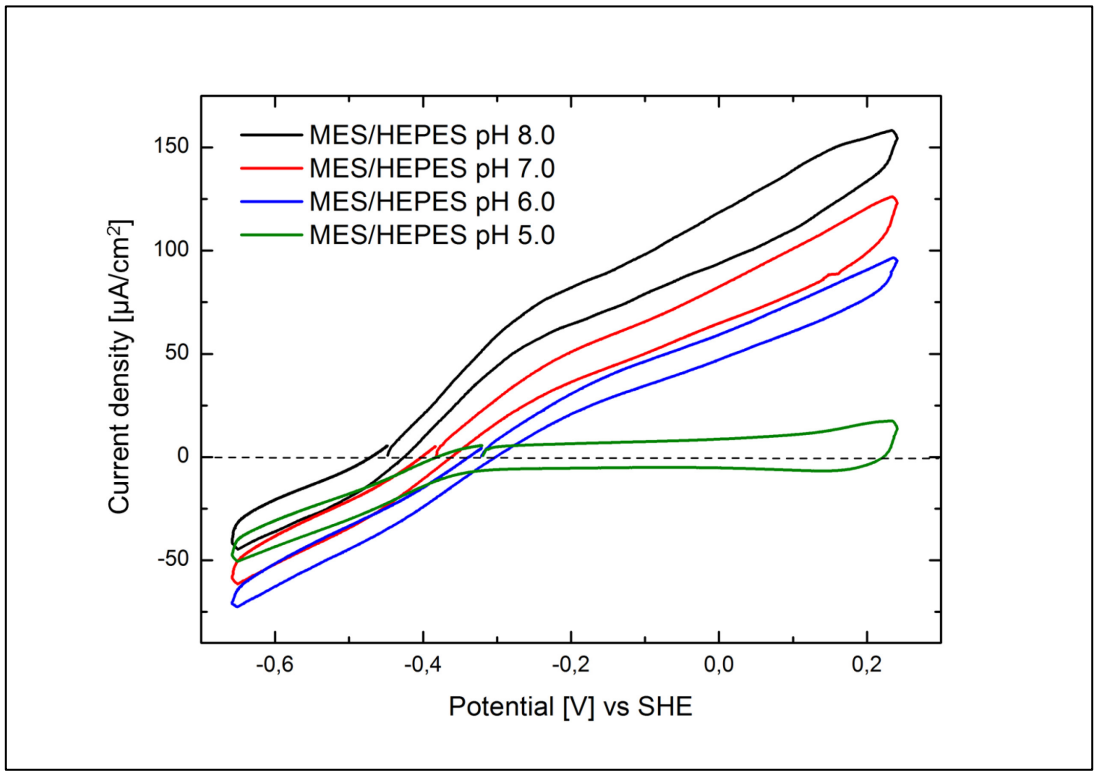

Figure 6-22 Cyclic voltammograms of maturated [FeFe]-hydrogenase a different pHs. Electrode rotation: 2000 rpm, MES/HEPES buffer system, scan speed: 0.2 mV/s, 1 bar H_2.

The shown pH dependency was also reported for [FeFe]-hydrogenase in a publication of Parkin et al..[39] The faster hydrogen oxidation at higher pH is likely due to a reduced number of protons available for re-oxidation of the hydrogen reduced enzyme. Also the thermodynamic potential of hydrogen changes with pH, as expected from the Nernst equation. The hydrogen production currents increase at lower pH as a result of the increase in the concentration of H^+. To demonstrate the change of potential with pH the Nernst equation for SHE can be rearranged to the following formulas:

$$E = 0 + \frac{0.059\ V}{2} \log \frac{c^2(H_3O^+)}{p(H_2)}$$

$$E = 0 + 0.059\ V \log c(H_3O^+)$$

$$\text{with } pH = -\log c(H_3O^+)$$

$$E = -0.059\ V\ pH$$

For several experiments with the unmaturated protein (Section 6.3.3) it was necessary to see if the maturated protein also works after adsorbing it to the electrode. The procedure described in Section 6.3.1 was used to adsorb the protein under anaerobic conditions. A cyclic voltammogram is shown in Figure 6-23.

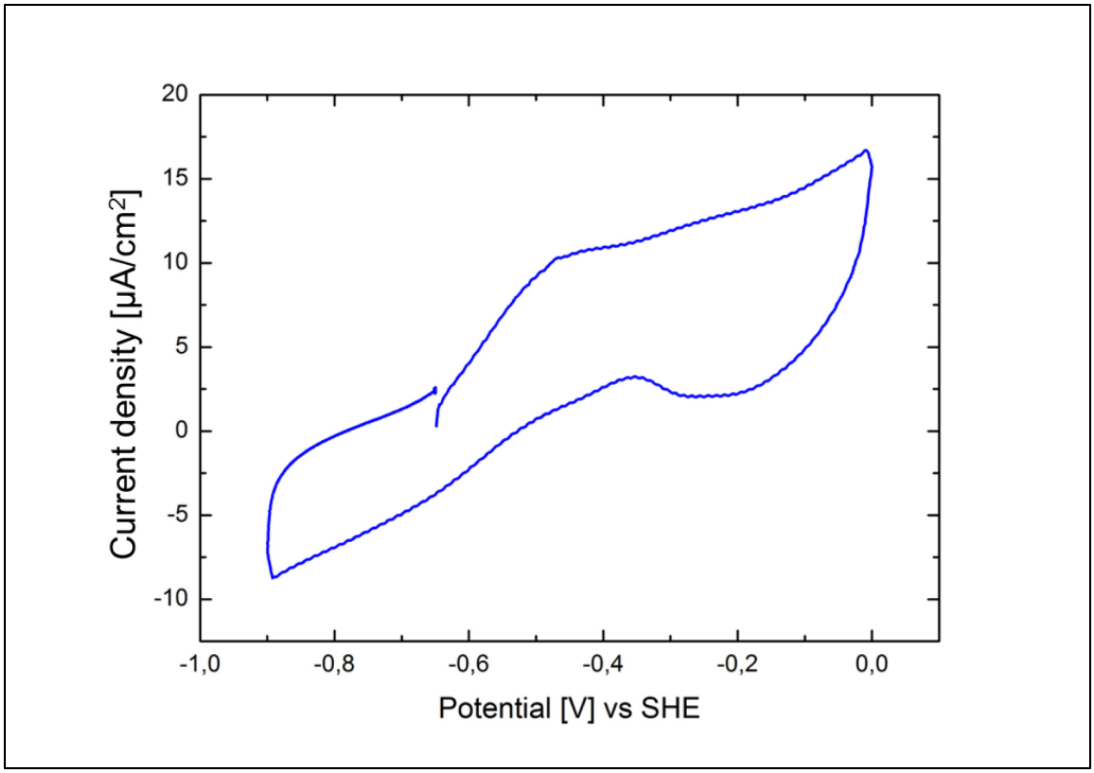

Figure 6-23 Cyclic voltammogram of maturated [FeFe]-hydrogenase adsorbed to the electrode. Electrode rotation: 2000 rpm, buffer mix system pH 7.0, scan speed 200 mV/s, 1 bar H_2.

The protein can be adsorbed to the electrode surface, but the catalytic current is quite low. This indicates low adsorption of the protein onto the electrode. It can be concluded that covalent attachment is the better immobilisation method for this protein. But it is also clear, that in the buffer mix system also the maturated [FeFe]-hydrogenase shows the high potential inactivation, which again underlines the similarity of both systems. Therefore, heterologous expression and the artificial maturation of the enzyme is an important tool for generation of large amounts of highly active protein that is identical to the one of natively purified protein.

6.3.3 *Electrochemical experiments on the unmaturated [FeFe]-hydrogenase*

To determine the redox potentials of the [Fe-S]-clusters, the unmaturated protein was adsorbed on a glassy carbon electrode. HOPGE and PGE electrodes were also tested but because the available electrodes of these types all had low surface areas, they gave poorer signals. 2 µL of protein were applied at approximately pH 6.0 at a concentration of 0.3 mM. Unfortunately, only very weak signals were observed and the film was not very stable, being lost completely after a few minutes. Further optimization by testing different PGE and HOPGE surfaces with higher surface areas may help. In addition, the protein buffer and electrochemistry buffer seem to be crucial in forming and maintaining a stable protein film. Figure 6-24 shows the best example of a cyclic voltammogram taken of a film of unmaturated protein from *D. desulfuricans*. Two peaks in the oxidative direction and two peaks in the reductive direction separated by approximately 170 mV are clearly observed. Background subtracted data are presented in the same figure and these have been simulated using Gaussian curves. The best fitting was achieved using three overlapping curves of equal area and equal peak width. Similar fits could also be achieved using two curves but with the higher potential curve having twice the area and a slightly larger peak width than the more negative potential curve.

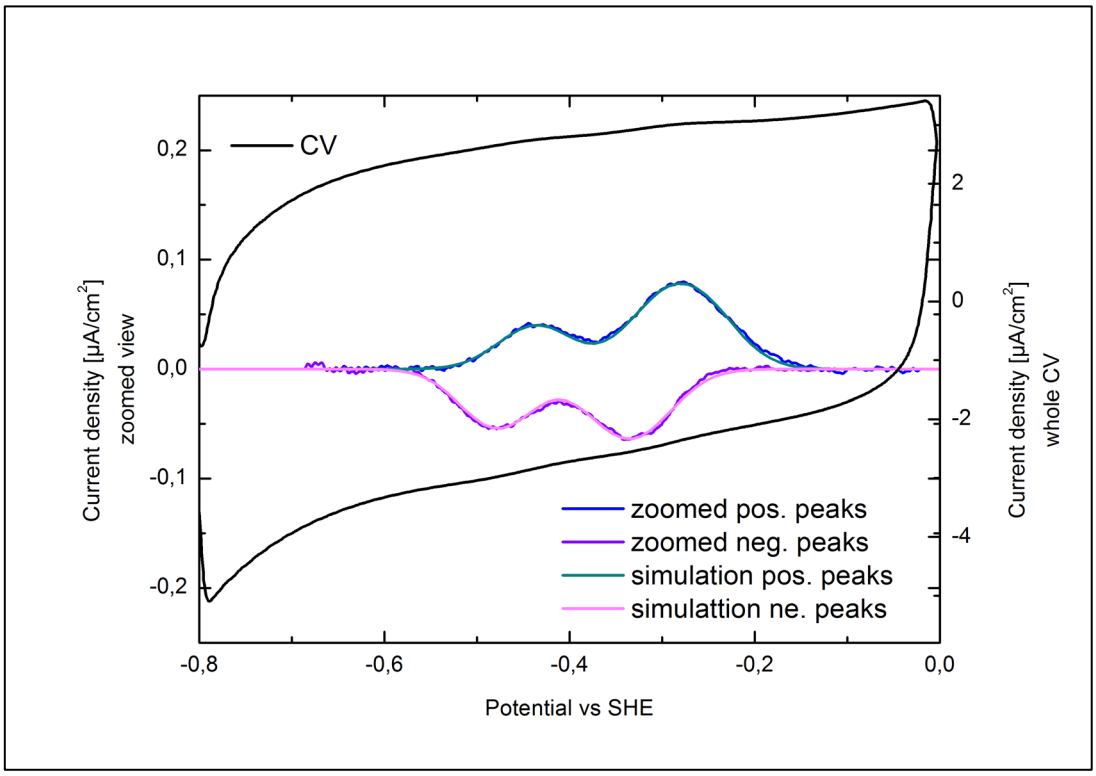

Figure 6-24 Smoothed CV of the adsorbed unmaturated protein is shown as a black trace. The signals of interest are zoomed and baseline corrected shown in blue and purple. The fit of these signals with a three signal fit is shown in cyan and pink. More details about data processing are given in the text.

Figure 6-24 shows the measured cyclic voltammogram and the zoomed areas of interest. For determination of the redox-potentials the data was modelled with three peaks as shown in the following Figure 6-25. The peak width at half the maximum height were fitted to 94 mV which is in approximate agreement to the expected value of 90 mV for a single electron process[151]. The data could also be modelled with two peaks but with a peak width of over 110 mV and twice the peak height for the higher potential peak. Since we expected to see three peaks and there is no good reason for expecting one cluster to have a higher stoichiometry than the other, we favour the former fitting approach. However, an additional problem is that the peak areas in the oxidative and reductive directions are slightly different. Most likely this is due to imperfect background subtraction of the small signals.

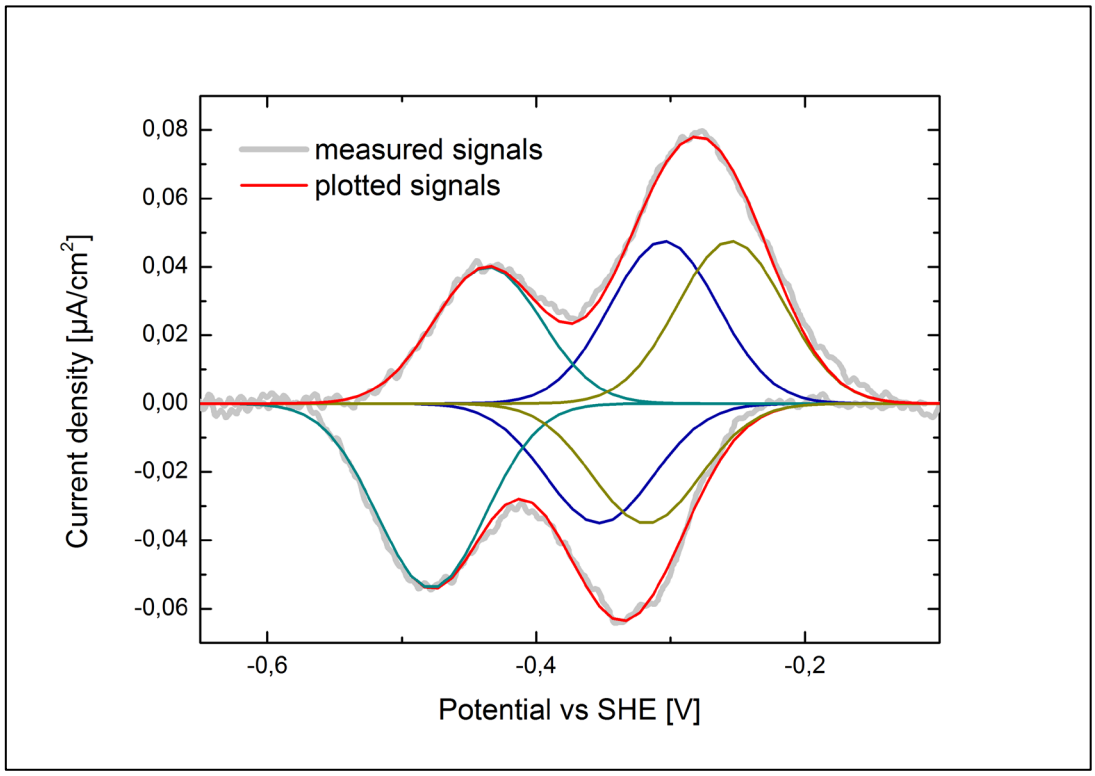

Figure 6-25 The zoomed signals from Figure 6-28 are shown as grey traces. The red trace shows the overall fit. The three separated fitting curves are shown in cyan, blue and dark yellow. Each colour belongs to one cluster. More details for the different peaks are given in the text below.

From Figure 6-25 three midpoint potentials for all three [Fe-S]-clusters could be determined. From this the midpoint potentials of

peak 1 = -0.33 ± 0.01 V, peak 2 = -0.46 ± 0.01 V and peak 3 = -0.29 ± 0.01 V vs SHE

were determined for the iron sulfur clusters in unmaturated [FeFe]-hydrogenase of *D. desulfuricans.* These values fit quite nicely to the potentials which were found from the EPR redox-titration in Section 4.2.2. Another value which can be calculated from this experiment is the coverage of the electrode by enzymes; here 0.92 pmol/cm^2 were reached. This is a quite low number, but fits to the received low response.

Another experiment was to observe the activation of the enzyme with electrochemistry, and thereby follow the insertion of the adt complex. In the beginning the enzyme was

covalently attached to the electrode and a one to one ratio of adt to protein was added to the solution in the electrochemical cell. However, here it was not possible to activate the covalently attached enzyme. To see if it is in general possible to activate the attached protein several concentrations of adt were directly added to the electrode surface with the attached protein. But even high concentrations of 1 mM adt were not able to activate the protein.

It is possible that the covalently attached protein is somehow effected by the maturation either because the adt binding cavity is blocked or by restriction of the necessary conformational changes involved in the process. Therefore, it was decided to test the activation with protein which is only adsorbed to the electrode allowing greater conformational freedom of the protein. However, this also failed to yield active hydrogenase. Further experiments are necessary to get a better idea in the activation process of the adt to be able to design afterwards an electrochemical experiment to follow the activation kinetics.

6.4 Summary

The largest part of this chapter concerned experiments with the native [FeFe]-hydrogenase from *D. desulfuricans*. It was shown that chloride is required to form the high potential inactivation state. In the absence of this anion, no HPI (or slower HPI) was observed. The influence of chloride is unclear and so far no explanation is possible. Chloride is present in all cells so it is likely that formation of the HPI state is not limited by this *in vivo*, but it may be possible that under certain conditions chloride is deficient and the hydrogenase cannot undergo HPI. Since, the hydrogenase is located in the periplasm it may be that the chloride concentrations fluctuate quite strongly. It is, therefore, also possible that the hydrogenase senses the chloride concentration and that it serves as a kind of signal which alters the enzyme reaction pathway under different conditions.

With chronoamperometric experiments it could be shown, that HPI of the enzyme is not only observed under hydrogen, as was reported by others[108], but also under nitrogen. Therefore, it can be concluded, that the blocking of the free coordination site is not specific to hydrogen or that blocking of the coordination site does not in fact take place and that another phenomenon explains the oxygen resistance in the HPI state. Maybe

also in this reaction the chloride plays an important role. It is known from Armstrong et al.[39] that there is no or at least lower HPI at low pH. It is suggested, that protonation of the enzyme influences the formation of the HPI state. For a pH lower than 6 a one electron transfer is postulated, while at a pH above 6 an additional one proton transfer is necessary to generate the HPI state, from this two different HPI states were suggested. This pH dependence results to two different options: either protonation occurs on the central atom of the adt ligand or protonation occurs at a coordinated OH^-/H_2O.[39] From the results of this thesis chloride might also affect the protonation of the enzyme and thereby the presence or absence of HPI, or somehow interact with a positively charged region of the protein, which may have the reverse effect to the interaction of positively charged protons with a negatively charged or neutral amino acid. From the literature it is confirmed, that the H_{ox} state of the enzyme shows an Fe^{I} Fe^{II} active site[37,108]. During the high potential inactivation maybe two different states are formed. From this, a scheme of the interaction with chloride can be proposed (see Figure 6-26).

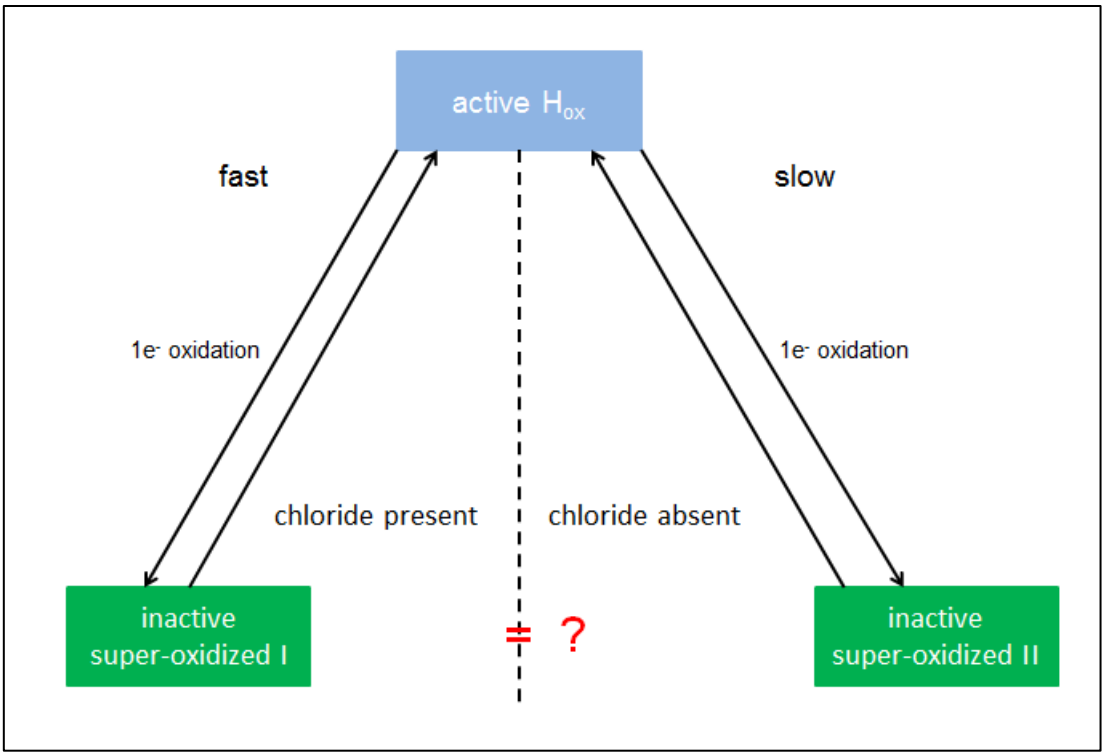

Figure 6-26 Possible scheme of the interaction between chloride and the active site of the [FeFe]-hydrogenase during high potential inactivation.

In Figure 6-26 the active enzyme is present in the H_{ox} state and one electron oxidation leads to formation of an inactive state which is in the presence of chloride stable and reactivates quite quickly (super-oxidized I). In the absence of chloride the active oxidized state (H_{ox}) cannot be recovered or is only very slowly recovered. This may be due to formation of a further oxidised state (super-oxidized II) or binding of a ligand such as water in the active site or a rearrangement of the protein structure or even dissociation of CO. Whether the two inactive states can interconvert with the addition or removal of chloride is unclear. For example it is not clear so far, if a transition between the two postulated HPI states is possible in the presence of chloride or not. Furthermore the electronic state of the iron in the "non chloride" intermediate is unknown. It seems that chloride and its properties is a new, interesting subject in the study of hydrogenases.

We were also able to adsorb and to covalently attach the maturated enzyme to HOPGE electrodes and measure hydrogen oxidation and production, and observe classical high potential inactivation in buffer mix. From these experiments, it was clear that covalent attachment show higher protein film stability and higher catalytic current, and is, therefore the more optimal approach. Nevertheless, the maturated enzyme showed lower activity than the native enzyme, which might be due to incomplete maturation of the enzyme or differences in the structure of the protein due to post-translational modification differences between the organisms or during protein preparation. It is known, for example, that aerobic purification of many proteins leads to oxidation of cysteines and methionines. This could alter the chemistry of the protein surface and change its interactions with the electrode surface. It would be interesting, to also test the influence of chloride, also for the artificially maturated enzyme, as this might give some insights, as to whether the influence of this anion is anyhow related to the oxygen stability of the native enzyme in its as-isolated state.

During this thesis it was also shown, for the first time, that the heterologously expressed, unmaturated [FeFe]-hydrogenase from *D. desulfuricans* could be adsorbed onto a glassy carbon electrode and the redox potentials for all three [Fe-S]-clusters in the enzyme measured. The potentials fit quite nicely to those measured by EPR redox-titration, which were reported in Section 4.2.2. The possibility to determine the redox potentials with electrochemistry provides an alternative method for comparison of redox potentials between the mutants generated in Chapter 5. Protein Film Voltammetry requires much less protein and much less time to determine the potentials of the clusters. However, the EPR and PFE methods are highly complementary, since EPR provides detailed information about the nature of the clusters and their interactions over the broad range of

potentials tested, while PFE allows for quick measurements of multiple samples in different buffer compositions, and at different temperatures. By measuring the different redox potentials of the mutants and considering the alterations in activities of the activated protein, new insights into how the properties of the [Fe-S]-clusters influence catalysis can be uncovered. It is interesting that all three clusters seem to have different redox potentials, which are separated by around 70 mV. At the moment no firm conclusions can be drawn about which potential belongs to which cluster. However, by considering the results from Chapter 4, it seems most likely that the [4Fe-4S]-cluster that forms the H-cluster has the most negative potential, since this EPR signal is lost in the maturated hydrogenase EPR spectrum. It is tempting to speculate that the most distal cluster from the H-cluster is the most positive potential cluster and the central cluster has an intermediate potential giving a sort of potential step effect. (see Figure 6-27 arrangement 1) However, it may be more rational for the enzyme to have the most positive potential cluster in the medial position such that electrons coming into the enzyme from the natural electron donor (likely a cytochrome) end up on the medial cluster first, allowing a second electron transfer to the distal cluster, giving the two electron reduced F-cluster chain that can then quickly reduce the H-cluster allowing hydrogen generation. A higher potential distal cluster would mean that instead the second electron transfer to the enzyme would be very slow because it would depend on the slower kinetics on transfer between the high potential distal cluster and the lower potential medial cluster (see Figure 6-27 arrangement 2). In the hydrogen oxidation direction, the case is reversed and in fact the enzyme would benefit from a high potential distal and low potential medial arrangement. It might be possible, that this potential arrangement changes in the different mutants of Chapter 5. Some of them show drastic changes in directionality of the catalytic activity which can be explained by the electron transfer between clusters with different potentials as just described. This again point out the necessity to determine the potential of the mutant clusters. The following Figure 6-27 illustrates the two possible cluster potential arrangements.

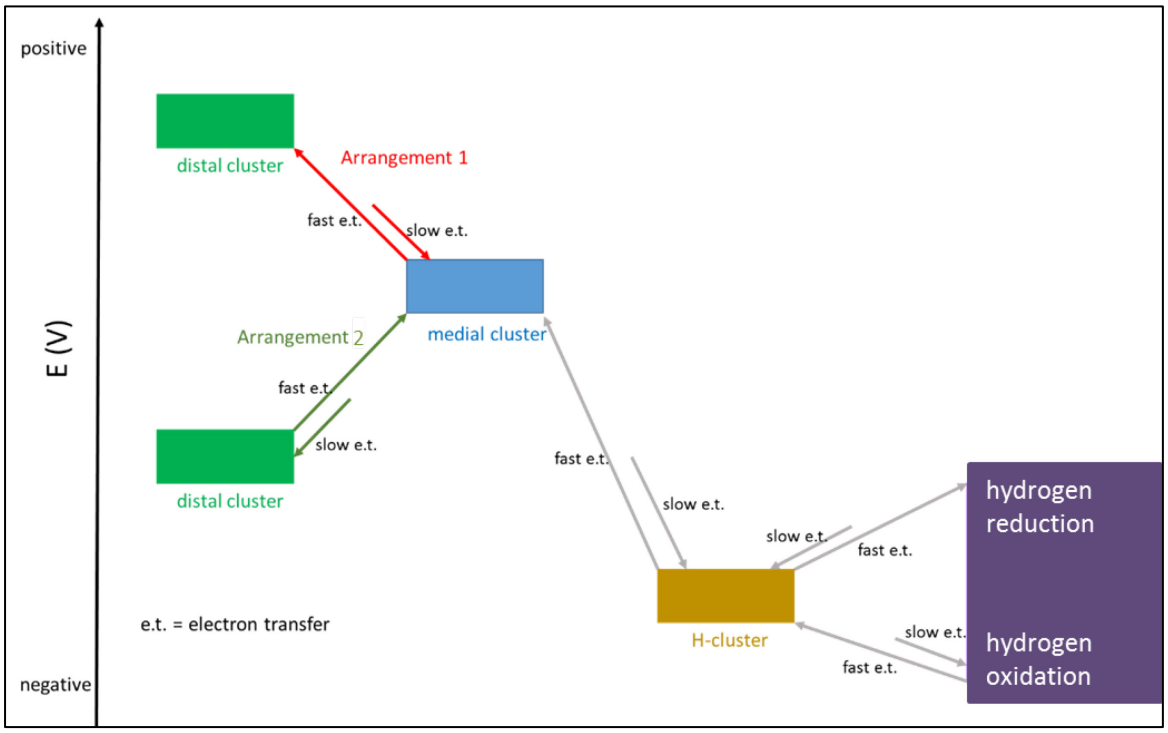

Figure 6-27 Scheme for both possibilities of arranging the cluster potentials of the distal and the medial cluster. Possibility 1 shows the highest potential at the distal cluster and possibility 2 the more likely arrangement with the highest potential at the medial cluster.

For summarizing this section Figure 6-28 shows the [4Fe-4S]-cluster arrangement of the unmaturated [FeFe]-hydrogenase from *D. desulfuricans* with the redox potentials determined from PFE in the possibility 2 arrangement, which is for us the most likely configuration in the wild type enzyme.

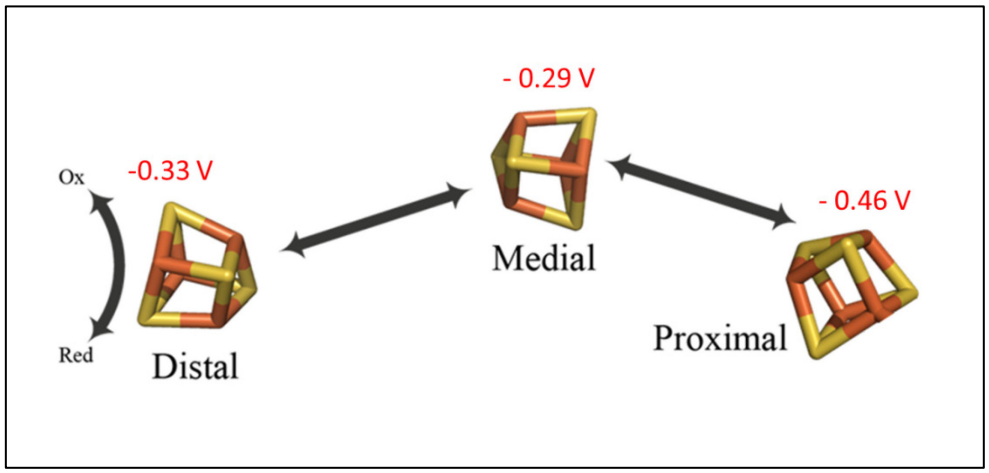

Figure 6-28 Possible arrangement of the cluster potentials, measured by PFE, for the [FeFe]-hydrogenase from *D. desulfuricans*.

Chapter 7 Summary and outlook

One major part of this thesis was the development and establishment of a heterologous over-expression system for the multi-subunit [FeFe]-hydrogenase from *Desulfovibrio desulfuricans* in *E. coli*. Therefore, a codon optimized sequence for both subunits was ordered and a plasmid, containing these hydrogenase sequences with an additional affinity tag was designed which allows a fast and simple purification procedure. These widen the scope of this method (heterologous expression of [Fe-S]-proteins) making it applicable for enzymes with two subunits. Further work is needed to see if it can be applied to enzymes with three or more subunits. However, initial experiments from Ogata and coworkers show that this method can be used for enzymes with three subunits, all of which contain [Fe-S]-clusters (Ogata, personal communication). Should it one day be viable to use isolated enzymes as components of fuel cells, methods for over-expression of the most active or most stable hydrogenases must be developed. This also leads to the confirmation, that this over-expression system is a powerful tool in enzyme production.

With this technique it was possible to generate high amounts of pure, unmaturated [FeFe]-hydrogenase. The advantage of unmaturated enzyme is the possibility to study the accessory [4Fe-4S]-clusters in the absence of the active site. The [FeFe]-hydrogenase from *D. desulfuricans* shows a ferredoxin-like cluster pair as well as an additional [4Fe-4S]-cluster and is therefore an interesting model to study interactions between this ferredoxin-like domain and the additional cluster, which extends the studies of other well-known ferredoxins. It could be shown in this thesis, that the unmaturated protein shows a unique EPR spectrum with a temperature dependent peak splitting, when reduced at negative potentials, which is attributed to the interaction between the H-cluster's [4Fe-S] and its nearest neighbour. At higher potential only the interaction between the clusters of the ferredoxin domain is observed and this appears to be temperature independent over the possible measurement range. Spin-spin interactions between

[Fe-S]-clusters are interesting to study because they provide information about the distances and orientations of the paramagnetic species in proteins. The simple case of two interacting spins is well-studied and relatively simple to simulate. The interaction

between more than two clusters becomes increasingly more complicated to simulate. However, here a system is presented with three interacting clusters, which at high temperature and at higher potential becomes much simpler. It should be possible, therefore, to get a complete understanding of this system and, thereby, provide further insight into the spin-spin interactions of iron-sulfur clusters. A further detail is that the interaction between the $[4Fe]_H$ and its neighbour disappeared after reconstitution of the H-cluster. From previous studies of *D. desulfuricans* it was not possible to identify the H_{sred} state, in which the 4Fe of the H-cluster is reduced. Here, both through EPR redox titration and PFE studies we determined that the potential in the unmaturated protein is approximately -460 mV. The potential of the H_{sred} state from *C. reinhardtii* HydA1 was determined to be -460 mV. The 4Fe cluster potential for unmaturated HydA1 was determined very recently to be -393 mV (unpublished results S. Rumpel). From these it can be suggested, that the H_{sred} state in *D. desulfuricans* might be observed at more negative potentials. Maybe it is not possible to observe this state thermodynamically, but it might be possible to observe it kinetically (freeze quench). The reason for the loss of the spin-spin interaction could be due to several other phenomena (increase in distance between the clusters or change of g-tensor orientation). The results presented in this thesis suggest that further work is needed to establish the reasons for the lack of the H_{sred} state in *D. desulfuricans* and furthermore, to look at the changes that happen to the [4Fe]-cluster upon maturation.

It was also possible for the first time to crystallize the unmaturated enzyme. One crystal gave X-ray diffraction to a resolution of 5 Å. The determination of crystallization conditions is an important step in structural analysis of proteins by X-ray diffraction. One future aim is to get a better resolution by testing different crystals, and, therefore, calculate an electron density map and solve the structure of this protein. By comparing the structure with the previously solved structure of the native enzyme, it should be possible to observe the structural differences that occur following maturation of the enzyme. Crystallization of the mutants described in this thesis would allow us to confirm the structural changes that lead to the changes in the EPR spectrum and the enzyme activity. It might be also possible to crystallize the maturated wild type enzyme as well as maturated mutants.

It could be also shown in this thesis that the unmaturated protein can be maturated with the $[2Fe]_H$ mimic adt (which was used for the maturation of the [FeFe]-hydrogenase from *C. reinhardtii*) to fully active hydrogenase. Therefore, it is clear, that the adt is a general mimic of the active site of [FeFe]-hydrogenases. It would be interesting to test additional

$[2Fe]_H$ mimics with different geometry or bridgeheads to probe the flexibility of the catalytic pocket of the enzyme. Also the maturated enzyme was characterized by EPR- in addition with FTIR-spectroscopy and compared to the native enzyme. From these results it is clear, that the heterologous expressed enzyme is in its oxygen sensitive states identical to the native enzyme. An interesting challenge would be the question, if it is possible to generate the oxygen tolerant, as isolated state, also from the over-expressed enzyme. This would allow detailed studies of the formation of this state and might help to design oxygen tolerant [FeFe]-hydrogenases.

To further understand the electron transfer through the accessory clusters site-directed mutagenesis experiments were performed to change their redox-potentials and analyze the effects. It could be shown, that all mutations can be maturated with adt but some show a change in the directionality of their activity. It was shown, that mutations at the histidine 58 show, unexpectedly, a dramatic increase in the hydrogen production activity. The most likely explanation for this is that in the hydrogen oxidation direction a high potential terminal cluster (that donates electrons to electron acceptors) is more quickly reduced by the H-cluster (and the medial cluster) than one with a more negative potential. It was proposed in this thesis that the most positive potential cluster is the medial one and so in the hydrogen oxidation direction the electron transfer from the H-cluster to the medial cluster is fast but then from the medial cluster to the terminal cluster is low. The mutations that increase the activity are likely to increase the terminal cluster potential to something similar or more positive than the medial cluster, increasing the rate of electron transfer from medial to terminal. In the opposite direction, hydrogen production, the higher potential terminal cluster is a disadvantage, as electrons “sit” there and block further electron acceptor oxidation. This concept may be more widely applicable to electron transfer enzymes, especially those where two electrons are required at once to reduce an electron acceptor (e.g. $2H^+$ to hydrogen or NAD^+ reductases which often use Flavin molecules as cofactors). Such mutations might also be possible in other [FeFe]-hydrogenases, such as the well-studied CpI hydrogenase from *C. pasteurianum* or thermostable enzymes such as those from *T. maritima* to see if that will cause a similar effect or if it is unique for the [FeFe]-hydrogenase from *D. desulfuricans*.

There are many aspects of the native enzyme that are not yet fully understood and were therefore part of this work. The enzyme shows a high potential inactivation (HPI) in protein film electrochemistry (PFE) experiments. To get a closer insight in this phenomenon further PFE experiments with covalently attached protein were done. It

could be shown, for the first time that chloride plays an important role in the formation of this HPI state, because it is only observed, when chloride is present in the electrochemistry buffer. It is completely unclear what chloride does and which part of the enzyme is affected. In the literature it was reported, that for HPI hydrogen needs to be present and that hydrogen is an integral component of the HPI state, bound in an unusual bridging position, but experiments in this thesis show, that HPI also occurs in the absence of hydrogen. It is, therefore, highly unlikely that the HPI state is explained by the model proposed by Léger and coworkers. Instead we propose that chloride plays an important role and that in its absence the enzyme becomes irreversibly inactivated, and that chloride somehow provides a protected HPI state. All of these results lead to further questions about what HPI really is and how this state is formed. It is obvious that this is an important and interesting subject for future studies.

As mentioned above, it was also possible to determine the redox-potentials of the [Fe-S]-clusters for the unmaturated enzyme, with EPR redox-titration as well as with an electrochemical set up. Both techniques show similar results. This shows that electrochemistry is a fast technique to determine redox potentials but it is not a well-established method for [FeFe]-hydrogenases and it needs further optimization. Of particular importance is the fact that the signals in PFE are extremely weak and sensitive to the pH and salt concentration in which the protein is applied to the electrode surface. This is also the case for other unmaturated [FeFe]-hydrogenases, none of which so far have been measured by PFE. Measurements of the mutants are planned for the future to be able to compare their potentials to the one from the wild type. It will be possible to study also other [Fe-S]-proteins with this technique and compare them, for example ferredoxins related to *D. desulfuricans.*

One would have imagined that after so many years of research, the [FeFe]-hydrogenases would be completely understood. However, as is obvious from this thesis there were still many questions to be answered. We managed to take a few steps further towards uncovering secrets of these fascinating proteins, the hydrogenases. Yet, perhaps we have actually ended up providing more questions and revealing that there are still many more things which need to be discovered.

But, in the end, is that not the joy of science?!

Reference List

1. Cammack, R.; Frey, M.; Robson, R. *Hydrogen as a Fuel - Learning from Nature;* Taylor & Francis Group: 2001.

2. Vignais, P. M.; Billoud, B.; Meyer, J. Classification and phylogeny of hydrogenases. *Fems Microbiology Reviews* **2001,** *25* (4), 455-501.

3. Vignais, P. M.; Billoud, B. Occurrence, classification, and biological function of hydrogenases: An overview. *Chemical Reviews* **2007,** *107* (10), 4206-4272.

4. Frey, M. Hydrogenases: Hydrogen-activating enzymes. *Chembiochem* **2002,** *3* (2-3), 153-160.

5. Appel, J.; Schulz, R. Sequence analysis of an operon of a NAD(P)-reducing nickel hydrogenase from the cyanobacterium Synechocystis sp PCC 6803 gives additional evidence for direct coupling of the enzyme to NAD(P)H-dehydrogenase (complex I). *Biochimica et Biophysica Acta-Protein Structure and Molecular Enzymology* **1996,** *1298* (2), 141-147.

6. Hemschemeier, A.; Melis, A.; Happe, T. Analytical approaches to photobiological hydrogen production in unicellular green algae. *Photosynthesis Research* **2009,** *102* (2-3), 523-540.

7. http://www.iubmb.org. **2014**.
Online Source

8. Fontecilla-Camps, J. C.; Volbeda, A.; Cavazza, C.; Nicolet, Y. Structure/function relationships of [NiFe]- and [FeFe]-hydrogenases. *Chemical Reviews* **2007,** *107* (10), 4273-4303.

9. Liu, X. M.; Ibrahim, S. K.; Tard, C.; Pickett, C. J. Iron-only hydrogenase: Synthetic, structural and reactivity studies of model compounds. *Coordination Chemistry Reviews* **2005,** *249* (15-16), 1641-1652.

10. Shima, S.; Pilak, O.; Vogt, S.; Schick, M.; Stagni, M. S.; Meyer-Klaucke, W.; Warkentin, E.; Thauer, R. K.; Ermler, U. The crystal structure of [Fe]-hydrogenase reveals the geometry of the active site. *Science* **2008,** *321* (5888), 572-575.

11. Tian, F.; Toon, O. B.; Pavlov, A. A.; De Sterck, H. A hydrogen-rich early Earth atmosphere. *Science* **2005,** *308* (5724), 1014-1017.

12. Vincent, K. A.; Cracknell, J. A.; Clark, J. R.; Ludwig, M.; Lenz, O.; Friedrich, B.; Armstrong, F. A. Electricity from low-level H-2 in still air - an ultimate test for an oxygen tolerant hydrogenase. *Chemical Communications* **2006,** (48), 5033-5035.

13. Zirngibl, C.; Vandongen, W.; Schworer, B.; Vonbunau, R.; Richter, M.; Klein, A.; Thauer, R. K. H-2-Forming Methylenetetrahydromethanopterin Dehydrogenase, A Novel Type of Hydrogenase Without Iron-Sulfur Clusters in Methanogenic Archaea. *European Journal of Biochemistry* **1992,** *208* (2), 511-520.

14. Korbas, M.; Vogt, S.; Meyer-Klaucke, W.; Bill, E.; Lyon, E. J.; Thauer, R. K.; Shima, S. The iron-sulfur cluster-free hydrogenase (Hmd) is a metalloenzyme with a novel iron binding motif. *Journal of Biological Chemistry* **2006,** *281* (41), 30804-30813.

15. Lyon, E. J.; Shima, S.; Boecher, R.; Thauer, R. K.; Grevels, F. W.; Bill, E.; Roseboom, W.; Albracht, S. P. J. Carbon monoxide as an intrinsic ligand to iron in the active site of the iron-sulfur-cluster-free hydrogenase H-2-Forming methylenetetrahydromethanopterin dehydrogenase as revealed by infrared spectroscopy. *Journal of the American Chemical Society* **2004,** *126* (43), 14239-14248.

16. Thauer, R. K.; Klein, A. R.; Hartmann, G. C. Reactions with molecular hydrogen in microorganisms: Evidence for a purely organic hydrogenation catalyst. *Chemical Reviews* **1996,** *96* (7), 3031-3042.

17. pymol. **2014**. Computer program structure modelling
Online Source

18. Lubitz, W.; Reijerse, E.; van Gastel, M. [NiFe] and [FeFe] hydrogenases studied by advanced magnetic resonance techniques. *Chemical Reviews* **2007,** *107* (10), 4331-4365.

19. Happe, R. P.; Roseboom, W.; Pierik, A. J.; Albracht, S. P. J.; Bagley, K. A. Biological activation of hydrogen. *Nature* **1997,** *385* (6612), 126.

20. Pierik, A. J.; Roseboom, W.; Happe, R. P.; Bagley, K. A.; Albracht, S. P. J. Carbon monoxide and cyanide as intrinsic ligands to iron in the active site of [NiFe]-hydrogenases - NiFe(CN)(2)CO, biology's way to activate H-2. *Journal of Biological Chemistry* **1999,** *274* (6), 3331-3337.

21. Lubitz, W.; Ogata, H.; Rudiger, O.; Reijerse, E. Hydrogenases. *Chemical Reviews* **2014,** *114* (8), 4081-4148.

22. Romao, C. V.; Pereira, I. A. C.; Xavier, A. V.; Legall, J.; Teixeira, M. Characterization of the [NiFe] hydrogenase from the sulfate reducer Desulfovibrio vulgaris Hildenborough. *Biochemical and Biophysical Research Communications* **1997,** *240* (1), 75-79.

23. Valente, F. M. A.; Oliveira, A. S. F.; Gnadt, N.; Pacheco, I.; Coelho, A. V.; Xavier, A. V.; Teixeira, M.; Soares, C. M.; Pereira, I. A. C. Hydrogenases in Desulfovibrio vulgaris Hildenborough: structural and physiologic characterisation of the membrane-bound [NiFeSe] hydrogenase. *Journal of Biological Inorganic Chemistry* **2005,** *10* (6), 667-682.

24. Pandelia, M. E.; Fourmond, V.; Tron-Infossi, P.; Lojou, E.; Bertrand, P.; Leger, C.; Giudici-Orticoni, M. T.; Lubitz, W. Membrane-Bound Hydrogenase I from the Hyperthermophilic Bacterium Aquifex aeolicus: Enzyme Activation, Redox Intermediates and Oxygen Tolerance. *Journal of the American Chemical Society* **2010,** *132* (20), 6991-7004.

25. Pandelia, M. E.; Infossi, P.; Giudici-Orticoni, M. T.; Lubitz, W. The Oxygen-Tolerant Hydrogenase I from Aquifex aeolicus Weakly Interacts with Carbon Monoxide: An Electrochemical and Time-Resolved FTIR Study. *Biochemistry* **2010,** *49* (41), 8873-8881.

26. Lubitz, W.; Reijerse, E. J.; Messinger, J. Solar water-splitting into H(2) and O(2): design principles of photosystem II and hydrogenases. *Energy & Environmental Science* **2008,** *1* (1), 15-31.

27. Nicolet, Y.; De Lacey, A. L.; Vernede, X.; Fernandez, V. M.; Hatchikian, E. C.; Fontecilla-Camps, J. C. Crystallographic and FTIR spectroscopic evidence of changes in Fe coordination upon reduction of the active site of the Fe-only hydrogenase from Desulfovibrio desulfuricans. *Journal of the American Chemical Society* **2001,** *123* (8), 1596-1601.

28. Pohorelic, B. K. J.; Voordouw, J. K.; Lojou, E.; Dolla, A.; Harder, J.; Voordouw, G. Effects of deletion of genes encoding Fe-only hydrogenase of Desulfovibrio vulgaris Hildenborough on hydrogen and lactate metabolism. *Journal of Bacteriology* **2002,** *184* (3), 679-686.

29. Hatchikian, E. C.; Magro, V.; Forget, N.; Nicolet, Y.; Fontecilla-Camps, J. C. Carboxy-terminal processing of the large subunit of [Fe] hydrogenase from Desulfovibrio desulfuricans ATCC 7757. *Journal of Bacteriology* **1999,** *181* (9), 2947-2952.

30. Nicolet, Y.; Piras, C.; Legrand, P.; Hatchikian, C. E.; Fontecilla-Camps, J. C. Desulfovibrio desulfuricans iron hydrogenase: the structure shows unusual coordination to an active site Fe binuclear center. *Structure with Folding & Design* **1999,** *7* (1), 13-23.

31. Verhagen, M. F. J. M.; O'Rourke, T.; Adams, M. W. W. The hyperthermophilic bacterium, Thermotoga maritima, contains an unusually complex iron-hydrogenase: amino acid sequence analyses versus biochemical characterization. *Biochimica et Biophysica Acta-Bioenergetics* **1999,** *1412* (3), 212-229.

32. Moser, C. C.; Page, C. C.; Farid, R.; Dutton, P. L. Biological Electron-Transfer. *Journal of Bioenergetics and Biomembranes* **1995,** *27* (3), 263-274.

33. Page, C. C.; Moser, C. C.; Chen, X. X.; Dutton, P. L. Natural engineering principles of electron tunnelling in biological oxidation-reduction. *Nature* **1999,** *402* (6757), 47-52.

34. McCullagh, M.; Voth, G. A. Unraveling the Role of the Protein Environment for [FeFe]-Hydrogenase: A New Application of Coarse-Graining. *Journal of Physical Chemistry B* **2013,** *117* (15), 4062-4071.

35. Liang, Z. X.; Klinman, J. P. Structural bases of hydrogen tunneling in enzymes: progress and puzzles. *Current Opinion in Structural Biology* **2004,** *14* (6), 648-655.

36. Peters, J. W.; Lanzilotta, W. N.; Lemon, B. J.; Seefeldt, L. C. X-ray crystal structure of the Fe-only hydrogenase (Cpl) from Clostridium pasteurianum to 1.8 angstrom resolution. *Science* **1998,** *282* (5395), 1853-1858.

37. Adamska, A.; Silakov, A.; Lambertz, C.; Rudiger, O.; Happe, T.; Reijerse, E.; Lubitz, W. Identification and Characterization of the "Super-Reduced" State of the H-Cluster in [FeFe] Hydrogenase: A New Building Block for the Catalytic Cycle? *Angewandte Chemie-International Edition* **2012,** *51* (46), 11458-11462.

38. Swanson, K. D.; Ratzloff, M. W.; Mulder, D. W.; Artz, J. H.; Ghose, S.; Hoffman, A.; White, S.; Zadvornyy, O. A.; Broderick, J. B.; Bothner, B.; King, P. W.; Peters, J. W. [FeFe]-Hydrogenase Oxygen Inactivation Is Initiated at the H Cluster 2Fe Subcluster. *Journal of the American Chemical Society* **2015,** *137* (5), 1809-1816.

39. Parkin, A.; Cavazza, C.; Fontecilla-Camps, J. C.; Armstrong, F. A. Electrochemical investigations of the interconversions between catalytic and inhibited states of the [FeFe]-hydrogenase from Desulfovibrio desulfuricans. *Journal of the American Chemical Society* **2006,** *128* (51), 16808-16815.

40. Patil, D. S.; Moura, J. J. G.; He, S. H.; Teixeira, M.; Prickril, B. C.; Dervartanian, D. V.; Peck, H. D.; Legall, J.; Huynh, B. H. Epr-Detectable Redox Centers of the Periplasmic Hydrogenase from Desulfovibrio-Vulgaris. *Journal of Biological Chemistry* **1988,** *263* (35), 18732-18738.

41. Pereira, A. S.; Tavares, P.; Moura, I.; Moura, J. J. G.; Huynh, B. H. Mossbauer characterization of the iron-sulfur clusters in Desulfovibrio vulgaris hydrogenase. *Journal of the American Chemical Society* **2001,** *123* (12), 2771-2782.

42. van Dijk, C. The effect of reoxidation on the reduced hydrogenase of Desulfovibrio vulgaris strain Hildenborough and its oxygen stability.FEBS **1983,***156* (2).

43. Mulder, D. W.; Shepard, E. M.; Meuser, J. E.; Joshi, N.; King, P. W.; Posewitz, M. C.; Broderick, J. B.; Peters, J. W. Insights into [FeFe]-Hydrogenase Structure, Mechanism, and Maturation. *Structure* **2011,** *19* (8), 1038-1052.

44. Guigliarelli, B.; Bertrand, P. Application of EPR spectroscopy to the structural and functional study of iron-sulfur proteins. *Advances in Inorganic Chemistry, Vol 47* **1999,** *47*, 421-497.

45. Posewitz, M. C.; King, P. W.; Smolinski, S. L.; Zhang, L. P.; Seibert, M.; Ghirardi, M. L. Discovery of two novel radical S-adenosylmethionine proteins required for the assembly of an active [Fe] hydrogenase. *Journal of Biological Chemistry* **2004,** *279* (24), 25711-25720.

46. Peters, J. W.; Szilagyi, R. K.; Naumov, A.; Douglas, T. A radical solution for the biosynthesis of the H-cluster of hydrogenase. *Febs Letters* **2006,** *580* (2), 363-367.

47. Voordouw, G. The Genus Desulfovibrio - the Centennial. *Applied and Environmental Microbiology* **1995,** *61* (8), 2813-2819.

48. Lobo, S. A. L.; Melo, A. M. P.; Carita, J. N.; Teixeira, M.; Saraiva, L. M. The anaerobe Desulfovibrio desulfuricans ATCC 27774 grows at nearly atmospheric oxygen levels. *Febs Letters* **2007,** *581* (3), 433-436.

49. Conrad, R. Soil microorganisms as controllers of atmospheric trace gases (H-2, CO, CH4, OCS, N2O, and NO). *Microbiological Reviews* **1996,** *60* (4), 609.

50. Hansen T.A. Metabolism of sulfate-educing prokaryotes. *Antonie van Leeuwenhoek* **1994,** *66* (1-3), 165-185.

51. Odom, J. M.; Peck, H. D. Hydrogen Cycling As A General Mechanism for Energy Coupling in the Sulfate-Reducing Bacteria, Desulfovibrio-Sp. *Fems Microbiology Letters* **1981,** *12* (1), 47-50.

52. Crabtree, G. W.; Dresselhaus, M. S. The hydrogen fuel alternative. *Mrs Bulletin* **2008,** *33* (4), 421-428.

53. Armstrong, F. A.; Belsey, N. A.; Cracknell, J. A.; Goldet, G.; Parkin, A.; Reisner, E.; Vincent, K. A.; Wait, A. F. Dynamic electrochemical investigations of hydrogen oxidation and production by enzymes and implications for future technology. *Chemical Society Reviews* **2009,** *38* (1), 36-51.

54. Happe, T.; Hemschemeier, A.; Winkler, M.; Kaminski, A. Hydrogenases in green algae: do they save the algae's life and solve our energy problems? *Trends in Plant Science* **2002,** *7* (6), 246-250.

55. Gaffron H.; Rubin J. Fermentative and photochemical production of hydrogen in algae. *The Journal of General Physiology* **1942,** *26* (2), 219-240.

56. Gfeller, R. P.; Gibbs, M. Fermentative Metabolism of Chlamydomonas-Reinhardtii .2. Role of Plastoquinone. *Plant Physiology* **1985,** *77* (2), 509-511.

57. Melis, A. Photosynthetic H-2 metabolism in Chlamydomonas reinhardtii (unicellular green algae). *Planta* **2007,** *226* (5), 1075-1086.

58. Nath, K.; Kumar, A.; Das, D. Hydrogen production by Rhodobacter sphaeroides strain OU001 using spent media of Enterobacter cloacae strain DM11. *Applied Microbiology and Biotechnology* **2005,** *68* (4), 533-541.

59. Li, C. L.; Fang, H. H. P. Fermentative hydrogen production from wastewater and solid wastes by mixed cultures. *Critical Reviews in Environmental Science and Technology* **2007,** *37* (1), 1-39.

60. Akhtar, M. K.; Jones, P. R. Deletion of iscR stimulates recombinant clostridial Fe-Fe hydrogenase activity and H-2-accumulation in Escherichia coli BL21(DE3). *Applied Microbiology and Biotechnology* **2008,** *78* (5), 853-862.

61. American Type Culture Collection www.atcc.org. **2014**.
Online Source

62. Kuchenreuther, J. M.; Grady-Smith, C. S.; Bingham, A. S.; George, S. J.; Cramer, S. P.; Swartz, J. R. High-Yield Expression of Heterologous [FeFe] Hydrogenases in Escherichia coli. *Plos One* **2010,** *5* (11).

63. Bernardi, G.; Kawasaki, T. Chromatography of Polypeptides and Proteins on Hydroxyapatite Columns. *Biochimica et Biophysica Acta* **1968,** *160* (3), 301.

64. GE Healthcare Chapter 9 Ion Exchange Chromatography. **2001**.
Online Source

65. Szybalski, W.; Kim, S. C.; Hasan, N.; Podhajska, A. J. Class-Iis Restriction Enzymes - A Review. *Gene* **1991,** *100*, 13-26.

66. Mandel, M.; Higa, A. Calcium-Dependent Bacteriophage Dna Infection. *Journal of Molecular Biology* **1970,** *53* (1), 159.

67. Hatchikian, E. C.; Forget, N.; Fernandez, V. M.; Williams, R.; Cammack, R. Further Characterization of the [Fe]-Hydrogenase from Desulfovibrio-Desulfuricans Atcc-7757. *European Journal of Biochemistry* **1992,** *209* (1), 357-365.

68. Winkler, M.; Hemschemeier, A.; Gotor, C.; Melis, A.; Happe, T. [Fe]-hydrogenases in green algae: photo-fermentation and hydrogen evolution under sulfur deprivation. *International Journal of Hydrogen Energy* **2002,** *27* (11-12), 1431-1439.

69. Wang, X. B.; Niu, S. Q.; Yang, X.; Ibrahim, S. K.; Pickett, C. J.; Ichiye, T.; Wang, L. S. Probing the intrinsic electronic structure of the cubane [4Fe-4S] cluster: Nature's favorite cluster for electron transfer and storage. *Journal of the American Chemical Society* **2003,** *125* (46), 14072-14081.

70. Fish, W. W. Rapid Colorimetric Micromethod for the Quantitation of Complexed Iron in Biological Samples. *Methods in Enzymology* **1988,** *158*, 357-364.

71. D.Heering . UTILS. **2015**.
Online Source

72. Wuthrich, K. The way to NMR structures of proteins. *Nature Structural Biology* **2001,** *8* (11), 923-925.

73. Berg JM; Tymoczko JL, S. L. Three-Dimensional Protein Structure can be determined by NMR Spectroscopy and X-Ray crystallograhy. In *Biochemistry*, 5th ed.; W H Freeman: New York, **2002**.

74. Jonic, S.; Venien-Bryan, C. Protein structure determination by electron cryo-microscopy. *Current Opinion in Pharmacology* **2009,** *9* (5), 636-642.

75. Doerr, A. Single-particle electron cryomicroscopy. *Nature Methods* **2014,** *11* (1), 30.

76. McPherson, A. *Introduction to macromolecular crystallography;* Wiley and Sons: **2003**.

77. Blow, D. *Outline of Crystallography for Biologists;* Oxford University Press: **2002**.

78. Drenth, J. *Principles of Protein X-Ray Crystallography;* 2nd ed.; Springer: **1999**.

79. Hagen W.R. *Biomolecular EPR Spectroscopy;* Taylor & Francis Group: **2009**.

80. Lottspeich, F.; Engels, J. B. *Bioanalytik;* **2006**; Vol. 2;.pp. 441-449.

81. Paul Schosseler . Basic Concepts of EPR. **2015**.
Online Source

82. Que L. *Physical methods in bioinorganic chemistry;* University Science Books: **2000**.

83. Kiley, P. J.; Beinert, H. Oxygen sensing by the global regulator, FNR: the role of the iron-sulfur cluster. *Fems Microbiology Reviews* **1998,** *22* (5), 341-352.

84. Hesse, M.; Meier, H.; Zeeh, B. Infrarot- und Raman-Spektren. In *Spektroskopische Methoden in der organischen Chemie*, 7 ed.; Thieme: Stuttgart, **1979**; pp 33-73.

85. Roseboom, W.; De Lacey, A. L.; Fernandez, V. M.; Hatchikian, E. C.; Albracht, S. P. J. The active site of the [FeFe]-hydrogenase from Desulfovibrio desulfuricans. II. Redox properties, light sensitivity and CO-ligand exchange as observed by infrared spectroscopy. *Journal of Biological Inorganic Chemistry* **2006,** *11* (1), 102-118.

86. VanderSpek, T. M.; Arendsen, A. F.; Happe, R. P.; Yun, S. Y.; Bagley, K. A.; Stufkens, D. J.; Hagen, W. R.; Albracht, S. P. J. Similarities in the architecture of the active sites of Ni-hydrogenases and Fe-hydrogenases detected by means of infrared spectroscopy. *European Journal of Biochemistry* **1996,** *237* (3), 629-634.

87. Pierik, A. J.; Hulstein, M.; Hagen, W. R.; Albracht, S. P. J. A low-spin iron with CN and CO as intrinsic ligands forms the core of the active site in [Fe]-hydrogenases. *European Journal of Biochemistry* **1998,** *258* (2), 572-578.

88. De Lacey, A. L.; Stadler, C.; Cavazza, C.; Hatchikian, E. C.; Fernandez, V. M. FTIR characterization of the active site of the Fe-hydrogenase from Desulfovibrio desulfuricans. *Journal of the American Chemical Society* **2000,** *122* (45), 11232-11233.

89. Gwyer, J. D.; Richardson, D. J.; Butt, J. N. Resolving complexity in the interactions of redox enzymes and their inhibitors: Contrasting mechanisms for the inhibition of a cytochrome c nitrite reductase revealed by protein film voltammetry. *Biochemistry* **2004,** *43* (47), 15086-15094.

90. Bard, A. J.; Faulkner, L. R. *Electrochemical Methods: Fundamentals and Applications;* 2. ed. ed.; Wiley: New York, **2001**.

91. Hirst, J.; Armstrong, F. A. Fast-scan cyclic voltammetry of protein films on pyrolytic graphite edge electrodes: Characteristics of electron exchange. *Analytical Chemistry* **1998,** *70* (23), 5062-5071.

92. Fichtner, C. Spektroskopische und elektrochemische Untersuchung der [NiFe]-Hydrogenase aus Desulfovibrio vulgaris Miyazaki F. **2005**.Universität Düsseldorf

93. Butt, J. N.; Armstrong, F. A. Voltammetry of adsorbed redox enzymes: Mechanism in the potential dimension. In *Bioinorganic Electrochemistry*, Hammerich, O., Ulstrup, J., Eds.; 2008; pp 91-128.

94. Leger, C.; Jones, A. K.; Roseboom, W.; Albracht, S. P. J.; Armstrong, F. A. Enzyme electrokinetics: Hydrogen evolution and oxidation by Allochromatium vinosum [NiFe]-hydrogenase. *Biochemistry* **2002,** *41* (52), 15736-15746.

95. Rudiger, O.; Abad, J. M.; Hatchikian, E. C.; Fernandez, V. M.; De Lacey, A. L. Oriented immobilization of Desulfovibrio gigas hydrogenase onto carbon electrodes by covalent bonds for nonmediated oxidation of H-2. *Journal of the American Chemical Society* **2005,** *127* (46), 16008-16009.

96. Engstrom, R. C.; Strasser, V. A. Characterization of Electrochemically Pretreated Glassy-Carbon Electrodes. *Analytical Chemistry* **1984,** *56* (2), 136-141.

97. Jeuken, L. J. C.; Armstrong, F. A. Electrochemical origin of hysteresis in the electron-transfer reactions of adsorbed proteins: Contrasting behavior of the "blue" copper protein, azurin, adsorbed on pyrolytic graphite and modified gold electrodes. *Journal of Physical Chemistry B* **2001,** *105* (22), 5271-5282.

98. Wenk, B. Die periplasmatische [FeFe]-Hydrogenase aus Desulfovibrio desulfuricans ATCC7757: Aufreinigung, Kristallisation, spektoskopische und elektrochemische Charakterisierung. **2010** Universität Düsseldorf.

99. Glick, B. R.; Martin, W. G.; Martin, S. M. Purification and Properties of the Periplasmic Hydrogenase from Desulfovibrio-Desulfuricans. *Canadian Journal of Microbiology* **1980,** *26* (10), 1214-1223.

100. Grande, H. J.; Dunham, W. R.; Averill, B.; Vandijk, C.; Sands, R. H. Electron-Paramagnetic Resonance and Other Properties of Hydrogenases Isolated from Desulfovibrio-Vulgaris (Strain Hildenborough) and Megasphaera-Elsdenii. *European Journal of Biochemistry* **1983,** *136* (1), 201-207.

101. Silakov, A.; Wenk, B.; Reijerse, E.; Albracht, S. P. J.; Lubitz, W. Spin distribution of the H-cluster in the H(ox)-CO state of the [FeFe] hydrogenase from Desulfovibrio desulfuricans: HYSCORE and ENDOR study of (14)N and (13)C nuclear interactions. *Journal of Biological Inorganic Chemistry* **2009,** *14* (2), 301-313.

102. Silakov, A. Investigation of the active site of the [FeFe] hydrogenase from Desulfovibrio desulfuricans. **2006**, Universität Düsseldorf.

103. Albracht, S. P. J.; Roseboom, W.; Hatchikian, E. C. The active site of the [FeFe]-hydrogenase from Desulfovibrio desulfuricans. 1. Light sensitivity and magnetic hyperfine interactions as observed by electron paramagnetic resonance. *Journal of Biological Inorganic Chemistry* **2006,** *11* (1), 88-101.

104. Adams, M. W. W.; Johnson, M. K.; Zambrano, I. C.; Mortenson, L. E. On the Novel H-2-Activating Iron-Sulfur Center of the Fe-Only Hydrogenases. *Biochimie* **1986,** *68* (1), 35-41.

105. Fauque, G.; Peck, H. D.; Moura, J. J. G.; Huynh, B. H.; Berlier, Y.; Dervartanian, D. V.; Teixeira, M.; Przybyla, A. E.; Lespinat, P. A.; Moura, I.; Legall, J. The 3 Classes of Hydrogenases from Sulfate-Reducing Bacteria of the Genus Desulfovibrio. *Fems Microbiology Reviews* **1988,** *54* (4), 299-344.

106. Vandam, P. J.; Reijerse, E. J.; Hagen, W. R. Identification of a putative histidine base and of a non-protein nitrogen ligand in the active site of Fe-hydrogenases by one-dimensional and two-dimensional electron spin-echo envelope-modulation spectroscopy. *European Journal of Biochemistry* **1997,** *248* (2), 355-361.

107. Popescu, C. V.; Munck, E. Electronic structure of the H cluster in [Fe]-hydrogenases. *Journal of the American Chemical Society* **1999,** *121* (34), 7877-7884.

108. Fourmond, V.; Greco, C.; Sybirna, K.; Baffert, C.; Wang, P. H.; Ezanno, P.; Montefiori, M.; Bruschi, M.; Meynial-Salles, I.; Soucaille, P.; Blumberger, J.; Bottin, H.; De Gioia, L.; Leger, C. The oxidative inactivation of FeFe hydrogenase reveals the flexibility of the H-cluster. *Nature Chemistry* **2014,** *6* (4), 336-342.

109. D.Zannoni; R.De Philippis *Microbial BioEnergy: Hydrogen Production;* 1 ed.; Springer Netherlands: **2014**; Vol. 38.

110. English, C. M.; Eckert, C.; Brown, K.; Seibert, M.; King, P. W. Recombinant and in vitro expression systems for hydrogenases: new frontiers in basic and applied studies for biological and synthetic H-2 production. *Dalton Transactions* **2009,** (45), 9970-9978.

111. Abo-Hashesh, M.; Wang, R. F.; Hallenbeck, P. C. Metabolic engineering in dark fermentative hydrogen production; theory and practice. *Bioresource Technology* **2011,** *102* (18), 8414-8422.

112. Adams, M. W. W.; Mortenson, L. E. The Physical and Catalytic Properties of Hydrogenase-Ii of Clostridium Pasteurianum - A Comparison with Hydrogenase-I. *Journal of Biological Chemistry* **1984,** *259* (11), 7045-7055.

113. Kamp, C.; Silakov, A.; Winkler, M.; Reijerse, E. J.; Lubitz, W.; Happe, T. Isolation and first EPR characterization of the [FeFe]-hydrogenases from green algae. *Biochimica et Biophysica Acta-Bioenergetics* **2008,** *1777* (5), 410-416.

114. Laffly, E.; Garzoni, F.; Fontecilla-Camps, J. C.; Cavazza, C. Maturation and processing of the recombinant [FeFe] hydrogenase from Desulfovibrio vulgaris Hildenborough (DvH) in Escherichia coli. *International Journal of Hydrogen Energy* **2010,** *35* (19), 10761-10769.

115. Girbal, L.; von Abendroth, G.; Winkler, M.; Benton, P. M. C.; Meynial-Salles, I.; Croux, C.; Peters, J. W.; Happe, T.; Soucaille, P. Homologous and heterologous overexpression in Clostridium acetobutylicum and characterization of purified clostridial and algal Fe-only hydrogenases with high specific activities. *Applied and Environmental Microbiology* **2005,** *71* (5), 2777-2781.

116. Morimoto, K.; Kimura, T.; Sakka, K.; Ohmiya, K. Overexpression of a hydrogenase gene in Clostridium paraputrificum to enhance hydrogen gas production. *Fems Microbiology Letters* **2005,** *246* (2), 229-234.

117. King, P. W.; Posewitz, M. C.; Ghirardi, M. L.; Seibert, M. Functional studies of [FeFe] hydrogenase maturation in an Escherichia coli biosynthetic system. *Journal of Bacteriology* **2006,** *188* (6), 2163-2172.

118. Sybirna, K.; Antoine, T.; Lindberg, P.; Fourmond, V.; Rousset, M.; Mejean, V.; Bottin, H. Shewanella oneidensis: a new and efficient system for expression and maturation of heterologous [Fe-Fe] hydrogenase from Chlamydomonas reinhardtii. *Bmc Biotechnology* **2008,** *8*.

119. Jo, J. H.; Jeon, C. O.; Lee, S. Y.; Lee, D. S.; Park, J. M. Molecular characterization and homologous overexpression of [FeFe]-hydrogenase in Clostridium tyrobutyricum JM1. *International Journal of Hydrogen Energy* **2010,** *35* (3), 1065-1073.

120. Zhao, J. F.; Song, W. L.; Cheng, J.; Zhang, C. X. Heterologous expression of a hydrogenase gene in Enterobacter aerogenes to enhance hydrogen gas production. *World Journal of Microbiology & Biotechnology* **2010,** *26* (1), 177-181.

121. Yacoby, I.; Tegler, L. T.; Pochekailov, S.; Zhang, S. G.; King, P. W. Optimized Expression and Purification for High-Activity Preparations of Algal [FeFe]-Hydrogenase. *Plos One* **2012,** *7* (4).

122. Esselborn, J.; Lambertz, C.; Adamska-Venkatesh, A.; Simmons', T.; Berggren, G.; Nothl, J.; Siebel, J.; Hemschemeier, A.; Artero, V.; Reijerse, E.; Fontecave, M.; Lubitz, W.; Happe, T. Spontaneous activation of [FeFe]-hydrogenases by an inorganic [2Fe] active site mimic. *Nature Chemical Biology* **2013,** *9* (10), 607-609.

123. Kellers, P. Strukturelle und funktionelle Charakterisierung der [NiFe]-Hydrogenase aus Allochromatium vinosum. **2008**, Universität Düsseldorf.

124. Goenka Agrawal, A. Molecular biological and spectroscopic characterisation of the [NiFe]-hydrogenase from Desulfovibrio vulgaris. **2005**, Universität Düsseldorf.

125. Milowska, K.; Gabryelak, T. Reactive oxygen species and DNA damage after ultrasound exposure. *Biomolecular Engineering* **2007,** *24* (2), 263-267.

126. Voordouw, G.; Niviere, V.; Ferris, F. G.; Fedorak, P. M.; Westlake, D. W. S. Distribution of Hydrogenase Genes in Desulfovibrio Spp and Their Use in Identification of Species from the Oil-Field Environment. *Applied and Environmental Microbiology* **1990,** *56* (12), 3748-3754.

127. Berggren, G.; Adamska, A.; Lambertz, C.; Simmons, T. R.; Esselborn, J.; Atta, M.; Gambarelli, S.; Mouesca, J. M.; Reijerse, E.; Lubitz, W.; Happe, T.; Artero, V.; Fontecave, M. Biomimetic assembly and activation of [FeFe]-hydrogenases. *Nature* **2013,** *499* (7456), 66.

128. Stripp, S. T.; Happe, T. How algae produce hydrogen-news from the photosynthetic hydrogenase. *Dalton Transactions* **2009,** (45), 9960-9969.

129. Berggren, G. O.; Fontecave, M.; Berggren, G. O.; Simmons, T.; Atta, M.; Gambarelli, S.; Mouesca, J.; Artero, V.; Fontecave, M.; Lambertz, C.; Esselborn, J.; Heppe, T.; Adamska, A.; Reijerse, E.; Lubitz, W. Artificial Maturation of [Fe Fe] Hydrogenases, Biomimetic Chemistry and Biological Machinery in Synergy. *Journal of Biological Inorganic Chemistry* **2014,** *19*, S69.

130. McGlynn, S. E.; Ruebush, S. S.; Naumov, A.; Nagy, L. E.; Dubini, A.; King, P. W.; Broderick, J. B.; Posewitz, M. C.; Peters, J. W. In vitro activation of [FeFe] hydrogenase: new insights into hydrogenase maturation. *Journal of Biological Inorganic Chemistry* **2007,** *12* (4), 443-447.

131. Darensbourg, M. Y.; Lyon, E. J.; Zhao, X.; Georgakaki, I. P. The organometallic active site of [Fe]hydrogenase: Models and entatic states. *Proceedings of the National Academy of Sciences of the United States of America* **2003,** *100* (7), 3683-3688.

132. Paufler, P. International Tables for Crystallography. Wondratschek, H. and Müller, U. [2nd]. **2011**. IUCr Journals.
Online Source

133. Beinert, H.; Holm, R. H.; Munck, E. Iron-sulfur clusters: Nature's modular, multipurpose structures. *Science* **1997,** *277* (5326), 653-659.

134. Cammack, R. Iron-Sulfur Clusters in Enzymes - Themes and Variations. *Advances in Inorganic Chemistry* **1992,** *38*, 281-322.

135. Meyer, J. Iron-sulfur protein folds, iron-sulfur chemistry, and evolution. *Journal of Biological Inorganic Chemistry* **2008,** *13* (2), 157-170.

136. Boll, M.; Fuchs, G.; Tilley, G.; Armstrong, F. A.; Lowe, D. J. Unusual spectroscopic and electrochemical properties of the 2[4Fe-4S] ferredoxin of Thauera aromatica. *Biochemistry* **2000,** *39* (16), 4929-4938.

137. Guerrini, O.; Burlat, B.; Leger, C.; Guigliarelli, B.; Soucaille, P.; Girbal, L. Characterization of two 2[4Fe4S] ferredoxins from Clostridium acetobutylicum. *Current Microbiology* **2008,** *56* (3), 261-267.

138. Dhanaraj, G.; Byrappa, K.; Prasad, V.; Dudley, M. *Springer Handbook of Crystal Growth;* 1 ed.; Springer Verlag Berlin Heidelberg: **2010**.

139. Weil, J. A.; Bolton, J. R. *Electron Paramagnetic Resonance: Elementary Theory and Practical Applications;* second ed.; Wiley: **2006**.

140. Li, H. X.; Rauchfuss, T. B. Iron carbonyl sulfides, formaldehyde, and amines condense to give the proposed azadithiolate cofactor of the Fe-only hydrogenases. *Journal of the American Chemical Society* **2002,** *124* (5), 726-727.

141. Frey, M. Hydrogenases: Hydrogen-activating enzymes. *Chembiochem* **2002,** *3* (2-3), 153-160.

142. Madden, C.; Vaughn, M. D.; Diez-Pérez, I.; Brown, K. A.; King, P. W.; Gust, D.; Moore, A. L.; Moore, T. A. Catalytic Turnover of [FeFe]-Hydrogenase Based on Single-Molecule Imaging. *Journal of the American Chemical Society* **2012,** *134*, 1577-1582.

143. Pandelia, M. E.; Nitschke, W.; Infossi, P.; Giudici-Orticoni, M. T.; Bill, E.; Lubitz, W. Characterization of a unique [FeS] cluster in the electron transfer chain of the oxygen tolerant [NiFe] hydrogenase from Aquifex aeolicus. *Proceedings of the National Academy of Sciences of the United States of America* **2011,** *108* (15), 6097-6102.

144. Bingemann, R.; Klein, A. Conversion of the central [4Fe-4S] cluster into a [3Fe-4S] cluster leads to reduced hydrogen-uptake activity of the F-420-reducing hydrogenase of Methanococcus voltae. *European Journal of Biochemistry* **2000,** *267* (22), 6612-6618.

145. Rousset, M.; Montet, Y.; Guigliarelli, B.; Forget, N.; Asso, M.; Bertrand, P.; Fontecilla-Camps, J. C.; Hatchikian, E. C. [3Fe-4S] to [4Fe-4S] cluster conversion in Desulfovibrio fructosovorans [NiFe] hydrogenase by site-directed mutagenesis. *Proceedings of the National Academy of Sciences of the United States of America* **1998,** *95* (20), 11625-11630.

146. Vincent, K. A.; Parkin, A.; Lenz, O.; Albracht, S. P. J.; Fontecilla-Camps, J. C.; Cammack, R.; Friedrich, B.; Armstrong, F. A. Electrochemical definitions of O-2 sensitivity and oxidative inactivation in hydrogenases. *Journal of the American Chemical Society* **2005,** *127* (51), 18179-18189.

147. Bryant, M. A.; Crooks, R. M. Determination of Surface Pka Values of Surface-Confined Molecules Derivatized with Ph-Sensitive Pendant Groups. *Langmuir* **1993,** *9* (2), 385-387.

148. Vincent, K. A.; Parkin, A.; Armstrong, F. A. Investigating and exploiting the electrocatalytic properties of hydrogenases. *Chemical Reviews* **2007,** *107* (10), 4366-4413.

149. Ogata, H.; Kellers, P.; Lubitz, W. The Crystal Structure of the [NiFe] Hydrogenase from the Photosynthetic Bacterium Allochromatium vinosum: Characterization of the Oxidized Enzyme (Ni-A State). *Journal of Molecular Biology* **2010,** *402* (2), 428-444.

150. Chouffai, D.; Capon, J. F.; De Gioia, L.; Petillon, F. Y.; Schollhammer, P.; Talarmin, J.; Zampella, G. A Diferrous Dithiolate as a Model of the Elusive H-ox(inact) State of the [FeFe] Hydrogenases: An Electrochemical and Theoretical Dissection of Its Redox Chemistry. *Inorganic Chemistry* **2015,** *54* (1), 299-311.

151. Hirst, J. Elucidating the mechanisms of coupled electron transfer and catalytic reactions by protein film voltammetry. *Biochimica et Biophysica Acta-Bioenergetics* **2006,** *1757* (4), 225-239.

Vector maps of the cloning vectors:

pUC57 vector:

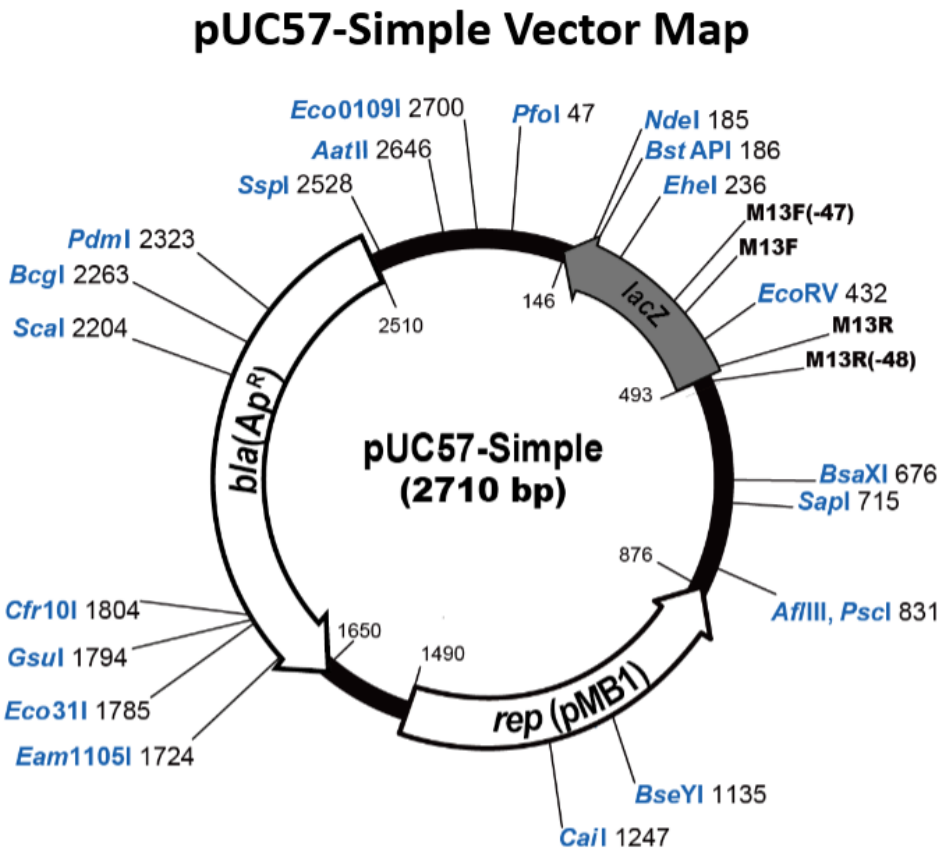

Multiple Cloning Sites:

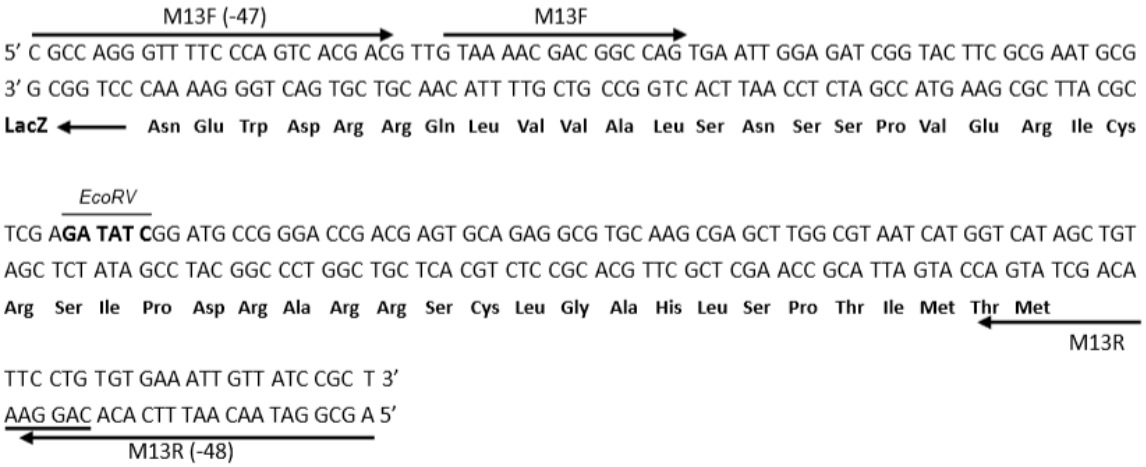

pACYC-Duet-1 vector:

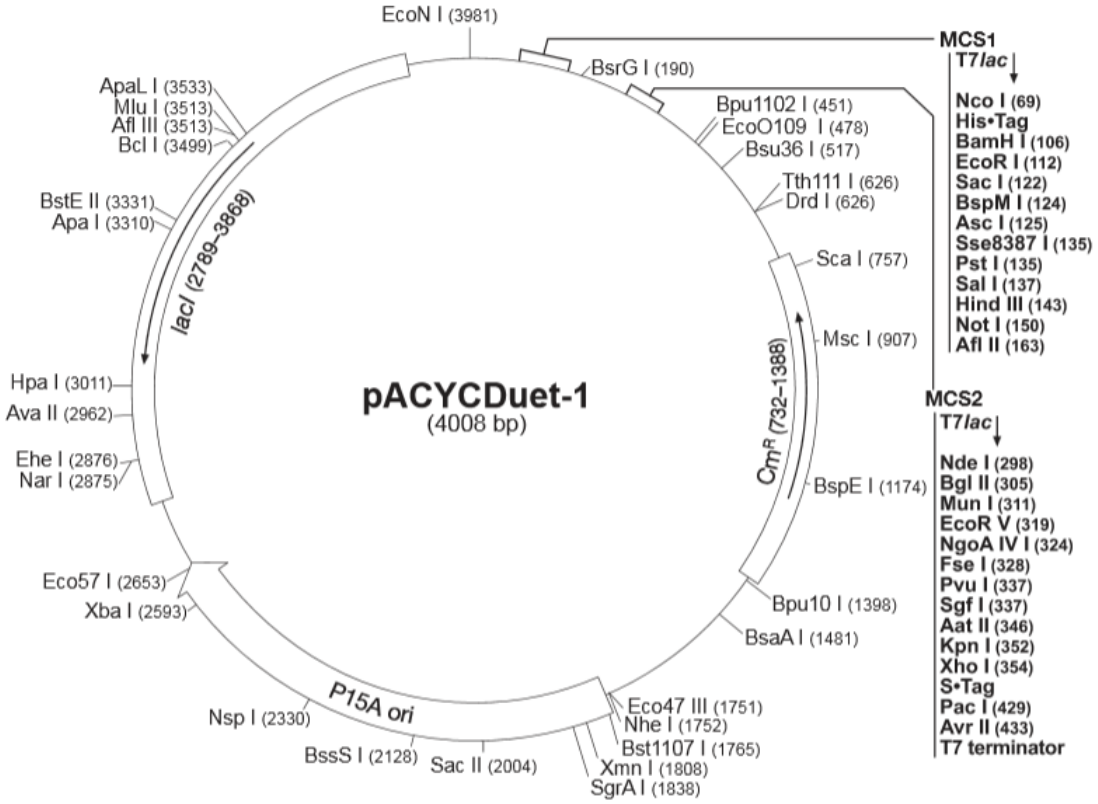

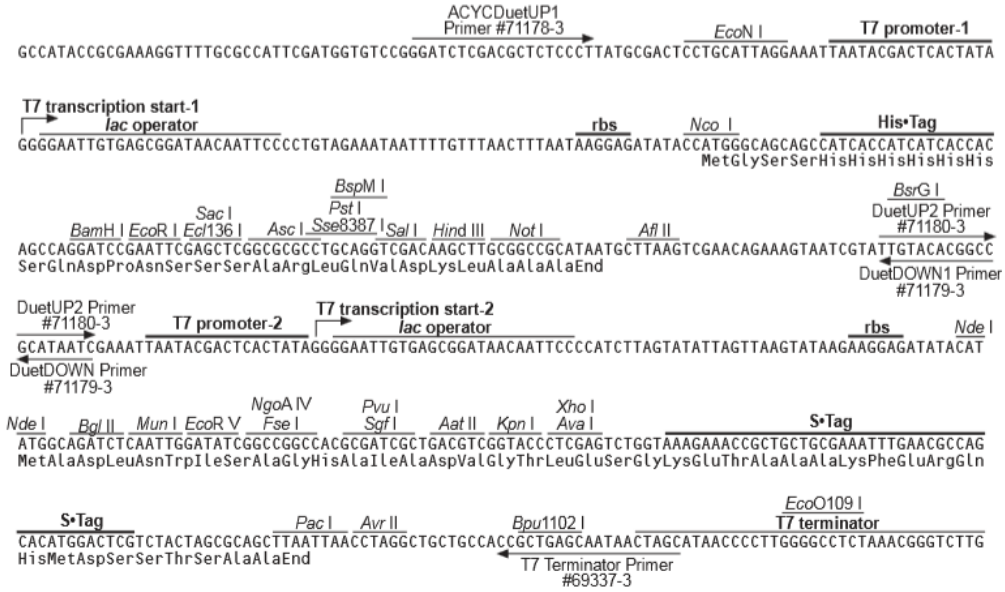

pACYCDuet-1 cloning/expression regions

amino acid	three letter code	one letter code	structure
alanine	Ala	A	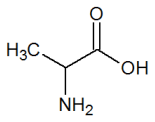
arginine	Arg	R	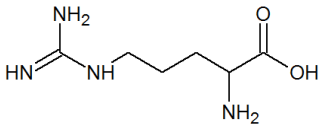
asparagine	Asn	N	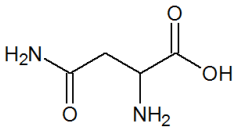
aspartic acid	Asp	D	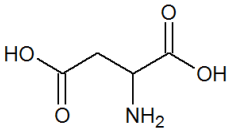
cysteine	Cys	C	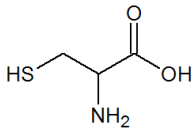
glutamic acid	Glu	E	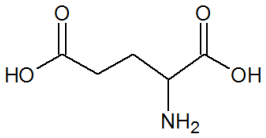
glutamine	Gln	Q	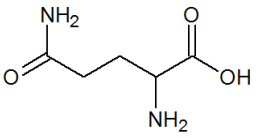
glycine	Gly	G	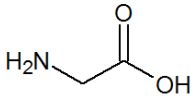
histidine	His	H	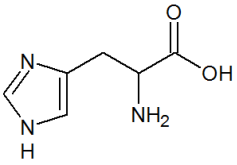
isoleucine	Ile	I	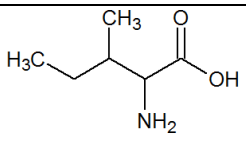

leucine	Leu	L	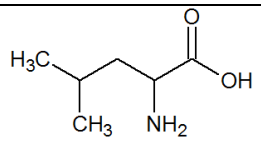
lysine	Lys	K	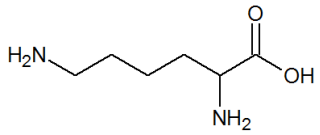
methionine	Met	M	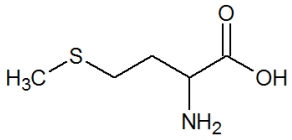
phenylalanine	Phe	F	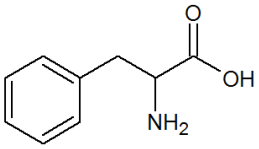
proline	Pro	P	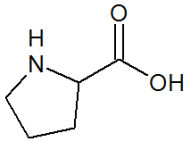
serine	Ser	S	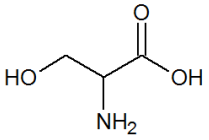
threonine	Thr	T	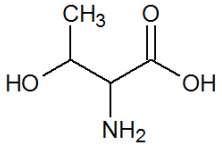
tryptophan	Trp	W	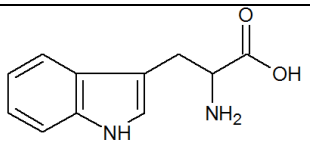
tyrosine	Tyr	Y	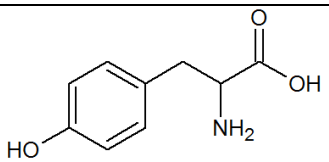
valine	Val	V	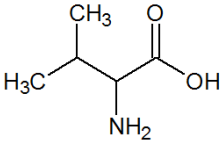

Reaction and possible degradation of diluted (~100 µM) adt in 100 mM Tris pH 8.0 over time (anaerobic conditions inside a glovebox with 2 % hydrogen)